Development of a Neuromechanical Model for Investigating Sensorimotor Interactions During Locomotion

by

Jeremy William Noble

A thesis

presented to the University of Waterloo

in fulfillment of the

thesis requirement for the degree of

Doctor of Philosophy

in

Kinesiology

Waterloo, Ontario, Canada, 2010

AUTHOR'S DECLARATION

I hereby declare that I am the sole author of this thesis. This is a true copy of the thesis, including any required final revisions, as accepted by my examiners.

I understand that my thesis may be made electronically available to the public.

Abstract

Recently it has been suggested that the use of neuromechanical simulations could be used to further our understanding of the neural control mechanisms involved in the control of animal locomotion. The models used to carry out these neuromechanical simulations typically consist of a representation of the neural control systems involved in walking and a representation of the mechanical locomotor apparatus. These separate models are then integrated to produce motion of the locomotor apparatus based on signals that are generated by the neural control models. Typically in past neuromechanical simulations of human walking the parameters of the neural control model have been specifically chosen to produce a walking pattern that resembles the normal human walking pattern as closely as possible. Relatively few of these studies have systematically tested the effect of manipulating the control parameters on the walking pattern that is produced by the locomotor apparatus. The goal of this thesis was to develop models of the locomotor control system and the human locomotor apparatus and systematically manipulate several parameters of the neural control system and determine what effects these parameters would have on the walking pattern of the mechanical model. Specifically neural control models were created of the Central Pattern Generator (CPG), feedback mechanisms from muscle spindles and contact sensors that detect when the foot was contact with the ground. Two models of the human locomotor apparatus were used to evaluate the outputs of the neural control systems; the first was a rod pendulum, which represented a swinging lower-limb, while the second was a 5-segment biped model, which included contact dynamics with the ground and a support system model to maintain balance.

The first study of this thesis tested the ability of a CPG model to control the frequency and amplitude of the pendulum model of the lower-limb, with a strictly feedforward control

mechanism. It was found that the frequency of the pendulum's motion was directly linked (or entrained) to the frequency of the CPG's output. It was also found that the amplitude of the pendulum's motion was affected by the frequency of the CPG's output, with the greatest amplitude of motion occurring when the frequency of the CPG matched the pendulum's natural frequency. The effects of altering several other parameters of the pendulum model, such as the initial angle, the magnitude of the applied viscous damping or the moment arms of the muscles, were also analyzed. The second study again used the pendulum model, and added feedback to the neural control model, via output from simulated muscle spindles. The output from these spindle models was used to trigger a simulated stretch reflex. It was found that the addition of feedback led to sensory entrainment of the CPG output to the natural frequency of the pendulum. The effects of altering the muscle spindle's sensitivity to length and velocity changes were also examined. The ability of this type of feedback system to respond to mechanical perturbations was also analyzed. The third and fourth studies used a biped model of the musculoskeletal system to assess the effects of altering the parameters of the neural control systems that were developed in the first two studies. In the third study, the neural control system consisted only of feedforward control from the CPG model. It was found that the walking speed of the biped model could be controlled by altering the frequency of the CPG's output. It was also observed that variability of the walking pattern was decreased when there was a moderate level of inhibition between the CPGs of the left and right hip joints. The final study added feedback from muscle receptors and from contact sensors with the ground. It was found that the most important source of feedback was from the contact sensors to the extensor centres of the CPG. This feedback increased the level of extensor activity and produced significantly faster walking speeds when compared to other types of feedback.

This thesis was successful in testing the effects of several control parameters of the neural control system on the movement of mechanical systems. Particularly important findings included the importance of connectivity between the CPGs of the left and right hip joints and positive feedback regarding the loading of the limb for establishing an appropriate forward walking speed. It is hoped that the models developed in this thesis can form the basis of future neuromechanical models and that the simulations carried out in this thesis help provide a better understanding of the interactions between neural and mechanical systems during the control of locomotion.

Acknowledgements

I would like to begin by acknowledging my doctoral advisor Dr. Stephen Prentice. His mentorship, guidance, support, patience and most importantly his friendship made this thesis possible. Steve was always there to encourage me when things seemed like they would never work and was always there to push me to go further with my work.

I would also like to acknowledge the contributions of my thesis committee: Dr. Clark Dickerson, Dr. Bill McIlory and Dr. John McPhee. Their feedback helped shape the projects in this thesis and helped improve the quality of the work. Particular thanks must be paid to Dr. John McPhee for providing access the DynaFlex Pro software package that was developed in his lab. Thanks also must be extended to Dr. McPhee's student Matthew Millard who provided a great deal of support with this software package. I would also like to thank my external examiner Dr. Brad McFadyen, your comments and insights helped improve the quality of this work.

I would also like to thank the members of the Gait and Posture Lab over my time at Waterloo. I have made many friends during this time that I am sure will last a lifetime. I would also like to thank fellow graduate students in the department for the comradery and friendship during my time here, there are too many names to list individually but the lunches, Friday afternoons on the patio and even the time in the gym or sports fields will not be forgotten.

Lastly, I would like to thank my amazing wife Maryanne. Without her love, support and encouragement this work could never have been completed. The last several years have definitely had their ups and downs, but I can't wait to see what happens next and to share those experiences with you.

Dedication

To my wife, Maryanne. Your unwavering support means the world to me and without it, this thesis would never have been possible.

Table of Contents

List of Figures

List of Tables

Chapter 1: Introduction

The study of the neural control of walking has been performed for close to 100 years (For a review see (Rossignol et al. 2006)). The study of walking intrigues researchers as it is our primary form of locomotion; it is required for independent living and recreational enjoyment of life. Despite all of the studies performed on human walking and the walking of other animals, the mechanisms that are involved in the control of human walking remain somewhat elusive, as it is impossible to directly measure activity within the human central nervous system (CNS). It is currently thought that the control of walking includes contributions from all levels of the CNS, from the spinal cord to the higher brain centres. Some of the neural pathways that are thought to be involved in the control of human walking are shown in Figure 1.1. Walking results from a complex interaction between the various neural pathways that are shown in Figure 1.1. The interaction and communication between these various pathways remains an area that requires a significant amount of research.

One of the paramount features of human walking is its' adaptability. We are able to change, or adapt, our walking pattern in order to walk in a number of different environments such as walking through an uneven rocky path while hiking. We are also able to adapt our walking pattern to accommodate obstacles in our walking path, for example, if we encounter an obstacle that is in our path, we are able to use vision to detect this obstacle, and select an appropriate strategy to avoid the obstacle. This may involve stepping over the obstacle, or walking around the obstacle. We are also able to adapt our walking pattern to overcome unexpected perturbations, such as a slip or a trip or a shove.

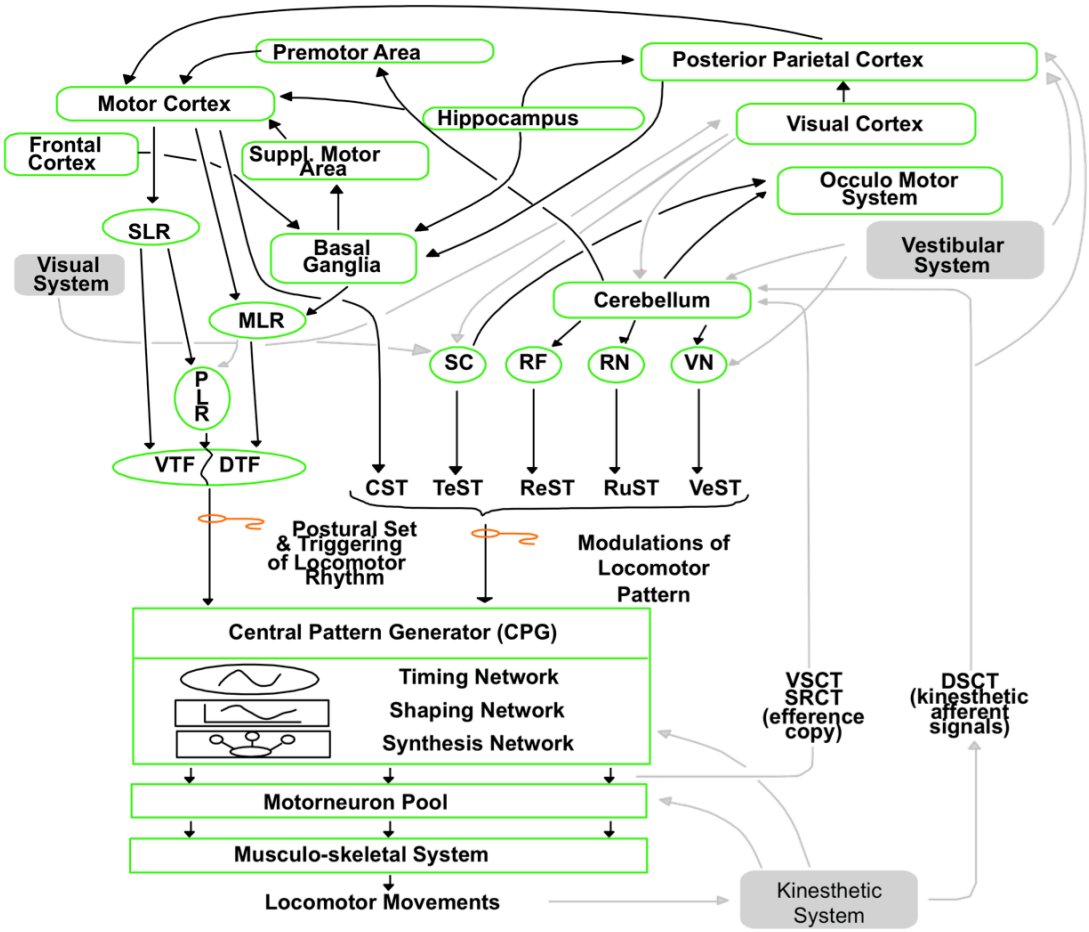

Figure 1.1: Illustration of some of the neural pathways involved in the control of human walking. The black arrows indicate efferent pathways, while the grey arrows represent afferent pathways, while the grey boxes indicate sensor systems used to control walking. The following acronyms are used in the figure: CST – Cerebrospinal Tract, TeST – Tectospinal Tract, ReST – Reticulospinal Tract, RuST – Rubrospinal Tract, VeST – Vestibulospinal Tract, SC – Superior Colliculus, RF - Reticular Formation, RN – Red Nucleus, VN – Vestibular Nuclei, SLR – Subthalamic Locomotor Region, MLR – Mesencenphalic Locomotor Region, PLR – Pontine Locomotor Region, VTF – Ventral Tectal Field, DTF – Dorsal Tectal Field, VSCT – Ventral Spinocerebelar tract, SRCT – Spino-Reticular Cerebellar-Tract, DSCT – Dorsal Spinal Cerebellar Tract. Figure adapted from Patla (1996).

As observed in Figure 1.1, the control mechanisms involved in the control of walking are quite complex, with neural substrates from various levels of the CNS contributing to the generation of an adaptable, efficient walking pattern. A simplified model of the control of walking is shown in Figure 1.2. The basic timing and shaping of the muscle activation patterns

observed during walking is thought to be produced by neural circuits in the spinal cord known as Central Pattern Generators (CPGs) (Grillner and Zangger 1979). These spinal circuits are capable of producing a basic walking pattern in the absence of sensory feedback, however there are a great deal of deficits in the observed walking pattern when no feedback is available (Grillner and Zangger 1984). The movement pattern that is produced during walking will activate various sensory receptors, from three main sensory systems: the vestibular system, the visual system and the kinesthetic system (Patla 1992). As shown in Figure 1.1, all of these sensory systems are capable of altering the output of the CPG, and thus altering the muscle activation patterns that will in turn affect the kinematics of the walking pattern. The sensory feedback may also alter the output of the CPG in order to adapt to changes in environmental conditions, or due to perturbations to the body.

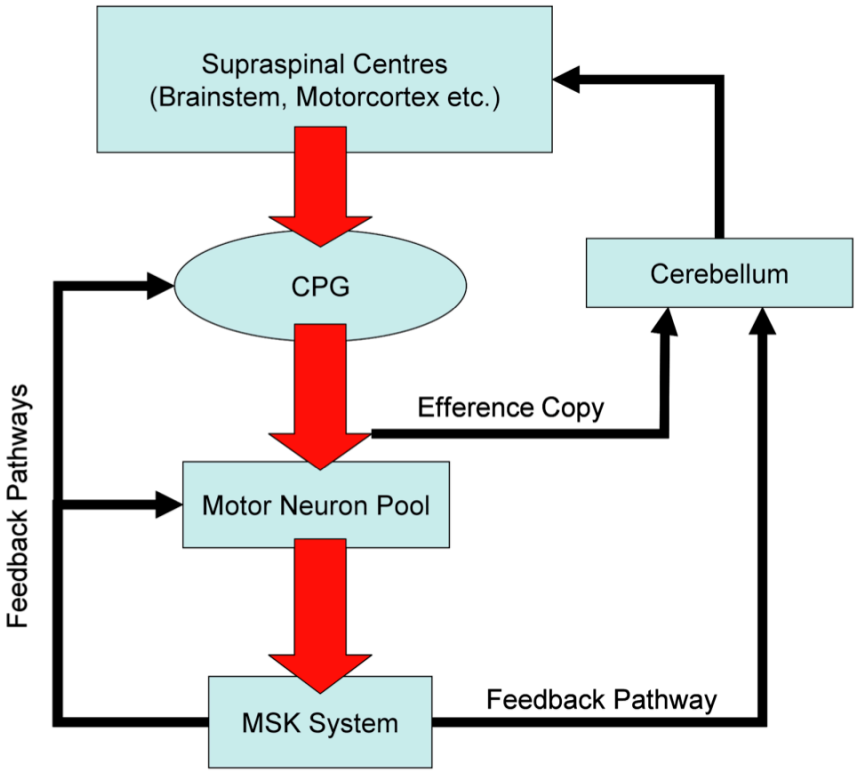

Figure 1.2: Conceptual model of the heterarchical organization of the control systems for human locomotion.

Because the neural centres that are involved in the control of walking are distributed across the various levels of the CNS, but each neural centre has an important role in the overall generation of the walking pattern, the organization of the locomotor control system has been described as a heterarchical control system (Cohen 1992). This is in contrast to a hierarchical control system where certain components of the control system have a higher precedence in determining the overall output of the system.

A great deal of research has been done examining the contributions of various neural substrates to the overall walking pattern. The typical paradigm used to determine the role of a neural centre during locomotion is to destroy or disable the neural substrate in question and observe what deficits occur in the walking pattern. In humans, the only ethical manner in which the function of these neural substrates can be determined is to examine the effect of degenerative processes, such as Parkinson's disease, or traumatic destruction of neural centres, through brain injury or stroke for example. For this reason, most of our knowledge regarding the neural control of locomotion comes from animal research, where neural centres can be systematically destroyed and the resulting movement patterns can be carefully analyzed. Another advantage of using animals for this type of research is that the activity of the neurons in these various neural centres can be directly measured, and correlated with movement patterns, thereby giving greater insight to the roles of these neural centres during the control of locomotion (Drew 1988).

An important aspect of the neural control of walking is the interaction between the various neural substrates involved. These interactions are difficult to assess in animal studies, and even more difficult to assess with human research participants. The importance of these interactions can be observed in Figure 1.1, where a number of the neural substrates illustrated receive input from more than one source, or may have projections to a number of other

substrates. For this reason it is sometimes difficult to assess which particular pathway is leading to a change in the walking pattern when the activity of a certain neural substrate is eliminated (Rossignol et al. 2006). One method that has been suggested as a promising approach to furthering our understanding of the interaction between various neural substrates is computational modeling (Pearson et al. 2006).

Computational modeling is a useful paradigm for testing hypotheses where the full details of the system in question are not fully understood (Lewandowski 1982). Computational modeling also allows us to test situations where *in vivo* experiments are not possible. To further our understanding regarding the neural control of human locomotion, three main systems must be represented in neuromechanical models, these include a model of the neural control system, a representation of the musculoskeletal system and a model representing the environmental dynamics where the simulations will take place. Recently, Pearson et al (2006) reviewed the progress on using neuromechanical models for enhancing our understanding of the neural control of mammalian locomotion. Pearson's group stresses that the use of neuromechanical models can provide a great opportunity to further our knowledge on the neural control of walking, as most of our current knowledge comes from isolated animal models, which usually do not have a full complement of sensory activity that is associated with normal walking behaviour. Also, the use of models allows for the simulation of conditions that are very difficult to achieve in human based experiments. For example, it is impossible to determine what the walking pattern would be if all sensory information from muscle spindles is eliminated, unless you have access to a patient with such a condition. However even with such a patient, it is nearly impossible to know how much sensory information is actually being processed as some information may remain. Additionally, patient populations may often have other conditions, which may also contribute to

altered neuromuscular control during walking. However with a neuromechanical model, we are able to systematically manipulate the contribution of each individual system or neural substrate to the overall control of walking and carry out simulations which show the effect of these changes on the kinematics of the walking pattern, and thus gain a deeper insight into how these systems contribute to the control of locomotion.

This thesis is divided into four separate studies that analyzed the interaction between CPG and sensory feedback mechanisms, primarily from kinesthetic systems. In these studies, the magnitude and timing of the feedback from simulated muscle spindles were systematically manipulated and the effects of these signals on the movement pattern of the locomotor apparatus were analyzed. The first two studies of the thesis featured a neural control model producing muscle activation signals, which in turn acted on a simple pendulum, which represented a swinging human lower limb, without any contact with the ground. This pendulum model allowed for the elucidation of some of the neural mechanisms involved in the control of rhythmic limb movements, particularly the modulation of the frequency and amplitude of the movement patterns. The first study of this thesis examined what effect of the amplitude and frequency of the neural control signals have on the motion of the pendulum system, in the absence of sensory feedback. The next study analyzed the effect of a simple reflex pathway that interacted with the CPG. The effect of this reflex pathway on the amplitude and frequency of the pendulums' motion was analyzed. In the final two studies of this thesis a more detailed musculoskeletal model, which represented a biped human and included contact dynamics with the ground, was used to analyze the effects of the previously examined neural control mechanisms. Humans have a unique ability to walk as bipeds, which allows for us to use the upper limbs to carry out other tasks as we are walking. This gives the CNS the important task of controlling balance of the

upper body during walking, however these tasks were not analyzed or modeled in this thesis. Study 3 analyzed the effect of the frequency of CPG output on the walking velocity and walking kinematics of a biped model. The final study analyzed how the addition of feedback from muscle spindles and ground contact sensors altered the movement patterns of the biped model and how the timing of the feedback signals altered the kinematics of the walking pattern.

Overall Thesis Goals and Study Objectives

The overall goal of this thesis is to better understand the neural control mechanisms involved in the control of locomotion, particularly how sensory feedback from the kinesthetic system alters the output of the CPG, and what effect this feedback would have on the overall walking pattern. The work towards this goal occurred in an incremental fashion. In Study 1, a model of the CPG was used to test the ability to interact with a simplified model of the musculoskeletal system. Study 2 added feedback pathways based on our physiological knowledge of how sensory information interacts with the CPG and used the same model of the musculoskeletal system used in Study 1. Study 3 investigated the feedforward control of walking through the use of a CPG interacting with a more detailed model of the musculoskeletal system, in the absence of sensory feedback. The final study of this thesis added sensory feedback to the model developed in Study 3 and analyzed how the magnitude and timing of this feedback altered the walking pattern of the biped musculoskeletal model.

Chapter 2: Review of Relevant Literature

This chapter will consist of an evaluation of past research that is relevant to methods used in this thesis. The review will begin with an examination of the neural mechanisms involved in the control of human walking. Next, the biomechanics of human locomotion will be briefly evaluated. This will be followed by an assessment of past research that has attempted to combine models of neural control with biomechanical models of human locomotion.

Neural Control of Human Locomotion

As noted in the introduction, the neural control of locomotion results from a complex interaction between neural substrates at various levels of the CNS. This section examines past investigations on the contributions of spinal circuitry, sensory mechanisms and higher brain centres to the control of human walking.

Central Pattern Generators

The concept of a Central Pattern Generator was first proposed by Brown (1911), who suggested that locomotion is produced by neurons that are within the spinal cord. The model proposed by Brown was termed the Half Centre Model, where there is a neuron (or group of neurons) that produce activity for the extensor muscles involved in locomotion and a similar neuron (or group) that produces the neural activity for the flexor muscles. Brown further suggested that a mutual inhibition between these flexor and extensor half centres would permit activity that allows for only one of these muscle groups to be active at a time, thus allowing a normal walking pattern to occur (Brown 1914). The production of an alternating neural output within a half centre occurs through mutual inhibition of the two neurons, such that only one

neuron can be active at a time and a fatigue property known as the adaptation effect, which prevents a neuron from firing indefinitely. One neuron, the flexor neuron for example, will begin in an active state, providing excitation to the flexor muscles and inhibiting the extensor half centre. When the flexor neuron stops firing due to the adaptation effect, the extensor neuron is allowed to begin firing, exciting the extensor motor neurons and inhibiting the flexor half centre. For this process to continue both half-centres need to be excited from an external source and the inhibitory connection between the two neurons must be sufficiently strong enough to inhibit the other half-centre (Brown 1914). The theories put forward by Brown were in contrast to the work of Sherrington who suggested that the walking pattern was the result of a chain of reflexes, where having a limb in a certain position would lead to a reflex that would lead to the next phase of walking (Sherrington 1910).

The debate whether walking was controlled by reflexes, or through CPGs, continued for several decades (Clarac 2008). Forssberg et al performed studies that were similar to the experiments that were initially performed by Brown and noted that a basic alternating walking pattern could be observed in cats following complete spinal cord transection, however there were deficits in the ability to produce adequate forward propulsion, body weight support and in balance control (Forssberg et al. 1980a). Some proponents of the reflexive control of locomotion suggested that since stretch reflexes are processed in the spinal cord, that the work of Forssberg did not conclusively prove that CPGs were involved in the control of locomotion. A series of follow-up experiments by several groups led to an increase in support for the idea of locomotor CPGs. Firstly, work by Grillner et al (1984) showed that a walking pattern could still be achieved when all sensory information was prevented from communicating with the spinal cord by means of a dorsal root transection. Immobilized preparations have also been used to demonstrate that

sensory information is not required to produce an alternating flexor-extensor motor neuron firing pattern ie. (McCrea 1996). In these animal preparations a drug that is an antagonist for acetylcholine is administered, thereby preventing muscle contraction from occurring and thus movement is not possible, which would eliminate any sensory information that would occur due to movement. The activity of the CPG in these preparations is usually elicited by applying a tonic stimulus to the mesencephalic locomotor region (MLR), in the midbrain. This tonic stimulus is known to produce alternating motor neuron output through descending connections to the spinal cord (Shik et al. 1966).

The work of Shik, who showed that non-phasic stimulation of the MLR produces alternating motor neuron output provides compelling evidence for the existence of CPGs within the spinal cord and provides insight into how such circuits may be used in the control of locomotion. Shik found that setting the magnitude of the tonic stimulation to the MLR could control the frequency (rate) of the motor neuron output. The magnitude of the tonic stimulation applied to the MLR was found to control the speed of locomotion of the cat, based on the increase in frequency and amplitude of the motor neurons outputs. Increasing the level of the tonic stimulation to the MLR was found to increase the speed of the locomotion of the cat, even changing the form of locomotion (ie. Walk → Trot → Gallop). The work of Shik has important implications for the neural control of locomotion. Firstly, it shows that the spinal cord is capable of producing an organized and patterned output, while receiving only a simple tonic input signal. This indicates that the circuitry responsible for the final production of walking patterns is likely located within the spinal cord. Secondly, the fact that the output of the CPG can be modified based on an external signal shows the importance of other neural substrates in the control of locomotion. A number of higher brain centres have projections onto the MLR, which would help

determine the frequency and amplitude of the CPG output, and thus the speed and mode of locomotion (Patla 1996).

Central pattern generators have often been described as simple circuits that help organize the basic timing and rhythm of the walking pattern, however there is a great deal of evidence that the output from CPG circuits also contain a great deal of information regarding the magnitude and shaping of the muscle activation patterns (Grillner and Zangger 1979). It has been shown that the complexity of the CPG output is greater when sensory feedback is acting on the CPG (Grillner and Zangger 1984), however when there are no sensory signals acting on the CPG the motor neuron output is still quite complex, in terms of timing and shaping.

Two approaches have been previously used to model the output of CPG circuits; the first is to use a simple oscillator model, such as a Van der Pol oscillator (Dutra et al. 2003), or the more popular Matsuoka model (Matsuoka 1985). The second approach used to model CPG output employs a more complex representation that may attempt to include mechanisms of controlling the magnitude and shaping of the CPG output. These approaches may include the use of artificial neural networks (ANNs) (Prentice et al. 1995; Prentice et al. 1998), statistical techniques, such as factor analysis (Patla et al. 1985) or complex networks of simulated neurons that use an integrate and fire model (Rybak et al. 2006). One reason for using a simpler oscillator model, rather than a more complex model to simulate CPG output for the control of human is that the full connectivity of neurons within the mammalian CPG is not known. The exact neural circuitry of the CPG has only identified in a few species, such as the lamprey (Grillner et al. 1987). Simpler models are also easier to integrate with other models, such as muscle models, and usually feature uncomplicated methods for controlling the frequency and the amplitude of the CPG model output.

The actual architecture of the mammalian CPG is likely organized into two separate systems, the first controls the timing and basic rhythm of the locomotor pattern, while the other system specifies the activation for the individual muscles required to produce an appropriate walking pattern (McCrea 2001). These features have been included in CPG models such as those by Prentice et al (1995, 1998). There is also more recent evidence that there may be a third level involved in the CPG circuitry which allows for integration of sensory signals with the CPG output (McCrea and Rybak 2008). Some of these features have been included in various models of CPG activity.

While there is some evidence that CPGs are used in the control of human locomotion, it is mainly indirect evidence that comes from patients who have suffered spinal cord injuries (Calancie et al. 1994; Dimitrijevic et al. 1998) or from infants, who have not yet developed independent walking patterns (Thelen 1979; Yang et al. 1998a). It is sometimes thought that the CPG does not play a large role in the control of human walking, and that human walking is mainly controlled through cortical processing, due to the deficits that are observed when the brain is injured traumatically, or via stroke. However it has also been noted that there is a large degree of similarity in the neural control systems across a variety of mammalian species, and there is no reason to believe that the human locomotor control system would not include the use of CPG circuits (Patla 1996). The exact role that the CPG plays in the control of human locomotion still remains somewhat unknown, but it is clear that complicated spinal circuits play a role in the control of locomotion (Duysens et al. 2002; MacKay-Lyons 2002).

Contribution of Somatosensory Input to the Control of Locomotion

While it has been observed that relatively normal locomotion can be observed in the absence of afferent feedback (Grillner and Zangger 1979), it has also been noted that this

walking pattern is not the same as the walking pattern that occurs with a full compliment of sensory information (Grillner and Zangger 1984). There have been numerous studies that have analyzed the role of sensory feedback on the control of locomotion, (for a review see (Rossignol et al. 2006)). These studies have ranged from the modulation of reflexes during normal locomotion (Capaday and Stein 1986) to analyzing the gait of a patient whose sensory nerve fibres have been completely abolished (Lajoie et al. 1996). Despite the large number of studies that have been performed on the role of sensory information in the control of human locomotion, there are no studies where the sensory signals have been systematically manipulated, due to restrictions in research methods. For example, it is not possible to test what would happen to the walking pattern if all sensory feedback from muscle spindle pathways were suddenly removed.

The somatosensory system takes information from a variety of sensors and provides the CNS with information regarding the position and motion of the body relative to itself and relative to the environment. Information from the somatosensory system originates from muscle spindles, which sense the magnitude and velocity of stretching of muscles, Golgi tendon organs that sense muscle loading, joint receptors which sense the position and movement of the joint, and cutaneous receptors that sense contact with the external environment. This section will focus on describing the mechanisms that are used to encode sensory information within the CNS and how these systems contribute to the control of locomotion.

Role of Muscle Spindles

Muscle spindles are small complex structures that are in a parallel with muscle fibres (extrafusal fibres) and have tendinous attachments within the structure of the muscle. In the middle of the tendinous attachments there are a contractile muscle fibres (intrafusal fibre), which are innervated by γ-motor neurons. The role of the γ-motor neuron is to maintain tension in the

intrafusal fibre during muscle contraction and is co-activated with the α-motor neuron, which innervates the extrafusal fibre. The intrafusal fibres are wrapped by sensory endings of IA afferent neurons, which are sensitive to stretching of the intrafusal fibre. Additionally there are different types of intrafusal fibres that exist in each muscle spindle with different sensitivities to changes in length or velocity, these include dynamic nuclear bag fibres which are primarily sensitive to changes in length, static nuclear bag fibres which are sensitive to changes in both length and velocity, and nuclear chain which are primarily sensitive to changes in length. All of these intrafusal fibres trigger type IA and type II sensory afferents, with the exception of dynamic nuclear bag fibres which only trigger type IA sensory afferents (Pearson and Gordon 2000).

When a muscle is stretched, there will be an increase in both IA and II afferent activity, which has been shown to code the velocity and the magnitude of the stretch (Pearson and Gordon 2000). The signals from the IA afferents have synapses directly onto the α-motor neuron of the muscle where the spindle signal originates. Thus, the stretch of a muscle will lead to a contraction of the muscle in question; this is the typical monosynaptic stretch reflex. The role of the stretch reflex is to correct any unexpected stretches that occur during motion and can help stabilize the body in event of a perturbation. The gain of this reflex can be modulated by neurons from a number of other pathways, a good example of this is that the stretch reflex is modulated during the gait cycle to have the highest impact when the muscle is expected to be active during the gait cycle (Capaday and Stein 1986).

Role of Golgi Tendon Organs during Locomotion

Golgi tendon organs (GTOs) are complex structures that are located at the musculotendinous junction and are in series with the extrafusal muscle fibres. The capsule of the

GTO contains a web of collagen fibres that pinch the endings of IB afferents when the muscle is loaded. Thus, the GTOs signal when a muscle is generating force. Information from these receptors has been shown to be important for timing the stance to swing transition in gait (Pearson 1995; Pearson 2004), regulating the extensor tone during the stance phase (Hiebert and Pearson 1999) and for responding to unexpected perturbations to the limb, such tripping over an object (Prochazka et al. 2002). The neural pathways involved in some of these responses will be discussed in upcoming sections.

Role of Cutaneous Inputs

Another source of important sensory information during locomotion is from cutaneous receptors, which are distributed throughout the skin, but have a high distribution within the sole of the foot (Perry et al. 2001). An early observation was that 'almost' normal locomotion was possible after removal of cutaneous receptors in the cat (Forssberg et al. 1977), however when the foot pads of the cat were deinnervated, it was found that the cats were unable walk in situations where precision foot placement demands were required, such as walking across the rungs of a ladder (Rossignol et al. 2006). Therefore it was concluded that these receptors play an important role in the control of foot placement during locomotion, in cats. This has also been shown in humans by reducing sensation of the plantar surface of the foot, by submersing the feet in ice-water, and having the participants terminate their walking. It was found that reducing this sensation led to more variable foot placement, and a lower level of control of the limb during stance phase which was evident through an increased loading rate in the ground reaction force profile (Perry et al. 2001).

Role of Joint Receptors

The final source of somatosensory information that is available to the CNS to help

control locomotion originates from joint receptors. These receptors consist of free nerve endings that innervate the joint capsules and ligaments of major synovial joints and are thought to code the position and velocity of the joint, with a particular increase in activity at the end-range of the joints (Proske and Gandevia 2009). The exact role of these receptors in the control of locomotion remains to be determined, as it is difficult to isolate and measure the activity of these afferents due to their small size. One method to investigate the contribution of these receptors is to analyze the motion of patients whose joint receptors have been completely destroyed, usually by means of joint replacement ie. (Byrne et al. 2002b), however, there is also a significant change in the mechanical properties of the joint that accompany the destruction of the joint receptors during surgery. To attempt to reduce the influence of the joint receptors without altering the mechanical properties of the joint, some researchers have attempted to inject the joint with a local anesthetic so that the signals from the joint receptors are eliminated, although this approach has only been used sparingly (Gage 2003).

Locomotor Control Mechanisms Reliant on Somatosensory Information

In his review, Rossignol (2006) highlighted four main roles for afferent information from somatosensory sources on the control of locomotion. These are: 1) blocking or triggering the locomotor pattern, 2) controlling the timing the locomotor pattern, 3) regulating the amplitude of the locomotor pattern and 4) correcting unexpected muscle stretches during walking. These functions of the sensory signals will be analyzed in the following sections.

Blocking or Triggering the Locomotor Pattern

Walking may only occur if the lower limbs are in an appropriate position to support the weight of the upper body. Early work, by Sherrington (1910), found that extending the hip joint

was sufficient stimulus to elicit the walking pattern in spinalized cats, which he argued was part of the fundamental walking pattern and an integral part of his reflex chaining theory of locomotor control. It has also been found that extension of the hip joint to the position that would normally occur at the end of the stance phase will trigger the walking pattern in human patients with spinal cord injuries, provided the contralateral limb is in a position to accept weight (Dietz 2003). Flexing the hip to a position beyond that experienced during the walking cycle has been found to prolong the extensor phase of the contralateral limb, while sustaining the flexor phase of the ipsilateral limb; this has been observed in decerebate cats (Conway et al. 1987), in humans who have experienced spinal cord injury (Pepin et al. 2003) and during treadmill stepping in infants (Yang et al. 1998b). It has also been observed that in MLR induced locomotion, in the cat, that passive movement of the hip joint to positions outside the normal range of motion observed during locomotion will result in the abolishment of the walking pattern, and moving the hip back into a position appropriate for walking will lead to the continuation of the walking pattern (Orlovsky and Feldman 1972). These experiments provide strong evidence that muscle afferents from the hip joint can play a powerful role in triggering or blocking the walking pattern while also ensuring coordination between the left and right limbs, so that adequate body support can be maintained at all times. These mechanisms have not been included in any neuromechanical model to date, as the positions of the limbs are usually set to be in a position that will allow walking to occur. Some of these sensory mechanisms will be examined in study 4 of this thesis.

Effects on Timing of the Locomotor Pattern

The next major role of muscle afferents during the control of locomotion is to maintain the timing of the locomotor pattern. The main way that this occurs in vivo is by controlling when

transitions between the stance and swing phase occur (Pearson 1995). In order for the transition from stance to swing to occur, the limbs must be in a suitable position, with the contra-lateral limb being able to support the weight of the body. Conceptual neural pathways involved in controlling this timing have been proposed by Pearson and are shown in Figure 2.1, these pathways describe how sensory information from the limb can be used to trigger phase transitions in conjunction with a half centre CPG model, as first proposed by Brown (1914). During late stance in human walking, there will be an unloading of the ankle extensors, which naturally occurs as the contra-lateral limb accepts weight and as the force in the ankle extensors begin to decrease due to the force-length relationship of the muscle. This decrease in loading is detected by Golgi tendon organs (GTOs; IB Pathways) of the ankle extensors and results in a removal of inhibition on the flexor half centre of the CPG and allows the flexor muscles of the limb to become active. In order to complete the transition between stance and swing, the activity in the extensor half-centre of the CPG must be inhibited. This is accomplished through the detection of stretch in the hip flexor muscles. Afferent information from IA pathways will then inhibit the extensor half-centre and allow the transition between the stance phase and swing phase (Pearson 1995). This pathway for afferent regulation of stance duration allows spinalized cats to adapt their walking speed to different rates prescribed by motorized treadmills (Grillner and Zangger 1979; Forssberg et al. 1980b). This phenomenon has also been observed in infant stepping (Yang et al. 1998a) and in adult humans with spinal cord injuries (Pepin et al. 2003). Therefore it is apparent that this pathway is present in humans, but the degree that this route is used for human locomotion remains in question.

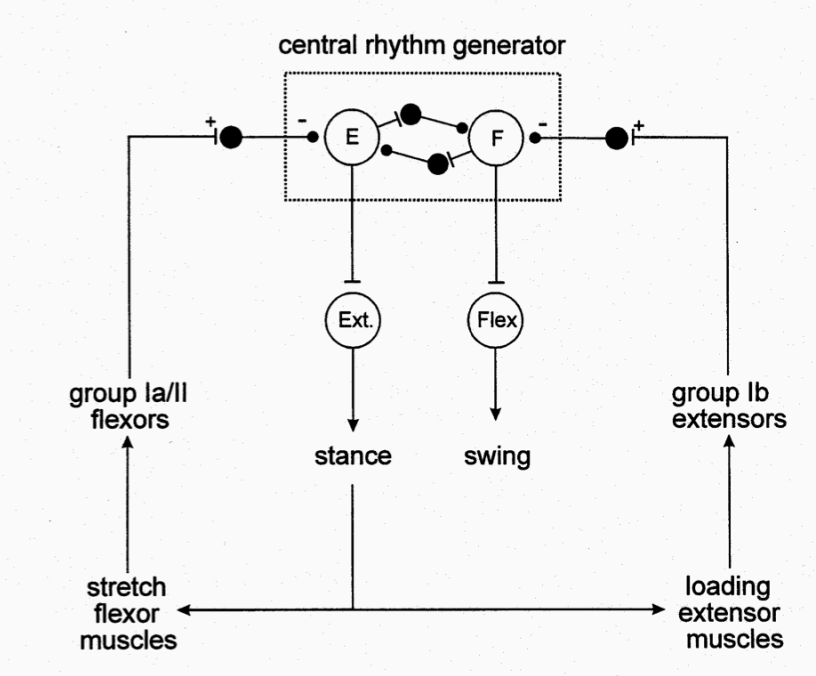

Figure 2.1: Afferent regulation of stance-to-swing transition. Adapted from Pearson (1995).

This mechanism for the control of stance duration is so powerful that it can allow for walking to take place in spinalized cats on a split-belt treadmill with the belts moving at different speeds (Forssberg et al. 1980b). Humans are also able to walk on split-belt treadmills although the difference in speeds between the two belts has to be fairly small (Prokop et al. 1995; Jensen et al. 1998). These experiments have led scientists to propose that there are individual CPG circuits for controlling each limb within the spinal-cord (Patla et al. 1985). Since this modulation of stance duration is observed in infant stepping, before the complete development of the cortico-spinal tract, it would appear that this pathway is innate, and of high importance for the control of locomotion (Yang et al. 1998a).

The role of this particular circuitry was assessed in a neuromechanical model by Ekeberg & Pearson (2005), and it was determined that this pathway for regulating the duration of the stance phase was crucial for ensuring a stable locomotor pattern. A similar rule was used to

control the timing of the stance to swing transition by Yakovenko et al (2004), it was once again found to be critical for producing a stable walking pattern. Therefore this mechanism should be included in the neural control model for this thesis. It is hypothesized that this particular pathway will help ensure a stable walking pattern by the model.

Controlling the magnitude of the locomotor pattern / load compensation

The third role of muscle afferent information during the control of walking is to help modulate the magnitude of muscle activation during walking. This can be observed by unloading the weight of a person while walking through the use of a harness (Dietz and Duysens 2000). By unloading the body weight of the subject, a decrease in the muscle activation magnitude of up to 50% may be observed. Another approach that has been used to study the role of afferent information for the control of the magnitude of the walking pattern has been to use "foot-in-hole" experiments, where a cat experiences as sudden unloading of the limb shortly after making contact with the ground, usually due to a trap-door apparatus being used. This sudden unloading of the limb results in a decreased level of activation in the extensors of the limb (Prochazka et al. 2002). Therefore it is apparent that the loading of the extensors, particularly at the ankle, joint plays an important role in controlling the magnitude of the extensor activation during walking.

A conceptual pathway for the mechanism of the control the magnitude of extensor EMG was proposed by Pearson (1995) and is shown in Figure 2.2. This figure shows that loading of the extensor muscles, as it normally occurs during stance phase, will have an excitatory effect on an interneuron that synapses with the motor neuron pool for the extensor muscles and an additional excitatory connection to the extensor half centre of the CPG. This information would be detected by GTOs within the extensor muscles, and transmitted through these pathways by IB muscle afferents. These connections provide positive feedback in response to loading the limb by

encouraging more extension to occur. The interneurons in the pathways allow other connections, such as those from higher centres in the CNS to modulate the influence of this positive feedback (Pearson 1995).

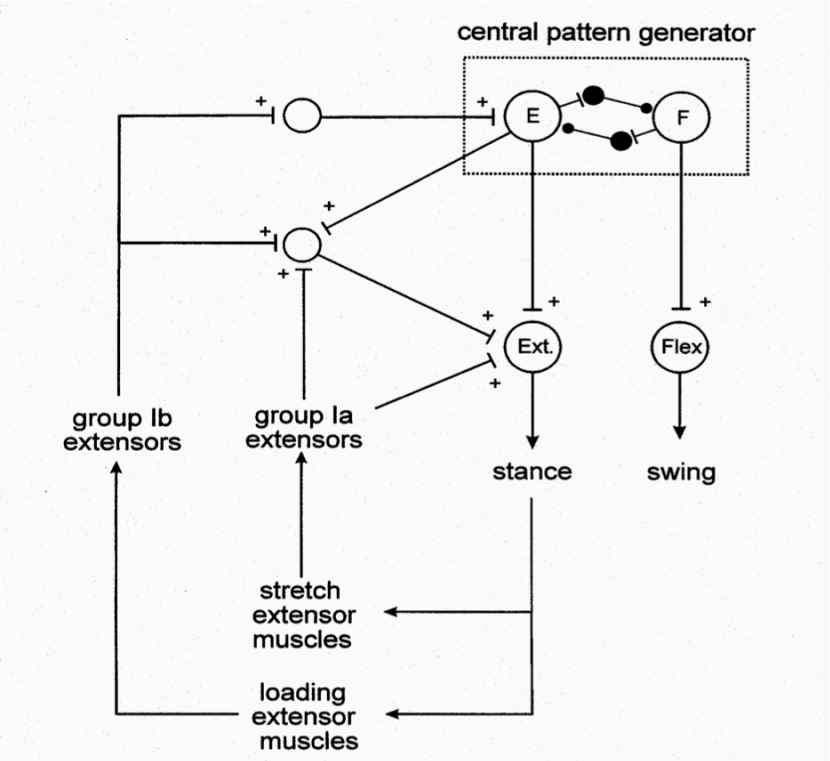

Figure 2.2: Conceptual pathways for afferent regulation of extensor magnitude during stance phase. Adapted from Pearson (1995).

In the conceptual pathway that was proposed by Pearson, there is also a negative feedback loop, which responds to yielding or unloading of the limb, which would result in stretching of the extensor muscles. This would be detected by muscle spindles, and results in excitation of the motor neuron of the muscle where the stretch was detected through a mono-synaptic stretch reflex. According to Pearson, the IA muscle afferents would also have an excitatory connection to the same interneuron that was between the IB muscle afferent and the motor neuron for the extensors. Thus, stretching of the extensor muscle during stance phase, due to unloading, such as the unloading that occurs in the foot-in-hole experiment should result in an

increased excitation of the extensor muscle of the limb, which has been observed to occur approximately 40-60ms after unloading of the limb (Prochazka et al. 2002).

One criticism of the conceptual pathway proposed by Pearson (1995) is that during fast walking, or running, there is insufficient time to respond to any unloading of the limb that occurs during stance phase using sensory information alone (Rossignol et al. 2006). It has also been proposed that the magnitude of the feedback provided by these pathways may be insufficient to adjust to changes in loading (Prochazka et al. 2002). These hypotheses were tested in a neuromechanical model by Yakovenko et al (2004). An interesting result from the simulations by Yakovenko et al was that the contribution of sensory information to the control of muscle activation magnitude decreased as the neural drive from the CPG was increased; this was attributed to the increased muscle stiffness that occurred with higher levels of central drive. Therefore it has been proposed that at higher walking speeds, or running, there is an increased neural drive from higher centres in the CNS, which results in higher joint stiffness, and therefore a decreased reliance on information from muscle afferents for the compensating for increased limb loading. However at normal walking speeds, the information from muscle afferents appears to be important for controlling the magnitude of extensor activity during the stance phase of walking (Rossignol et al. 2006).

Correcting Unexpected Stretches During Locomotion

Knowing the neural pathways involved in the basic mono-synaptic stretch reflex, this particular role of muscle afferents during locomotion seems to be the most obvious. Sensory information from muscle afferents will allow the locomotor control system to adapt do different environmental conditions, or more dramatic changes such as changes in the mechanical properties of the musculoskeletal system (Noble and Prentice 2006). Sensory information from

muscle afferents is also critical to make an appropriate response following a slip or a trip (Marigold et al. 2003), and failing to make an appropriate response based on this sensory information may increase the potential for a fall to occur (Marigold and Eng 2006). The initial response following a trip or a perturbation to the walking pattern is generated by mono-synaptic stretch reflexes, then followed by longer latency responses that include the influence of higher centres in the CNS (Marigold and Patla 2002). There is strong evidence that the magnitude of stretch reflexes are strongly modulated depending on the phase of the locomotor cycle where the perturbation takes place (Capaday and Stein 1986). For example, the magnitude of the Soleus H-reflex, which is an electrical analogue of the stretch reflex, has its highest magnitude during the stance phase, after toe-off there is a dramatic decrease in the magnitude of the reflex. Thus the stretch reflex is modulated to ensure that a muscle stretch cannot prevent the important contraction of the soleus to provide propulsion during late stance phase (Capaday and Stein 1986). It is thought that this modulation of the stretch reflex throughout the gait cycle occurs through pre-synaptic inhibition of the IA afferent (Edamura et al. 1991).

Other Pathways Involving Muscle Afferents

The four roles of sensory information from muscle afferents just discussed are by no means a complete description of all the potential roles of sensory information during walking, as there have been hundreds of studies published on sensory contributions to the control of locomotion. One example of an additional role of afferent information originating from muscle spindles have been found by analyzing recordings of neurons in the Dorsal-Spinal-Cererbellar Tract (DSCT) (Bosco and Poppele 1997). This work showed that this tract utilizes population coding to code for the position and movement of the limb axis. It is thought that the cerebellum can use this information to compare the expected limb position and movement to the actual

position, and make corrections through higher brain centres and brainstem nuclei (Morton and Bastian 2006).

Contribution of Other Sensory Systems to the Control of Locomotion

In addition to the somatosensory system, the control of locomotion is also dependant on sensory signals from the visual and vestibular system. Some of the functions of these sensory systems will be briefly examined in this section. The visual system has two primary roles in the control of locomotion. Firstly, the visual system is normally the only sensory system that provides information about the location of objects in the external environment (exteroceptive information), thus visual information is obviously the primary sensory system that provides information that is used for navigation and guidance during walking. This information is also used to navigate around obstacles and through complex terrains and allows the other centres in the CNS to make appropriate adjustments to the locomotor pattern. The second function of the visual information is to provide information about the position and motion of the body with respect to the environment (exproprioceptive information) (Patla 1996). The exproprioceptive information is critical for judging our motion within the environment (optic flow) and for helping judge the orientation of the body within the environment (ie. Maintaining an upright trunk posture) (Marigold 2008).

Another source of exproprioceptive information originates from the vestibular system. The vestibular apparatus is located in the inner ear and is responsible for detecting angular and linear accelerations of the head. The first role of the vestibular system is to help stabilize the gaze during walking (Pozzo et al. 1990) and maintain an upright trunk posture in the frontal plane (Pozzo et al. 1995). Vestibular information has also been shown to have increased importance for maintaining a straight path during walking when visual information is not available (Fitzpatrick

et al. 1999). Like somatosensory and visual information, vestibular information is modulated throughout the gait cycle, with the magnitude of the response from the vestibular system having a different response depending on the timing within the gait cycle, with the influence from the vestibular apparatus being greatest during the double support phase (Bent et al. 2004).

Contribution of other Neural Systems

Although it has been observed in a number of animal studies that fairly normal walking patterns can be achieved with only contributions of spinal pattern generators and sensory information, there are certain deficits that still exist in the walking patterns in these preparations, particularly in the control of balance and navigating more complex terrains (Patla 1996). This section will examine the contributions of brainstem nuclei, the cerebellum and cortical structures to the neural control of locomotion. As was shown in Figure 1.1, a number of these neural pathways will act by modifying the activity of the neurons in the CPG, meaning that these pathways from higher brain centres have projections onto the spinal cord and are able to influence the final motor neuron output.

Brainstem Structures

The first role of the structures within the brainstem is to set the appropriate postural tone so that walking can take place. Work by Mori (1987) has shown that the postural tone in the extensor muscles can be increased though neuronal activity in the ventral tegmental field (VTF) and similarly decreased by stimulating neural activity in the dorsal tegmental field (DTF). For example, increasing the firing rate of the VTF neurons will cause a cat to go from a lying posture to a standing posture. Mori also found that stimulation of the MLR would only induce locomotion if there were an appropriate balance activity between the VTF and the DTF, or an appropriate level of postural tone. If there is not an appropriate level of postural tone then

stimulation of the MLR will not generate motor neuron outputs that would generate a locomotor pattern.

An appropriate level of postural tone must be maintained throughout the entire locomotor cycle, not just during the initiation of gait. As discussed in the previous section, sensory information from muscle receptors helps ensure that the magnitude of output from the CPG is at an appropriate level during walking. Sometimes during locomotion it is necessary to make online adjustments to the locomotor patterns to accommodate or avoid obstacles during walking. Adjustments to the walking pattern are potentially destabilizing and may result in loss of support or in a loss of balance if the adjustment is not accompanied by an increase in activity of postural muscles. It has been widely reported that the motor commands for voluntary movements are accompanied by a feedforward command to stabilize the body, (for review see (Massion et al. 2004)). During obstacle avoidance some reticulo-spinal neurons (RSNs) in the Pontomedullary Reticular Formation (PMRF) appear to provide a general signal for the timing and magnitude of support that is required (Prentice and Drew 2001). This appears to generate an increased extensor tone in the support limb, while the contra-lateral limb is stepping over the obstacle. It is thought that this method of control is similar to how postural control is maintained while executing reaching movements. It is also believed that RSNs act on interneurons between the CPG and the motor neurons for the limb, which can therefore enhance the firing rate in the extensor motor neuron, and hence the extensor tone in the limb. Previous work investigating the influence of the reticular formation has found that the stimulation of RSNs leads to a phasic response where flexor or extensor neurons will increase in activity depending on the phase when the stimulation is delivered and is capable of altering the timing of the gait cycle (Drew and Rossignol 1984). Cats who have lesions to PMRF neurons show great difficulty walking, particularly in

maintaining an appropriate level of postural tone, illustrating the importance of these neurons to the control of locomotion (Rossignol et al. 2004).

Another pathway that acts on the CPG and originates in the brainstem is the rubrospinal pathway. This pathway originates in the red nucleus within the brainstem and has projections to neurons within the spinal cord. In cats, it has been observed that this pathway is involved in coordinating the action of the various muscles within a single limb, particularly during voluntary modifications to the locomotor pattern, such as stepping over an obstacle (Lavoie and Drew 2002). However, in humans the relative number of neurons in the rubrospinal pathways is quite small relative to the number of neurons in the cat, therefore the relative contribution of this pathway to the control of human locomotion is thought to be rather small. However the contributions of this pathway to the control of human walking are not very well understood (Nathan and Smith 1982; Massion 1988; ten Donkelaar 1988).

As previously discussed, the vestibular system has a large influence on the control of the walking pattern. The vestibular apparatus within the inner ear has projections onto the vestibular nuclei within the brainstem, which then in turn have projections onto neurons within the spinal cord, which help influence the walking pattern. The final major pathway that originates within the brainstem and helps influence the control of locomotion is the tectospinal tract. This pathway originates in the Superior Colliculus and has projections to neurons within the spinal cord. This pathway helps control orientating to objects in the external environment and steering through unique projections to each limb (Patla 1996).

Role of the Cerebellum

The cerebellum plays a very important role in the control of human locomotion. Firstly, the cerebellum is important in controlling the magnitude of the vestibulo-ocular reflex

(VOR), which is important for stabilizing the visual field during locomotion (Goldberg 2001). Next, the cerebellum receives input from kinesthetic sources both the dorsal and ventral spino-cerebellar tracts (Patla 1996), both of these pathways are ascending pathways that provide information from muscle afferents to higher centres within the CNS. The ventral spino-cerebellar tract carries information from the muscle spindles which is compared to signals from the motor areas of the brain and are compared within the cerebellum, this comparator function is critical for motor learning and for error correction (Ghez and Thach 2001). Signals from the dorsal spino-cerebellar tract have been found to use population coding to code information regarding the position and movement of the limb axis (Bosco and Poppele 1997). This pathway helps provide adaptability to the walking pattern, providing updated information on the locomotor pattern to higher brain centres (Morton and Bastian 2006). Patients who have suffered damage to the cerebellum often demonstrate a decreased level of coordination, or an ataxic gait (Palliyath et al. 1998; Ilg et al. 2007) and have difficulty adapting to novel mechanical conditions, such as adding mass to the limbs (Ilg et al. 2008).

Role of Higher Brain Centres

Higher brain centres also play a crucial role in adapting the walking pattern to navigate through complex environments. This was shown in experiments by Drew (1988) , where an increase in activity within the primary motor cortex of the cat was observed as the flexion of the limb was increased to step over an obstacle in the walking path. These commands from higher centres would have to be integrated with the walking pattern that is being generated by the CPG, so that forward progression can be maintained as the cat is stepping over the obstacle. These modifications to the walking pattern to step over an obstacle in the path have been termed voluntary gait modifications, since they require a voluntary adjustment to be made to the walking

pattern once the obstacle is detected by the visual system. The main pathway involved in these voluntary gait modifications is the cortico-spinal tract (CST), or pyramidal tract. It has been shown in cats that neurons in this pathway increase their activity during a voluntary gait modification, such as stepping over an obstacle (Drew 1988). It has also been observed that the increase in activity in these neurons is phase locked with the increased activity of the flexor muscles that is required to step over the obstacle. Therefore, the increased activity in the CST can be thought of as a basic command to increase flexion in the limb during swing phase. More recent evidence indicates that this control signal is not a simple command to increase flexion of the limb, but rather is a complex signal, which appears to encode muscle activity for individual muscles; this was found by analyzing the activity of individual neurons within the motor cortex (Lavoie and Drew 2002). This command signal to increase flexion will have to be integrated with the spinal circuitry to ensure that a stable walking pattern can continue. It has been suggested that descending signals from the CST would be integrated with interneurons within the locomotor circuitry within the spinal cord , this would allow for a flexible control of limb flexion during the swing phase, while allowing the basic locomotor pattern to continue (Drew et al. 2004). Research has also shown that there are collateral pathways from neurons within CST to the reticular formation neurons, which highlights the integration of voluntary movements and changes in posture (Kably and Drew 1998).

The basal ganglia are involved in the control of locomotion, although there are no direct connections from the basal ganglia to any structures that control limb movement. Deficits observed by patients who have Parkinson's disease such as a difficulty initiating movement, freezing and decreased amplitude of movement highlight some of the contributions of the basal ganglia to the control of locomotion (Rogers 1996).

Integration of Neural Systems

In order to achieve successful locomotion a number of neural centres must generate appropriate activity. All of the neural substrates that have been previously discussed must be functioning properly in order to achieve a stable and adaptable locomotor pattern. The interaction between these pathways is critical for ensuring an appropriate locomotor pattern. A figure illustrating the interaction between these various neural substrates was shown in Figure 1.1. The neural pathways involved in the interactions between the sensory systems and the motor systems involved in the control of locomotion were reviewed by Rossignol et al (2006). Most of our knowledge regarding the neural pathways involved in walking either comes from animal work, or from studies of human patients who have suffered damage to a particular neural substrate. The interaction between all of the neural substrates is very difficult to assess with the research methods that are typically used for the study of the neural control of locomotion.

The interaction between the neural systems involved in walking has been studied in two ways. The first method is to systematically alter the outputs of two separate systems and assess the impact on the resulting walking pattern. An example of this was a study by Desphande and Patla (2005), which examined the interaction between the vestibular system and the visual system by systematically altering the vestibular input, through the use of Galvanic Vestibular Stimulation and the optic flow, with the use of prism goggles, and examined resulting effect on the walking direction. Despite the valuable information that can be gained from *in vivo* experiments such as these, the neural pathways involved in these interactions are still difficult to assess and the exact nature of the interaction cannot be determined.

The second method used to study the interactions between various neural systems is to use computational modeling. A review on this technique was recently published by Pearson et al

(2006). This technique involves creating computational models of the neural control systems involved in the control of walking (both motor and sensory) along with a model of the musculoskeletal system. Using these types of computational models it is possible to simulate conditions that cannot be tested *in vivo* or *in vitro*. The main drawback for these types of models is that we cannot model either the neural control systems or the musculoskeletal systems completely accurately. These types of models have been valuable to gain insight into the interaction between the neural control models and the mechanical systems. A common finding of a number of these simulations is that the neural and mechanical systems involved in locomotion are very much entwined with each other (Taga et al. 1991) and that the frequency of the CPG often becomes entrained to the natural frequency of the limb movement, highlighting the importance of sensory information in the control of locomotion.

From a control perspective, animal locomotion is a result of a combination of feedforward control, as provided by the CPG, and feedback control, as provided by the sensory pathways that will act on the locomotor circuits. This combination is thought to be optimal as the advantages of both control schemes can result in less errors during the control of rhythmic movements (Kuo 2002). The use of a purely feedforward control system is not adequate for the control of walking, primarily because the system would be unable to respond to any perturbations that would occur during walking. A purely feedback system would also be inadequate because the system would be reliant on receiving perfect information regarding the position and movement of the limbs, which is not possible due to errors in signal transmission and processing. Therefore an ideal locomotor control system would take advantage of both feedforward and feedback mechanisms in order to minimize movement errors.

Comparing Locomotion to Other Rhythmic Limb Movements

The neural control of locomotion is thought to be similar to a number of other rhythmic limb movements, such as cycling or simply swinging the lower limb in humans, or scratching or the paw-shake response in animals (Rossignol 1996). All of these types of motions are thought to be controlled by CPGs and modulated by sensory pathways (Zehr 2005). A common feature among many rhythmic limb movements, including walking, is entrainment of neural signals to the natural frequency of the limb, meaning that the CPG will use sensory information to match its output frequency to the resonant frequency of the limb (Taga et al. 1991). This feature of rhythmic limb movements allows for maximal displacement, or movement amplitude, for the amount of effort used, resulting in a metabolically and mechanically efficient movement pattern (Doke et al. 2005). The interaction between the CPG and the sensory signals that are involved in entrainment between the CPG and the limb movement will be investigated in Chapter 4.

Biomechanics of Human Locomotion

Just as there is a long history of research on the neural control of locomotion, there is an equally long history examining the biomechanics of human locomotion. Both the kinematics, kinetics and muscle activation patterns of human walking have been well documented (For review see Winter (1991)). The joint kinematics of human walking show a high degree of consistency and repeatability both within and between individuals and have been well adapted to meet a number of the demands of walking. Winter (1991) highlighted several key objectives for locomotor control that must be achieved biomechanically. These are highlighted below:

1) Maintenance of support of the upper body.
2) Maintenance of an upright posture and balance of the upper body.

3) Control of foot trajectory to achieve ground clearance and a gentle heel contact (avoiding slips and trips).
4) Generation of mechanical energy to maintain an appropriate forward velocity and have the ability to increase forward walking velocity, if required.
5) The ability to absorb mechanical energy for shock absorption or to decrease the forward walking velocity.

Winter (1991)

All of the above listed objectives must be accomplished in order to successfully walk. In addition to these objectives, the walking pattern must be adaptable so that the individual may successfully navigate unique environment. The chosen walking pattern should also be energetically efficient so that the individuals can walk for long periods of time without becoming fatigued. This section will briefly examine the biomechanical requirements of human locomotion, with a focus on which biomechanical aspects should be included in neuromechanical simulations of human locomotion.

Generation of Upper Body Support

The neural control mechanisms involved in generating support for the upper body have already been examined in this chapter; this section will focus on the mechanical requirements of supporting the upper body during walking. The vertical motion of the body's centre of mass (COM) has been well documented during walking (Iida and Yamamuro 1987; Winter 1991). This pattern consists of a cyclical pattern at twice the stride frequency being used during walking. The typical "double-hump" vertical ground reaction force profile that is observed during normal walking is responsible for generating this pattern, where the first positive peak corresponds to the upward acceleration of the COM the valley between the two peaks

corresponds to downward acceleration of the COM and the second peak corresponds to another upward acceleration of the COM (Winter 1991).

Supporting the upper body during locomotion must be accomplished through a combined net extensor moment of all of the major joints of the lower limb (hip, knee and ankle). Winter (1980) found that despite large amounts of variability in the joint moments produced over the gait cycle by the hip and knee joints, that the sum of these two moments produced a moment with substantially less variability, possibly indicating some neural redundancy that occurs in the control of these joints (Winter 1995b). When this combined moment is summed with the moment from the ankle joint, which is very consistent from stride to stride, the result is a time-series curve that closely resembles the shape of the vertical ground reaction force, showing a robust synergy of the musculature of the lower limb to help achieve support of the upper body (Winter 1980). This synergy between the hip and the knee joints is so robust, that when a correlation is carried out between the instantaneous moments observed at the hip and the knee joint over the stance phase that there is a 1:1 trade-off in the moments, showing a strong negative correlation between these values (Winter 1995b).

Control of Balance During Walking: Sagittal and Frontal Plane

Humans are unique in that we are able to primarily use a bipedal gait. While this is evolutionary useful in a number of ways, it also is inherently unstable. Therefore, the locomotor control system must have a robust balance control system. A number of studies have been carried out to better understand the control of balance during human locomotion (For reviews see: Misiaszek (2006) or Winter (1995a)), however only the basic concepts will be covered here. In basic terms, if the body's centre of gravity (COG)(a downward vector projecting from the body's COM) falls outside of the body's base of support (area surrounding the feet's contact area with

the ground) the body will be unstable and prone to falling. However during gait we are able make quick transitions from one base of support to another and the forward momentum that is inherent with progress in the forward direction helps maintain stability; this concept has been termed dynamic stability (Hof et al. 2005). The control of balance can be divided into two distinct control strategies, reactive control and proactive control. In reactive control, sensory systems are used to detect disruptions to balance and an appropriate motor response is generated by the CNS to recover balance, during walking this recovery strategy usually involves taking a step that will place the base of support in appropriate position to recover balance (Hill 2004). The CNS has been shown to be quite flexible in recovering balance and is able to cope with limitations such as narrow walkways and limited visual information situations.

Proactive control of balance during walking involves using learned knowledge regarding perturbations to make appropriate responses as the perturbation occurs. For example during push-off, a horizontal acceleration will be created in the direction of progression, which will tend to destabilize the upper-body in the forward direction. This destabilizing force is countered by an extensor joint moment at the hip joint to reduce the destabilizing effect of the push-off force (Winter 1991). The net extensor moment generated at the hip joint is time-locked with the destabilizing force, showing that the CNS is using learned information regarding the destabilizing force to generate an appropriate response as the perturbation is occurring (Winter 1991). A similar phenomenon has been observed in the frontal plane during walking to keep the trunk upright during walking (MacKinnon and Winter 1993).

Control of Foot Trajectory during Walking

In order to avoid tripping or slipping during walking the trajectory of the foot must be carefully controlled during the swing phase. It has been shown that during normal walking that

the toe clears the ground by a very small margin (approximately 0.5cm) (Winter 1992). This small level of toe clearance leaves very little room for error or else a trip will occur; therefore it is critical that foot trajectory is well controlled. Heel contact with the ground at the termination of the swing phase also occurs with the same degree of precision. When the heel makes contact with the ground it does so with a very low velocity in both the horizontal and vertical directions (Winter 1992). By making contact with the ground at low velocity the chance of slipping is greatly reduced and any transient force that would occur from making contact with the ground is eliminated.

Although it has been shown that some degree of muscle activation is required to achieve a proper kinematic pattern during swing phase, a great deal of the dynamics involved in the swing phase of walking are determined by the mechanical properties of the lower limb (Whittlesey et al. 2000). It has been shown that the CNS has accurate knowledge regarding the mechanical properties of the lower limb and incorporates these mechanical properties when producing motor patterns during swing phase. The net kinematic pattern observed during swing phase is the result of the interaction of the joint moments produced by muscles and passive moments that are created by the motion of the limb (Zernicke et al. 1991). It has been observed that the CNS takes advantage of these passive forces to simplify the swing motor patterns observed during swing phase in level walking (Zernicke and Smith 1996), during obstacle avoidance (Patla and Prentice 1995) and while recovering from a trip (Eng et al. 1997).

Generation and Absorption of Energy during Human Walking

In order to progress in the forward direction during walking the human body must do work. It has been shown that people must generate approximately 0.375 J/step/kg during walking, this has been shown be consistent across people of various sizes (Browning et al. 2009).

Most (approximately 80%) of the total energy that is generated during the gait cycle is done so by the plantar flexors of the ankle joint during late stance phase (Winter, 1991). This burst of energy generation is generated is the primary source of forward propulsion during walking (Neptune et al. 2004).

Significant absorption of energy also occurs during the gait cycle to help maintain the normal walking pattern. During early stance, the knee extensors absorb a significant amount of energy to prevent the collapse of the lower limb as the weight is transferred to the support limb (Winter 1991). During early-to-mid stance, the ankle plantar flexors also absorb a significant amount of energy to help control the velocity of the upper body's progression (Winter 1991). The swing phase is also controlled by the absorption of energy. During early swing the knee extensors absorb a energy to control the upward velocity of the foot after push off, while the knee extensor absorb energy during late swing to control the velocity of the foot prior to heel-contact (Mills and Barrett 2001).

Despite the amount of energy generated and absorbed over the walking cycle, human walking is very energetically efficient. It has been shown that humans naturally choose to walk at a speed that minimizes the metabolic cost of walking. This allows for walking to occur over long distances without fatigue developing and allows for a great deal of mobility (Saibene and Minetti 2003). This efficiency is the result of allowing the body to interact with the gravitational field in an ideal manner to achieve forward motion.

Modeling the Musculoskeletal System

Various approaches have been used to model the dynamics of the musculoskeletal system. The most common approach is to model the musculoskeletal system as a series of linked rigid bodies (Kingma et al. 1996). This technique allows for the determination of joint

kinematics and kinetics through the application of Newtonian mechanics, but is reliant on a number of assumptions. Firstly, it must be decided on how many segments are appropriate to model the system in question. For some motions, such as quiet standing, it may be appropriate to model the entire body as a single segment and analyze the motion of the body's COM relative to the ground (Winter et al. 1998). However for more dynamic movements, it may be necessary to model the body as a large number of linked segments. For analyzing kinematics and kinetics of human locomotion, studies have used anywhere from a single segment (Doke et al. 2005), to upwards of 13 segments (Anderson and Pandy 2001) depending on the level of analysis that is necessary. For example, many early studies examining the control of human balance and walking lumped the entire upper body into a single segment, known as the head, arms and trunk (HAT) segment (Winter 1991) , doing this however neglects the large amount of motion within that is possible within these segments. However, if the goal of the study at hand is to analyze the motion within the trunk, then a more detailed model is needed. For example the goal of a study by Callaghan et al was to analyze the kinematics and kinetics of the low back during walking, therefore the pelvis and the remainder of the to trunk was modeled separately (Callaghan et al. 1999).

In order to determine the joint kinetics using a linked segment model, it is important to have accurate knowledge of the anthropometrics of the subject being modeled. Important anthropometric information includes the mass of the individual segments, the location of the centre of mass for each segment and the moment of inertia of the segment about the segment centre of mass or an end of the segment. Usually this information comes from studies of the mechanical properties of cadavers (Dempster 1955). The main limitation with the information provided by Dempster is that the original sample is a small group of elderly men; this has led

some researchers to look into alternative methods to determine the anthropometrics of the individual subjects. Some approaches used to gain subject specific anthropometric information are regression equations (Zatsiorsky 2002) or individual scanning using dual X-ray absorptiometry (DEXA) (Durkin et al. 2002).

Forward Dynamics

Most of the work that has been previously discussed uses the process of inverse dynamics to make inferences on the control of human locomotion. Inverse dynamics is the process of determining joint kinetics from kinematic information, anthropometric information and information regarding external forces through the application of Newtonian mechanics. The process of inverse dynamics has been particularly useful for helping to determine some of the neural control mechanisms involved in the control of walking (Winter 1995b). The opposite of the process of inverse dynamics is known as forward dynamics and involves integration of the equations of motion of a system to determine the kinematics of the system (and possibly forces applied to the external environment by the system) from a set of applied forces or moments of force (Winter 2004). The process of forward dynamics is considerably more complex than inverse dynamics. This section will examine some of the issues involved in completing a forward dynamics analysis of human motion.

Just as in inverse dynamics, the anthropometric properties of the system being modeled must be known and similar procedures are often used to determine the information. The next step in a forward dynamics analysis is to determine the equations of motion of the system. The equations of motion for a single rigid body are quite easy to determine analytically, however for more complex systems with multiple segments it is necessary to use alternate techniques to determine the equations of motion for the system. Without going into detail, Lagrangian

mechanics are most commonly used to determine the equations of motion when the details of the system are known (Winter 2004). A more common approach is to use a computer software package such SD/FAST (PTC Inc, Needham MA) or DynaFlex Pro (Maplesoft Inc, Waterloo ON). These software packages allow the user to describe the properties of a mechanical system and the equations of motion are determined in a form that can be linked with other software packages to carry out simulations of the system.

Once the equations of motion are known and the applied forces or moments of force are known, simulation of the system can be carried out to determine the motion of the system through integration. Essentially the equations of motion are integrated forward in time, with knowledge of the applied forces and moments, to determine the motion of the system. A number of different techniques can be used to integrate the equations of motion, with each technique having advantages and disadvantages when compared to each other. The biggest distinction between the various integrators is whether they use a fixed time-step or a variable time step to determine the next point in time. Variable time step integrators are more computationally robust, in that if there is minimal change in the signal that a large time step can be taken and if a large change occurs in the signal then smaller time steps can be taken in order to gain a more accurate representation of the signal.

The main challenge with forward dynamics is usually to find a set of applied moments and forces that will produce the desired kinematics. Several techniques can be used to determine the appropriate moments of force and applied forces, with the most common method currently being dynamic optimization (Anderson and Pandy 1999). This method uses a first guess at the applied moments and then integrates the equations of motion to determine the kinematics and compares this set of kinematics to the desired kinematics or an objective function was

determined *a priori*. Once this comparison is made, the applied moments of force are altered and the process is repeated until the optimization criteria is achieved. Some optimization criteria that have been used with dynamic optimization include achieving maximal jumping height (Anderson and Pandy 1999), using the most efficient walking pattern (Anderson and Pandy 2001) or matching kinematic patterns that were measured in vivo (Piazza and Delp 1996; Millard 2006). This approach is suitable for finding moments of force that match a pre-determined movement pattern, or where an objective function can be clearly defined. The main drawback to this approach is that it is very computationally intensive, often taking several hours to determine a solution.

One of the most difficult problems with creating simulations of human walking with forward dynamics is that the interaction between the foot and the ground is very difficult to accurately represent. Early studies did not attempt to model this at all and simply chose to affix the foot to the ground during the stance phase (Pandy and Berme 1988), however a drawback to this approach is that an artifact is introduced in the kinematics and kinetics of the simulation when the contact with the ground is released (Gilchrist and Winter 1996). The most common method to approximate the dynamics of the interaction between the ground and the foot is to model the sole of the foot as a series of stiff non-linear springs with moderate damping (Gilchrist and Winter 1996; Anderson and Pandy 2001). The use of this approach determines the penetration depth of a contact point with the ground and determines the force applied to the foot based on the compression of the spring damper complex.

An other method that has been used to predict the applied moments and forces is the use of control systems that are based on models of the motor control systems rather than an optimization approach, this technique promises to greatly enhance our understanding of the

neural mechanisms involved for motor control (Pearson et al. 2006). These types of simulations create computational representations of the neural control mechanisms of the motion of interest, which in most of these simulations is walking. The output of the neural control models usually specifies the activation pattern for a number of muscles, which in turn determine the applied moments of force for a forward dynamics simulation. A unique feature of these types of simulations is that feedback can be integrated with the neural control models that originate from the results of the forward dynamics simulation, allowing the creation of models that can probe the influence of the sensory systems on the motor control.

There are two approaches that can be used when determining the moments of force that will be applied during a forward dynamics simulation that is controlled by a neural control model. The first is a direct approach where the joint moments are directly determined by the neural control model, such as the model created by Taga (1991). The preferred approach is to create a muscle model that captures the dynamics of muscle contraction. This model usually involves the determination of muscle force based on the current length, velocity and activation state. The details of the methods used to model muscle force output will be examined in the next section.

Modeling Muscles

Skeletal muscle is responsible for the generation of force to support and propel the mammalian skeletal system. Skeletal muscle possesses a number of interesting properties that influence the force output of the muscle and therefore would be of interest when creating muscle driven forward dynamic models. A number of these properties will be examined in this section.

Active and Passive Force-Length Relationship

The first property of skeletal muscle that will be examined is the active Force-Length relationship. It is well known that the maximum force output of a muscle is dependent on the length of the sarcomeres within the muscle (Rassier et al. 1999). This is due to the overlap of the thick (myosin) and thin (actin) filaments within the sarcomere. If the sarcomere is too long there will not be an adequate crossover between the thick and thin filaments, therefore the number of force generating cross bridges that can be formed will be reduced and force output will be limited. If the sarcomere is too short, then the force output will also be limited due to an inadequate number of cross-bridges being formed due to compression of the sarcomere. When the muscle is very short or very long, the amount of force that can be produced by the muscle is significantly reduced, in the middle of this range there is an ideal length where the muscle will produce the maximum active force; this particular length is known as the resting muscle length. When modeling the muscle force output based on a neural activation signal it is important to know the coordinates of the origin and the insertion of the muscle, so that the muscle's length can be accurately determined; this information is available from a number of sources (ie. Hoy et al. (1990)). It is also important to have knowledge of the resting muscle length of the muscles being modeled, this information is also available from literature sources (Hoy et al. 1990).

When a muscle is passively stretched, there is an exponential increase in the force observed within the muscle fibre. The structural protein Titin is responsible for this exponential increase in force (Rassier et al. 2005). This passive muscle force is an important consideration in the modeling of human locomotion as these passive forces have been shown to exert significant forces during normal human walking (Whittington et al. 2008). To help facilitate the modeling of the passive force relationship equations have been developed to predict the passive force from

skeletal muscle based on the length of the muscle relative to the resting length of the muscle (McGill and Norman 1986).

Force-Velocity Relationship

When the velocity of muscular contraction increases, there is a significant decrease in the force production of the muscle due to a decreased ability to generate force by the cross bridges when cycling quickly and due to viscosity of the muscle tissue (Winter 2004). This phenomena was studied by Hill (1938) who published an equation to represent the Force-Velocity relationship for isotonic concentric contractions as a rectangular hyperbola that could be expressed with constants related to the energy used during these contractions (Hill 1938). The work of Hill has provided the basis of all muscle models since the publication of this seminal paper.

Hill's equation can be used to predict the level of force at a given velocity for concentric contractions; however the behaviour during eccentric contractions is quite different. During eccentric contractions with maximal activation an increase in force above the maximal resting force is observed (Winters and Stark 1987). This increase in force is due to the extra force that is required to break apart bound cross-bridges during the lengthening of the muscle (Winter 2004). Further investigation of the eccentric portion of the force velocity relationship has shown that this increase in force is most pronounced when the activation of the muscle is close to maximal and that submaximal eccentric contractions lead to more modest increases in the force relative to the maximum isometric force (Winters 1990). It has also been found that there are differences in the force-velocity relationship depending on the type of contraction that is taking place. Sutarno and McGill (1995) found that during submaximal isovelocity eccentric contractions that there was a decrease in the force output relative to the maximal isometric force, which was compared

to the isotonic eccentric contractions that were described by Winters which increased in force relative to the maximal isometric force (Winters 1990).

It is difficult to capture all the nuances of the force-velocity relationship in a muscle model. In particular the eccentric side of the force velocity model is particularly difficult to model, therefore it is often simplified to only reflect the isotonic case during eccentric contractions (Caldwell 2004). To model the force velocity relationship of skeletal muscle the simplest approach is to normalize the parameters of the model to produce a dimensionless gain factor, which is applied to the output force, depending on the velocity of the muscle. This approach has been used by McGill and Norman (1986) to model the force velocity relationship in an EMG driven model of the lumbar spine. To do this it is necessary to choose parameters that describe the shape of the concentric portion of the Force-Velocity relationship, the maximal shortening velocity and the maximum force that may be produced by an eccentric contraction.

Excitation Contraction Coupling

There is a delay of approximately 10-30 ms between the time when a muscle activation signal can be detected using EMG and the force output of the muscle, this has been termed they electro-mechanical delay, or excitation-contraction coupling (ECC) (Winter 2004). This delay is not actually a simple delay in the temporal domain but differences between the activation signal and the force output of the muscle are also observed within the frequency domain. A delay is also observed in the decrease in force once the neural stimulation of a muscle fibre has been terminated.

This delay is primarily due to the dynamics of calcium ion release and reuptake within the sarcoplasmic reticulum of the muscle fibre (Caldwell 2004). A neural signal to a motor unit will lead to the release of calcium ions from the sarcoplasmic reticulum and then a short time

later these calcium ions will bind to the contractile apparatus within the sarcomere, allowing force to develop. Following the end of the stimulation signal from the neuron all of the calcium ions in the sarcoplasm must be reabsorbed into the sarcoplasmic reticulum. This process takes longer than the release of the initial release of the calcium ions and therefore force is sustained in the muscle fibre for a brief period after the neural signal has stopped stimulation of a muscle fibre (Caldwell 2004).

In muscle models it is important to have an accurate model of excitation contraction coupling as this feature can dramatically affect the muscle force output. In forward dynamics models there are often distinctions made between neural stimulation signals (usually designated by the variable u or y) and muscle activation signals (usually designated by a). In most studies the dynamics of the ECC process are approximated with a first order transformation, with separate time constants for an increase in the muscle activation signal and muscle deactivation (Anderson and Pandy 1999).

Other Muscle Models

There are a number of other features of muscle contraction that have not been addressed in this review, such as the history dependence of force output (Rassier and Herzog 2005) or the different muscle force dynamics that could be expected from different muscle fibre types (Cheng et al. 2000). While more complete muscle models exist for predicting the muscle force output based on the neural activation and the state of the muscle, it is also important to consider the computational cost that accompanies the increased level of detail of the muscle model. For most neural-mechanical simulations, a fairly simple muscle model is usually used. These models usually focus on representing some of the key features that would alter force output of a muscle, such as the active and passive force-length relationship, the force-velocity relationship and

excitation contraction coupling, while having a small number of variables in model to ensure quick computation (Yakovenko et al. 2004). While this modeling approach may not allow for the most robust estimates of muscle force, it does allow for a quick estimation of the muscle force that is suitable for driving a forward dynamic simulation, with low levels of computational resources while capturing the dynamics of the force-length and force-velocity relationships.

Models integrating biomechanics and neural control

All of the neural pathways, or neural circuits that were mentioned earlier in this chapter, seamlessly act in concert with each other to allow locomotion to occur. Because of the invasive techniques that are required to measure the individual pathways, it is only usually possible to measure these pathways in animal preparations. Additionally, the invasive techniques used to measure the pathways often require that only one neural substrate can be isolated at a time. This has led to a great deal of research being done on individual neural substrates, but there is only limited work analyzing the interaction between the various neural pathways involved in the control of human locomotion.

It has been suggested that one possible technique to investigate these interactions is through computational modeling (Pearson et al. 2006; Rossignol et al. 2006). Computational modeling allows for the activity in individual pathways to be systematically manipulated and thus the function of the pathways in the control of locomotion can be better understood. In order to fully understand how these pathways contribute to the control of walking, the model must also include a mechanical (musculoskeletal) component so that the effect of manipulating a pathway's activity can be observed in the kinematics of the musculoskeletal model.

Recently, Pearson et al (2006) reviewed the progress on using neuromechanical models for enhancing our understanding of the neural control of mammalian locomotion. Pearson's

group stresses that the use of neuromechanical models can provide a great opportunity to further our knowledge on the neural control of walking, as most of our current knowledge comes from isolated animal models, which usually do not have a full complement of sensory activity that is associated with normal walking behaviour. Also the use of models allows for simulation of conditions that are very difficult to achieve in human based experiments. For example, it is impossible to determine what the walking pattern would be if all sensory information from muscle spindles is eliminated, unless you have access to a patient with such a condition, which is exceedingly rare. However with a neuromechanical model, we are able to systematically manipulate and control the contribution of each individual pathway to the overall control of walking, and thus gain a deeper insight into how locomotion is controlled.

Several neuromechanical models have been previously been published to analyze the control of walking in the cat, humans, stick insects and reptiles, and swimming behaviour in the lamprey (Taga et al. 1991; Taga 1995a; Taga 1995b; Taga 1998; Ogihara and Yamazaki 2001; Dutra et al. 2003; Gunther and Ruder 2003; Yakovenko et al. 2004; Ekeberg and Pearson 2005; Paul et al. 2005; Yu and Ikemoto 2007; Jo 2008). Each of these models have contributed to our knowledge on the neural control of locomotion, however there are some significant limitations of most these models, which will be highlighted in the following paragraphs. This thesis will build upon the knowledge from these previous neuromechanical models by investigating the interaction between signals from a CPG, muscle afferents and descending commands from supraspinal structures. The goal of this section is to analyze what has previously been included in these neuromechanical models, and determine the best strategy to develop a neuromuscular model, which will further enhance our knowledge of the control of human locomotion.

Taga (1991, 1995, 1998):

Taga developed a series of models to understand the interaction between neural and mechanical systems involved in human locomotion (Taga et al. 1991; Taga 1995a; Taga 1995b; Taga 1998). This series of papers presented a pioneering model and included the first published model that combined a model of the neural control systems involved in the control of locomotion with a representation of the human musculoskeletal system and was able to achieve a stable walking pattern. Taga tested the hypothesis that the basic locomotor pattern is the result of entrainment between neural and mechanical systems. This hypothesis states that the neural control system receives feedback regarding the movement of the mechanical system, which will alter future neural output to incorporate the mechanical properties of the limbs into the motor output. Taga et al state that this system is self-organizing, meaning a stable locomotor pattern will emerge spontaneously.

The first model by Taga et al. (1991) included a 2D four segment linked segment model, with thighs and leg segments for both limbs. Although no foot was modeled there was an ankle moment included that acted at the point of contact with the ground. The neural oscillators (or CPG) were represented by a system of differential equations, that were based on equations presented by Matsuoka (1985). Feedback pathways were represented by simple reflex patterns, which were essentially an extended version of the simple stretch reflex, with additional feedback about the inertial angles of the segments being modeled. Each joint had an individual CPG, where the oscillators applied torques in opposite directions, mimicking extensor and flexor torques. The values of the time constants (τ & τ') from Matsuoka's differential equations (Matsuoka 1985) were chosen such that the frequency of the hip oscillator was twice of that for the knee and ankle joints, based on observed walking patterns. In order to achieve the proper

intralimb coordination pattern, the extensor neurons for the knee and ankle joints where inhibited by both the hip flexor and extensor neurons, thus the knee and ankle neurons became excited when the hip neurons were not active. Also included in the model were somatosensory sensors for the "feet" of the model, which signaled whether or not the feet were in contact with the ground, these somatosensory signals modulated some of the pathways that were involved in the detection of inertial angles.

The results of the simulations from this model show that walking patterns can be achieved with a model of the human neural control system when coupled with a fairly simple model of the musculoskeletal system. The CPG model used is a neural oscillator model that does not take any shaping of the muscle activation patterns into account. The shaping of the neural activity results from interaction with the sensory systems. Also, most of the sensory systems modeled were gross estimates of the function of the actual systems at best, therefore were not a good estimate of reality. Lastly, the while the model was stable under a number of conditions, it was unable to initiate or locomotion, without falling, and could only modulate its speed within 10% of the chosen walking speed.

The initial model by Taga was expanded to include the contribution of both mono- and biarticular muscles, with an enhanced control system and a more detailed model of the musculoskeletal system (Taga 1995a). This enhanced model showed a great improvement in terms of the degree of adaptability of the walking patterns. The model was able to moderate its walking speed over a fairly large range, react to a mechanical perturbation (a shove from behind), and even walk up a slight incline (Taga 1995b). The control system used to produce the walking pattern was based on similar principles as the earlier model, where a sensory feedback from the muscles acts on the CPG output to generate a walking pattern represents an entrainment

between the limbs and the neural systems. The neural input for the biarticular muscles were weighted averages the half-centre neurons for the joints that the muscle crossed although there was no justification given for the chosen weights. This model was further enhanced by using some simple control algorithms to allow it to step over an obstacle in its path (Taga 1998). This model used information regarding the distance from the obstacle to regulate its step length as the model approached the obstacle and to initiate the step over the obstacle at an appropriate distance to the obstacle. Additionally a descending command was modeled to increase the flexion of all the joints of the lower-limb for the step over the obstacle. The method used to increase the flexion of the limb did not correspond to the kinetic pattern that is observed in humans during this task, where active flexion of the knee joint also leads to flexion of the hip and ankle joints (McFadyen et al. 1993; Patla and Prentice 1995).

Wadden & Ekeberg (1998):

A neuromechanical model was developed for a single limb, of a non-specific animal by Wadden and Ekeberg (1998), in order to test the integration of a hierarchical distributed control system for the control of locomotion. This model included a neural drive signal from higher centres that controlled the speed of locomotion, CPG circuits, sensory feedback pathways providing information on the position of the joints, and stretch reflexes to prevent excessive stretching of muscles in the model. The model was able to produce stable locomotion at slow (0.14 m/s) and normal (1.4 m/s) walking speeds, and was able to transition between the chosen walking speeds.

While this model was based upon principles that are known about the organization of animal locomotor control systems, the fidelity of the model was lacking, as the CPG component was simply a neural oscillator that was formed by connecting three neurons and thus was unable

to provide a great deal of shaping to the muscle activation profiles. The neural network that was used to form the control algorithm was also based on the concept that each individual component of the stepping cycle is controlled independently, rather than has a whole.

One positive aspect of this model is that the model was able to adapt to various levels of loading during the stance phase, thus showing that the sensory feedback pathways involved were successful at adapting the walking pattern to different situations. However, these sensory pathways do not have a great deal of correspondence to known sensory pathways.

Paul et al (2005):

A neuromechanical model of human gait, based on the principles of known neural pathways was presented by Paul et al (2005). This is a significant improvement on previous neuromechanical models, as the contribution levels of various pathways could be modulated, so that the overall effect of these pathways could be reduced or even eliminated. Even though the neural components of the model were based on known neural pathways, and stable walking patterns could be achieved, the overall walking pattern was not of the same quality of previously reported neuromechanical models, taking short rapid steps, and walking at a very low walking speed. Also there were no supra-spinal inputs included in the model, other than a tonic stimulation of the CPG circuit, which only served to activate the CPG. Also details on the methods used to train the neural networks involved in the model were not stated therefore it is difficult to know which features of the neural system were serving as an objective function.

Another issue with model was with the CPG model used, which was similar to the half-centre concept proposed by Brown (1914). This CPG model results in an oscillatory behaviour, with no possible shaping being done by the spinal circuits, and therefore any modulation of muscle activity was solely done through sensory pathways. An examination of the motor neuron

activity while the CPG is being activated reveals sharp impulsive increases and decreases in motor neuron activity, which resulted in somewhat jerky walking patterns.

A feature that was not included in this model and may allow this model to produce more realistic walking patterns is the inclusion of stretch reflex modulation during the gait cycle. It has been shown that stretch reflex pathways are modulated during the walking cycle such that the reflex for a particular muscle has a gain that is proportional to the magnitude of the muscle's normal activity (Capaday and Stein 1986). This modulation ensures that activation of stretch reflexes will only occur when they are task relevant, for example in walking extensor muscles will have their highest level of activation during stance phase, a stretch during this period would indicate a lack of support for the limb, and therefore activation of the stretch reflex would be task relevant. During the swing phase, activity in the extensor muscles is minimal, as there is no need to support the limb while flexion is occurring, a stretch of most of the extensors will occur during this flexion, and correcting for this stretch would be inappropriate for the task. The mechanism for this modulation appears to be pre-synaptic inhibition of the IA sensory neurons and was not included in the model by Paul et al. Lastly, sensory pathways from the muscle receptors to the CPG were not included in this model. These pathways have been shown be important in the control of phase transitions during walking and in the modulation of the extensor tone during walking (Donelan and Pearson 2004). These pathways have been shown to be important for maintaining a stable walking pattern in other neuromechanical (Yakovenko et al. 2004; Ekeberg and Pearson 2005).

In conclusion, this model made significant improvements on previous neuromechanical models, by creating control systems that are based on known neurophysiological pathways;

however improvement could be made on modeling the subcomponents of their neural control system, to gain a better understanding of the contributions to these systems.

Ekeberg & Pearson (2005):

A three dimensional model of the musculoskeletal system of the cat was constructed that was controlled by a finite state controller which took the cat through a walking cycle with four distinct phases, swing, touchdown, stance and liftoff (Ekeberg and Pearson 2005). Sensory feedback was then integrated into the model to determine the relative importance of two factors that have been identified as being important for signaling the stance-to-swing transition in the cat; ankle extensor muscle unloading and hip position. It was found that the signal from the ankle extensor proved to be the dominant signal for signaling the stance to swing transition and steady state gait could be achieved with input from this pathway alone. With the sensory pathways in place this model could also respond to small perturbations, such as a small shove, slips, and changes in the grade of the walking surface.

A drawback of this model was that many features of the walking pattern were pre-determined, and specified with the finite state controller. Therefore a complete model of the locomotor control system was not presented. This model also tested the effect of coupling the control systems for the contralateral limbs, and found that this coupling helped ensure stability of the walking pattern after a perturbation had occurred. This coupling was however not necessary to provide normal steady state locomotion.

Yakovenko, Gritsenko & Prochazka (2002, 2004):

This group created a model of the lower limbs of the cat to help determine the role of stretch reflexes during normal walking (Prochazka et al. 2002; Yakovenko et al. 2004). This model was based on the finding that during “foot in hole” experiments where the muscle is

suddenly stretched, when it is expecting to make contact with the ground that there is only a minor increase in the level of muscle activity, indicating that the stretch reflex may have only a small contribution to the overall walking pattern. It was approximated that the stretch reflexes contribute about 30% of the overall muscle activity observed during walking.

This model used pre-defined muscle activation patterns to initially drive the model; these muscle activation profiles represented the output of the CPG, in the absence of sensory information. These activation patterns were then subjected to a model of the stretch reflexes, and Ib pathways, associated with GTOs. The model also included some Finite-State rules to induce phase transitions during walking; these are similar to the functions for phase transitions that were modeled by Ekeberg & Pearson (2005). It was found that these IF-THEN rules enhanced the stability the walking pattern of the model.

The overall findings of this model were that stretch reflex pathways could help enhance the walking pattern when central drive from the CPG is low, however under normal circumstances a steady state walking pattern can occur simply due to the intrinsic stiffness of the limb. A strength of this model is that it was tested with a very high number of parameters for the musculoskeletal system and the neural control model and established a range of values for these parameters that produced a stable walking pattern.

Jo (2008):

A recent model by Jo (2008) used a neuromechanical model to simulate human walking, with the ability to superimpose a voluntary movement over the walking pattern using a control system that is similar to the neural control mechanisms for stepping over an obstacle that has been proposed based on observation in cats (Drew et al. 2004). This model included a CPG which was based on similar concept as the finite-state controller that was published by Ekeberg

& Pearson (2005), where muscle activation patterns were chosen to accomplish five sub-tasks during walking (as opposed to 4 subtasks used by Ekeberg & Pearson). The neural signals that were developed by this CPG model drove a 7 segment, 18-muscle representation of the musculoskeletal system.

This model made two unique contributions to the field of neuromechanical model development. The first was that the system that was used to control the balance was based on systems that may be present in human locomotor control systems. This concept was based on some long latency reflex loops, with some intelligence build into the reflexes, that Jo termed Cerebro-cerebellar long-loop feedback system. A circuit that is based on our current understanding of how the cerebellum processes data did the intelligent processing for this feedback loop. The details of this feedback process were published in a separate paper (Jo and Massaquoi 2007). The balance control scheme that was used in this paper proved to be quite robust as the model was able to walk with the upper-body segment of the model in significantly flexed position and still maintain a regular walking pattern. The balance recovery model was also adapted in a different paper to be able to recover from tripping and push type perturbations in another paper (Jo 2007).

The second unique aspect of this paper was the superimposition of voluntary movements on top of the normal walking pattern. These voluntary movements included stepping over an obstacle and generating a voluntary kick during the swing phase. The processing to achieve these specific walking patterns was not expressly detailed within the paper however.

Concluding Remarks

The neural control and biomechanics of human walking have long interested researchers. Recently a trend towards integrating the knowledge from these two fields has resulted in the

publication of several computational models that are combining our knowledge of the control mechanisms and the mechanics of the musculoskeletal system test hypotheses regarding the control of walking and make manipulations that are not possible with traditional experimental techniques. Current computer technology is also facilitating the development of these models; simulations that used to take days to execute can now be carried out in seconds.

The development of these neuromechanical models is a challenging task. One must decide on the amount of detail to include when creating the neural control models and the models of the musculoskeletal system. Often increasing the complexity of either of these models is a paralyzing process as the increased complexity complicates the control of the system. There are a number of methods that can be used to find solutions to complicated control problems such as artificial neural networks or genetic algorithms, which are essentially forms of optimization techniques.

One could argue that the foundation neuromechanical simulation has not been laid. Many complicated and complex models have been published but several of the basic model interactions that occur within these models have not been tested and the effects of altering the parameters of the models have not been demonstrated. One of the overall goals of this thesis will be to understand the interactions between the neural and mechanical representations and systematically manipulate a number of parameters of both models to examine the effect on the motion of the mechanical system and processing within the neural control models.

Chapter 3: Use of a Pendulum Model for Testing Neuromechanical Interactions during Feedforward Control of Rhythmic Limb Movements

Introduction

The basic rhythm of the locomotor pattern is thought to be produced by spinal circuits known as Central Pattern Generators (CPGs). These circuits are capable of producing rhythmic motor output in the absence of any sensory feedback. The exact circuitry involved in these neural networks is only known in a few cases, for example in the lamprey (Grillner et al. 1987), however rhythmic motor outputs can be observed in the absence of sensory feedback in a number of species (Forssberg et al. 1980a; Dimitrijevic et al. 1998). While it is thought that CPG circuits contribute to the basic timing and inter-limb coordination of the locomotor pattern, it is realized that these networks are not capable of providing full body weight support, balance control or proper propulsion; it is thought that higher centres within the CNS are responsible for these tasks (Rossignol 1996; Drew et al. 2004; Rossignol et al. 2004). One important feature of CPG circuits that has been observed is that the burst frequency of the CPG can often be controlled by the magnitude of a simple tonic signal (Shik et al. 1966; Dimitrijevic et al. 1998). While it is known that the frequency of the CPG output can be controlled by these simple signals the kinematic results of altering the frequency of the CPG output remains somewhat unknown. The goal of this study is to develop a computational model of a CPG, which will be based on the work of Matsouka (Matsuoka 1985; Matsuoka 1987) and determine what effect altering the frequency of CPG output has on a simple musculoskeletal system (MSK-S). Since the kinematic

pattern observed will be partially determined by a number of parameters of the musculoskeletal system, a number of these parameters will be systematically altered to determine their effect on the combined action of the CPG and the MSK-S. The work completed in this chapter will allow for the development of models that will be used in the following studies of this thesis, and enhance our understanding of the role of feedforward control of rhythmic limb movements, such as walking.

One of the most important considerations for locomotor control is the efficient use of energy during walking. An important goal of walking is to be able to move in the forward direction in the most efficient way possible. One method that has been suggested to increase the efficiency of rhythmic limb motions is to produce oscillatory joint torques at a frequency close to the natural frequency of the limb (Taga et al. 1991). This allows for maximal movement amplitude with minimal exertion of energy by the biological system. It has been shown that during walking and other limb movements that people activate their muscles at a frequency that is close to the natural frequency of the limb, thereby achieving maximal movement amplitude, with minimal effort (Doke et al. 2005). Analytical studies of periodically driven damped pendulums has shown that motion of the pendulum is different depending on whether the driving torque is occurring at frequencies less than or greater than the natural frequency of the pendulum (Bryant and Miles 1990; Hatsopoulos 1996; Kuo 2002). When the frequency of the torque driving the pendulum is greater than the natural frequency of the pendulum then it has been shown that the pendulum's frequency will match the frequency of the driving torque. However, when the frequency of the driving torque is less than the natural frequency of the pendulum then more complex kinematics will emerge due to interactions between the natural motion of the

pendulum and the frequency of the neural drive, thus controlling the pendulum becomes much more problematic at these frequencies (Hatsopoulos 1996; Williams and DeWeerth 2007).

A model commonly used to test the neural mechanisms involved in the control of rhythmic limb movements is a simple pendulum, usually with mechanical properties (mass, moment of inertia) that are similar to the human lower limb ie. (Bryant and Miles 1990; Obusek et al. 1995; Hatsopoulos 1996; Selles et al. 2001; Kuo 2002; Futakata and Iwasaki 2008; White et al. 2008). The pendulum is usually driven by a torque motor at the revolute joint of the pendulum, and is lightly damped such that a sustained force input is required to maintain a stable kinematic pattern. This approach provides an elegant model to test interactions between the control systems that determine the force of the pendulum and mechanical influences on the motion of the pendulum. The pendulum model obviously does not represent the dynamics that are involved in making contact with the ground, but can adequately represent the motion of the swinging lower limb when the knee is locked and has been shown to have reasonable correspondence to the energetics and mechanics of a swinging human leg (Doke et al. 2005).

A number of previous studies have examined the interaction between neural control systems and mechanical systems, however there are two issues which have not been examined in detail. The first is the inclusion of the dynamics involved in muscle contraction, such as the force-length and force velocity relationships. The second is that the mechanical system modelled often does not have a great degree of correspondence to the human musculoskeletal system. The mechanical model used is typically a pendulum, for reasons previously discussed, or an oscillating mass. For example, Kuo (2002) showed that a rhythmic swinging pattern could be attained using neural oscillators that were based on either feedforward or feedback mechanisms or a hybrid system that combined both feedforward and feedback mechanisms. This paper

showed that a hybrid mechanism was best for achieving rhythmic motor pattern and deal with potential perturbations. Despite making some valuable insights into the neural mechanisms involved in locomotor control, the motor pattern produced by the control systems were based on control theory to achieve a specific set of kinematic parameters in all conditions, instead of allowing the model to assume what ever kinematic patterns naturally emerge. This paper also did not test the ability to control rhythmic limb movements at different frequencies. A number of other studies have compared the motion patterns of pendulums or other mechanical systems that were driven by control systems with feedforward commands and with the inclusion of feedback, but few studies have analyzed the amplitude response of the movement patterns to different CPG frequencies.

The overall goal of this study was to develop a simplified model of the musculoskeletal system whose muscles were driven by a simple model of a CPG control system and analyze how the magnitude and frequency of the neural drive affected the magnitude and frequency of the musculoskeletal system in the absence of sensory feedback. The components involved in the musculoskeletal model and in the neural control model were described, and are used extensively in other models in this thesis. The specific goals and hypotheses for this study were outlined following the description of the model so that the specific hypotheses could be tested and discussed with respect to specific variables within the model. The next chapter in this thesis analyzed contributions of feedback to the motion of the pendulum system described in this chapter.

Methods and Model Descriptions

Mechanical Model

A simple damped pendulum was used as a model for the limb during rhythmic movements. A pendulum model has been used in a number of previous studies to investigate the control of rhythmic limb movements (Obusek et al. 1995; Hatsopoulos 1996; Kuo 2002; Iwasaki and Zheng 2006; White et al. 2008). The model attempted to replicate the anthropometrics of an average sized male's lower limb. The limb was represented as a rod pendulum that rotated about a revolute joint at the proximal end. The total mass of the pendulum was 12.5 kg, with a length of 1 m. To more accurately represent the distribution of mass of the human lower limb, the centre of mass of the pendulum was 0.4 m from the revolute joint. The moment of inertia of the pendulum was set to be similar to a human lower limb, with a value of 1.04 $kg.m^2$. The origins of the muscles were 0.1m from the revolute joint, with the extensor muscle being behind the revolute joint and the flexor muscle being in front of the joint. The muscles were attached to the rod pendulum 0.3m from the revolute joint.

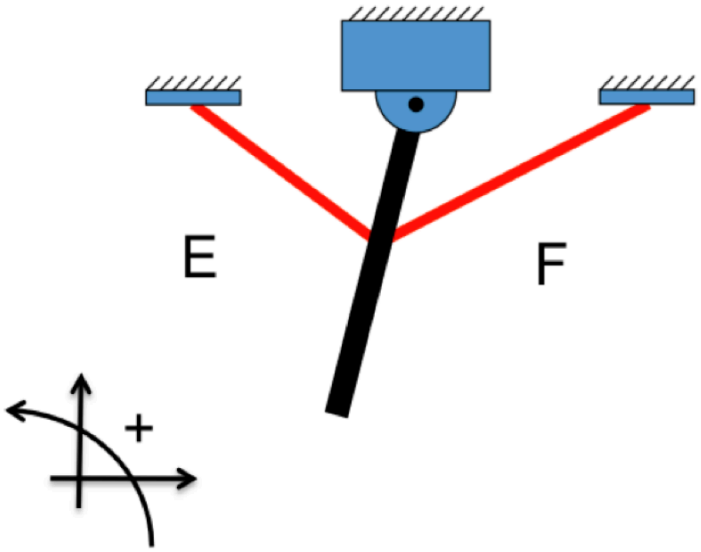

Figure 3.1: Schematic diagram showing the positioning of the two muscles in the pendulum model. The muscle to the right, which induces a positive rotation, is labeled as the flexor, while the muscle to the left, which induces rotation in the negative direction, is labeled as the extensor.

A torque motor was used to drive the pendulum at the revolute joint. The torque applied by this torque motor is determined through the use of Hill-type muscle models, representing the flexor and extensor muscles. To prevent continual motion of the pendulum in the absence of an applied torque, viscous damping was applied at the revolute joint with a damping constant of 5 Nm.s/rad, unless otherwise specified. The resistive moment provided by the viscous damping was given by the following equation:

$$M_d = -B\omega_P$$

Equation 3.1

Where M_d was the damping moment applied at the revolute joint, B was the damping constant, and ω_P was the angular velocity of the pendulum.

Muscle Model

A Hill type muscle model (Zajac 1989) was used to convert muscle activation signals to muscle forces, which in turn actuated the mechanical model. Muscle activation was first determined from a neural drive signal, which originated from the CPG model, which will be described later in this chapter. The muscle activation signal was slightly delayed from the neural drive signal, due to a process known as Excitation-Contraction Coupling (ECC) (Caldwell 2004). The ECC process was modelled by adding a first order delay to the neural drive signal. The differential equation used to represent the ECC process was based on the model by Anderson and Pandy (2001) and is shown in Equation 3.2.

$$\dot{a} = \left(\frac{1}{\tau_{rise}}\right)\left(y^2 - ya\right)\left(\frac{1}{\tau_{fall}}\right)\left(y - a\right)$$

Equation 3.2

Where a was the muscle activation signal, y was the neural drive signal that was determined by the CPG model, $\tau_{rise} = 20$ ms and $\tau_{fall} = 40$ ms and represented the time constants for the rise and fall of muscle activation signals, respectively. This activation signal then served as the activation input to the muscle model that is described below.

Overall, the force produced by a muscle was determined by the following equation (McGill and Norman 1986):

$$F_{mus} = a(P_0 \Omega \delta) + F_{pass}$$

Equation 3.3

Where, F_{mus} was the force produced by the muscle, P_o was the maximum isometric force that could be produced by the muscle, a, δ and Ω were dimensionless scaling factors relating to activation, muscle length and muscle velocity respectively. The dimensionless scaling factor Ω

represented the active force-velocity relationship of skeletal muscle and was varied depending on the type of contraction. The force-velocity scaling factor for concentric muscle contractions was given by:

$$\Omega = \frac{P_0 \cdot b - V \cdot a}{P_0 (V + b)}$$

Equation 3.4

Where P_o was the maximum isometric force that could be produced by the muscle and V was the velocity of shortening for the muscle. The constants a and b were constants which determined the shape of the force-velocity curve. Hill's constants a and b were given by the following relationship (McGill and Norman 1986):

$$\frac{a}{P_o} = \frac{b}{V_{\max}} \text{ Where, } \frac{a}{P_0} = 0.25$$

Equation 3.5

Where V_{max} was the maximum shortening velocity where force may be produced and was taken from literature sources, to be 10 l_o/s (Anderson and Pandy 1999).

In the eccentric case, the force-velocity relationship was given by (Caldwell 2004):

$$\Omega = \frac{P_s - S(P_s - 1)}{S - V}$$

Equation 3.6

Where P_s was the maximum force that may be produced eccentrically and was set to 1.8 times *Po* (Caldwell 2004) and S was a variable which describes the shape of the eccentric portion of the Force-velocity curve, and is given below:

$$S = \frac{b(Ps-1)}{1+(a/P_0)}$$

Equation 3.7

Hill's constants *a* and *b* were the same for both the eccentric and concentric portions of the force-velocity curve. Note that the equations defining *S* and *Ω* have been normalized to P_o, to produce a dimensionless value.

The active force length relationship (δ) was defined by the following equation (McGill and Norman 1986):

$$\delta = \sin\left[\pi\left(\frac{L}{L_0} - 0.5\right)\right] \text{ Where,}$$

$$0.5 \le \frac{L}{L_0} \le 1.5$$

Equation 3.8

If L/L_0 was outside of these bounds then δ = 0. Graphs illustrating the active force length and force-velocity relationships were shown in Figure 3.2.

The passive muscle force was calculated using the methods of McGill and Norman (1986). The equation for this is shown below:

$$F_{Pass} = P_0 e^{7.675(l/l_0)-10.671}$$

Equation 3.9

Where, P_o was the maximum isometric force that could be produced by the muscle, and (l/l_o) was the length of the muscle normalized to the muscle's resting length. The parameters used in the muscle model were shown in Table 3.1.

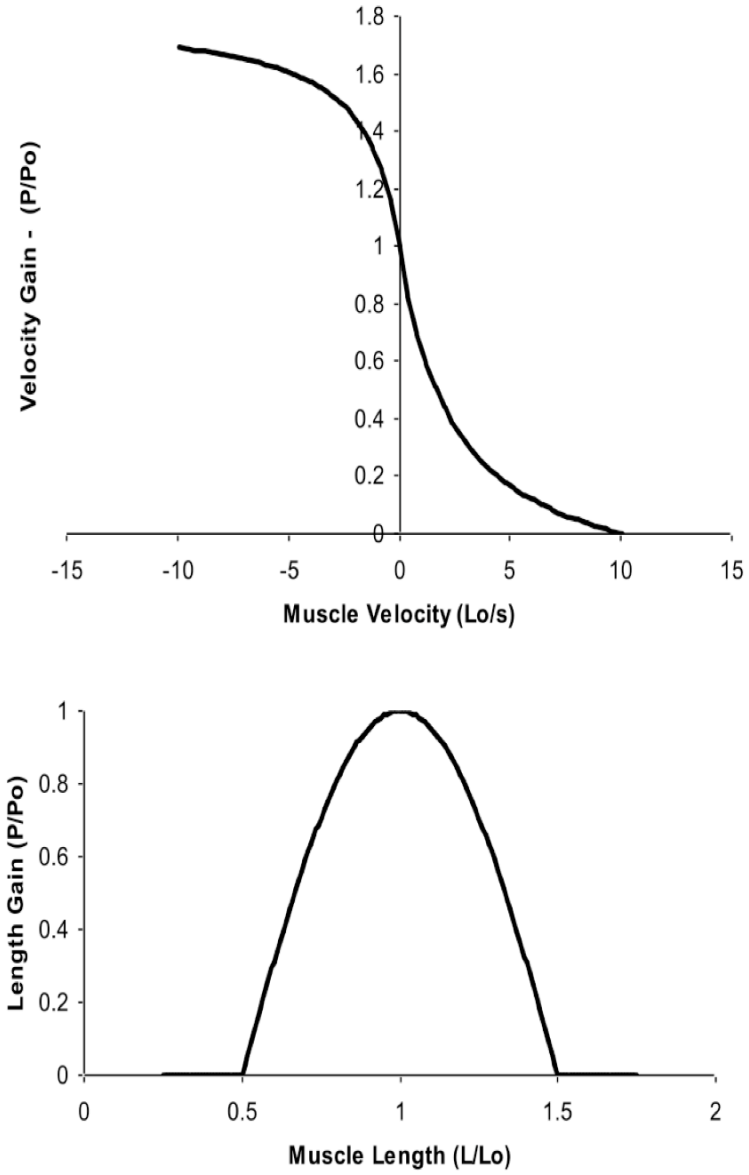

Figure 3.2: Force-Velocity relationship (top), and active Force-Length used in the muscle model.

Table 3.1: Parameters used in the muscle model

Symbol	Description	Value
P_o	Maximum Isometric Muscle Force	2000 N
P_S	Maximum Eccentric Muscle Force	1.8 * P_o
L_o	Resting Length	0.383 m
V_{max}	Maximum rate of shortening where force can be produced	10 L_0/s
τ_{rise}	Time constant for rise of muscle activation signal	0.020 s
τ_{fall}	Time constant for decrease in muscle activation	0.040 s
$\boldsymbol{L_{SEC}}$	**Length of Series Elastic Component**	**0.2 m**
a	Shaping factor for F-V relationship	0.25 * P_o = 500
b	Shaping factor for F-V relationship	V_{max} * 0.25 = 2.5

Central Pattern Generator Model

The numerical CPG model was based on a set of differential equations that were first introduced by Matsuoka (1985). These equations produced a pair of continuously alternating signals that correspond to the flexor or extensor half centre in the half centre CPG model, first proposed by Brown (1911). These differential equations use the concepts of mutual inhibition and the adaptation effect to produce a reciprocal firing pattern for two half-centre neurons. Mutual inhibition means that the two half neurons had inhibitory connections such that only one of the two neurons could have been active at any given time. The adaptation effect reduced the magnitude of output after a period of sustained output; this effect was critical for producing the oscillatory patterns. The basic organization of the mutually inhibitory half centre CPG model was shown in Figure 3.3.

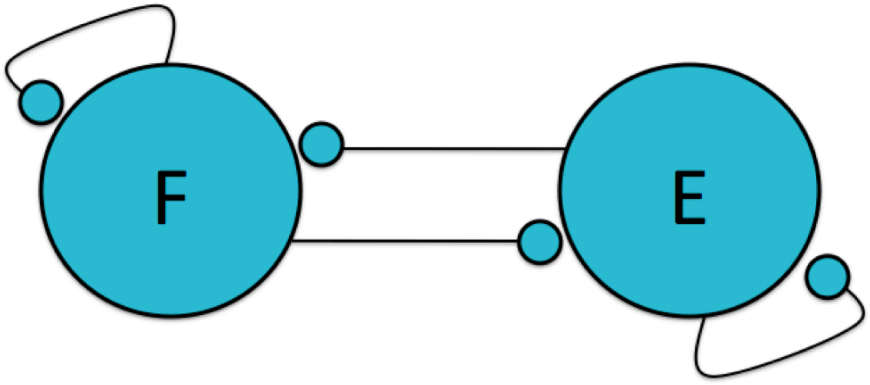

Figure 3.3: Basic Half Centre CPG Model. The flexor neuron is indicated with an 'F', while the extensor neuron is indicated with an 'E'. The circular synaptic connections indicate an inhibitory connection. The adaptation effect is represented by the neuron's inhibitory connection to themselves.

The output of the neurons was given by the equations below:

$$y_F = \max(0, u_F) \text{ and } y_E = \max(0, u_E)$$

Equation 3.10

Where, y_F and y_E were the outputs of the flexor and extensor neurons respectively. The *max* function in Equation 3.10, forced the output of the neurons to be positive in all circumstances. The inner state of the flexor and extensor neurons were represented by u_F and u_E respectively and were calculated as shown in the differential equations, in Equation 3.11.

$$\dot{u}_F = \frac{1}{\tau_{rise}}\left(q_t - u_F - \beta v_F - w y_E\right)$$

and

$$\dot{u}_E = \frac{1}{\tau_{rise}}\left(q_t - u_E - \beta v_E - w y_F\right)$$

Equation 3.11

Where y_F and y_E were the outputs for the flexor and extensor neurons, respectively, and u_F and u_E were the internal states of the flexor and extensor neurons respectively. A time

constant, τ_{rise}, was used to regulate the rise time of the output of the neurons and was set to 10 ms, based on literature values (Matsuoka 1985; Taga et al. 1991). The weighting factor w specifies the strength of mutual inhibition between the flexor and extensor half-centres; the value of w was set to -2.0 in all cases. A tonic input q_t specified the magnitude of the output, v_F and v_E were the adaptation terms for the neurons that influenced how long the neurons remained active before their activity diminished, and β was a weighting factor. The values of v_F and v_E were given by the following differential equations:

$$\dot{v}_F = \frac{1}{\tau_{ad}}\left(y_F - v_F\right) \text{ and } \dot{v}_E = \frac{1}{\tau_{ad}}\left(y_E - v_E\right)$$

Equation 3.12

Where, τ_{ad} was the time constant for the adaptation effect and the was primary mechanism used to control the burst frequency of the CPG model (Matsuoka 1987).

Matsouka (1985) specified the conditions where these equations will produce an oscillating output, and introduced mechanisms for frequency control and the ability to modulate the pattern of output (Matsuoka 1987). This model has been used in a number of previous studies combining neural and mechanical models, ie. (Taga et al. 1991; Asai et al. 2003) and has been shown to have the ability to integrate feedback signals into the neural processing (Taga et al. 1991; Asai et al. 2003) and included the ability to construct networks consisting of several neurons (Matsuoka 1985; Taga et al. 1991; Asai et al. 2003). The neural signals produced by the Matsuoka model were continuous, non-spiking signals. More complex CPG models have been constructed that include spiking neurons (Simoni and DeWeerth 2007), however the output of these types of CPG models did not lend themselves to acting as neural drive signals for Hill-Type muscle models. The output signals produced by the Matsuoka CPG model could be

compared in nature to linear envelope EMG signals, and the magnitude of the signal could be conceptualized as representing the firing rates of the neurons (Taga et al. 1991).

Overall Dataflow Through The Model

The CPG model that was previously described first generates neural signals. Two main parameters were used to modulate the output of the CPG model q_t and τ_{ad}, which were expected to control the magnitude and frequency of the CPG output respectively. Once the neural output of the CPG was determined the ECC model determined the muscle activation patterns. These muscle activation patterns then served as input to the muscle model, which determined the muscles' force based on the current muscle activation and the state of the muscles, which was affected by the motion of the pendulum. The net joint moment was then determined based on the muscle forces and the moment arm (r), which was also affected by the angle of the pendulum. The calculated net joint moment was then applied to the revolute joint at the pivot point of the pendulum and the velocity and angle of the pendulum was determined by integrating the equations of motion for the pendulum system.

A flowchart outlining the flow of data through the model was shown in Figure 3.4.

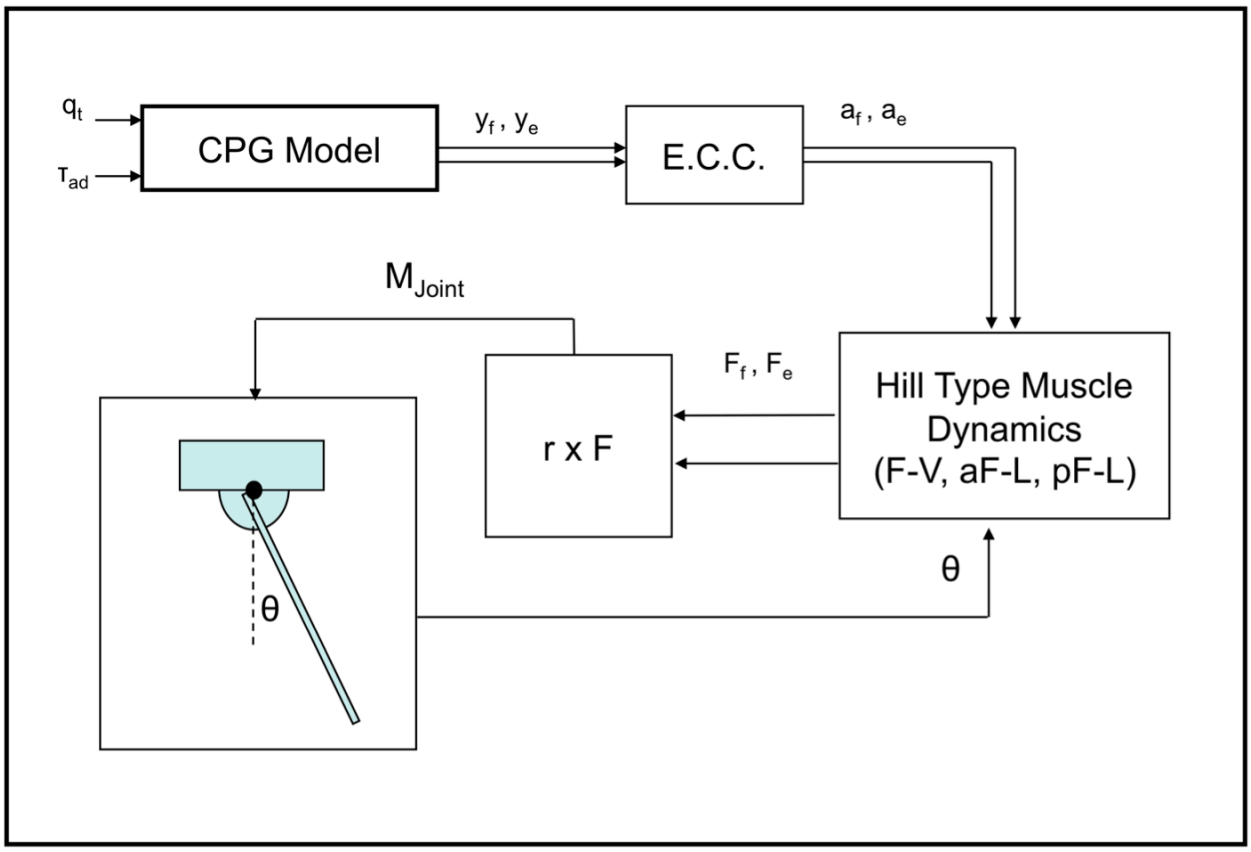

Figure 3.4: Flowchart outlining the flow of data through the Feedforward pendulum model.

Simulation Properties

All simulations were carried out with Simulink version 6.1, a component of MATLAB (The Mathworks Inc., Natwick MA). Simulink is a graphical tool for solving models that are based on differential equations. All simulations for this portion of the thesis used the *ode45* solver to integrate the differential equations that determine the model, which is a variable step Runge-Kutta based solver. The solver took an initial time-step of 10^{-4} s, and had a maximum step size of 10^{-2} s and a minimum step size of 10^{-15} s. Relative and absolute tolerances were set to 10^{-5} units and zero-crossing control was enabled. The mechanical system used in this study was

defined using SimMechanics, which is a component of Simulink used to create mathematical representations of mechanical systems.

Unless otherwise stated all simulations took place with the initial conditions shown in Equation 3.13. The acceleration due to gravity (g) was nominally set to 9.81 m/s^2 in the negative vertical direction for all simulations in this chapter.

$$\left[\theta_0, \dot{\theta}_0\right] = \left[-45^\circ, 0^\circ / s\right]$$

Equation 3.13

Simulation Goals and Hypotheses

Goal 1:

The first goal of this study was to determine the effects of the parameters of the CPG model on the frequency and amplitude of the CPG output. The parameters tested were τ_{ad} and q_t, which were expected to control the frequency and the magnitude of CPG output respectively.

It was hypothesized, based on the work of Matsuoka (1987), that the amplitude of the output of the CPG will be directly (linearly) related to the value of q_t. It was also hypothesized that the burst frequency of the CPG model would be able to be controlled by the time constant of the adaptation effect (τ_{ad}), however this relationship would not be as predictable as the relationship between q_t and the amplitude of the output.

Goal 2:

The second goal was to determine the natural frequency of the pendulum and analyze the effect of adding viscous damping and by adding muscles to the pendulum model.

Considering the mechanical properties of the pendulum system, it was hoped that the natural frequency of the pendulum would be similar to the human lower limb. It was expected

that the addition of muscles would increase the natural frequency of the pendulum system, as the passive muscle force model will introduce an additional joint moments that will reverse the motion of the pendulum earlier. It was expected that the joint damping would decrease the natural frequency of the pendulum somewhat, as it would slow down the motion of the pendulum as the pendulum passed the neutral position, therefore increasing the cycle time.

Goal 3:

The third goal was to determine how a torque driven, damped pendulum interacted with the CPG model. The simulations that addressed this goal drove the pendulum, with the signals generated by the CPG model, and assessed what effect the amplitude and frequency of the CPG output had on the motion of the pendulum.

It was expected that the interaction between the neural and mechanical systems would be complex. Based on past research it was hypothesized that the frequency of the pendulum system would become entrained (or match) the frequency of the neural signals produced by the CPG model (Hatsopoulos 1996). It was expected that the amplitude of the pendulum's motion would be greatest when the frequency of the CPG output was close to the natural frequency of the mechanical pendulum. When the frequency of the CPG was less than the natural frequency of the pendulum, the behaviour of the pendulum was expected to be complex, with frequency components that represented the natural frequency of the pendulum and the frequency of the CPG.

Goal 4:

The final goal of this study was to determine the impact that the choice of muscle attachment properties had on the motion of the pendulum. This set of simulations analyzed the effect that the location of the muscle attachment points had on the motion of the pendulum.

It was expected that changing the location of the muscle attachment points would have a dramatic effect on the motion of the pendulum, primarily due to the changes in the moment arms of the muscles that accompanied the changes in muscle attachment points. It was also expected that the properties of the muscle model, particularly the resting length of the muscle, would have an effect on the motion of the pendulum system when the muscle attachment points were changed.

Simulation Descriptions and Results

Experiment #1: Modulation of CPG Frequency and Amplitude

The CPG model that was previously described was successful in creating an oscillating output that was reciprocally active between two neurons. Sample outputs of the two neurons of the CPG model are shown in Figure 3.5. The frequency of the CPG's output was able to be controlled by specifying the value for the adaptation time constant (τ_{ad}), the output of the CPG model at several values of τ_{ad} is shown in Figure 3.6.

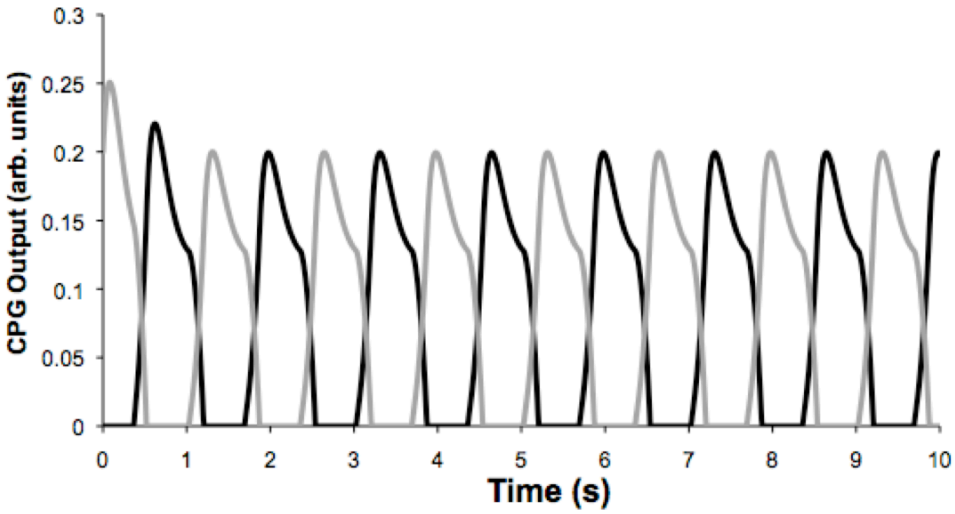

Figure 3.5: Sample output from the half centre CPG model. The black line represents the output of the flexor neuron, while the grey line represents the output of the extensor neuron. This output was obtained with the value of q_t set to 0.4 and τ_{ad} set to 0.5s.

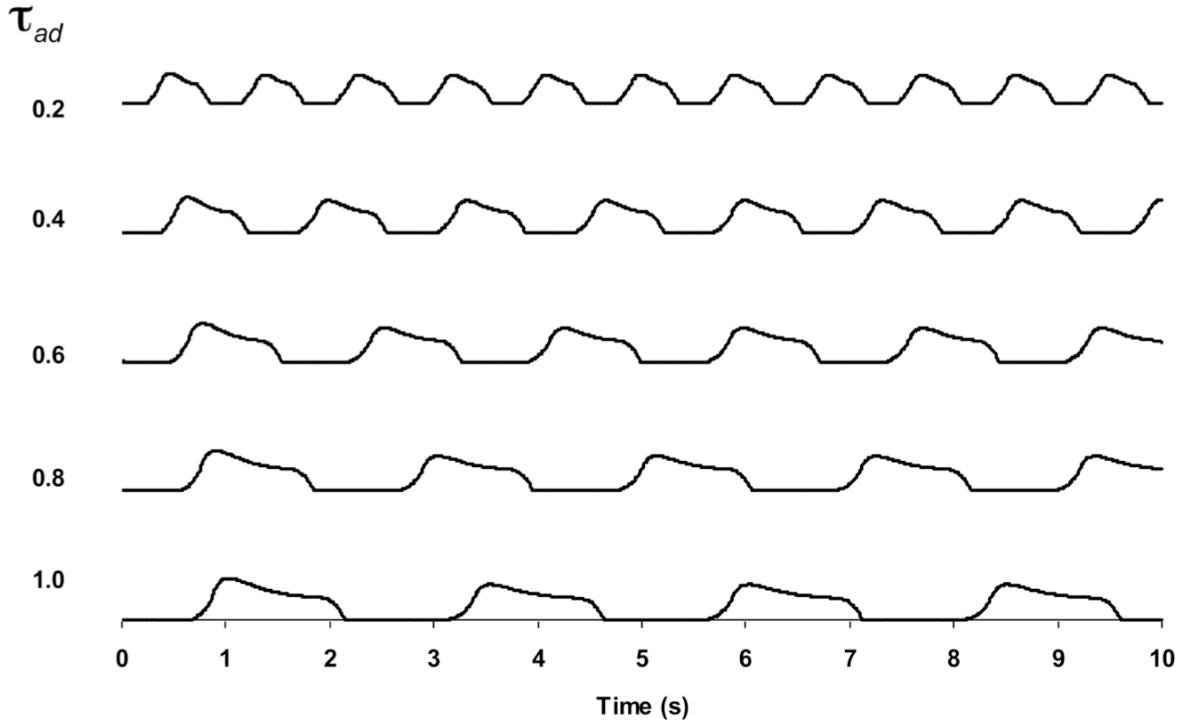

Figure 3.6: Effect of τ_{ad} on the frequency of the CPG output. Only the output of the flexor neuron is shown.

A total of 4500 simulations were carried out to determine the combined effects of the time constant of the adaptation effect (τ_{ad}) and the value of the tonic input to the CPG model (q_t). The 4500 simulations were divided into 9 sets of 500 simulations where q_t was set to values between 0.125 and 1.125, in increments of 0.125. The value of τ_{ad} was increased from 0.01s to 5s, in increments of 0.01s for each value of q_t. The frequency of the output of the CPG (ω_{CPG}) was found to be directly controlled by the value of τ_{ad}, regardless of the value of q_t. A plot showing the frequency of the CPG across a range of values of τ_{ad} is shown in Figure 3.7. The value of q_t increased the magnitude of the neural output in a linear fashion (Figure 3.8). The

magnitude of the CPG output was also affected by the value of τ_{ad}. The amplitude of the CPG output increased in a logarithmic fashion as the value of τ_{ad} was increased (Figure 3.9).

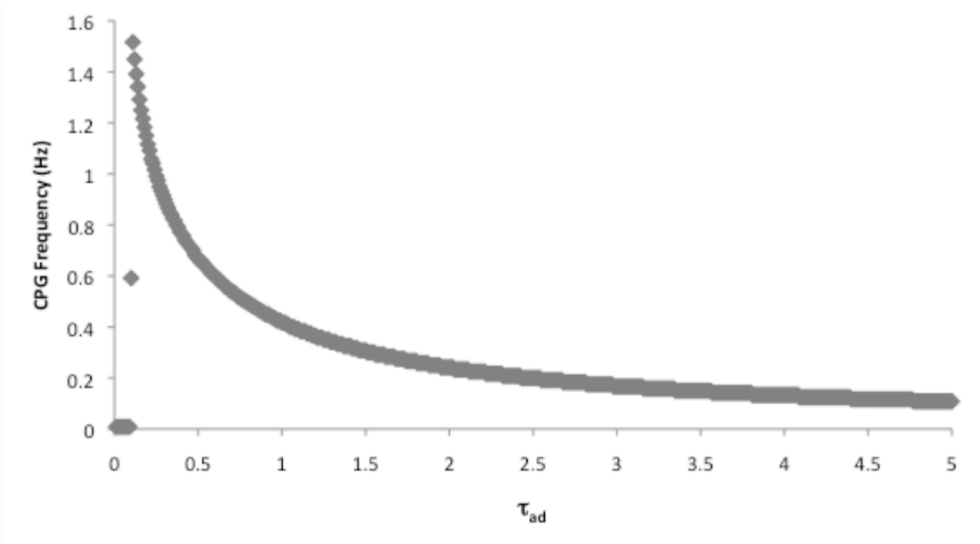

Figure 3.7: Frequency of the CPG at various values of τ_{ad}. The data points for different values of q_t would overlay the points shown in the graph

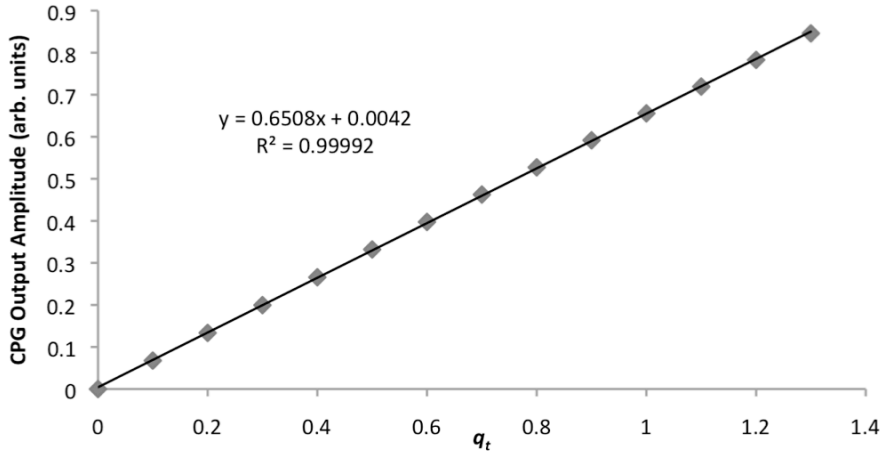

Figure 3.8: Effect of q_t on the magnitude of the output of the CPG model at a set value of τ_{ad} (τ_{ad} = 0.6).

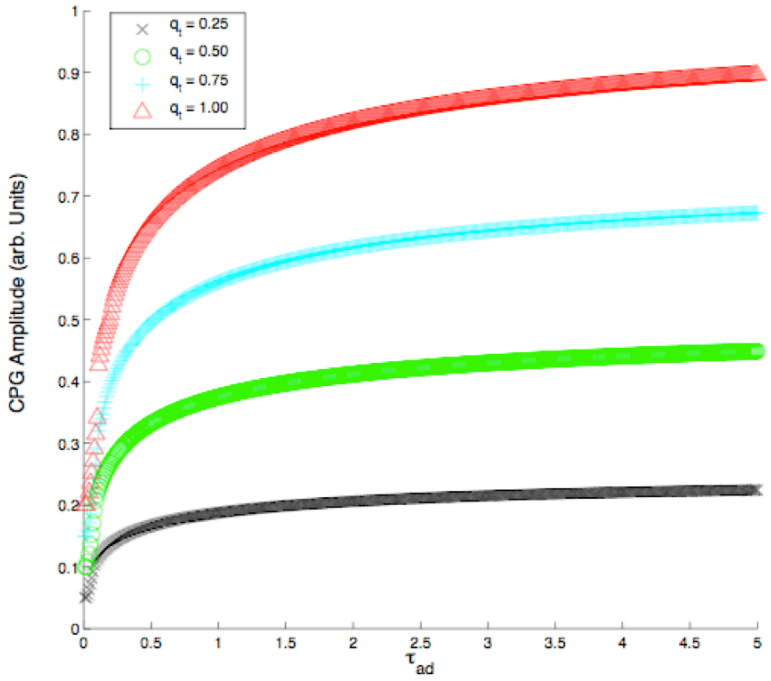

Figure 3.9: Amplitude of CPG output at various levels of q_t and τ_{ad}.

As observed in Figure 3.7, the CPG did not produce an oscillatory output at low values of τ_{ad}. A peak frequency of 1.5 Hz was observed, which corresponds to a τ_{ad} value of 0.11s. After the peak frequency was obtained, the frequency of output that was created by the CPG decreased in an asymptotic fashion as the value τ_{ad} increased. The range of frequencies produced by the CPG model should be adequate to allow a wide range of walking speeds. A CPG frequency of 1.5 Hz corresponds to a cadence of 90 steps/minute per limb, or a maximum net cadence of 180 steps/minute for a biped model. Because the amplitude of the CPG was dependent on both the values of q_t and τ_{ad}, a bode plot, which compares the amplitude of the CPG output to the frequency of the CPG, was used to analyze the amplitude response of the CPG output across frequencies of the CPG output (Figure 3.10). It was seen in this bode plot that the amplitude of the CPG output was lower at higher CPG frequencies, or smaller values of τ_{ad}. This was because the short time constant of the adaptation effect means that the neuron began to inhibit itself more

quickly and thus a lower maximum amplitude could be achieved. There appeared to be a discontinuity in the relationship between the CPG frequency and the amplitude of the CPG output at relatively high CPG frequencies and was particularly noticeable in Figure 3.10 when q_t = 0.75 or 1.0, and may represent some change in behavior of the CPG model when the CPG reached that particular frequency.

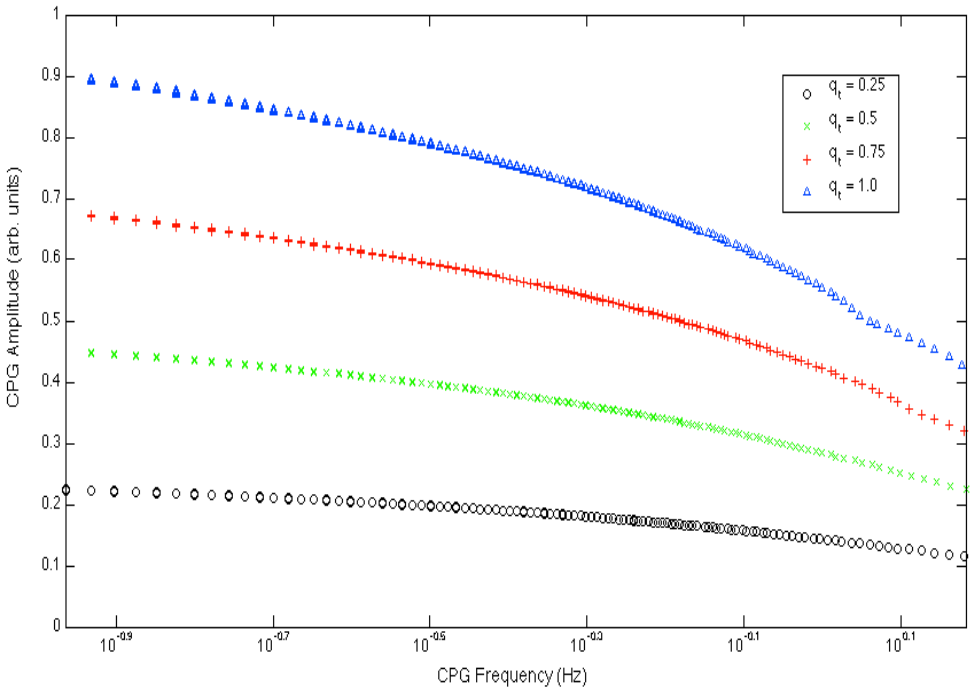

Figure 3.10: Bode blot showing the amplitude response of the CPG at various values of q_t.

Experiment #2: Determining the Natural Motion of the Pendulum System

Two sets of simulations were carried out to determine the natural frequency of the pendulum, when no neural input was provided to the muscles. For the first series of simulations the muscles were completely removed from the model, so that the only forces acting on the pendulum were the gravitational force and the damping torque. The second set of simulations were conducted with the muscles intact, such that the passive muscle forces also created a moment of force about the joint of the pendulum. For both sets of simulations the damping was

varied between 0 and 10 Nm.s/rad in increments of 1 Nm.s/rad, in order to determine what effect the level of viscous damping would have on the results.

For these simulations the average frequency of the pendulum was determined by calculating the time between successive zero crossings in the angular displacement of the pendulum (θ_P), since Fourier analysis was not appropriate due to the lack of a stationary signal. The angular displacements from these simulations were shown in Figure 3.11. It was observed that in both sets of simulations the natural ranging between 0.6 and 0.7 Hz, these values showed congruence with the natural frequency of the swinging human leg that was measured in vivo by Doke et al (2005). It was observed that the addition of muscles to the model caused an increase in the frequency of the pendulum of approximately 0.05 Hz. It was also observed that moderate amounts of damping led to an increase in the frequency of the pendulum. However when the damping was increased further, a decrease in the frequency of the pendulum was observed. These results were shown in Figure 3.12.

Considering the results of these simulations it was determined that a damping constant of 5 Nm.s/rad would be used in future simulations for this study. This damping value produced a movement pattern that would be expected to occur when the human leg was swung with no muscular activation. This assumption is difficult to justify empirically because it is usually not possible to have a human swing their leg without any muscle activation.

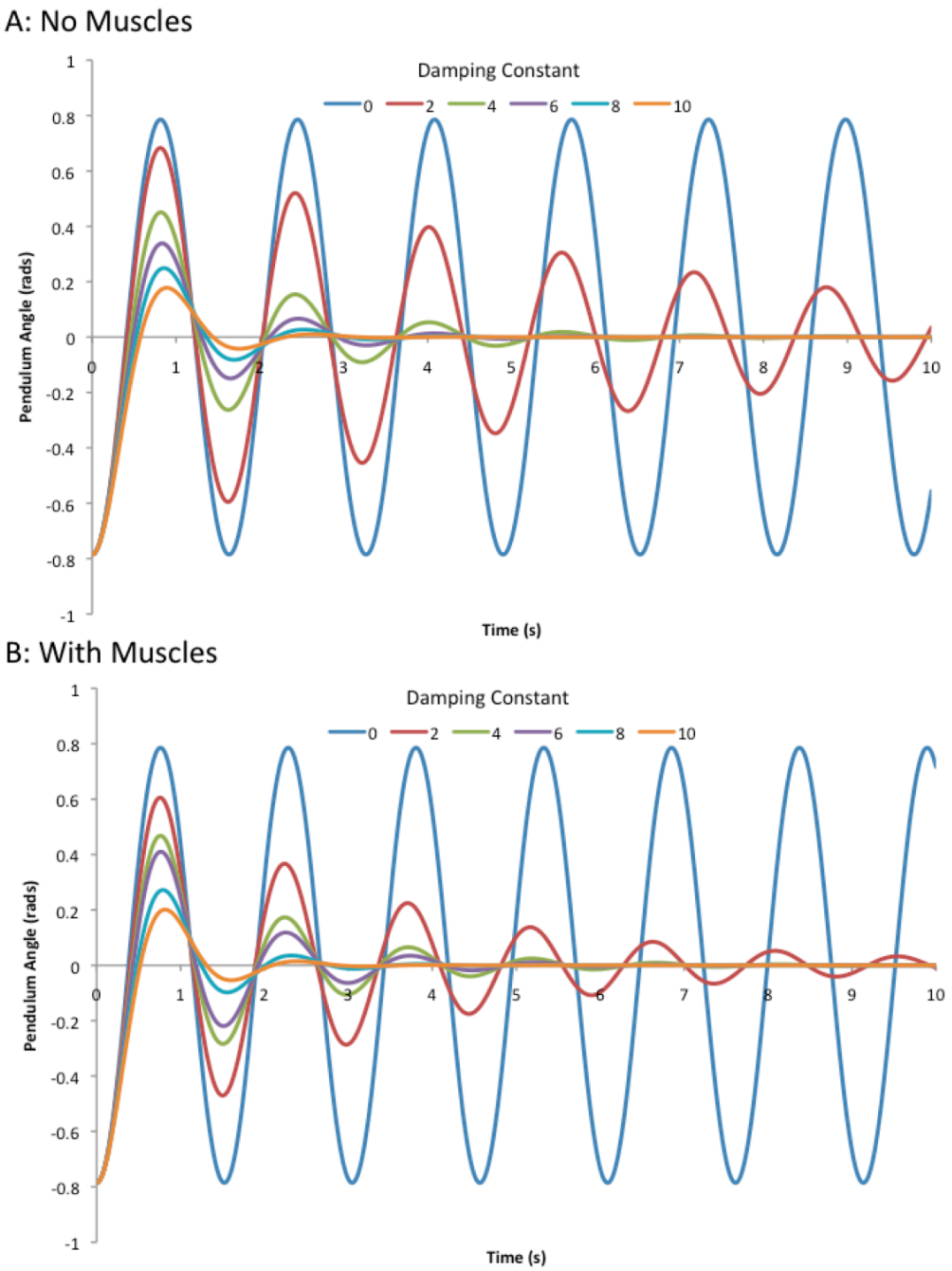

Figure 3.11: Motion of the damped pendulum, with no neural input with various damping constants. The top figure shows the motion of the pendulum with the muscles detached from the pendulum, while the bottom figure shows the motion of the pendulum with the muscles intact.

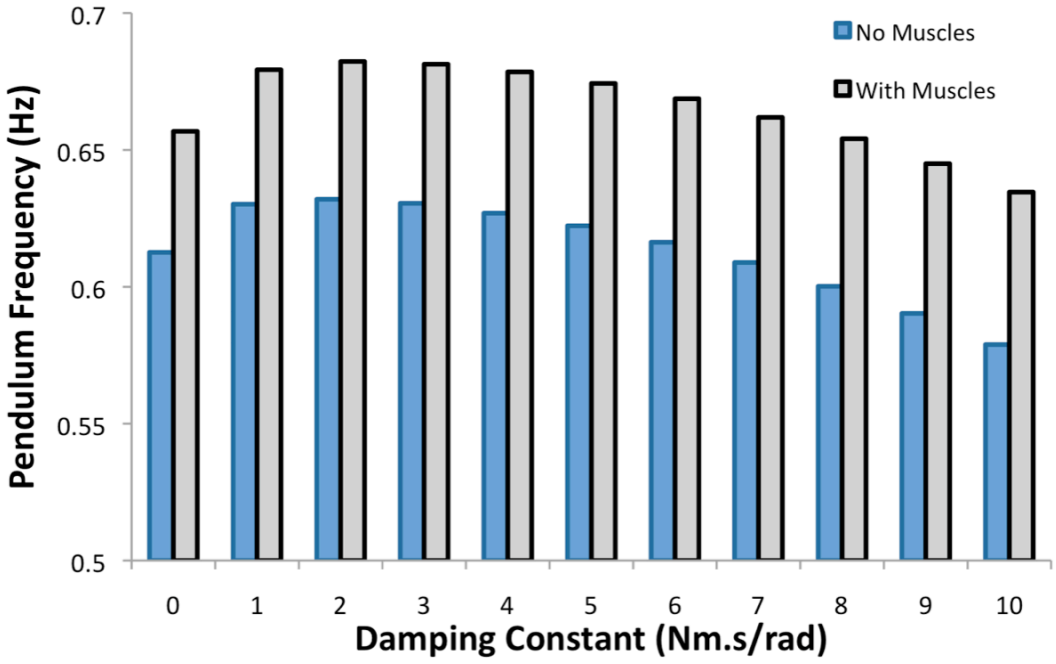

Figure 3.12: Frequency of the pendulum at various levels of damping, with and without the muscles attached to the pendulum, with no neural input.

Experiment #3: Feedforward Control of Rhythmic Limb Motion With a Central Pattern Generator

The set of CPG parameters that were tested in Experiment #1 of this chapter were repeated for this series of simulations, however this time the neural outputs created by the CPG model acted as muscle activation input signals to the muscle models, which produced a moment of force that drove the pendulum. To summarize, a total of 4500 simulations were carried out to determine the combined effects of the CPG amplitude and frequency on the motion of the pendulum system. The 4500 simulations were divided into 9 sets of 500 simulations where q_t was set to values between 0.125 and 1.125, in increments of 0.125. The value of τ_{ad} was increased from 0.01 to 5, in increments of 0.01 for each value of q_t. Each simulation used a 120s simulation time, of which the last 100s of the simulation were analyzed, thereby avoiding any effects on the pendulum's motion that were a result of the chosen initial conditions.

The motion of the pendulum was quantified in three ways, peak amplitude, frequency and phase relative to the CPG signals. The peak amplitude of the pendulum was determined by finding the highest positive peak in the angular displacement of the pendulum (θ_P) within the last 100s of the simulation. A discrete Fourier transform (DFT) algorithm was used to determine the power spectral density function (PSDF) of the θ_P over the 100s analysis period. The frequency with the peak power in the PSDF was determined for each simulation and chosen to represent the main frequency of oscillation of the pendulum. The phase of the pendulum's position relative to the CPG signals was determined through the use of a cross-correlation function between θ_P and a signal representing the net output of the CPG (CPG_{NET}), which was shown in Equation 3.14, this equation produces a single value represented the combined output of the CPG, with flexor activity being represented by a positive value and extensor activity represented by a negative value, to match the convention of θ_P.

$$CPG_{NET} = y_F - y_E$$

Equation 3.14

The cross-correlation function between CPG_{NET} and the angular displacement was carried out using Equation 3.15 (Nelson-Wong et al. 2009)

$$R_{xy}(\tau) = \frac{\frac{1}{N}\sum_{i=1}^{N}(x_i - \bar{x})(y_{i+\tau \cdot f_s} - \bar{y})}{\frac{1}{N}\sqrt{\sum_{i=1}^{N}(x_i - \bar{x})^2 \sum_{i=1}^{N}(y_i - \bar{y})^2}}$$

Equation 3.15

Where, N was the number data points in the analysis period (10000), τ was the temporal phase shift, f_s was the sampling rate of the signals (100 Hz) and x and y were the signals for which the cross-correlation was being determined (CPG_{NET} and θ_P). The phase shift between the neural signals and the mechanical motion of the pendulum was determined by finding the phase shift value (τ) that corresponds to the maximum correlation between CPG_{NET} and θ_P, this phase shift was then divided by the cycle time of the pendulum to allow for a normalized representation of the phase shift, that could be compared regardless of the pendulum's frequency.

Sample output from simulations where the motion of the pendulum was determined by the CPG model are shown in Figure 3.13, across various values of τ_{ad}. Graphs showing the peak amplitude of the pendulum's motion across all values of τ_{ad} tested were shown in Figure 3.14. Some discontinuities were evident in the relationship between τ_{ad} and the peak amplitude of θ_P, particularly when q_t was set to higher values. When q_t was set to 0.75 there was a large discontinuity noted when τ_{ad} reached 0.72s. These discontinuities have been observed in other studies of torque driven pendulums (Bryant and Miles 1990) and were attributed to a change in behaviour due to decreasing the frequency of the applied torque below the resonant frequency of the pendulum (ω_r). When q_t was greater than or equal to 1.0 there were a few simulations where a steady state oscillation was achieved where θ_P reached values greater than 180 degrees (π radians) however due to limitations with the angular conventions used the peak value of θ_P was set to π radians for these simulations.

There are several interesting results that can be observed in Figure 3.13. Firstly, there was an interaction between the neural and mechanical systems. This was observed most directly when higher values of τ_{ad} were used for the simulation, where the primary frequency of oscillation was observed to be similar to the frequency of the CPG signals, however there were

also oscillations in θ_P that were similar to the natural frequency of the pendulum. In Figures 3.14 & 3.15, it was observed that for all levels of q_t that were tested, there was a peak in the amplitude observed at relatively similar values of τ_{ad}, however this was not the same exact value for all values of q_t. To examine this further, a bode plot was made to analyze the amplitude response of the pendulum in response to the frequency of the CPG and is shown in Figure 3.15.

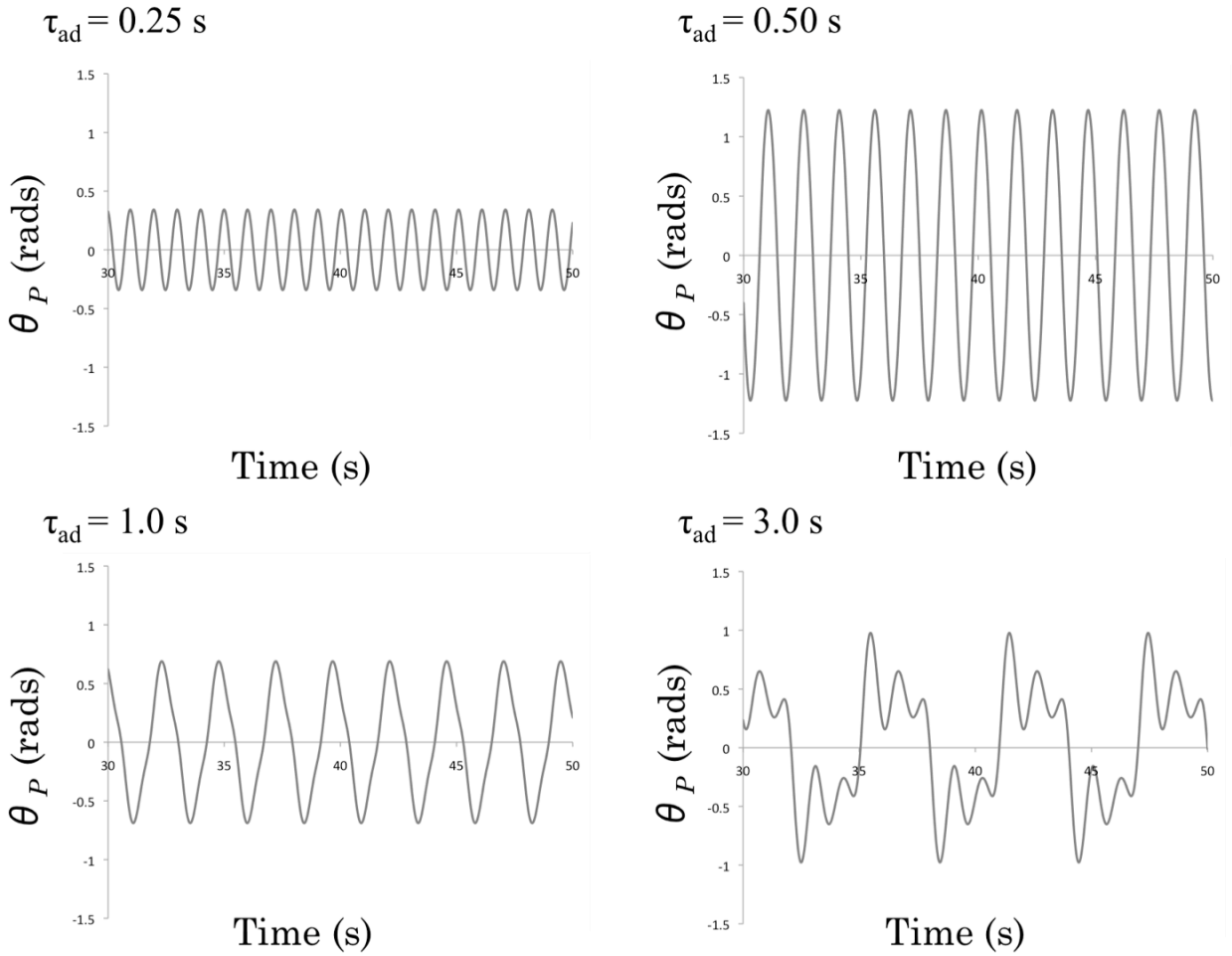

Figure 3.13: Examples of the angular displacement of the pendulum at various levels of τ_{ad}. All figures show 20s of simulation time with q_t set to 0.5 for all simulations shown. This figure illustrates how the natural frequency of the pendulum will be superimposed on the motion caused by the CPG if the frequency of the CPG is less than the natural frequency of the pendulum.

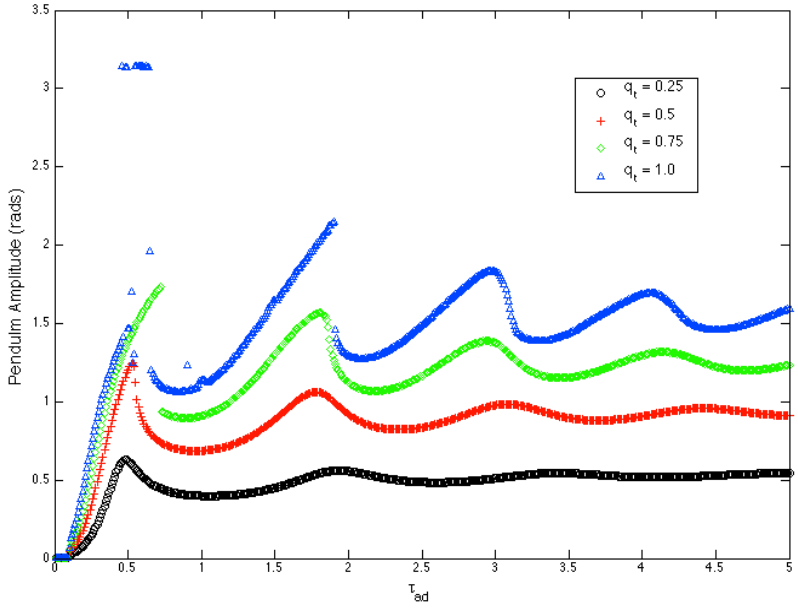

Figure 3.14: Pendulum's amplitude response to different values of τ_{ad}, at 4 different levels of q_t.

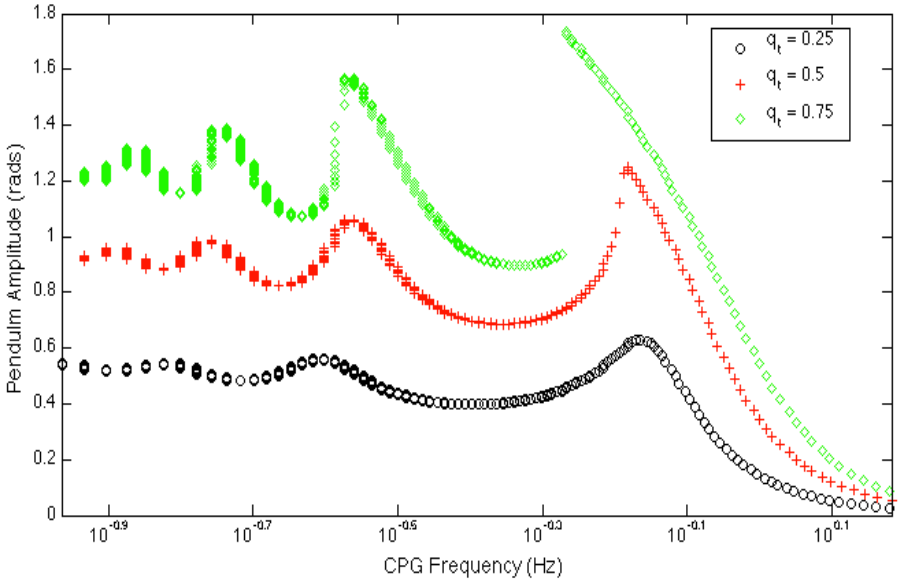

Figure 3.15: Bode blot showing the relationship between the frequency of the CPG output and the amplitude of the pendulum, with q_t at 0.25 (black circles), 0.50 (red crosses), and 0.75 (green circles).

The resonant frequency (ω_r) of the pendulum was determined for each value of q_t that was tested by determining the pendulum frequency where the pendulum had the greatest root-mean-square (RMS_E) energy. The formula used to determine the energy of the pendulum system is shown in Equation 3.16 (Bryant and Miles 1990). The values of ω_r for some of the various levels of q_t tested were shown in Figure 3.16; the resonant frequency of the pendulum was not calculated for simulations where the peak value of θ_P was greater than 180˚. A bode plot showing the value of RMS_E for various values of q_t was shown in Figure 3.17. To facilitate comparisons between different levels of q_t the frequency axis of the bode plot was normalized to the resonant frequency for each series of simulations. The analysis of this bode plot revealed the peak level of energy was observed at the resonant frequency for each value of q_t.

$$E = \frac{1}{2}\dot{\theta}_p^2 + 1 - \cos\theta_P$$

Equation 3.16

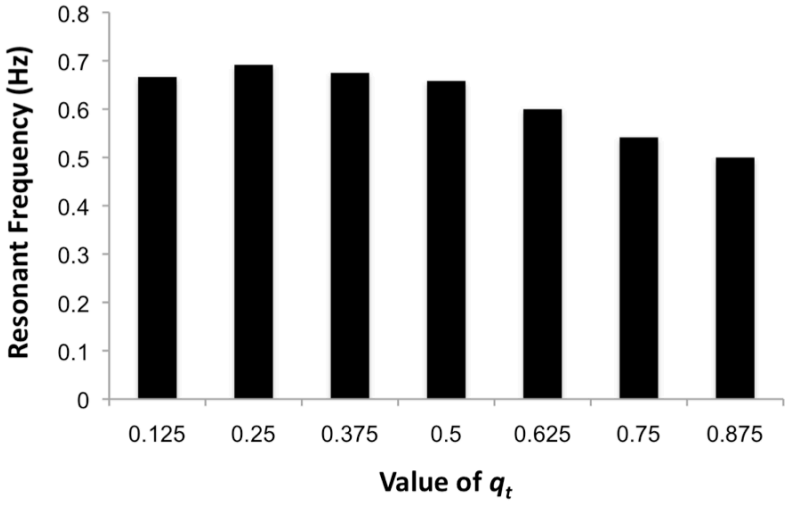

Figure 3.16: Resonant frequency (ω_r) of the pendulum at different values of q_t.

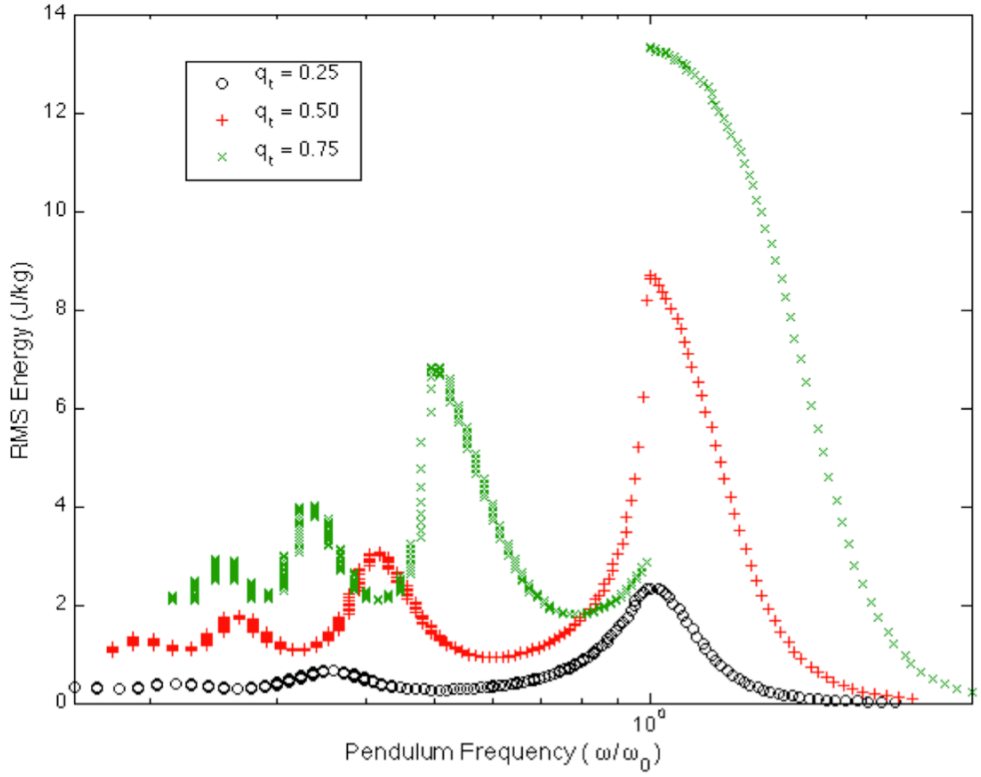

Figure 3.17: Bode plot with the frequency normalized to the resonant frequency of the system.

For all simulations carried out in this study the dominant frequency of the pendulum became entrained to the burst frequency of the CPG, which was observed from the direct relationship between the CPG frequency (ω_{CPG}) and the frequency of θ_P. Plots of these relationships were shown in Figure 3.18 for various levels of q_t. It was seen in Figure 3.18 that there was a very strong linear relationship between the frequency of the CPG and the frequency of the pendulum (R^2 = 0.9962). Additionally, the slope of the regression equation was very close to unity indicating that frequency of the pendulum is being directly determined by the frequency of the CPG output. It was also noteworthy that this relationship remained constant across all values of q_t tested.

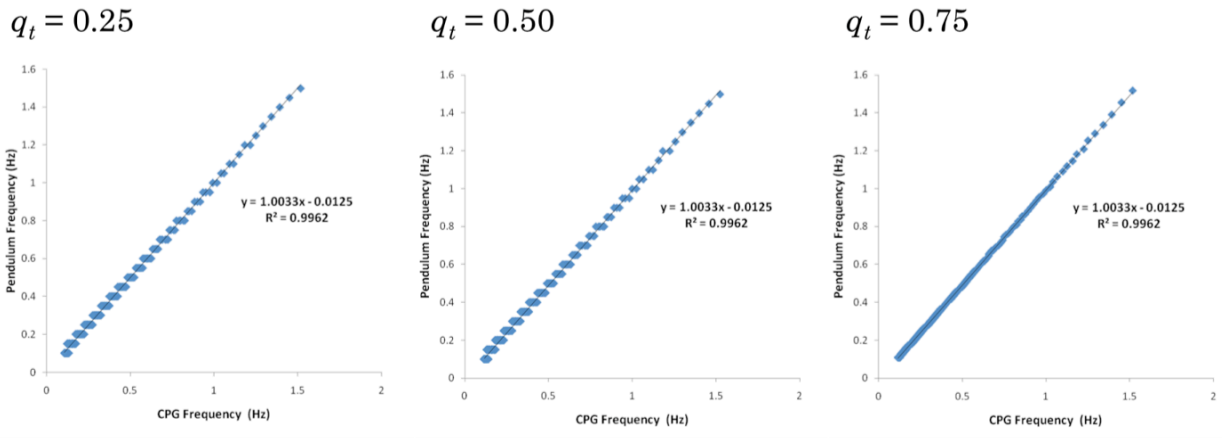

Figure 3.18: Comparison of the frequency of the CPG output and the primary frequency of oscillation of the pendulum. Results are shown for q_t = 0.25, 0.50 & 0.75.

It was seen in Figure 3.17 that when ω_{CPG} was greater than ω_r that the behaviour of the pendulum was quite predictable, but when ω_{CPG} was less than ω_r the behavior of the pendulum was not predictable. This was because when ω_{CPG} was less than ω_r the pendulum was still oscillating at a frequency of that was close to ω_r, with the frequency being created by the oscillations being superimposed on the natural motion of the pendulum, as seen in Figure 3.13.

The difference in phase between θ_P and ω_{CPG} was also analyzed. The phase shift between the two signals was found using the cross correlation function shown in Equation 3.15. The phase shift that was determined by the cross-correlation function was then divided by the cycle time of the pendulum to express the phase shift as a ratio of the cycle time. A phase ratio of either 0.0 or 1.0 indicates that θ_P and ω_{CPG} were exactly in phase, while a phase ratio of 0.5 indicated that θ_P and ω_{CPG} were completely out of phase. The results from this analysis were shown in Figure 3.19. It was observed that for values of ω_{CPG} greater than ω_r, the CPG output

was slightly output phase with θ_P, however as ω_{CPG} approached ω_r, the CPG output became more in phase with the motion of the pendulum. When ω_{CPG} was just greater than ω_r, the CPG becomes synchronized with the motion of the pendulum, however when the CPG was set to ω_r the CPG slightly leads the pendulum angle. A discontinuity occurred in the relationship when ω_{CPG} was equal to ω_r. The relationship between the phase ratio and ω_{CPG} became much more variable when ω_{CPG} was less than ω_r. As ω_{CPG} continued to decrease, the variability continued to increase and the phase ratio indicated that the CPG and angle of the pendulum became more out of phase.

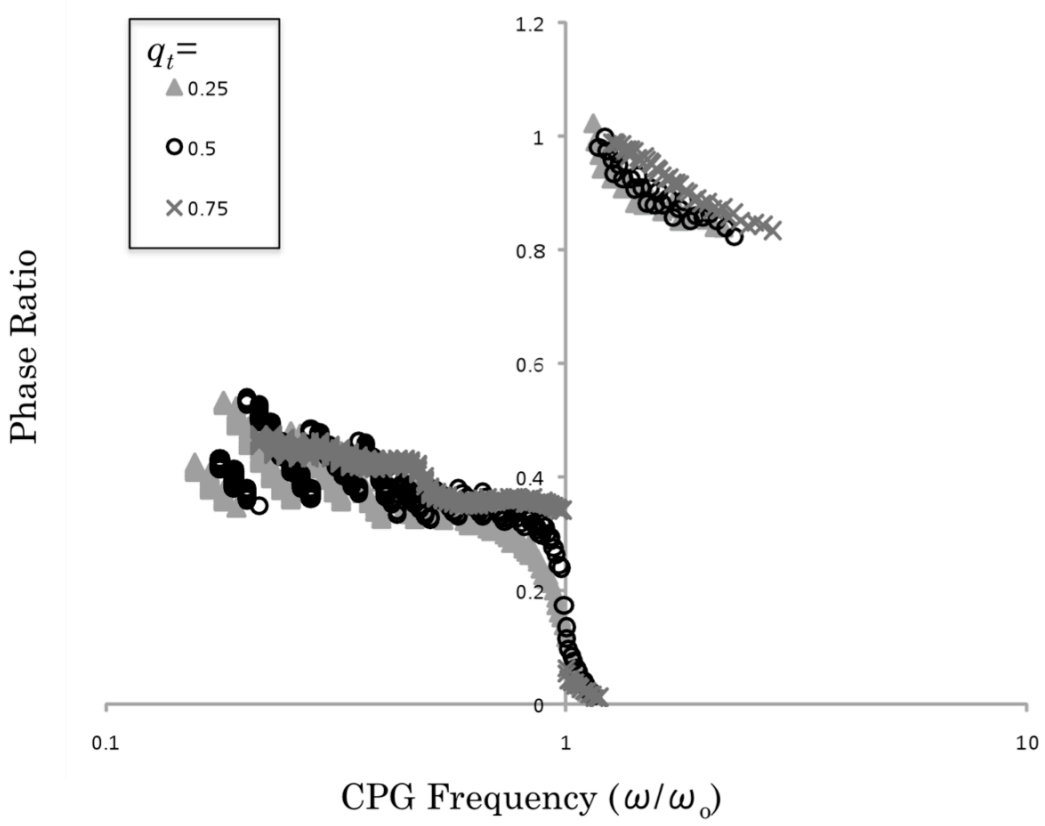

Figure 3.19: Phase ratio of the CPG and the angular displacement of the pendulum at various levels of q_t. A phase ratio of 0.0 or 1.0 indicates that CPG_{NET} was completely in phase with θ_P, while a phase ratio of 0.5 indicates that CPG_{NET} was completely out of phase with θ_P.

Experiment #4: Determining the Effects of Initial Conditions and Viscous Damping on the Motion of the Torque Driven Pendulum

To assess the effect of initial conditions of the simulation on the motion of the pendulum a series of simulations were carried out with the initial angle of the pendulum set to various angles. These simulations were carried out with the pendulum angle set to the following angles at the start of the simulation: -60°, -45°, -30°, -15°, 0, 15°, 30°, 45°, and 60°. Set values for the CPG properties were used throughout this series of simulations, with τ_{ad} and q_t both being set to 0.5. Once again the motion of the pendulum was assessed in terms of amplitude, frequency and phase relative to the joint torques. It was found that the motion of the pendulum was primarily dictated by the action of the CPG. As shown in Figure 3.20, the motion of the pendulum became synchronized with the CPG within one cycle, and that following the first cycle the motion of the pendulum was identical regardless of the pendulum angle at the start of the simulation.

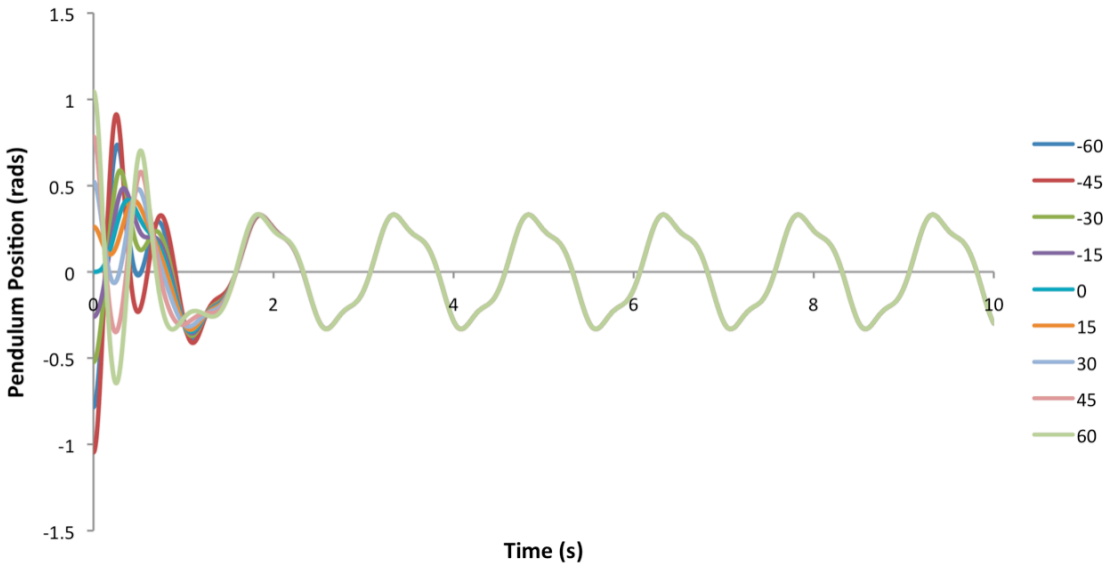

Figure 3.20: Motion of the pendulum with various initial conditions.

To determine the effect of the damping constant while the pendulum was being driven by signals from the CPG model; simulations were carried out with the damping constant being applied to pendulum being incremented from 0 to 20 Nm.s/rad, by 0.1 Nm.s/rad. The properties of the CPG were similar to the previous simulations, as were the variables analyzed, except the initial conditions were set to -30° and 0°/s, which was shown to have no effect on the motion of the pendulum in the previous series of simulations.

The amount of damping applied to the pendulum had very little effect of the overall motion of the pendulum, when the pendulum was being driven by signals from the CPG; the damping constant had no effect on the frequency of the pendulum, and only had a small effect on the amplitude of the pendulum's motion. A comparison of the motion of the pendulum with two different damping constants was shown in Figure 3.21.

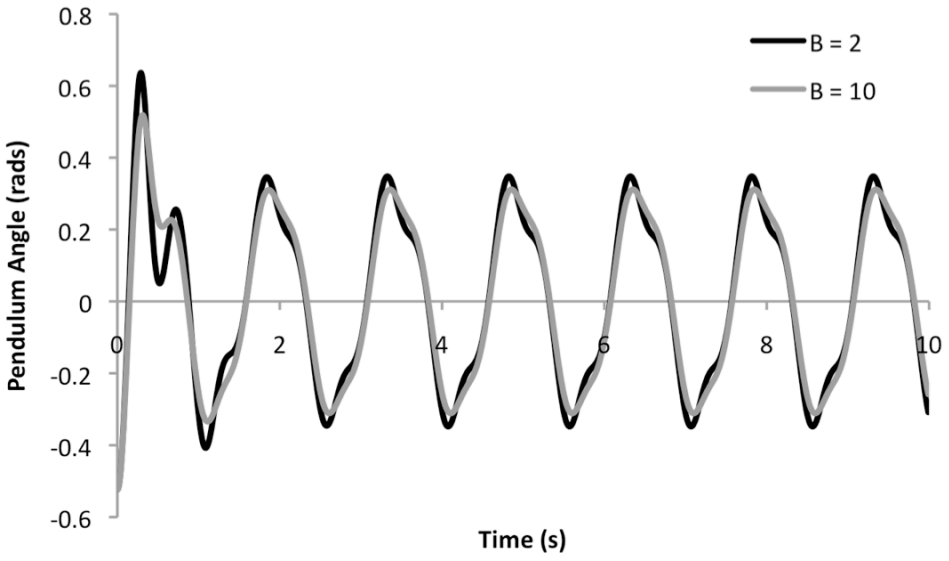

Figure 3.21: Pendulum motion with two different damping constants (B). The black line shows the motion of the pendulum when B = 2 Nm.s/rad, while the grey line shows the motion of the pendulum when B = 10 Nm.s/rad.

Experiment #5: Examining the Role of Muscle Attachment Properties on the Motion of the Pendulum System

The goal of the next set of simulations was to examine the effect of the mechanical properties of the system on the motion of the pendulum. To manipulate the mechanical properties of the system, the moment arm of the muscles driving the pendulum were altered by systematically adjusting the position of the proximal muscle attachment points. Two series of 300 simulations were carried out, with the horizontal distance between the proximal muscle attachment points and the revolute joint of the pendulum being varied between 0.01m to 0.3 m, in increments of 0.001m. In the first set of simulations, the resting lengths (l_o) of the muscles were set to be the same as all the previously described simulations. Therefore, moving the muscle attachment points would alter the portion of the active Force-Length curve that was used during the simulations. For the second set of simulations the resting length was adjusted such that the relative muscle length (l/l_o) was always the same as the previously described simulations and thus the effects seen were primarily due to the changes in the moment arm, instead of muscle mechanics.

These simulations were carried out with the same set of parameters for the CPG model, ($q_t = 0.5$, $\tau_{ad} = 0.25$s) which corresponded to a CPG frequency of approximately 1 Hz. The initial conditions of the pendulum were the same as those used in the simulations in experiment 2.

It was found that the horizontal distance between the muscle attachment and the joint had no effect on the frequency of the pendulum. There was also no effect on the frequency of the pendulum in the two different muscle conditions (Fixed Resting Length, or Adjusted Resting length). The amplitude of the pendulum's motion was dramatically altered by the muscle attachment location and by the muscle condition; a figure illustrating the pendulum's amplitude

across the range of muscle attachment distances tested is shown in Figure 3.22 for both muscle conditions.

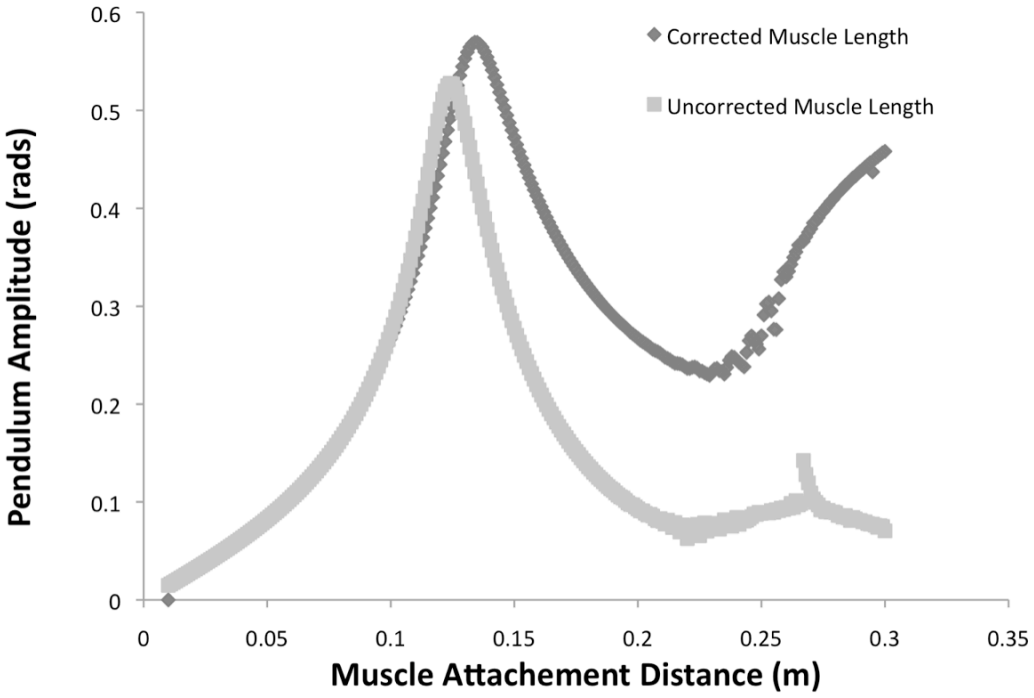

Figure 3.22: Amplitude of the pendulum motion compared to the horizontal distance between the muscle attachment points and the joint of the pendulum. Each point on the plot represents the results of a single simulation. The light curve illustrates the results when the resting length of the muscle was fixed, while the darker curve shows the results when the resting length was adjusted for the position of the attachment point.

Both muscle conditions resulted in very small pendulum amplitudes when the muscle attachment points were close to the revolute joint of the pendulum, due to the small moment arm. As the muscle attachment point increased in distance from the joint, the pendulum amplitude then increased, until maximum amplitude was observed when the muscle attachment distance was between 0.1m and 0.15m. Both muscle conditions increased at a similar rate, however the

peak pendulum amplitude was slightly higher for the condition where the resting length was adjusted to the muscle attachment location. After the peak pendulum amplitude was reached, a decrease in the pendulum amplitude was noted for both muscle conditions. In the simulations where the resting length was adjusted the amplitude of the pendulum stabilized and began to increase dramatically. In the simulations where the resting length of the muscles remained constant there was a dramatic decrease in the amplitude of the pendulums motion after the peak amplitude was reached. Simulations where the muscle attachment distance was greater than 0.3m were not possible because the motion of the pendulum became erratic in both muscle conditions, due to the large moment arm of the muscles.

Over the range of muscle attachment distances tested, there was a fairly linear relationship between the muscle attachment distance and the moment arm of the muscles (Figure 3.23). The effect of the muscle attachment distance on the muscle length and the active-force length coefficient of the muscle model were shown in Figure 3.24.

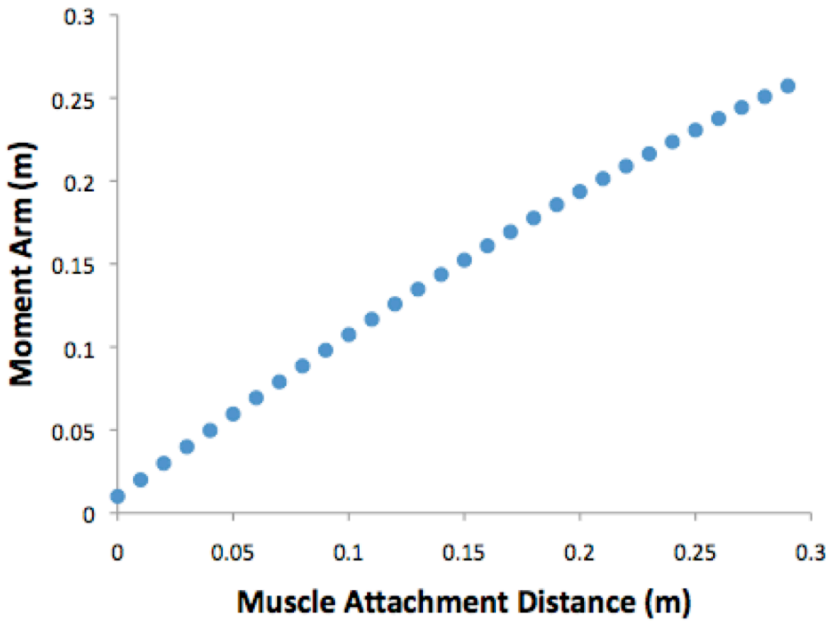

Figure 3.23: Moment arm as the muscle attachment distance increases. Moment arm is measured when the pendulum is in a neutral position.

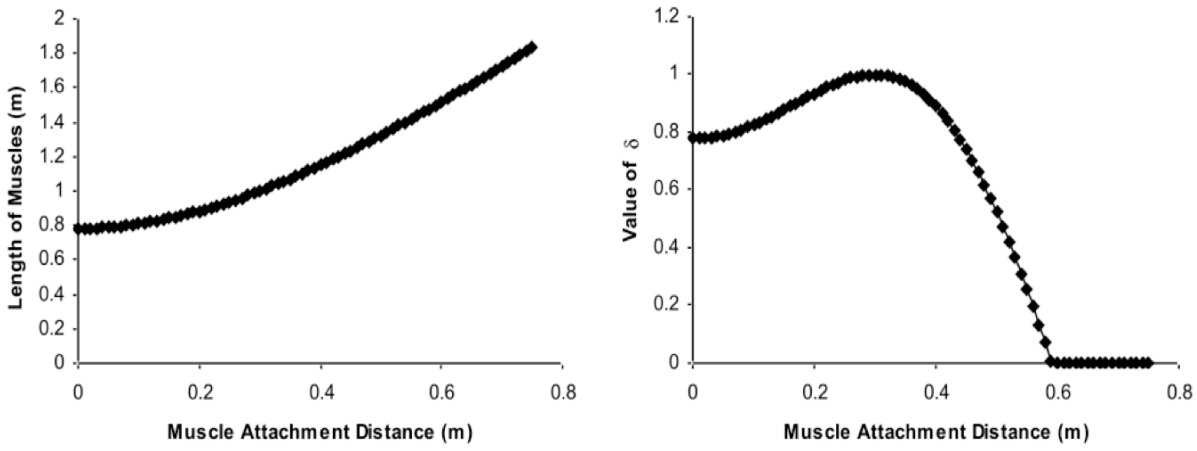

Figure 3.24: Length of the muscles in the model as a function of muscle attachment distance (Left), Value of δ (right), which is the gain of the active force length relationship, as a function of muscle attachment distance.

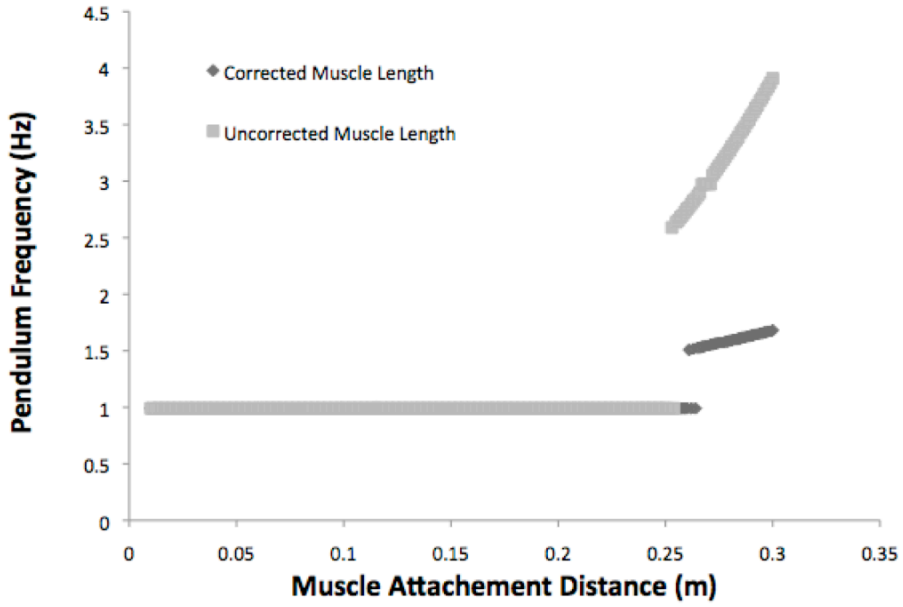

Figure 3.25: Frequency of the pendulum's oscillation across various muscle attachment distances. The light points illustrate the results when the resting length of the muscle was fixed, while the darker points shows the results when the resting length was adjusted for the position of the attachment point.

When the muscle attachment distance was greater than 0.25m, the movement became erratic for both muscle conditions, the motion of the pendulum showing dramatic changes in both amplitude and frequency. This result appears to be due to a combination of the large moment arm that was at these distances and the high levels of passive force developed by the muscles during these simulations. The components of the muscular moment for these simulations were shown in Figure 3.26. It can be seen from panel D of this figure that the largest component of the moment generated by the muscles was due to the passive muscle force, which had the largest contribution to the muscle force, particularly at higher muscle attachment distances.

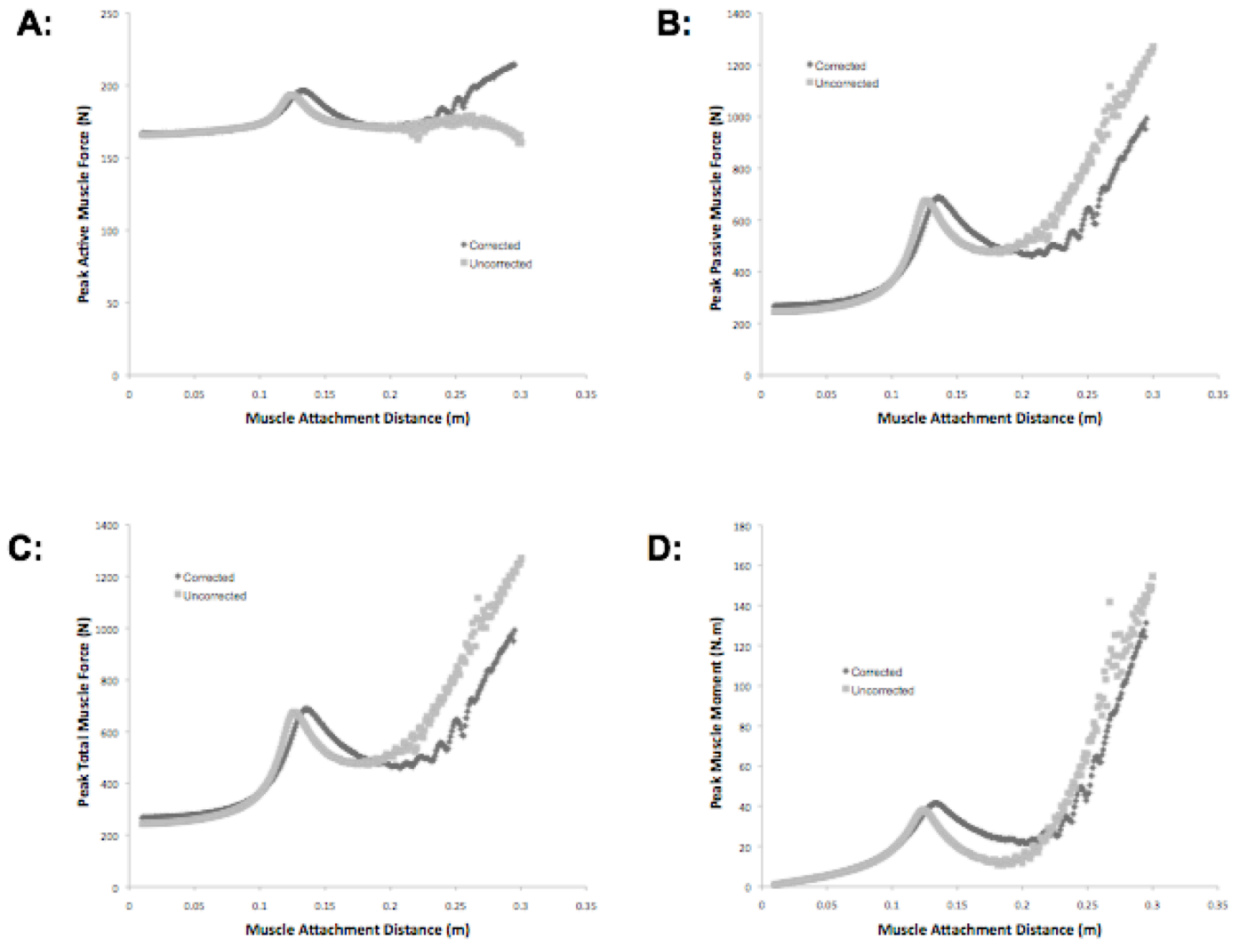

Figure 3.26: Components of the muscle moment during across the range of muscle attachment distances tested. A) Peak active muscle force, B) Peak passive muscle force, C) Peak Total muscle force and D) Peak muscle moment. The light points illustrates the results when the resting length of the muscle was fixed, while the darker points shows the results when the resting length was adjusted for the position of the attachment point.

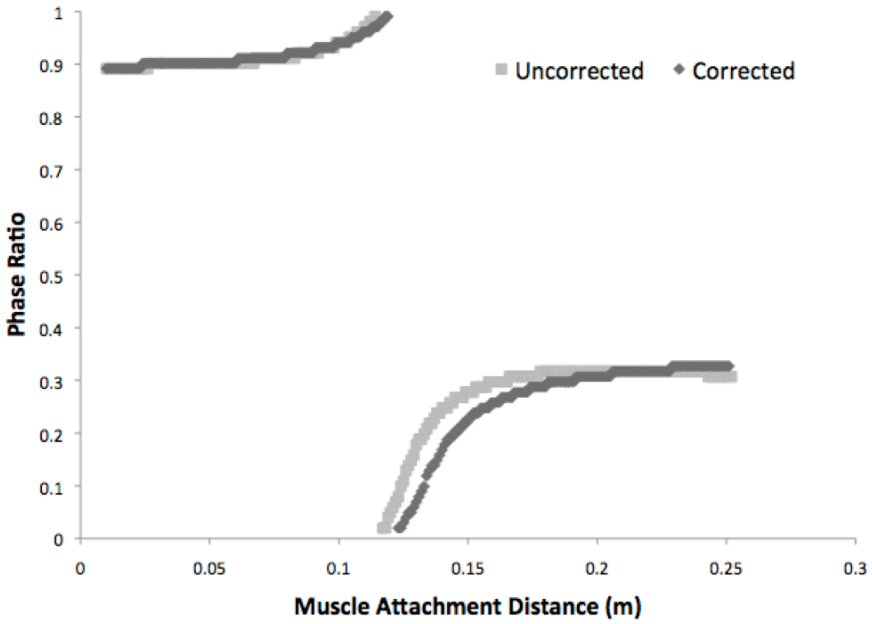

Figure 3.27: Phase ratio of the pendulum across various muscle insertion distances. The light curve illustrates the results when the resting length of the muscle was fixed, while the darker curve shows the results when the resting length was adjusted for the position of the attachment point.

The muscle attachment distance also affected the relationship between the phase of the pendulum and the CPG. The phase ratio across the range of muscle attachment distances that produced a stable oscillation were shown in Figure 3.27. At low muscle attachment distances the joint torque that was created by the muscles was close to being in phase with the motion of the pendulum, thus the joint torque aided the motion of the pendulum, which resulted in motion of greater amplitudes for these simulations. The pendulum's peak amplitude occurred when the CPG was perfectly in phase with the motion of the pendulum. As the muscle attachment distance continued to increase, the CPG output became more out of phase with the motion of the pendulum. There was little difference in the phase relationship between the two muscle conditions tested.

Discussion

In this study a simple CPG model was developed based on the work of Matsuoka (1985). The outputs of this CPG model were linked to a muscle model that produced forces that created a joint moment and drove a pendulum. The pendulum served as a model of the human lower limb and helped develop a better understanding of the feedforward mechanisms involved in the control of rhythmic limb movements, such as those used during walking, and the interaction between neural control systems and the mechanical apparatus involved in these types of movements. Results pertaining to the specific hypotheses made earlier in this chapter will be addressed individually in the following paragraphs.

The first goal of this study was to implement a CPG model based on some physiological principles and analyze the ability to control the magnitude and frequency of the output by altering some of the parameters of the model. It was decided to base this model on work previously published by Matsouka (1985) due to ease of implementation, the ability to construct networks of several neurons and the ability to incorporate feedback mechanism into the model, which was examined in the next chapter. As hypothesized it was found that the magnitude of the output of the CPG model could be directly controlled by adjusting the magnitude of the tonic input (q_t) that was provided to the model. The magnitude of the CPG model's output was found to increase linearly with the value of q_t. It was found that the frequency of the CPG was most easily controlled by manipulating the value of the time constant of the adaptation effect of the neurons (τ_{ad}), which specified how long the neurons' activity would remain active when the same inputs were present. As hypothesized, the relationship between the value of the time constant and the frequency of output from the CPG was not a direct relationship, but rather a peak frequency was observed after the value of τ_{ad} reached a critical value and then decayed in a

hyperbolic fashion, approaching 0 Hz as the value of τ_{ad} increased. It has been shown that stable oscillations occur in the Matsuoka oscillator when τ_{ad} is greater than τ_{rise} (Matsuoka 1985).

The methods of frequency and amplitude modulation of the CPG model may be entirely different than those observed in animal models. In the cat, it has been observed that the modulation of the frequency and amplitude of CPG output can be modulated by a single tonic signal, thought to originate in the Mesencephalic Locomotor Region, stimulating the CPG (Shik et al. 1969). The methods involved in frequency modulation of the Matsuoka were plausible, however it was likely that frequency modulation was accomplished by integrating sensory signals with the CPG to ensure that the walking pattern remained stable (Rossignol et al. 2006). The Matsuoka model of the CPG used in this chapter was a representation of a very simple neural circuit that produced an alternating oscillatory output between two neurons. Typically, neural oscillators are a poor model of the spinal circuitry involved in the control of locomotion, because it has been shown that the output of CPGs possess not only timing information for muscles, but also some basic information regarding the shape of the muscle activation pattern (Forssberg et al. 1980a; Forssberg et al. 1980b). It is often thought that these two features (timing and shaping) occur in two independent levels within the CPG and have been included in more complex models of CPGs (ie. (Rybak et al. 2006)), however for the purposes of this study the Matsuoka model of the CPG proved to be adequate to test the interaction between the feedforward control mechanisms and the mechanical features of the locomotor apparatus.

The second goal of this study was to analyze the effect of adding muscles and viscous damping on the natural motion of a pendulum. The natural frequency of a system is the frequency at which the system oscillates once it is set into motion. Although the natural frequency of a pendulum was easily calculated for a pendulum whose mass was distributed at the

distal end of the pendulum, there were no simple methods to directly calculate the natural frequency of a rod pendulum and the addition of muscles and damping torques would further complicate this issue. To test the effect of the muscles and viscous damping on the motion of the pendulum, a series of simulations were carried out that examined the frequency of the pendulum when no neural output was specified. As expected the addition of muscles to the model increased the natural frequency of the pendulum, likely as a result of the passive muscle forces causing an earlier reversal of the pendulum's motion during each cycle. The addition of viscous damping to the revolute joint of the pendulum led to an increase in the natural frequency of the pendulum (compare 0 Nm.s/rad to 1 Nm.s/rad in Figure 3.12). However, increasing the damping constant further led to a slight decrease in the natural frequency of the pendulum, due to overall slower motion of the pendulum. The natural frequency of the pendulum that was observed in this series of simulations showed close correspondence to the natural frequency of the lower limb that was calculated *in vivo* by Doke et al (2005).

It was found that the primary frequency of the pendulum's oscillation was directly determined by the frequency of the CPG model's output, which was determined by setting the value of τ_{ad}. A previous modeling study by Hatsopoulos (1996) also showed that the frequency of a mechanical system was directly determined by the frequency of a neural oscillator. The amplitude of the pendulum's motion was also affected by the motion of the frequency of the CPG's output, with the greatest amplitude of oscillation occurring when the frequency of the CPG was close to the natural frequency, or resonant frequency, of the pendulum. Interestingly the natural frequency of the system was affected by the magnitude of the tonic input to the CPG model (q_t), where higher values of q_t tended to cause a slight increase in the natural frequency of the system, which was likely due to the higher torques that were being applied to the pendulum

to reverse its motion more quickly, leading to a decreased cycle time. It was also found that the torques produced by this model were significantly higher than those measured in vivo by Doke et al (Doke et al. 2005) which led to extremely large angular displacement of the pendulum when the tonic input to the CPG model (q_t) was greater than 0.75. The maximum torque observed by Doke et al was approximately 70 N.m, while the model presented produced up to 85 N.m when q_t was set to 1.0.

The difference in phase between the movement of the limb and the phase of the CPG signals had not been extensively examined in previous work. Doke et al, (2005) showed that as the frequency of limb swinging increased that torque generated by the hip joint became more out phase with the hip joint angle, indicating that larger amounts of negative work was being performed to reverse the movement of the limb. Modeling work by Verdaasdonk et al (2005) showed that resonance tuning (oscillating the limb at the limb's natural frequency) to the limb occurred in a most efficient manner when the CPG signals are 90 degrees out of phase. Both of these studies however included the influences of sensory feedback mechanisms in their results. It was found that without feedback mechanisms influencing the motion of the pendulum, that the phase relationship between the CPG and the position of the pendulum was highly dependent on the frequency of oscillation. When the frequency of the CPG was less than the natural frequency of the pendulum the CPG signal tended to be out of phase with the pendulum's motion, but as the frequency of the CPG approached the natural frequency of the pendulum system the CPG and the pendulum became almost in phase with each other. As the frequency of the CPG continued to increase above the natural frequency of the pendulum the CPG became more out of phase with the pendulum but the CPG was actually leading the pendulum rather than lagging as

was observed when the frequency of the CPG was less than the natural frequency of the pendulum.

The entrainment between the CPG and the motion of the pendulum was shown to be very strong in all the simulations presented, which was shown through close matching of the frequency of the pendulum and the CPG output. The entrainment between the CPG and the pendulum was most evident in the series of simulations that were carried out to test the effect of the initial conditions on the motion of the pendulum, where the pendulum became entrained to the CPG's output within a single cycle, regardless of the initial angle of the pendulum.

When the CPG model was driving the pendulum, the amount of viscous damping had little effect on the motion of the pendulum, with increased damping only leading to a small decrease in the peak angular displacement of the pendulum. The primary reason for adding damping to the pendulum was to require the constant addition of energy to the system, as was required to achieve progression in the forward direction during walking. Therefore the damping moment represented forces that performed negative work during walking, such as the braking force following ground contact (White et al. 2008). Light damping was also required to ensure computational stability during the forward integration of the equations of motion, that was required to carry out forward dynamics (Anderson and Pandy 1999). As mentioned previously it was difficult to justify the level of damping that was used in this model empirically since it was difficult to assess the level of damping that would be present in the human joints *in vivo*.

The series of simulations where the muscle attachment distances were altered revealed some interesting findings regarding the role of muscle dynamics in the control of rhythmic limb movement. Increasing the muscle attachment distance altered both the active force-length and passive force-length relationships, and therefore altered the moment that was applied to the

pendulum. The maximum isometric force that could be developed in skeletal muscle occurred when there was an optimal level of overlap between actin and myosin fibres (Zajac 1989). The peak muscle force coincided with the peak amplitude of the pendulum's displacement. The passive muscle force increased dramatically as the muscle attachment distance increased, which contributed to a higher total muscle force. To further investigate the effect of the muscle dynamics on the motion of the pendulum a series of simulations were carried out where the resting length of the muscle was adjusted to be the same relative length for each muscle attachment distance. Changing the resting length of the muscles to be similar relative to the muscle resulted in only minimal differences compared to when the resting length was held constant. This could indicate that the major changes in the peak amplitude of the pendulum were due to changes in the moment arm, rather than the difference in muscle properties. The biggest contributor to the increased muscle force in each series of simulations was the passive muscle force. Due to the large passive muscle forces the amplitude of the pendulum's displacement was limited and thus the range of the active force-length curve that was utilized.

One of the primary goals of this study was to develop a set of models that will be used to investigate the interaction between neural and mechanical systems during locomotion; these models include the CPG model that was based on the work of Matsuoka and the Hill-type muscle model and combination of these models with a computational model of a mechanical system. This set of models will be instrumental for the development and implementation of other models that will be presented later in this thesis. The simulations in this study showed how the frequency of rhythmic limb movements could be controlled through the use of feedforward control mechanisms. Strong entrainment was observed between the output of the CPG model and the motion of the pendulum model in all the simulations that were carried out for this study. While

setting the frequency of the CPG could control the frequency of the pendulum's motion, the amplitude response of the pendulum was only predictable when the frequency of the CPG was less than the natural frequency of the pendulum. This study also found that the resonant frequency of the coupled CPG was affected by the attachment of muscles, the amount of damping applied to the pendulum, and the amplitude of the CPG signals. This study also examined the sensitivity of the model to different muscle attachment properties and found that the motion of the model was not overly sensitive to the properties of the muscle model, however the moment arm of the muscles led to a significant increase in the amplitude of the model.

Chapter 4: Effect of Muscle Stretch Feedback on the Control of Rhythmic Limb Movements: a neuromechanical simulation.

Introduction

Feedback from sensory systems, particularly from muscle receptors, is critical for the production of rhythmic limb motions such as walking. Although it has been shown in both animal studies (Grillner and Zangger 1984) and in a human patient (Lajoie et al. 1996) that walking can occur in the absence of sensory feedback from muscle receptors, the walking pattern that is observed differs substantially when compared to the normal walking pattern. In the human patient there was an increased dependence on other sensory systems, particularly the visual system. Although feedback has been implemented in a number of neuromechanical models, the methods that have been used to do so have varied widely. The goal of this study is to evaluate how a feedback system based on a stretch reflex interacts with a feedforward mechanism based on a central pattern generator (CPG).

Very few studies have investigated the integration between feedforward and feedback controls for rhythmic limb movement. Kuo (2002) showed that a hybrid control system, consisting of both feedback and feedforward mechanisms proved to be ideal for controlling rhythmic movements. Feedforward systems have the advantage that they can be easily adjusted to achieve a desired rhythmic kinematic pattern, but they are unable to cope easily when the system is perturbed. Feedback systems can respond to perturbations however they are reliant on knowing the exact state of the system at all times, and thus are susceptible to errors due to sensor noise or delays in the feedback system. Kuo (2002) showed that a system was able to maintain

the most stable rhythmic motor pattern and respond most effectively to perturbations when a combination of feedforward and feedback mechanisms was used.

A number of previous studies have been carried out to analyze the effect of feedback on the motion of an oscillating system that is driven by an oscillator model such has a CPG (Hatsopoulos 1996; Iwasaki and Zheng 2006; Simoni and DeWeerth 2007). These models have integrated a neural control model with a representation of a mechanical system with a single degree of freedom. Feedback from the position of the mechanical system was used in these simulations to alter the output of the CPG and consequently the motion of the mechanical system. The feedback used in these studies has typically been negative feedback from the position of the mechanical system to inhibit one of the half centres of the CPG. The efferent neural drive is then altered resulting in a change to the motion of the system. It has been shown that this type of feedback leads the mechanical system to oscillate at the systems' natural frequency, when a hybrid control system was used (Williams and DeWeerth 2007). This phenomenon is known as sensory entrainment and has also been observed in more complex neuro-mechanical models such as the model presented by Taga (1991). These studies have all used negative feedback regarding the position of the system to force the system; very few studies have analyzed the effect of different feedback schemes. A recent study by Williams and DeWeerth (2007) used positive feedback mechanisms where feedback that also originated from the position of the mechanical system, and used these mechanisms to control the motion of the pendulum. It was found that this type of feedback mechanism system is also capable of inducing sensory entrainment to the natural frequency of the mechanical system, and was able to do so over a greater range of control system parameters (Feedback gains, etc.). All of these studies, which have investigated how sensory feedback leads to entrainment between neural and

mechanical systems, have only used direct positional feedback and have not used information that would be physiologically provided by muscle receptors. Another drawback to these studies is that the effector system which causes movement of the mechanical systems has neglected the dynamics that are involved in muscle contraction (force-velocity & force-length relationships).

One of the goals of this study is to investigate the potential for stretch information from simulated muscle spindle models to lead to sensory entrainment between neural and mechanical systems. Muscle spindles provide information not only about the stretch of a muscle but also the velocity of the stretch. It is unknown how this information will affect the entrainment between neural and mechanical systems. The following sections will examine the structure and function of muscle spindles and will examine different approaches that can be used to model muscle spindle output.

Muscle Spindles

Muscle spindles are specialized sensory receptors that are embedded in parallel with muscle fibres (extrafusal fibres) in skeletal muscle, and have tendinous attachments within the structure of the muscle. In the middle of the tendinous attachments is a contractile muscle fibre (intrafusal fibre), which is innervated by γ-motor neurons. The role of the γ-motor neuron is to maintain tension in the intrafusal fibre during muscle contraction, and is co-activated with the α-motor neuron, which innervates the extrafusal fibre (Prochazka et al. 1985). The intrafusal fibres wrapped by sensory endings of Ia afferent neurons, which are sensitive to stretching of the intrafusal fibre. Additionally, there are different types of intrafusal fibres that exist in each muscle spindle with different sensitivities to changes in length or velocity, these include dynamic nuclear bag fibres which are primarily sensitive to changes in velocity, static nuclear bag fibres which are sensitive to changes in both length and velocity and nuclear chain fibres which are

primarily sensitive to changes in length. All of these intrafusal fibres trigger type Ia and type II sensory afferents, with the exception of dynamic nuclear bag fibres which only trigger type Ia sensory afferents (Pearson and Gordon 2000).

When a muscle is stretched, there is an increase in both Ia and II afferent activity, which has been shown to code both the velocity and the magnitude of the stretch (Pearson and Gordon 2000). If a muscle shortens quickly, without the activation of the gamma-motor neuron, the spindle activity will quickly diminish since tension is quickly lost in the sensory region of the receptor. Therefore the essential feature that must be included when modeling the receptor is that the output of the receptor must respond to changes in muscle length and muscle velocity, while also showing a decrease in activity when the muscle suddenly becomes slack. To communicate with other portions of the model, the muscle spindle should output a continuous signal that roughly correlates to the firing rate of the sensory neurons.

Modeling Muscle Receptors

This section will focus on analyzing different methods to represent muscle receptors in a neuromechanical model and determine which method would best suit the needs of the current model. The goal in modeling muscle receptors for this thesis is to create a transfer function that maps appropriate inputs (muscle length and velocity for spindles, and muscle force for GTOs), to a time series signal that would represent the firing rate of the afferent neurons from that receptor. Before considering which approach to use when modeling muscle spindles, it is important to consider the function of muscle spindles. In previous work there have been attempts to model the activity of Ia neurons based on muscle length and velocity information. Three primary methods have been previously used to represent the output of muscle receptors:

Linear transfer functions – These are the most simple muscle spindle models, simply consisting of a linear combination of the stretch velocity of the muscle and the length of the muscle. These models do not incorporate any dynamics of the muscle spindle outputs (Matthews and Stein 1969; Paul et al. 2005).

Non-linear transfer functions – These representations typically begin with a linear combination of muscle velocity and length, however they also include a non-linear model based on the dynamics of muscle spindle output. This is usually accomplished by a frequency domain transformation of the weighted sum of the muscle velocity and length. Examples of models that have this approach include those proposed by Chen and Poppele (1978), Houk et al. (1981), and Hasan (1983).

Non-linear models, based on physiological behaviour of muscle receptors - These models attempt to predict the length of the sensory region in the spindle by using techniques similar to a Hill-muscle model. It is thought that these methods would provide better estimates of Ia activity, however these models are quite onerous to implement in a large-scale model (Hulliger et al. 1985; Cheng et al. 2000).

Despite a number of previous researchers developing models to predict Ia output based on muscle length and velocity, there has been only one study that has compared the output of a muscle spindle model to activity measured from Ia afferents during locomotor activity (Prochazka and Gorassini 1998). This study compared six different models of muscle spindle output to measured Ia activity over a step cycle and found that all of the models tested provided relatively good matching when compared to the ensemble firing rate of Ia afferent neurons of the hamstring muscle during cat locomotion. A few of the methods tested were able to match the firing rate of the Ia neurons very closely, particularly models that introduced a non-linearity in

the velocity term. Raising the velocity term by a power of 0.5 or 0.6 provided the best fit to the firing rate of the spindle discharge collected from animal locomotion (Prochazka and Gorassini 1998).

For the implementation in the neuromechanical model in this thesis, the muscle spindle model should be relatively simple as it is not desirable to significantly increase the computational demands of the neuromechanical model to implement the muscle spindle model. The muscle spindle model used for this research will be a transfer function that maps appropriate inputs (muscle length and velocity for spindles) to a time series signal that represents the firing rate of the afferent neurons from that receptor. The spindle transfer function that is used in the neuromechanical model presented here is based on the function that Prochaska and Gorassini (1998) found was the best match to the ensemble firing rate of neurons recorded during locomotion in cats.

Goals and Hypotheses

The overall goal of this study was to create a neuromechanical model that will enable simulations to be carried out which will test the interactions between neural and mechanical systems when a combination of feedback and feedforward are used for controlling rhythmic limb movements. The feedback and feedforward control mechanisms will be based on the well known stretch reflex which induces a muscle that is stretched quickly to contract and inhibits the contraction of the antagonist muscle (Pearson and Gordon 2000). This work will expand on previous simulations including feedback pathways that are based on known neural pathways and by including feedback from simulated muscle spindles, with both a stretch and velocity component. Specific simulation goals and hypothesis related to these simulations are listed below.

Goal 1:

The first goal of this study was to create a muscle spindle model that could be used in future neuromechanical simulations and test how the output from this muscle spindle model would interact with the CPG model that was developed in Chapter 3. It was hypothesized that due to the circuitry involved in the CPG that facilitates mutual inhibition, excitation of one of the half centre (HC) neurons by the spindle model output would lead to prolonged excitation of that HC neuron and inhibition of the opposite HC.

Goal 2:

The second goal of this study was to assess the ability of a feedback only system to control the motion of the pendulum system. To accomplish this goal the magnitude of the feedback from the muscle spindle models was systematically manipulated, while the feedforward control mechanism was turned off. Since it is known that that the Matsuoka oscillator should synchronize to the frequency of input signals (Williams and DeWeerth 2007), it was expected that the oscillations would be close to the natural frequency of the pendulum. It was expected that the properties of the HC neurons in the model will also affect the frequency of the pendulum's motion, however this effect is not expected to be large. It was expected that the amplitude of the pendulum's motion would be primarily dictated by the magnitude of the feedback signal.

Goal 3:

The third goal of this study was to determine how the modeled feedback mechanisms would interact with the feedforward CPG model to control the motion of the pendulum system. The weight of the feedback gain was systematically manipulated, such that various combinations of feedforward and feedback were used to control the pendulum. It was hypothesized that the

frequency of the CPGs output will be primarily determined by the frequency of the feedback signals rather than the time constant of the adaptation effect when only feedforward mechanisms are used, as was shown in Chapter 3. Based on the results from Chapter 3 it was expected that the frequency of the pendulum would closely match the frequency of the CPGs output.

Goal 4:

The goal of the next series of simulations for this study was to analyze the effect that the gains of the spindle model (velocity and length gains) and the feedback delay has on the motion of the pendulum. It was hypothesized that the gain of the velocity terms of the spindle model would have a significant impact on the motion of the pendulum with higher velocity gains leading to an increase in the frequency of the CPG and the pendulum, while increasing the gain for the length input would have little impact on the frequency of the CPG or the pendulum but would affect the amplitude of the motion. It was hypothesized that changing the transmission delay of the spindle model will have little effect on the frequency or amplitude of the CPG or the pendulum however the phase relationship between the pendulum and the CPG would be altered.

Goal 5:

The goal of the final series of simulations was to compare how the various control strategies modelled are able to cope with a mechanical perturbation to the pendulum. To accomplish this, a small force was applied to the bottom of the pendulum at a set interval and the time that was required for the pendulum to return to the normal periodic pattern was determined. This method of applying the perturbation will allow for an analysis of a wide variety of responses due to the fact that the direction of the applied force will not always match the direction of the pendulum's motion (some of the perturbations will aid the pendulum's motion, some will resist the pendulum's motion).

Methods

Brief descriptions of the models used in this study are presented in this section. Some of the models used in this chapter were presented in greater detail previously in the thesis. Detailed descriptions of the simulations that were carried out for this study are found in the next section and are presented in conjunction with the simulation results.

Muscle Spindle Model

The muscles' feedback signals originated from muscle spindle models based on the work of Prochaska and Gorrasini (1998). This model consisted of a nonlinear transfer function of the muscle length and velocity. The following equation was used to first estimate the muscle spindle output.

$$MS_{OUT} = K_{vel} \cdot v_{mus}^{p} + K_{len} \cdot l_{mus} - 1$$

Equation 4.1

Where MS_{Out} was the muscle spindle output, v_{mus} was the stretch velocity of the muscle, p was an exponent for the nonlinearity of the muscle velocity relation, l_{mus} was the length of the muscle and K_{vel} and K_{len} were gains for the muscle velocity and length components respectively. For *Equation 4.1*, the muscle velocity term must be positive to give a real output (since $p < 1$), a positive muscle velocity corresponded to muscle stretch. If the muscle was shortening, the muscle spindle model would only output a value based on the current muscle length and not the velocity of shortening.

The combined output was then subjected to a first order delay, which was given in the frequency domain by:

$$H(s) = \frac{1}{\tau s + 1}$$

Equation 4.2

Where τ was the time constant for the delay and *s* was the Laplace operator. The final output was then, where K_{IA} is a gain for the overall muscle spindle output, which was always set to 1.0, since the gains of these signals were modified by the overall feedback gain (FB_{GAIN}):

$$S = K_{IA} \cdot MS_{Out} \cdot H(s)$$

Equation 4.3

The spindle output was then subjected to a 15 ms transmission delay to represent the dynamics in the firing rate of the muscle spindles. The spindle model response to a short ramp stretch was shown in Figure 4.1.

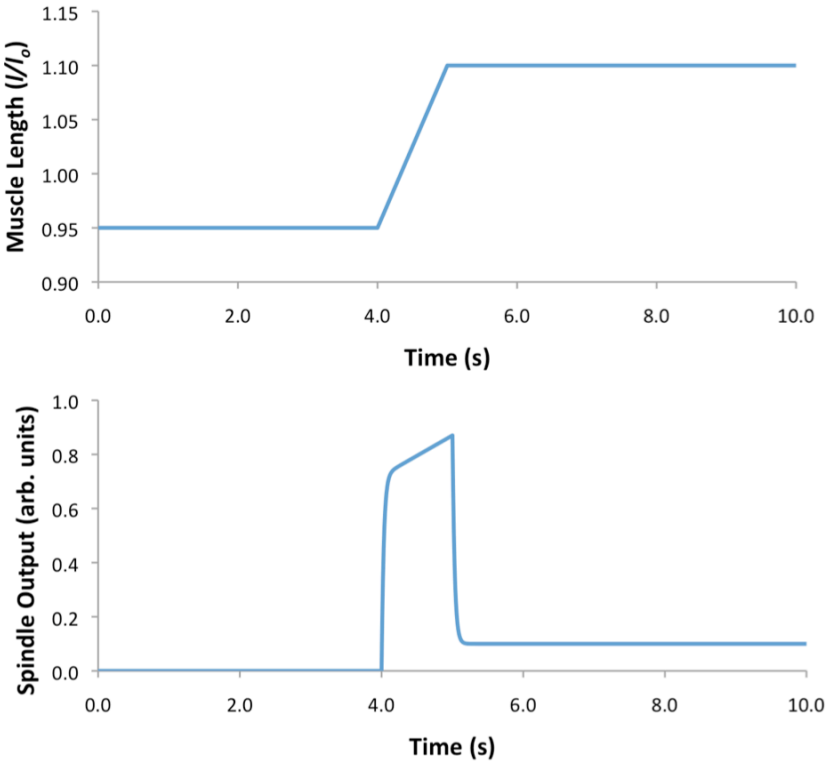

Figure 4.1: Spindle response to a step stretch in a muscle. The parameters of the spindle model were set to the following: K_{vel} = 2 and K_{len} = 1, and τ = 15 ms.

Integration of Feedback Signals with the CPG Model

The feedback system implemented was a modified version the stretch reflex, where a stretch of a muscle led to increased muscle spindle output, this signal was then mono-synaptically transmitted onto the α-motor neuron of the same muscle that was stretched, causing a muscle contraction to occur in the stretched muscle (Pearson and Gordon 2000). The Ia output triggered from the stretched muscle also synapsed on an inhibitory interneuron which inhibited the antagonist muscle of the stretched muscle (Pearson and Gordon 2000). This mechanism was implemented with the muscle spindle model and the pendulum model. The connections of the Ia neuron signals to the neurons in the CPG model are shown in Figure 4.2.

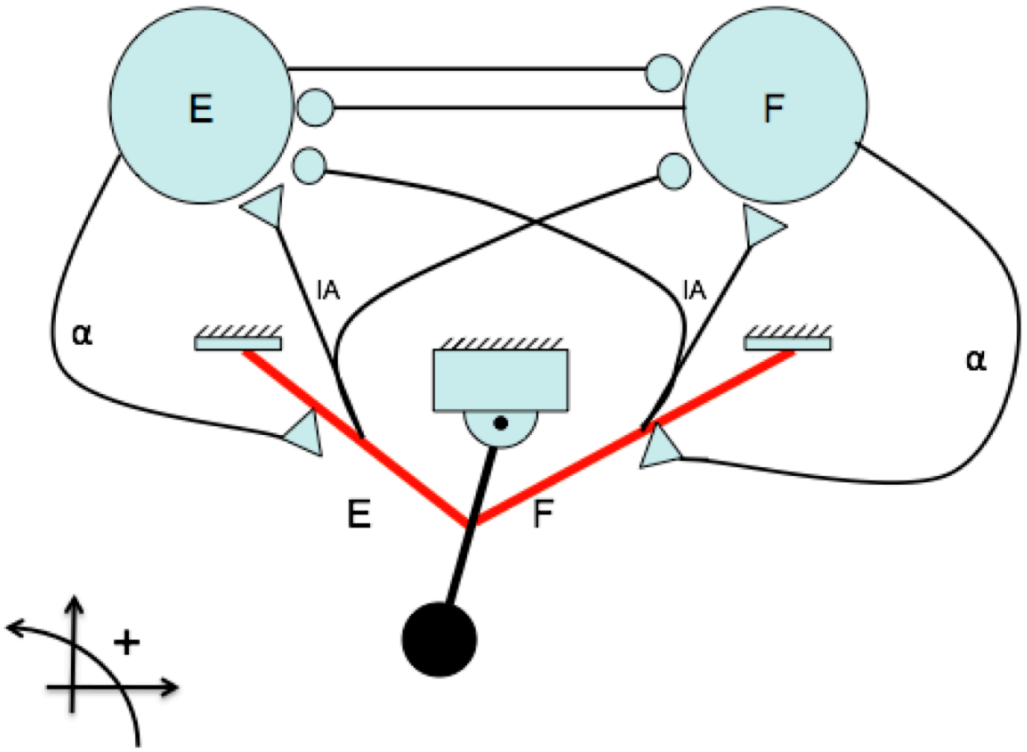

Figure 4.2: Feedback mechanisms used to control the pendulum system. The 'E' represents the extensor half centre neuron, and extensor muscle; while the 'F' represents the flexor half centre neuron and muscle. The round synapses represent inhibitory connections, while

triangular synapses indicate exhibitory connections. The α represents the α-motor neuron, and IA represents the primary afferent neurons from the muscle spindle model.

Prior to the integration of the spindle model outputs and the CPG model, the spindle outputs were subject to a delay of 15ms (unless stated otherwise) to mimic any synaptic delay in the monosynaptic stretch reflex (Pearson and Gordon 2000). The signals from the muscle spindle model were integrated with the CPG model by adding an additional term to the calculation of the inner state of the HC neurons, as shown in Equation 4.4.

$$\dot{u}_F = \frac{1}{\tau_{rise}}(q_t - u_f - \beta v_f - wy_E - FB_{gain}Q_{fbF})$$

and

$$\dot{u}_E = \frac{1}{\tau_{rise}}(q_t - u_e - \beta v_e - wy_F - FB_{gain}Q_{fbE})$$

Equation 4.4

Where, FB_{gain} was a scalar gain that can be applied, Q_{fb} was the summed output of the spindle output for that particular neuron and was calculated as shown in *Equation 4.5*. The remaining variables were defined previously in Chapter 3.

$$Q_{fbF} = S_e - S_f \text{ and } Q_{fbE} = S_f - S_e$$

Equation 4.5

Where, S_e and S_f were the outputs for the spindle model for the extensor and flexor muscles respectively. A negative value in the inner state model of the neurons will contribute to an increase in activity of that neuron, which was why subtraction occurs between the spindle outputs.

The output of the HC neurons was then calculated in the same method that has been previously used in Chapter 3, which was taking the value of the inner state if it was positive, or if it was negative choosing a value of zero for the output of the neuron, as shown in *Equation 4.6*.

$$y_F = \max(0, u_F) \text{ and } y_E = \max(0, u_E)$$

Equation 4.6

Musculoskeletal Model

The musculoskeletal model that was used for simulations was the same as the pendulum model used in Chapter 3. The model consisted of a computational representation of a rod pendulum with a length of 1m and the centre of mass (CoM) of the pendulum 0.4m from the revolute joint at the proximal end. The model was actuated by two muscles, which attached to the pendulum 0.3m from the revolute joint while the opposite ends of the muscles were fixed in space 0.1m from the revolute joint in the anterior and posterior direction. One muscle tended to cause counter-clockwise rotation of the pendulum and was innervated by the flexor HC neuron while the other muscle caused a clockwise rotation of the pendulum and was innervated by the extensor HC neuron. The damping moment was also applied in the same manner as that was used in Chapter 3.

A flow chart illustrating the flow of data through model was shown in Figure 4.3.

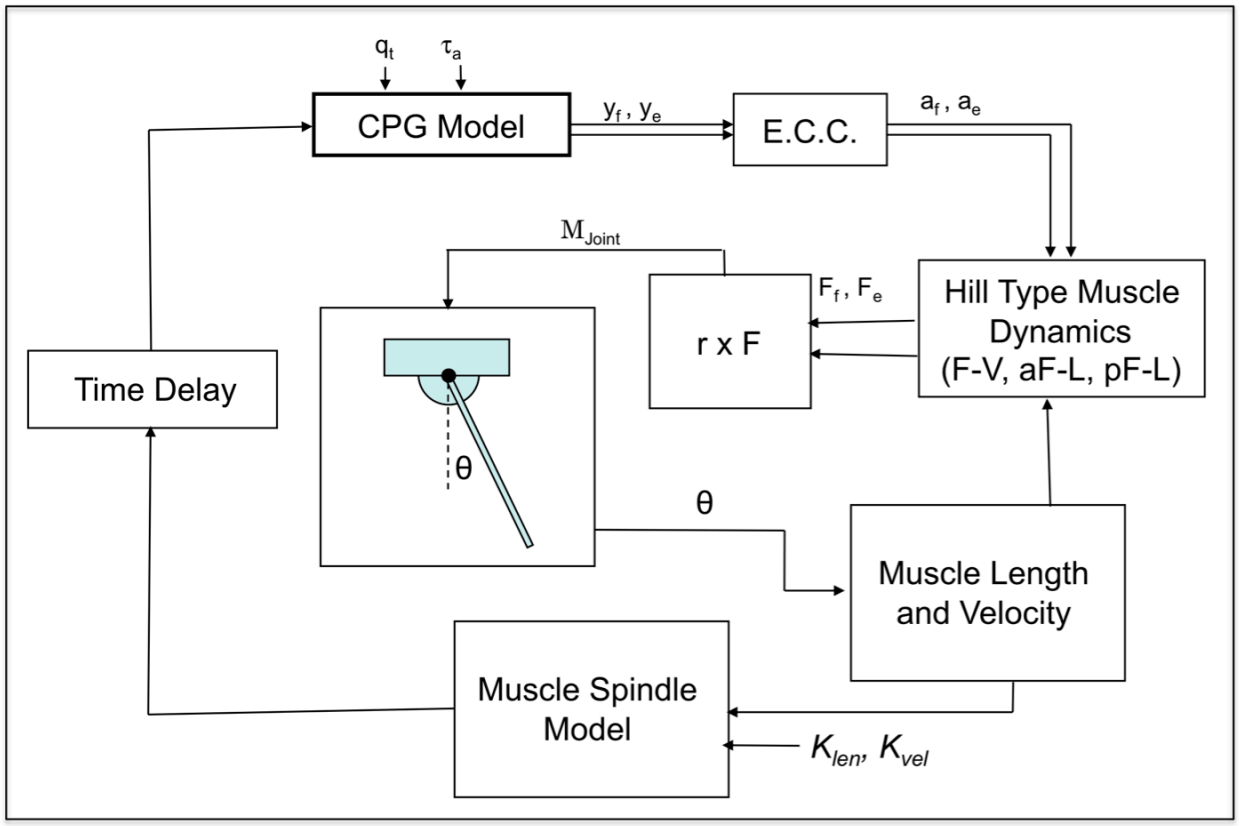

Figure 4.3: Flowchart illustrating the flow of data through the hybrid control pendulum model. See set for the description of all the variables.

Forward Dynamics and Simulation Properties

All simulations were carried out with Simulink version 6.1, a component of MATLAB (The Mathworks Inc., Natwick MA). Simulink is a graphical tool for solving models that are based on differential equations. All simulations for this study used the *ode45* solver to solve the differential equations that determine the model, which is a variable step Runge-Kutta based solver. The solver took an initial time-step of 10^{-4} s, and had a maximum step size of 10^{-2} s and a minimum step size of 10^{-15} s. Relative and absolute tolerances were set to 10^{-5} units and zero-crossing control was enabled. The mechanical system used in this study was defined using SimMechanics, which is a component of Simulink that is used to create models of mechanical systems.

All simulations took place with the initial conditions shown in Equation 4.7:

$$\left[\theta_0, \dot{\theta}_0\right] = \left[-45^\circ, 0^\circ / s\right]$$

Equation 4.7

Dependent Variables

Four main variables were used as dependent variables in the analysis of the models' output, these are the amplitude of the peak angular displacement of the pendulum (in radians), the frequency of the pendulum's motion (in Hz), the amplitude of the peak output of the CPG neurons (in the arbitrary units of the CPG's output, that was related to the firing rate of the neurons) and the burst frequency of the CPGs output. For all simulations carried out for this study it was assured that the CPG and the pendulum both achieved a periodic solution (by observing closed loops on the phase plots of the variables) and analysis of the dependent variables occurred over the final 100s of the 120s simulations to ensure that any artifacts from the chosen initial conditions would not affect the results. All signals were sampled at 100 Hz for analysis. The frequency variables were determined by finding the frequency where peak power occurred on the power spectral density function (PSDF) for that variable. The global maximum during the 100s analysis period of the angular displacement of the pendulum and net CPG output signal was recorded and it was verified graphically that this value was representative of the amplitude of the periodic output of these signals.

Simulation Descriptions and Results

Experiment #1: Integration of Feedback Signals with the CPG model

Because of the first order delay that was used to simulate the temporal dynamics of the sensory signals in the muscle spindle model, the magnitude of the output of the HC neurons was

affected by the duration of the sensory signal. To test the effect that the duration of the sensory input had on the magnitude of the output of the HC neurons, a series of simulations were carried out where a step input was applied to the spindle model of the same magnitude but of different durations. The stretch was always initiated at the same phase of the HC neurons output, since the same initial conditions and frequency were used for the CPG output for each simulation. Input durations of 0.05, 0.1, 0.25, 0.5, 1, 2.5 and 5s were tested. The feedback gain (FB_{GAIN}) was set to 1.0 for all simulations in this experiment, since the goal was to determine the effect of the duration of the feedback signals on the CPG output. The effect of the duration of the signal on the peak magnitude of the HC neuron's output was shown in Figure 4.5. The effect of the duration of sensory signals on the amplitude of the CPG model's output was shown in Figures 4.4 and 4.5.

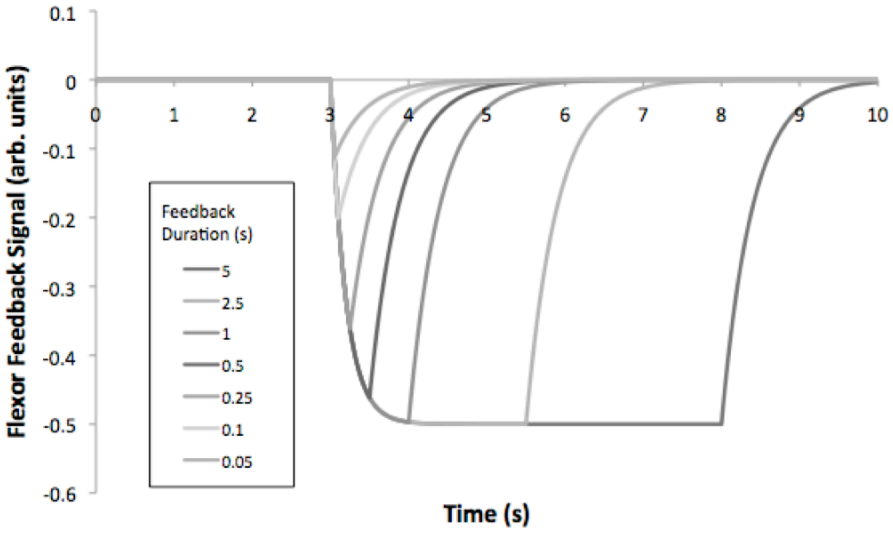

Figure 4.4: Effect of the duration of the feedback signal on the magnitude of the feedback signals.

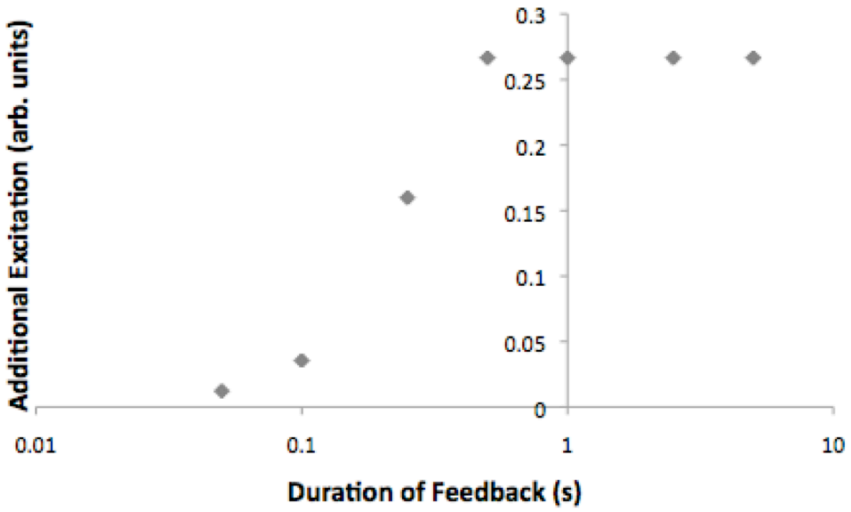

Figure 4.5: Effect of the duration of the feedback signals on the amplitude of the CPG signals. The ordinate indicates the additional excitation that is observed above the baseline signals.

The effect of the sensory signals on the output of the CPG was shown in Figure 4.6, the following CPG model parameters were used for this simulation: $\tau_{ad} = 0.5$, $q_t = 0.5$, since these parameters would produce signals of a moderate amplitude at frequency that was close to that of the stride frequency in normal human walking. It was seen that a simulated stretch of the flexor muscle leads to a prolonged excitation of the flexor HC neuron and a prolonged inhibition of the extensor HC, thus illustrating that the neural connectivity was functioning as it should.

The mutual inhibition property in the neural connections used in this model of the neurons meant that excitations of one HC neuron in the CPG would automatically lead to inhibition of the other neuron in the CPG. Therefore the neural connectivity in the model used means that the sensory signals would have the same effect on the CPG model's output if only one of the HC neurons was excited by the feedback signal or if one was inhibited and one was

excited. This feature was observed in Figure 4.7, where the same output from Figure 4.6 was observed when sensory information was only received through the flexor HC.

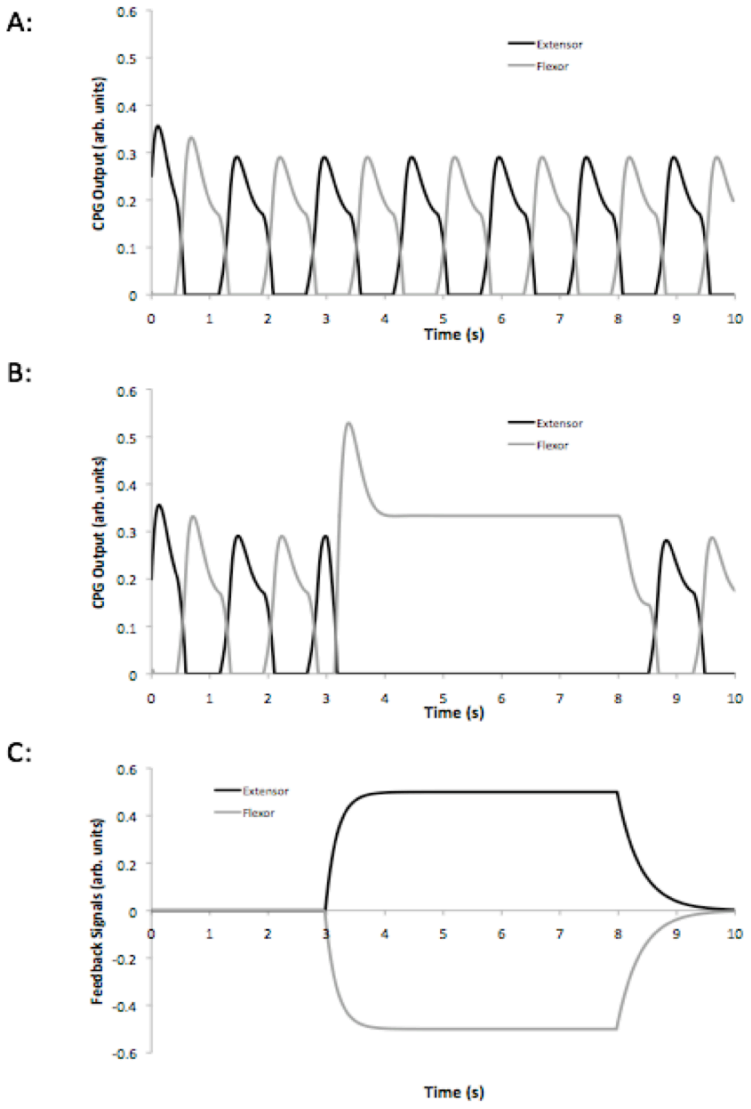

Figure 4.6: Effect of feedback signals on the output of the CPG model. The top panel (A) shows the normal CPG output when τ_{ad} = 0.5, and q_t = 0.5. The middle panel (B) shows the CPG output when the extensor neuron is inhibited and the flexor neuron receives excitatory input. The bottom panel (C) shows the feedback signals that were used to create the CPG output in B. The black lines represent signals related to the extensor HC, while the grey line represent signals related to the flexor HC.

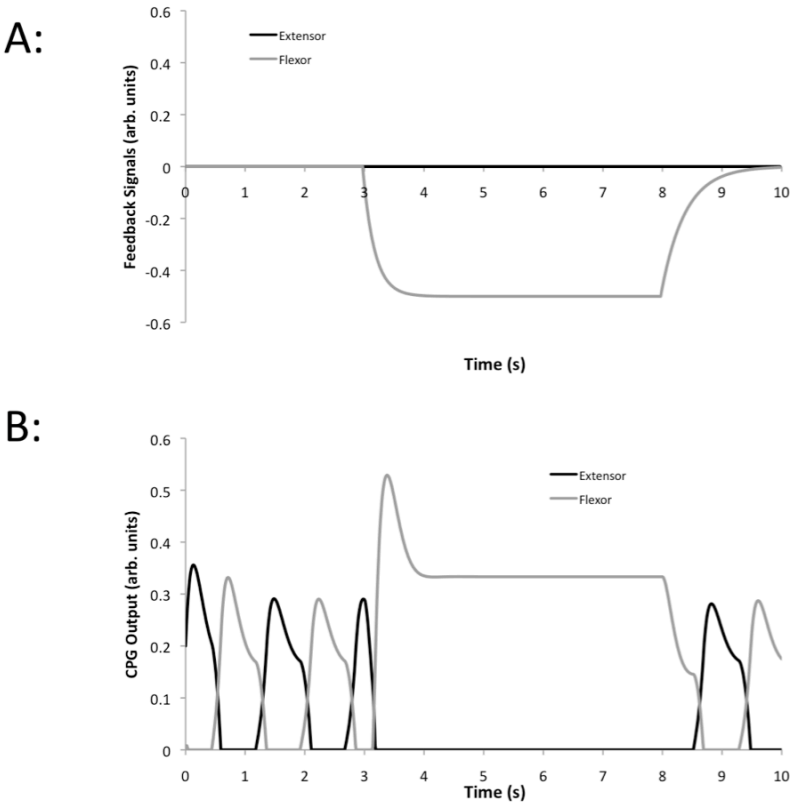

Figure 4.7: The feedback signals (A) and the CPG output (B), when feedback is only delivered through the flexor half centre. Note that the CPG output is the same as that when feedback was received through both HC neurons.

Experiment #2: Feedback Control of Rhythmic Limb Movements

To eliminate the influence of the oscillating output of the CPG and isolate the feedback mechanisms in the model, a series of simulations was carried out with the tonic input to the CPG (q_t) set to zero. Since the properties of the HC neurons, specifically the time constant of the adaptation effect of (τ_{ad}), may still influence the output of HC neurons, a series of simulations were carried out where both the feedback gain (FB_{GAIN}) and τ_{ad} were systematically manipulated. A total of 2050 simulations were carried out for this experiment, with values of τ_{ad} ranging between 0.01s and 4.91s, in increments of 0.1s, and the value of FB_{GAIN} varying between 0 and 2, in increments of 0.05. The amplitude and frequency of the pendulum was assessed for each of these simulations. The range of parameters was chosen to represent a wide range of the chosen

variables and the increments between the values were set so that the large number of simulations could be carried out in a reasonable time frame, as each simulation took approximately 1 minute to carry out.

It was found that at levels of FB_{GAIN} greater than 0.15 the pendulum was able to sustain a stable oscillating pattern, when only feedback was used. The amplitude of the pendulum's motion increased, and then leveled off as the value of FB_{GAIN} increased. The value of τ_{ad} appeared to only have an effect on the amplitude of the pendulum when the feedback gain was set to a moderate value ($FB_{GAIN} < 1$). The pendulum's amplitude across various levels of FB_{GAIN} and τ_{ad} tested was shown in Figure 4.8.

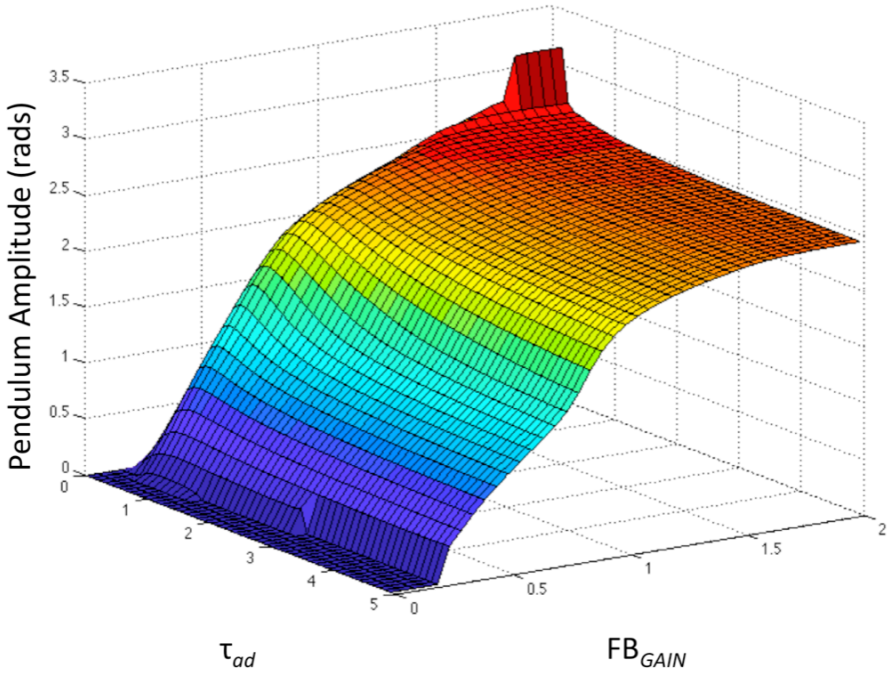

Figure 4.8: Pendulum amplitude across the ranges of FB_{GAIN} and τ_{ad} tested, when the pendulum was only driven by feedback signals.

Figure 4.9 isolated a few of the levels of FB_{GAIN} tested to illustrate that once the level of FB_{GAIN} was greater than 1.0, there was minimal impact on the amplitude of the pendulum's

motion. This was because the maximum muscle moment was achieved when the level of FB_{GAIN} was just greater than 1.0 and reached a plateau at the maximal value. A figure illustrating the peak muscle moment during the simulations in this experiment was shown in Figure 4.10. It was also observed in Figure 4.9, that τ_{ad} had the greatest effect on the amplitude of the pendulum when the level of FB_{GAIN} was less than 1 and had the greatest effect when a moderate FB_{GAIN} was used (0.25-0.5). It can also be observed that the magnitude of the pendulum's motion was much greater than was observed when only feedforward control mechanisms were used, such as in Chapter 3, due to significantly higher output magnitudes from the HC neurons, and consequently higher joint moments were observed. This was somewhat problematic as angular displacements greater than 90° would lead to the muscles crossing over the revolute joint of the pendulum, as no muscle wrapping algorithm was used. Appropriate levels of joint moments and angular displacements were attained when moderate levels of feedback were used (FB_{GAIN} between 0.25-0.5).

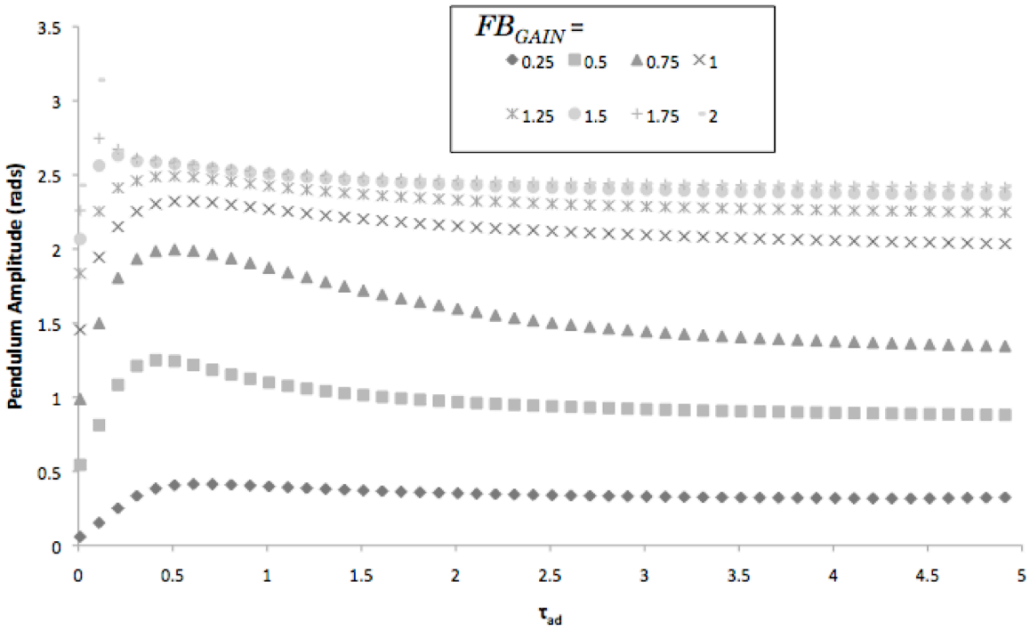

Figure 4.9: Effect of τ_{ad} on the amplitude of the pendulum when only feedback is used to control the motion of the pendulum. The results are shown across various levels of FB_{GAIN}.

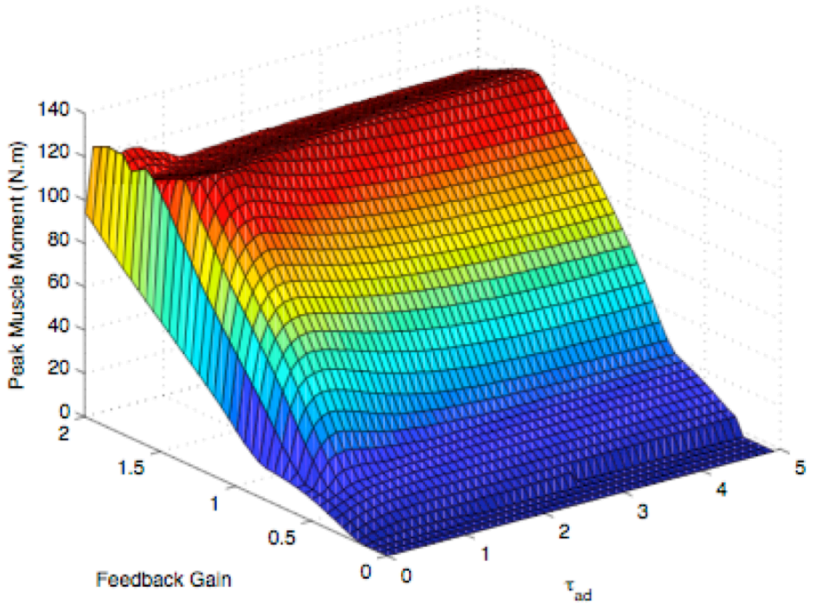

Figure 4.10: Peak muscle moment generated across various values of FB_{GAIN} and τ_{ad}.

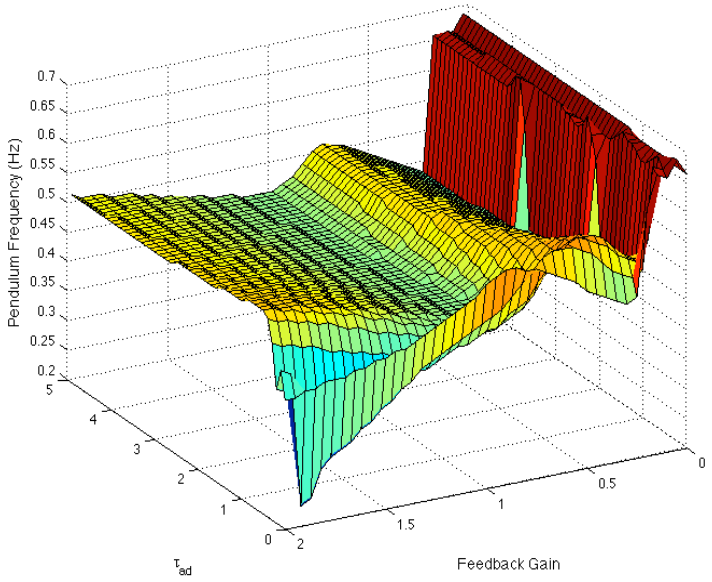

Figure 4.11: Effect of the feedback gain and the value of τ_{ad} on the frequency of the pendulum. When a feedback only configuration was used to control the pendulum ($q_t = 0$).

The frequency of the pendulum across the various values of τ_{ad} and FB_{GAIN} tested was shown in Figure 4.11. It was seen that the frequency of the pendulum was primarily dependant on the value of the feedback gain (FB_{GAIN}), with time constant of the CPG's adaptation effect (τ_{ad}) only having a minor influence on the frequency of the pendulum. For the majority of the simulations tested, the pendulum appeared to be fairly well matched to the natural frequency of the pendulum system (approximately 0.5 Hz), however there was some modulation of the frequency that was evident across the various levels of FB_{GAIN}, indicating that sensory entrainment was not occurring when only feedback was used to control the rhythmic limb movements. At low levels of FB_{GAIN} higher pendulum frequencies were observed, however the amplitude of the pendulum's motion was very low in these conditions, thus the frequency of oscillation was of little importance for these conditions.

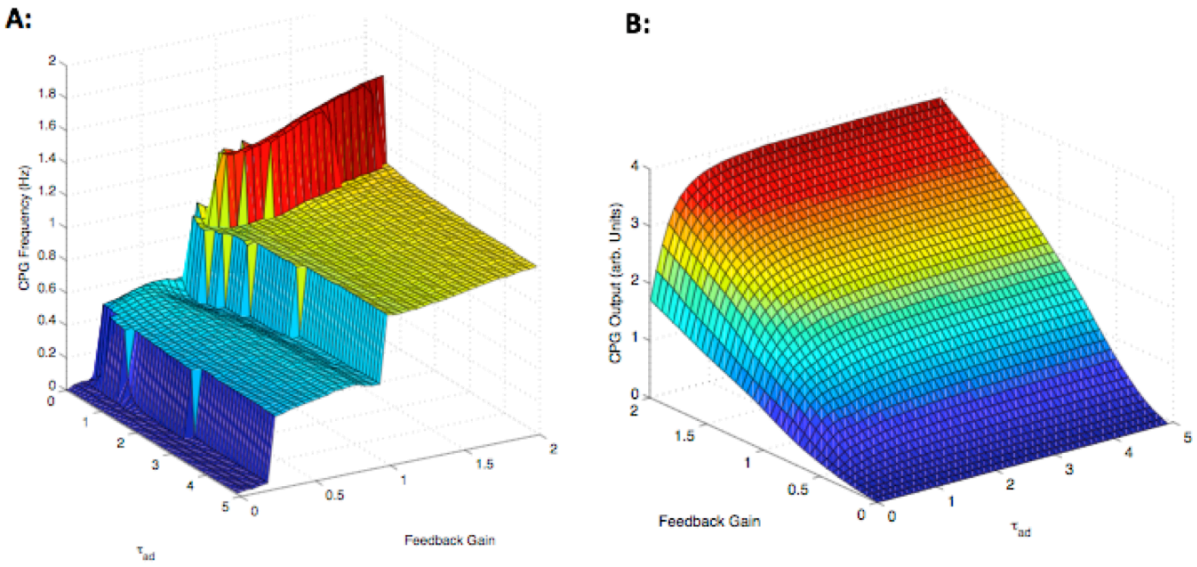

Figure 4.12: Properties of the CPG output when only driven by feedback from the muscle spindle models. Panel A shows the frequency of the CPG output across the values of FB_{GAIN} and τ_{ad} tested, while Panel B shows the amplitude of the CPG output for the same conditions. Note the different orientation of the graphs; the graphs have been oriented in the positions shown to best view the data.

The frequency and amplitude of the HC neurons output for this series of simulations were shown in Figure 4.12. The frequency of the CPG output at moderate feedback gains (0.25-1.0) appeared to be fairly well matched to the pendulum's frequency. When the feedback gain was greater than 1.0, the frequency of CPG output was doubled to twice the frequency of the pendulum, due to large spikes in the CPG output that occurred due to high magnitudes of spindle output. In some cases when τ_{ad} was short and the feedback gain was greater than 1.0, the frequency of the CPG output was further increased, to three times the natural frequency of the pendulum. The amplitude of the CPG increased in a linear fashion with the value of FB_{GAIN}. The value of τ_{ad} appeared to have minimal effect on the frequency and amplitude of the CPG output, except when the value of the time constant was very small, which led to a decrease in the amplitude and increase in the frequency of the CPG's output. Due to differences in the frequency between the pendulum and the output of the CPG model, differences in phase between the CPG and the pendulum could not be examined in an intuitive manner. A figure showing sample time series data for the pendulum's motion and CPG output was shown in Figure 4.13, for two different levels of FB_{GAIN}. This figure illustrates that the frequency of the pendulum's motion was the same regardless of the FB_{GAIN} value, however the amplitude pendulum was affected by this gain.

$FB_{GAIN} = 0.50$

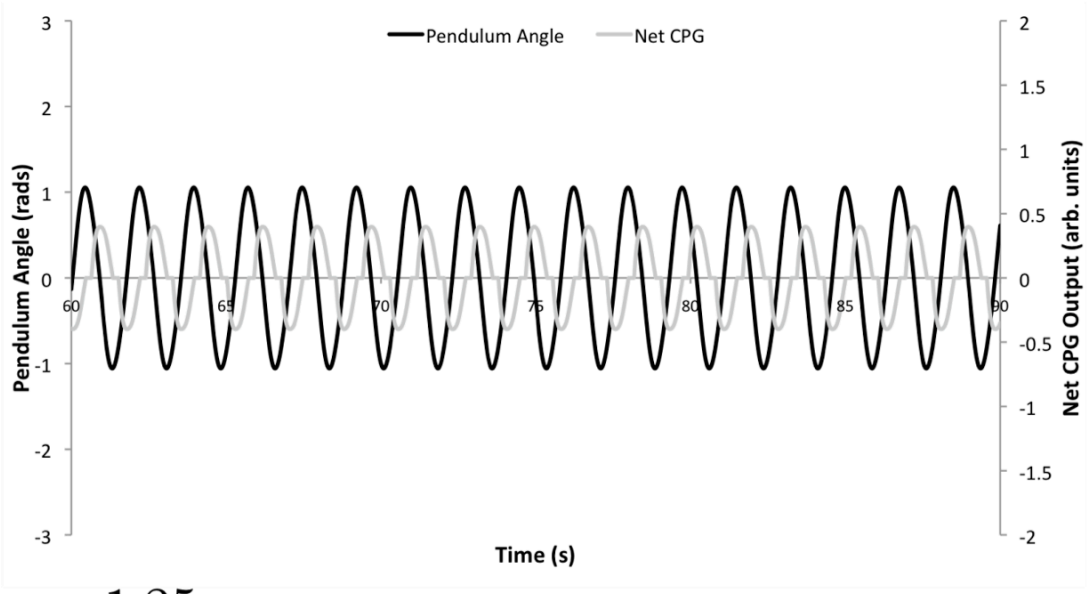

$FB_{GAIN} = 1.25$

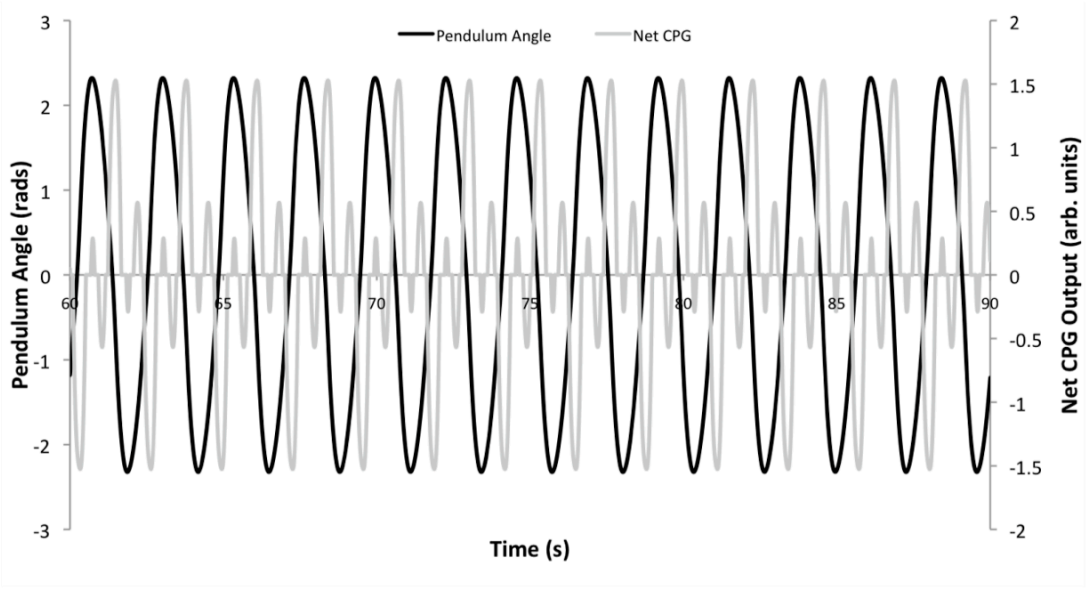

Figure 4.13: Motion of the pendulum (black line) and CPG_{NET} values (grey line) when FB_{GAIN} = 0.5 (top) and when FB_{GAIN} = 1.25 (Bottom) and q_t is set to zero. A total of 30 seconds of simulation time are shown for both graphs.

Experiment #3: Combination of Feedforward and Feedback Mechanisms For Control of Rhythmic Limb Movements

The next series of simulations were carried out to assess the ability of a hybrid control system, which used a combination of feedforward and feedback mechanisms to control the motion of the pendulum. To accomplish this goal, the series of simulations that were carried out for Experiment #2 in this chapter were repeated with the tonic input to the CPG model being set to 0.125, 0.25 and 0.50 (q_t). To summarize, a total of 2050 simulations were carried out at each level of q_t (0.125, 0.25 or 0.50) for this experiment, with values of τ_{ad} between 0.01s and 4.91s, in increments of 0.1s and the value of FB_{GAIN} varied between 0 and 2, in increments of 0.05.

The amplitude and the frequency of the CPG output and of the pendulum were illustrated in Figure 4.14 across the ranges of τ_{ad} and FB_{GAIN} that were tested when q_t was set to 0.125. As observed in Figure 4.14 it was found that the feedback mechanisms dominated the control of the pendulum in this configuration and the parameter that primarily affected the motion of the pendulum was the gain of the feedback (FB_{GAIN}), as altering the value of τ_{ad} did not significantly alter the motion pattern of the pendulum. There was no observable difference in the motion of the pendulum between the set of the simulations with q_t being set to 0.25 or 0.125. To further investigate the effect that the tonic input had on the motion of the pendulum, the amplitude and frequency of the pendulum's motion was plotted across the range of τ_{ad} tested when the feedback gain was set to 1.0 ($FB_{GAIN} = 1.0$) at all the values of q_t that were tested (See Figure 4.15). In this plot both the frequency and amplitude of the pendulum were very similar when the tonic input to the pendulum was at lower levels ($q_t = 0$, 0.125 or 0.25), however when q_t was set to a higher level, the motion of the pendulum became erratic, with the pendulum often surpassing the maximum displacement that was permitted (π radians). This was only evident at lower levels of

τ_{ad} ($\tau_{ad} < 1.0$). At higher values of τ_{ad} with the higher tonic input the amplitude of the pendulums motion was slightly higher, but the frequency of the pendulum's motion was the same, further illustrating the entrainment that occurs between the mechanical pendulum and the neural CPG system.

While the feedback from the muscle spindle models did dominate the output of the CPG, and thus the motion of the pendulum, there were some observable differences in the results of this series of simulations and the previous series of simulations where only feedback was used. The largest difference between the two series of simulations was that the level of the feedback gain where the CPG increased from the natural frequency of the pendulum, to twice the natural frequency of pendulum, was significantly lower with the hybrid feedforward-feedback control scheme; this was observed by comparing of Figures 4.12 (panel A) and 4.14 (panal B). When no feedforward control was used the jump to twice the natural frequency occurred when FB_{GAIN} was equal to 1.0, however when the feedforward component was activated this jump occurred when FB_{GAIN} was approximately 0.5. The addition of the feedforward component from the CPG also appeared to force the pendulum to oscillate at its' natural frequency over a much larger range of the parameters tested, this was seen by comparing panel D of Figure 4.14 to 4.11.

To test the effect that the mutual inhibition property of the Matsuoka oscillator had on the behavior of the system, an additional series of 2050 simulations were carried out with the connections between the two HC neurons removed and all other model parameters being held to the same values. The results of this series of simulation were shown in Figure 4.16. It was found that an oscillatory output was observed in CPG and the pendulums' motion, even when the reciprocally inhibitory connections were removed, however the results of the simulations showed some vast differences when compared to the output when connections were present between the

HC neurons of the CPG, this was particularly evident at lower values of τ_{ad} where the neural output was erratic. At higher values of τ_{ad}, the frequency of the CPG output was again dominated by the sensory entrainment from the muscle spindles, which allowed the frequency of the pendulum to match its natural resonant frequency.

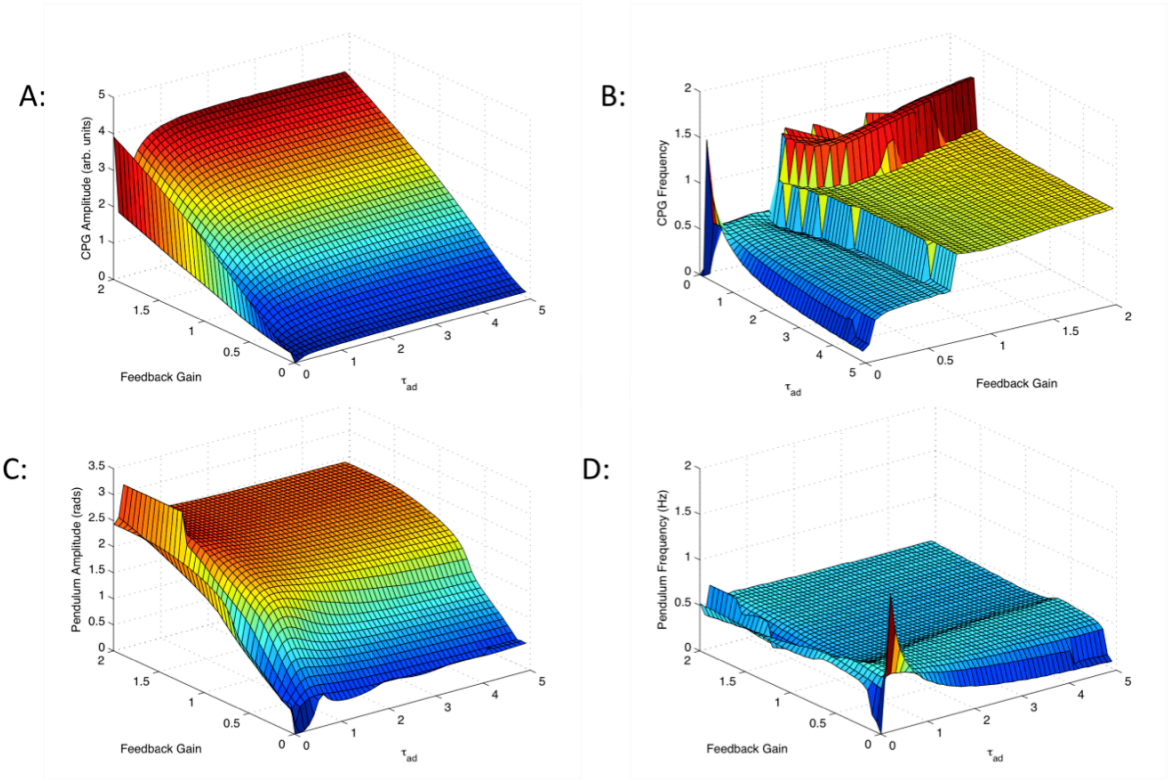

Figure 4.14: Effect of the feedback gain and the value of τ_{ad} on the amplitude (A) and frequency (B) of the CPG output, as well as the amplitude (C) and the frequency (D) of the pendulum's motion when a combination feedforward and feedback control was used. Note that the orientation of panel B has been rotated to better illustrate the simulation results.

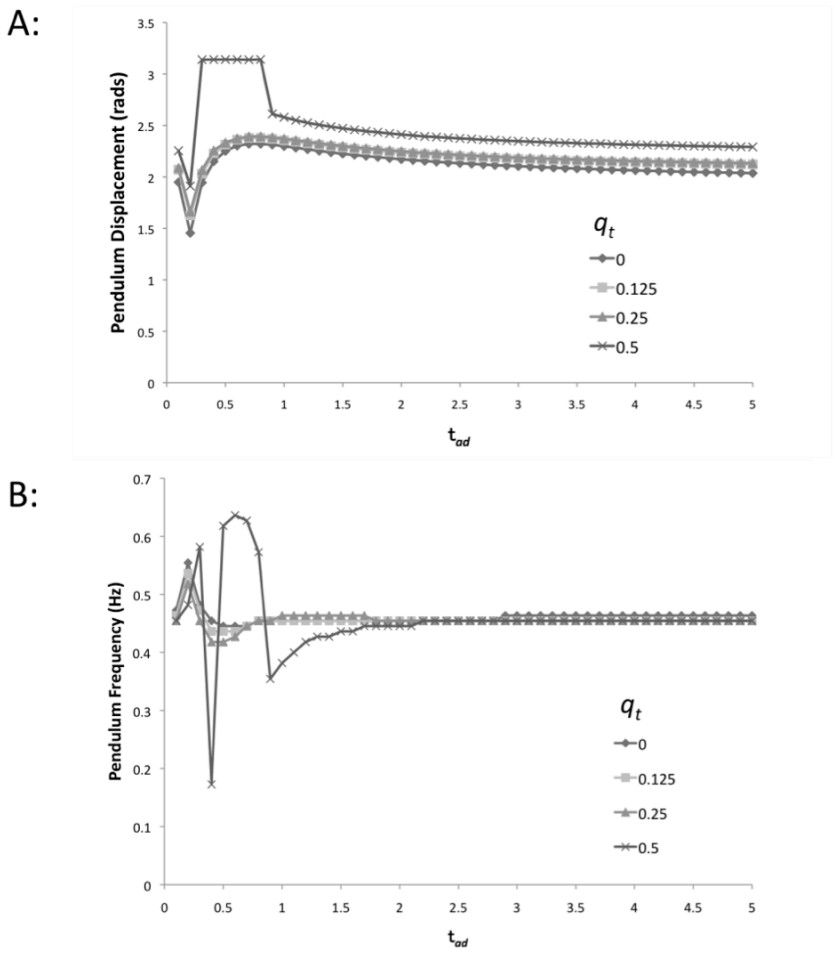

Figure 4.15: Amplitude (A) and frequency (B) of the pendulum across the range of values of τ_{ad} and q_t that were tested, when the feedback gain was set to 1.0 ($FB_{GAIN} = 1.0$).

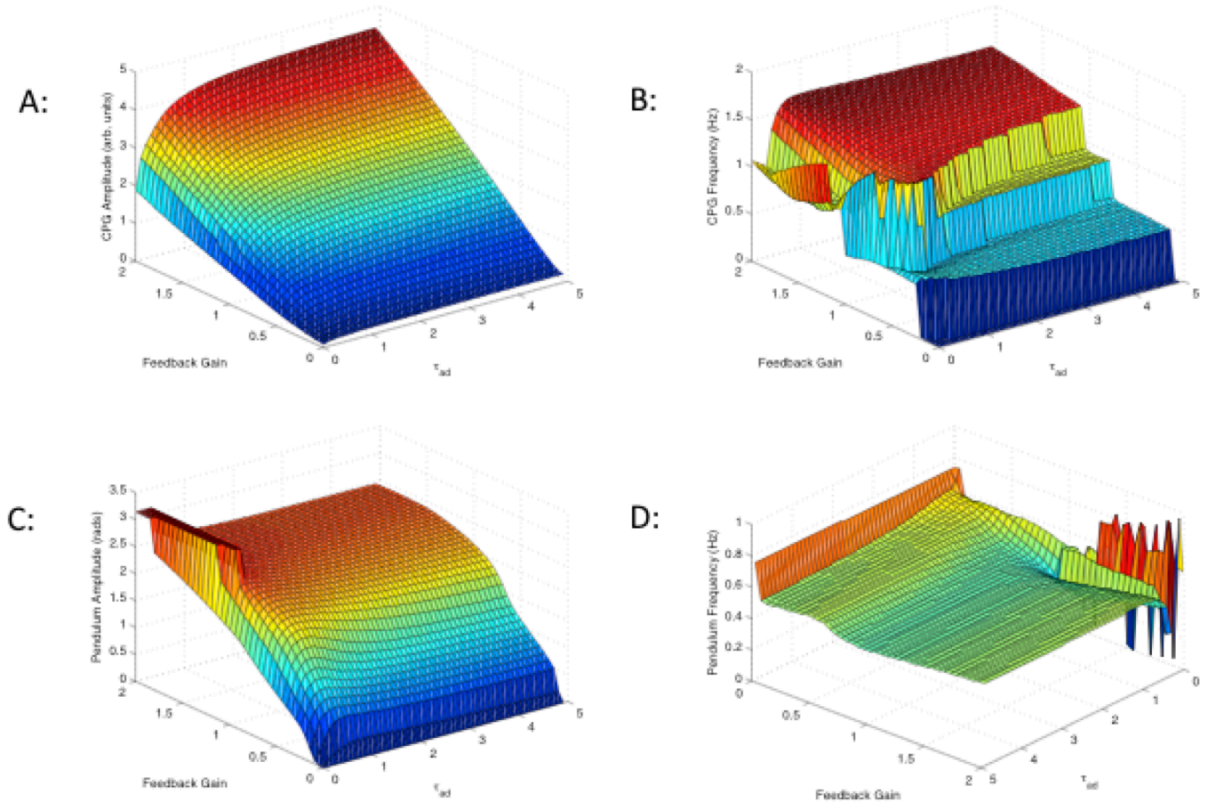

Figure 4.16: Effect of the feedback gain and the value of τ_{ad} on the amplitude (A) and frequency (B) of the CPG output, as well as the amplitude (C) and the frequency of the pendulum's motion when a combination feedforward (q_t = 0.25) and feedback control was used, however the reciprocal connections were removed between the flexor and extensor half centre neurons. Note that the orientation of panel B has been rotated to better illustrate the simulation results.

Experiment #4: Effect of the Feedback Delay and Muscle Length and Muscle Velocity Feedback Gains

A series of 5151 simulations were carried out to determine the combined effect of the timing and the magnitude of the feedback signals on the motion of the pendulum system. The transmission between the muscle spindle output and the connection to the HC neurons of the CPG was varied between 0 and 50ms in increments of 1ms, while the feedback gain (FB_{GAIN}) was varied between 0 and 1.0 in increments of 0.01. The tonic input to the CPG (q_t) was nominally set to 0.25 for all simulations while the time constant of the adaptation effect of the

neurons (τ_{ad}) was set to 0.25 s, the exact parameters that were chosen for the CPG parameters where not important for this particular simulation, as the feedback delay was being investigated.

The feedback delay had a small effect on both the frequency and amplitude of the CPG output and the motion of the pendulum, however most of the changes observed in this series of simulations were associated with changing the gain of the feedback signals. The results from this series of simulations were shown in Figure 4.16. The feedback gain was able to alter the frequency of both the CPG and the pendulum at higher feedback gains ($FB_{GAIN} > 0.8$), where the feedback signals tended to cause spikes in the CPG output, as previously shown in Figure 4.13. The delay in the feedback loop had somewhat of an effect on the phase relationship of the CPG and the pendulum, with higher feedback delays tending to cause the CPG and the pendulum's motion becoming more in phase, this was shown in Figure 4.17; phase difference results were only shown for the simulations where $FB_{GAIN} = 1.0$, however the results were similar across all feedback gain levels.

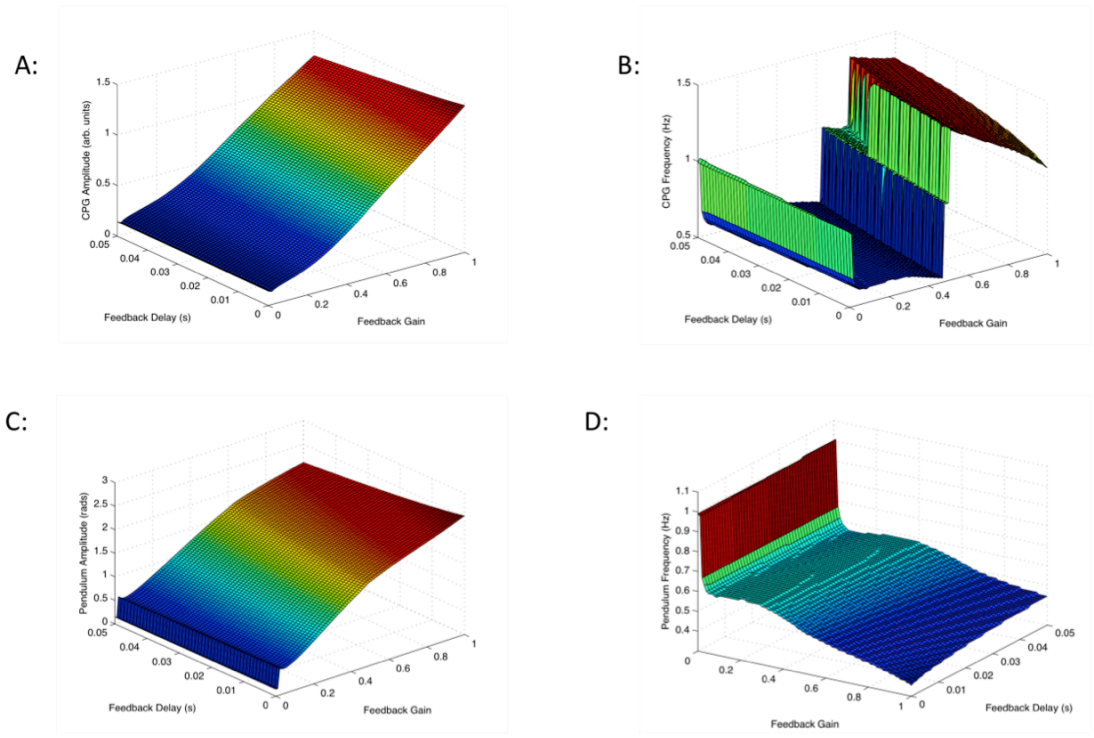

Figure 4.16: Combined effect of gain and the temporal delay of the sensory feedback on the amplitude (A) and frequency (B) of the CPG output, and amplitude (C) and frequency (D) of the pendulum's motion. Note the orientation of panel D has been altered relative to the other panels in order to best illustrate the results

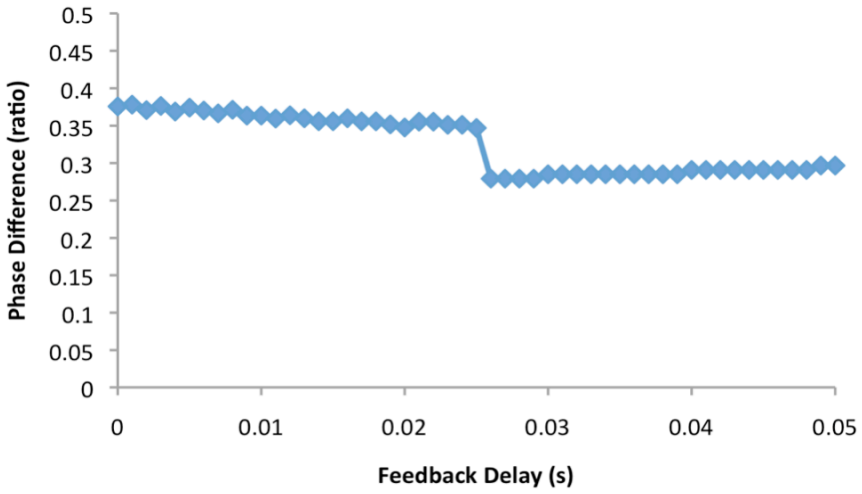

Figure 4.17: Phase difference between the net CPG output and the motion of the pendulum. The phase ratio indicates the difference in the cycle time of the CPG and the pendulum, expressed as a ratio of the CPG's cycle time. A phase ratio of 1.0 or 0.0 indicates that the CPG and the pendulum are exactly in phase, while a phase ratio of 0.5 indicates that the CPG and the pendulum are exactly out of phase.

To test the effect that the specific gains that relate muscle length and velocity to spindle output have on the output of the CPG and the motion of pendulum, a series of 2092 simulations were carried out. The muscle velocity gain, K_{Vel} from Equation 4.1, was systematically altered between 0 and 4.0, in increments of 0.1 while the muscle length gain (K_{Len}) was incremented from 0 to 5.0, also in increments of 0.1. A larger range of velocity gains was tested because results from pilot testing revealed that the dependent variables were more sensitive to changes in the velocity gain than the length gain. For all the simulations of this experiment, the time constant of the CPG's adaptation effect (τ_{ad}) was set to 0.5s while the tonic input to the CPG (q_t) was set to 0.25, so that all the results of this series of simulations would be comparable to the previously presented results. The feedback gain was nominally set to 0.75 for all of the simulations for this experiment.

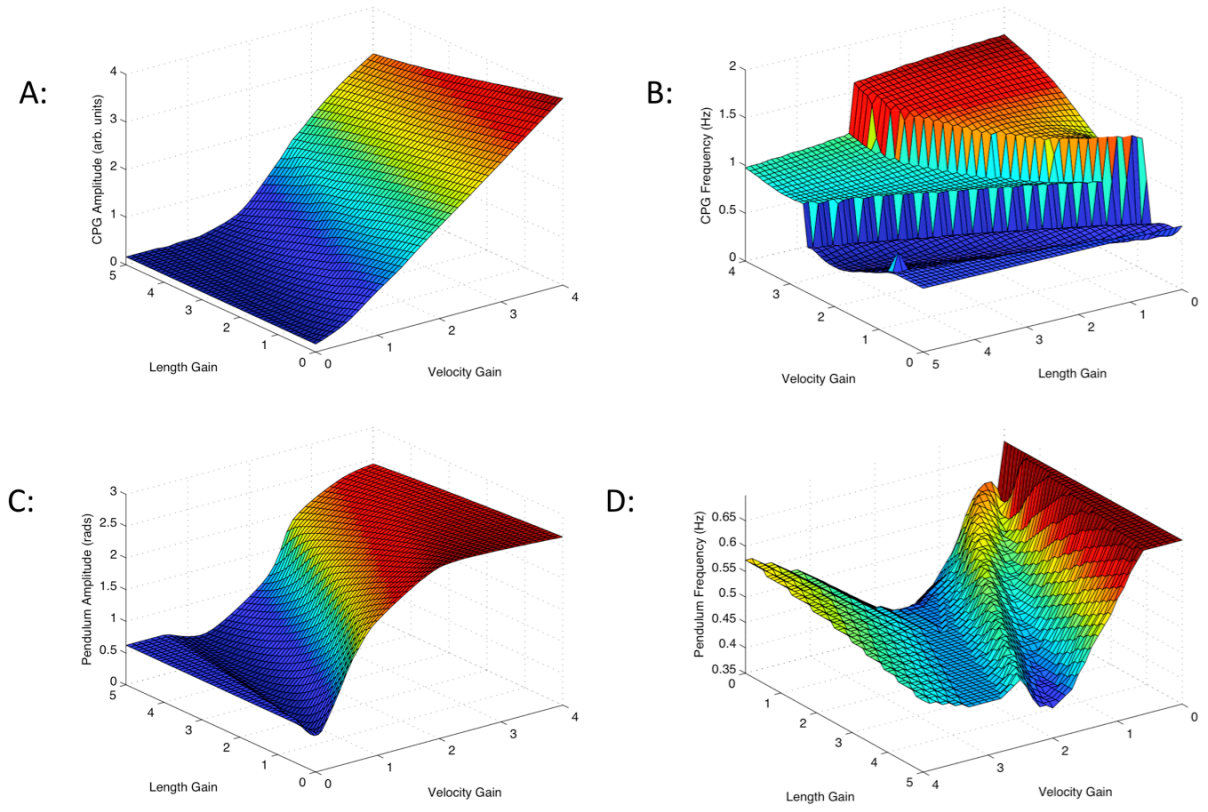

Figure 4.18: Combined effect of muscle length and velocity gains on the amplitude (A) and frequency (B) of the CPG output, and amplitude (C) and frequency (D) of the pendulum's motion. Note the orientation of panel D has been altered relative to the other panels in order to best illustrate the results.

As can be observed in Figure 4.18, both the length and velocity gains affected the amplitude and frequency of the CPG and consequently the motion of the pendulum. The muscle velocity gain had the largest effect on the amplitude of the CPG's output, due to the spike in the spindle signal that was caused by a muscle stretching. Increasing the muscle length gain actually led to a slight decrease in the amplitude of the CPG's output for reasons that will be discussed later. Increasing the length gain had little effect on the frequency of the CPGs output; however increasing the velocity gain had a significant effect on the frequency of the CPG's output. As the velocity gain increased, there were additional spikes in the output of the CPG that increased the frequency to multiples of the natural frequency of the pendulum. The amplitude of the

pendulum's motion was primarily affected by the velocity gain in the spindle model, with higher velocity gains leading to larger displacements of the pendulum. The length gain had the opposite effect on the amplitude of the pendulums displacement, with an increase in the length gain leading to a decrease in the pendulum's amplitude.

Experiment #5: Effect of Control System Parameters on the Response to Mechanical Perturbations

A series of nine simulations were carried out to analyze the effect of the neural control system configuration on the ability to respond to a mechanical perturbation. There were a total of 3 control configurations that were tested; a feedforward only control system, a feedback only control system and a hybrid control system consisting of feedback and feedforward control components. Three simulations were carried out in each of these configurations, with perturbations being delivered to the distal end of the pendulum at a magnitude of 0N (no perturbation), 20N or 40N. These particular perturbation force levels were chosen for analysis because perturbations greater 40N tended to cause erratic motion when a FF control scheme was used exclusively. The perturbation force was always applied to the distal end of the pendulum, in the positive-x direction as indicated in Figure 4.3. These perturbation forces tended to cause an increase in flexion of the pendulum, using the defined reference system. Perturbations were applied at an interval of 20s. The duration of application of the force was 0.4s in all instances, as larger impulses led to erratic motion of the pendulum. An attempt was made to keep all of the parameters of the neural control model as similar across this series of simulations; τ_{ad} was set to 0.5s for all simulations, which resulted in all of the control methods used. For the feedback only simulations, the tonic input to the CPG was set to 0 ($q_t = 0$), so that all of the neural activity was determined from the feedback from the spindle models. For the feedforward only simulations,

the gain of the feedback components was set to 0 ($FB_{GAIN} = 0$) so that the spindle output would have no effect on the output of the CPG. The tonic input to the CPG for the feedforward control simulations was set to 0.7, in attempt to match the pendulum's angular displacement that was observed in the other simulations when FB processes were used. For the feedforward-feedback hybrid simulations, FB_{GAIN} was set to 1.0 while q_t was set to 0.25, to attempt to have the same magnitude of output from the CPG and pendulum motion. In the feedback only simulations, FB_{GAIN} was also set to 1.0, to maximize the amplitude of the feedback signals.

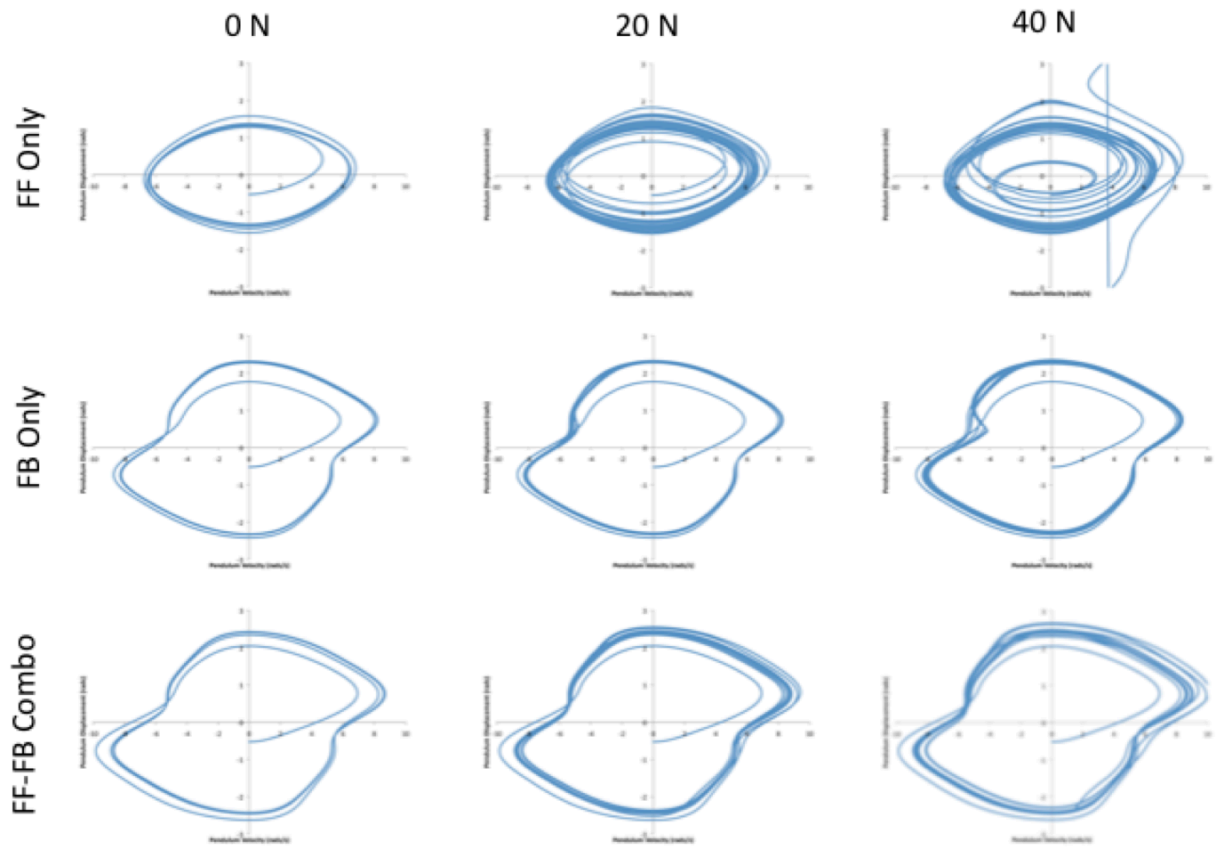

Figure 4.19: Phase plots illustrating the effect of the perturbations on the periodic motion of the pendulum. The horizontal axis of each graph shows the pendulum's angular velocity in rads/s while the vertical axis shows the pendulum's displacement in radians. The top row shows the results for the feedforward only simulations, the second row shows the results of the feedback only simulations while the bottom row shows the combined feedforward control results. The vertical line on the top-right phase plot indicates that the pendulum exceeded the maximum displacement (π radians) on that particular cycle. The leftmost column of plots shows the motion of the pendulum when no perturbation was applied, the middle column shows the motion of the pendulum when a 20N perturbation was applied, and the right-most column shows the motion of the pendulum when a 40 N perturbation was applied. .

Phase plots illustrating the motion of the pendulum in these simulations were shown in Figure 4.19. It was observed from the large excursions from the normal motion pattern during the perturbations in the top row of Figure 4.19 that the perturbations were most disruptive to the pendulum's motion when feedforward control was exclusively used. Predictably, the excursions from the normal motion pattern due to the perturbations were much smaller when a feedback

only control scheme was used. When a combination of FF and FB was used the excursions caused by the perturbations were slightly larger than those observed when only FB was used, however they were substantially smaller than the excursions that were observed when FF was used. The FB control scheme used in this chapter was able to respond to perturbations that were delivered during any phase of the pendulums motion with fairly little disturbance to the overall motion pattern of the pendulum. However when only FF control was used, the pendulum was less able to tolerate perturbations that caused an acceleration of the pendulum's motion (ie. the pendulum was advancing in the positive rotational direction when the perturbation was applied), this type of perturbation led to a large displacement of the pendulum, and in one case with the larger magnitude perturbation caused the pendulum to make a complete rotation about the revolute joint.

These results were quantified by assessing the range of magnitude of the phase vector (p) over the duration of the simulations. The phase vector is a vector from the origin of the phase plot to an individual point on the phase plot (Hamill 2000). The magnitude of the phase vector was determined for each point of the 100s analysis period with the following formula:

$$\overline{p} = \sqrt{\varpi^2 + \theta^2}$$

Equation 4.8

The range of the phase vector magnitude was then determined by subtracting the minimum phase angle over the 100s analysis period from the maximum phase vector over the same period. This measure proved to be sensitive to the amount of disruption that the perturbations imposed on the pendulum's motion. One issue with this particular measure is that it is also sensitive to the average displacement of the pendulums motion. To rectify this, the amount of additional motion that was introduced by the perturbation was calculated by subtracting the phase vector magnitude

range when no perturbation was applied, for each control system. The effect of the perturbations on the range of the phase vector magnitude for each control system was shown in Figure 4.20. The results from this figure quantified the observations that were made in the phase plots that the FB-Only control system was best able to maintain the rhythmic limb motion pattern in the presence of perturbations, while the FF-Only performed the worst. The FF-FB combination control system provided a moderate level of ability to respond to the perturbations, and it can be seen that the performance of this control system was in between that of the FF-only and the FB-only control systems.

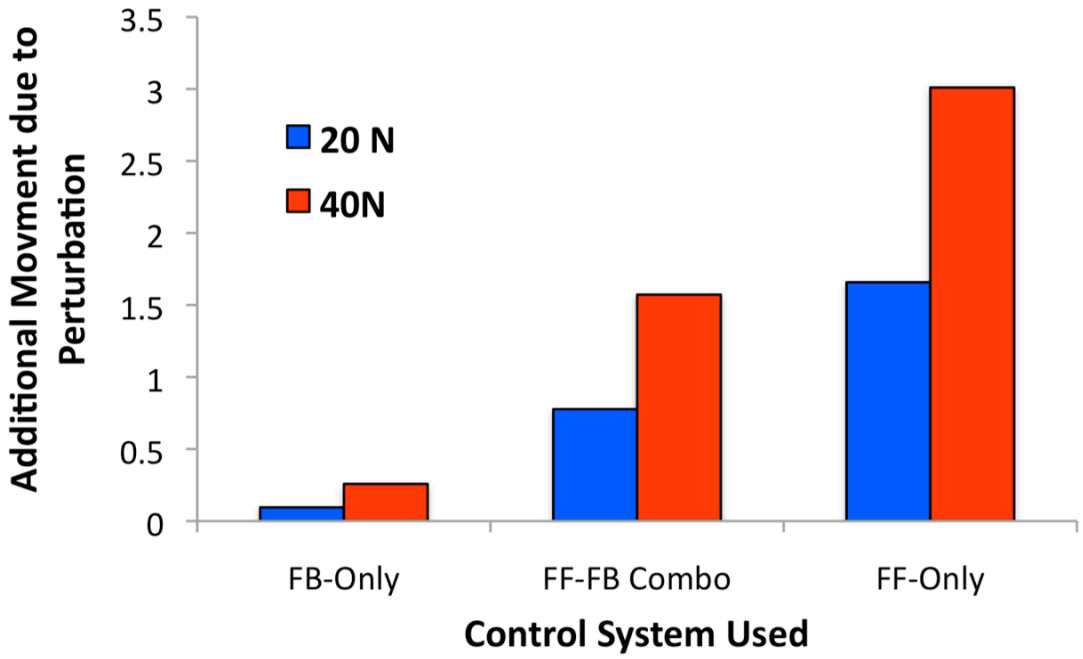

Figure 4.20: Amount of additional motion caused by the perturbation (at each perturbation level), as measured by the range of the phase vector magnitudes relative to the no perturbation conditions. Results are shown for each control system that was tested. Higher values indicate that the perturbation was more disruptive to the pendulum's motion.

Discussion

This chapter examined the role of feedback in conjunction with a neural oscillator for the control of rhythmic limb movements. The feedback was provided by simulated muscle spindles, which provided feedback to the neural oscillator based on the length and the velocity of the muscles. A number of the simulations carried out for this chapter were carried out to determine the effect of certain model parameters on the CPG and the motion of the pendulum. The insights gained from running these simulations was useful in the following chapter where the biped model was adapted to use a hybrid feedback-feedforward control system. It was discussed how the results from the current series of simulations would impact the control of the feedback parameters for the walking biped model. The main finding of the simulations carried out for this chapter was that feedback from the muscle spindle models tended to cause entrainment between the natural frequency of the pendulum and the CPG output. This finding was similar to the results of those who have used this type of control system in neuromechanical simulations to control rhythmic motion patterns (Hatsopoulos 1996; Iwasaki and Zheng 2006), however improved on these previous studies by using feedback mechanisms with a higher level of biological fidelity.

The first series of simulations for this study examined how feedback signals from the muscle spindle models interacted with the output of the Matsuoka oscillator. It was found that feedback exerted a powerful influence on the output of the HC neurons, where the output of the HC neurons was primarily determined by the feedback signals. It was also shown that the reciprocal inhibition feature of the Matsuoka oscillator had some important implications when feedback was introduced. Since the flexor and extensor neurons in the CPG were mutually inhibitory, inhibiting one of the neurons would have the same effect as exciting the opposite

neuron, confirming the hypothesis for this series of simulations. It was also shown that the duration of the feedback signal had an important effect on the magnitude of the output of the HC neurons, where a brief burst from the muscle spindles had little effect on the amplitude of the HC's output, whereas a sustained input from the muscle spindles led to a much larger increase in the amplitude of the HC neurons.

The next series of simulations examined the ability to control the motion of the pendulum with a feedback only control system, with the feedback originating from the muscle spindle models. It was found that this control configuration led to entrainment between the natural frequency of the pendulum and the frequency of the neural output of from the HC neurons, however the feedback gain was able to modulate the frequency of the pendulums motion to some degree, with a peak frequency occurring when the feedback gain was approximately 0.7. Following the peak in the frequency there was a small decrease in the pendulum and then as the magnitude of the feedback gain continued to be increased there was a slow increase in the frequency. This showed that there was incomplete entrainment between the natural frequency of the pendulum and the frequency of the neural oscillators output with the feedback configuration that was chosen, as the frequency of the pendulum was not consistently observed to be at the natural frequency of the pendulum. Not surprisingly, it was also shown that the amplitude of the pendulum's movement was determined by the magnitude of the feedback gain, as higher feedback gains led to larger magnitudes of output from the CPG and consequently higher muscle activation levels. It was also found that the choice of properties of the HC neurons, particularly the time constant of the adaptation effect of the neurons (τ_{ad}), had the potential to alter both the frequency and amplitude of the CPG's output, even though no tonic input was provided to the CPG.

The following series of simulations used a hybrid control system, using both feedback and feedforward control schemes, to control the movement of the pendulum. It was found that this control configuration led to entrainment between the neural output and the natural frequency of the pendulum over a wide range of control parameters, which was shown by the frequency of the pendulum matching the natural frequency of the pendulum. The amplitude of the pendulum's motion was also very similar across the same range of control parameters that led to sensory entrainment. Sensory entrainment has been observed in this type of control configuration in previous studies using neuromechanical simulations of rhythmic limb movements (Hatsopoulos 1996; Iwasaki and Zheng 2006; Futakata and Iwasaki 2008) and neuromechanical simulations of walking of human walking (Taga et al. 1991). This entrainment has also been observed in rhythmic limb movements in humans; Doke et al (2005) analyzed the motion patterns of rhythmic leg swinging and found that individuals preferred to swing their leg at the lower limb's natural frequency. It was seen that the control configuration used for this series of simulations was resistant to changes in parameters, including the feedback gain, the time constant of the adaptation effect and the tonic input to the CPG. This means that in a hybrid configuration it was difficult to modify the magnitude and frequency of the pendulum; it is not known what effect this will have on the more complex biped model.

The next series of simulations examined the effect of the feedback delay between the signals from the muscle spindle model and the CPG model. The control system used to control human movement is unique in that both feedforward and feedback aspects are used to control all movements, but what was unique about the movement control system is that there is a significant delay in the feedback system, meaning that feedforward components must account for this delay when sending movement commands. In the normal mono-synaptic reflex the delay between the

stretch of the muscle and contraction of that muscle was approximately 20-30ms. Other feedback pathways involved in the control of human movement had longer latencies, about 250 ms. In this chapter, we were focused on the interaction of feedforward and feedback control components for the control of rhythmic limb movements, and tested feedback delays of between 0ms and 50ms; these values were chosen to represent the range of times that would be used in short latency reflexes (30-50 ms), and to determine what the effect would be with faster reflexes. It was hypothesized that altering the delay of the feedback would have little effect on the magnitude or frequency of the pendulum however it would affect the phase relationship between the CPG output and the angle of the pendulum. It indeed was found that the delay of feedback signals had little effect on the magnitude or frequency of the pendulum's motion, however had a small effect on the phase between the CPG and the pendulum, as was previously hypothesized.

The greatest effect on the frequency and amplitude of the pendulum was seen when the length and velocity gains of the spindle model were altered. It was originally hypothesized that the velocity gains would have a larger effect on the motion of the pendulum, when compared to the length gain, however, as shown in Figure 4.17, both the length and velocity gains had an effect on the motion of the pendulum. The velocity gain did seemed to have a larger effect on the amplitude of the pendulum's motion, however the frequency of the pendulum was affected by both the length and velocity gains. This study was the only work that has manipulated the gains of a spindle type model to determine the effect on rhythmic limb movements. It was unknown how these spindle gains match the sensitivities of human muscle spindles, however the spindle gains chosen for the majority of the simulations in this chapter to match dynamic spindle output that was recorded during cat locomotion (Prochazka and Gorassini 1998).

The final series of simulations was carried out to determine how the type of feedback used affected the ability to respond to a mechanical perturbation. It was found that the feedback control system was best able to respond to perturbations, by quickly returning the pendulums motion to the normal rhythmic pattern, and showing the least amount of angular displacement due to the perturbations. This finding was contrary to the finding of Kuo (2002), who showed that hybrid systems were best able to respond to perturbations. There were some differences between the present study and that of Kuo which may have explained the difference in findings, including the fact that Kuo tested the ability of a system to respond to perturbations with several different combinations of feedback and feedforward control (which in this model would be altered by manipulating FB_{GAIN} and q_t, respectively), as this was a primary goal of Kuo's paper. In this study only a single combination of the two control parameters was tested, therefore if more combinations were tested, instances may be found where the hybrid system would be able to better respond to the perturbation. Another difference between the present study and that of Kuo (2002) was that the feedback was in Kuo's model was directly determined by the angular displacement and the velocity of the pendulum, but with no feedback delay and no transformation that would represent the output of muscle spindles. Lastly, Kuo used only spring-type muscles and Hill-Type dynamics were not included in the model. These differences could potentially explain some of the differences that were observed between the Kuo's model and the present model.

Differences in terminology may also explain some of the differences in results between the present study and that of Kuo (2002). The feedforward control mechanism that was described by Kuo featured a state prediction component, which predicted the pendulum's kinematics based on the moment of force that was applied. The control systems modelled in this study had no such

state-prediction modelled and based on control theory would be better described as open-loop control, where an input is specified and the resulting motion pattern is allowed to naturally emerge.

Another similar model tested the ability to respond to perturbations, in a neuromechanical model of a swinging forearm. Verdaasdonk (2007) created a model of a swinging forearm that was controlled by a Matsuoka oscillator and received feedback based on a muscle spindle model that was similar to that used in this study and found that the system led to sensory entrainment between the neural control system and the natural frequency of the limb. The system was also able to respond to perturbations of larger magnitudes than were used in this study. However this study compared the ability of the neural control system to respond to perturbations with different control configurations (FB, FF and FF-FB hybrid), while the FF control system wasn't able to tolerate perturbations with a force greater than 40N, the other control systems were able to respond to much larger perturbations, similar to the study presented by Verdaasdonk (2007). The ability of the hybrid control system to respond to perturbations was expanded beyond that shown by Verdaasdonk (2007), who always delivered the perturbation at the same phase of the of the mechanical system's cycle. In this study the perturbation every 20s regardless of the position of the pendulum within its cycle. Therefore the system had to be able to respond to perturbations at any phase of its cycle.

The overall goal of this chapter was to create a model to test some of the control parameters that will be used in the following study where feedback aspects will be introduced in the neural control system for the biped model. It was found that that adding feedback from simulated muscle spindles led to the neural control system forcing the pendulum to oscillate at its' natural frequency and facilitate the ability to respond to a perturbation. The results of this

study were helpful to help choose appropriate parameter settings for the simulations when feedback was used in the biped control model.

Chapter 5: Feedforward Control of Walking Speed in a Biologically Inspired Biped Model

Introduction

Experimental work performed on animals has determined that circuitry within the spinal cord is able to produce motor neuron output that is consistent with a walking pattern, without the need for sensory input (Brown 1911; Grillner and Zangger 1979; Grillner and Zangger 1984). These circuits have been termed central pattern generators (CPGs) (Grillner and Zangger 1979). In spinalized animal preparations, for example in the cat, the activity of the CPG can be activated and the movement patterns that are caused by the motor output generated by the CPG is able to be realized (Grillner and Zangger 1979). In these preparations, a surgical procedure removes all of the sensory inputs to the spinal cord (dorsal roots severed) and activating the CPG circuitry can generate a basic walking pattern. The walking pattern that is produced by these spinalized cats is far from complete; these animals often have problems supporting their body weight and must be supported in a harness and often have problems generating forward propulsion. Despite the deficits that are observed in the walking patterns produced by the CPG, there is evidence that these circuits have connectivity to higher centres and are able to produce walking patterns at different frequencies based on simple tonic changes in input. A region in the brainstem (mesencephalic locomotor region or MLR) where the magnitude of a tonic input is able to modulate the frequency of the CPG output to produce different speeds and modes (ie. walk, trot and gallop) of locomotion (Shik et al. 1969).

The role that the CPG plays in the control of human locomotion remains relatively unknown. There is evidence from patients who have suffered spinal cord injuries (SCI) that circuitry exists within the spinal cord capable of producing alternating limb movements (Dimitrijevic et al. 1998). It has also been found that the activity of these circuits may be expressed during infancy (Yang et al. 1998a). However the contributions of these circuits remain unknown due to the complexity of the human locomotor control system (MacKay-Lyons 2002). Recent work has even questioned the contributions of CPG circuits to the walking pattern in SCI patients because of the adaptability of the walking patterns that is still observed following incomplete injury (Ivanenko et al. 2009). Despite the complicated mechanisms involved in the control of human locomotion it is still assumed that the CPG does play a role in the maintenance of a locomotor rhythm (Rossignol et al. 2006) and CPG models have formed the basis of most neuromechanical simulations of human walking to date (Taga 1998; Ogihara and Yamazaki 2001; Paul et al. 2005; Jo 2008).

Although several previous neuromechanical simulations have used CPG models to form the basis of their neural control model, the range of movement patterns that can be produced by the CPG in isolation has not been examined. Of the previously published neuromechanical simulations of human walking, no simulation has examined the movement patterns that are produced by the isolated CPG, or examined the ability of the walking speed to be modulated by controlling the frequency of the CPG output. The primary goal of this study is develop a computational representation of the human musculoskeletal system that allows for motor patterns from various CPG models to produce motion using a forward dynamics approach. Once this model of the musculoskeletal system has been developed the ability to generate a locomotor

pattern will be investigated, and the ability of walking speed to be controlled by altering the frequency of CPG output will be investigated.

Musculoskeletal Model Considerations

The mechanical model used to test the neural control mechanisms modeled in the CPG must meet a certain set of requirements. Firstly, since we are interested in the control mechanisms involved in human locomotion, the model should have mechanical properties that are similar to human anthropometrics and should have mechanical degrees-of-freedom that represent the major actions of the involved joints in human locomotion. To date, all of the studies that have used neuromechanical models to study the control of locomotion have used a two-dimensional model where the motion was restricted to the sagittal plane (Taga et al. 1991; Taga 1995a; Ogihara and Yamazaki 2001; Paul et al. 2005; Yu and Ikemoto 2007; Zhang and Zhu 2007; Jo 2008). This level of detail is adequate for testing the neural mechanisms involved in locomotor control since the majority of motion occurs in the sagittal plane during walking. By limiting our analysis to the sagittal plane, certain aspects of the walking pattern are being ignored, for example there is a significant amount of action that takes place in the frontal plane to control balance of the upper body (MacKinnon and Winter 1993) and the pelvic motion during walking has been well documented for helping increase step length (Winter 1991). There have been some models that that include higher numbers of degrees of freedom ie. (Anderson and Pandy 2001) however these representations require much greater computational resources and are dependent on optimization methods to determine neural control patterns.

The mechanical properties, including segment lengths, segment centre of mass location, and moment of inertia for the mechanical model will be based on human anthropometrics of a 50^{th} percentile male (Winter 2004). Ideally, the neural control models developed in this thesis

should not be specific to one particular representation of the musculoskeletal system, but rather should be adaptable to be used on models of different sizes and different anthropometric parameters, although only one mechanical model will be tested for this thesis.

Early neuromechanical models neglected the dynamics of muscle contraction, or simply used a torque motor to actuate the joints of the mechanical model (Taga et al. 1991; Taga 1995a), while more recent models have included some aspects of the dynamics of muscle contraction in the model (Ogihara and Yamazaki 2001; Yakovenko et al. 2004; Paul et al. 2005). Additionally, the muscles in some previous neuromechanical model did not have very good anatomical correspondence to the organism being captured, for example Paul et al.'s (2005) model includes a generic flexor and a generic extensor at each joint and does not include any biarticular muscles, which have been shown to play an important role in the control of walking (Wells 1988; Van Ingen Schenaug et al. 1994; Zajac et al. 2002). The muscle models used in this study will be similar to those used in previous chapters, incorporating the active and passive force-length relationships, the force-velocity relationship, and excitation-contraction coupling. Although no biarticular muscles will be used in this model for computational purposes, the muscles placed in the model will be based on anatomical data from previous models of the lower-limb.

Often neuromechanical models will place constraints on the ROM of the joints to prevent non-physiological joint angles, particularly at the knee joint to prevent hyperextension. This is often justified as incorporating the effects of passive tissues such as ligaments and bony stops in the model (Paul et al. 2005). Constraints on joint ROM are usually implemented by creating a function relating the joint's angular displacement and a resistive moment that is applied at the joint; this function is usually an exponential opposition where reaching the end-points of the joint ROM will generate a dramatic increase in this resistive moment. The mechanical analog to this

implementation is having rotational springs placed at the joints, whose stiffness increases in a non-linear fashion when prescribed angular thresholds are reached. This approach will be used in the mechanical model developed in this chapter, with a model that was developed from joint stiffness values recorded from human subjects *in vivo* (Silder et al. 2007).

One challenging aspect of modeling the musculoskeletal system during locomotor movements is to determine how to represent interactions between the ground and the foot. Previous models have forced a direct connection between the foot and the ground during the stance phase (Taga et al. 1991), but the main problem with this approach is that a smooth transition from stance to swing is impossible, as there must be a defined release point (Gilchrist and Winter 1996). A preferred approach is to model some of the viscoelastic properties of the foot to more accurately represent the interaction between the foot and the ground. This approach has been used in the past and there are several models that can be implemented to capture the interaction between the foot and the ground (Gilchrist and Winter 1996; Anderson and Pandy 2001). Typically a series of non-linear spring damper systems are used to determine the vertical ground reaction force based on the penetration depth of a contact point into the ground. The number of viscoelastic elements can range from two per foot (Peasgood et al. 2007) to 9 per foot (Gilchrist and Winter 1996). The horizontal ground reaction forces typically use a form of a friction, based on the relative velocity of the contact point to determine the horizontal ground reaction force (Gilchrist and Winter 1996; Peasgood 2004; Paul et al. 2005). Often the foot will be modelled as two segments, with a stiff rotational spring between the two segments ie. (Gilchrist and Winter 1996), this will enhance the concordance with ground reaction force measurements made i*n vivo*. For the purposes of this thesis, it is not necessary to have a robust foot-ground interaction model, as we are more interested in the neural control mechanisms

involved in locomotion. The primary concern is that the contact model should be easily implemented and uses as few computational resources as possible. A viscoelastic contact model based on the work of Peasgood (2004) and refined by Millard (2006) will be used in this thesis.

Neural Control Model Considerations

Muscle activation patterns will be generated by a CPG model that is based on the work of Matsouka (1985) who published a set of differential equations that produce reciprocal oscillations of two neurons based on the properties of mutual inhibition and an adaptation effect . The advantages of the Matsouka oscillator as a CPG model have been described earlier but the most relevant benefit for this chapter is that the Matsouka model can be easily expanded to incorporate connections from several neurons as was first shown by Taga (1991). This allows for networks of neurons to be connected and generate output patterns based on the activity of several neurons, and allows neural connections to be established between the contralateral neurons and between the neurons for the other joints in the ipsilateral limb.

Evidence from animals (Whelan 1996; Gorska et al. 1999) and from human walking (Dietz et al. 1994; Prokop et al. 1995; Reisman et al. 2005) on split-belt treadmills indicates that the neural control of each limb may be relatively independent, therefore a separate CPG may be used for the control of each limb. Though this control may be independent between limbs there is also evidence that there are neural connections between contralateral sides (Rossignol et al. 2006). It has been proposed that these connections help make the walking pattern more stable by ensuring that the hips angular displacements are at an appropriate phase with respect to each other. This coupling between hip joints has been shown to help increase the stability of the walking pattern in a neuromechanical model by Ekeberg and Pearson (2005). While it is evident that there is some coupling in the control of the contralateral hips, the degree that this coupling

plays a role in the control of walking remains unclear. Therefore the CPG model that will be developed in this study will consist of two half-centres that control the flexion-extension pattern for each hip joint, while having neural connections between the contralateral half-centres with a weighting factor that can be manipulated to reveal the role of contralateral connections between hip joints in the control of locomotion.

Goals and Hypotheses

Goal #1:

To develop a computational model of the human musculoskeletal system that may be used to test hypotheses regarding the neural control of human locomotion. The specific requirements of this model have been described above, but in general this model should have a close approximation of the mechanical properties of the human locomotor apparatus and should respond to neural signals produced by separate neural control models with appropriate motion.

Goal #2:

To develop a basic model of CPG circuits that is involved in the control of locomotion. This model should provide the mechanisms to test the role of contralateral connections between neurons and connections between joints on the ipsilateral side. The frequency of output should also be able to be controlled to test the role that this has on the control of walking speeds.

Goal #3:

To test the ability of the walking speed of the mechanical model to be controlled by the frequency of the CPG output. Additionally, the role of contralateral connections between the half-centres involved in producing muscle activation patterns of the hip joints needs further determination.

The effect of connections between the neurons that control joints within the ipsilateral limb (ie. Hip to Knee connections) will also be examined.

It is hypothesized that a basic locomotor pattern will be able to be achieved by the mechanical model that is developed in this study, when the model is provided with adequate weight support. However, due to the lack of feedback mechanisms represented in the neural control models in this study there will be a great amount of variability in the joint motion, which will be observed in phase diagrams (plots of joint velocity vs. joint angle) of the joints of the lower limb. It is further hypothesized that the walking speed of the mechanical model will be able to be controlled by altering the frequency of output of the CPG model, though there will be variability in this relationship due to the lack of feedback in the control mechanisms. Lastly, it is hypothesized that the stability of the walking pattern will be improved by adding connections between appropriate neurons in the CPG model. These connections include those between the half-centres of the contralateral hip joints, and the ipsilateral hip and knee joints. Improved stability of the walking pattern will be evident through less variability in the phase diagrams of the joints of the lower limb of the mechanical model.

Methods

Summary of Experiments Performed in This Study

The following was a summary of the simulations that were performed in this study with the specific goals of each simulation.

Experiment #1:

Once the mechanical model was constructed, the first series of simulations tested the ability of the walking speed of the model to be controlled by altering the frequency of the CPG

output. For this experiment, muscle activation patterns were only provided to the muscles actuating the hip joints of the model, while the knee was passively controlled. Similar approaches have been used to test the control systems of walking robots (Lewis et al. 2003). This simulation also tested the effect of providing inhibitory connections between the contralateral neurons of the hip joints. A series of simulations were also carried out to independently examine the weight of these inhibitory connections.

Experiment #2:

The second set of simulations for this study examined the ability to control walking speed by altering the frequency of the CPG model when knee muscles were added to the model. This series of simulations also examined the effect of adding neural connections between the CPG neurons of the hip joint and the ipsilateral knee joint.

Experiment #3:

The final series of simulations carried out for this study examined the effect of the body weight support system that was used in the above simulations. In this series of simulations, the stiffness of the spring that supports the body weight of the mechanical model was manipulated and the effect on the walking speed was examined.

Mechanical Model Description

The mechanical model consists of five segments, which were divided into two lower-limbs, each consisting of a thigh and a shank and a lumped head arms and trunk segment (HAT). The anthropometric properties of the segments are given in Table 5.1. The segments were articulated by a total of 4 revolute (pin) joints, corresponding to the hip and knee for each limb. Overall, the model had seven degrees of freedom (pitch angle and two translations (vertical and

horizontal) of the trunk segment, rotation about each hip, and rotation about each knee. The mechanical model was implemented in Dynaflex Pro (Motion Pro Inc, Waterloo, ON) and exported to C++-code, which was implemented as an S-Function within Simulink (ver. 1.6), which is a graphical tool for solving dynamic models based on differential equations and a component of MATLAB R14 (The Mathworks Inc, Natwick, MA). A schematic of the mechanical model was shown in Figure 5.1.

Table 5.1: Anthropometric properties of the Mechanical Model

Segment	Mass (kg)	Moment of Inertia ($kg.m^2$)	Length (m)	COM ratio *
HAT	37.81	2.1901	0.55886	0.5
Thigh	7.88	0.1488	0.44019	0.466
Shank	3.54	0.03960	0.37585	0.442

* COM ratios were given as a proportion of the segment length from the proximal end of the segment.

Upper Body Support System Model

Because balance control mechanisms were not implemented in the model at this time, it was required that the HAT segment be supported during simulations of the model. The HAT segment was supported by a spring-damper, attached to a mass-less rigid body above the segment; this rigid-body was then attached to a frictionless prismatic joint, which allowed translation in the direction of progression. This support system for the HAT segment also restricted rotation (pitch) of the HAT, thus reducing the total degrees of freedom for the model to 6. Such an arrangement was akin to a body weight support harness that would be used for rehabilitation or gait research ie. (McGowan et al. 2008). The detailed properties of the support system were given in Appendix A.

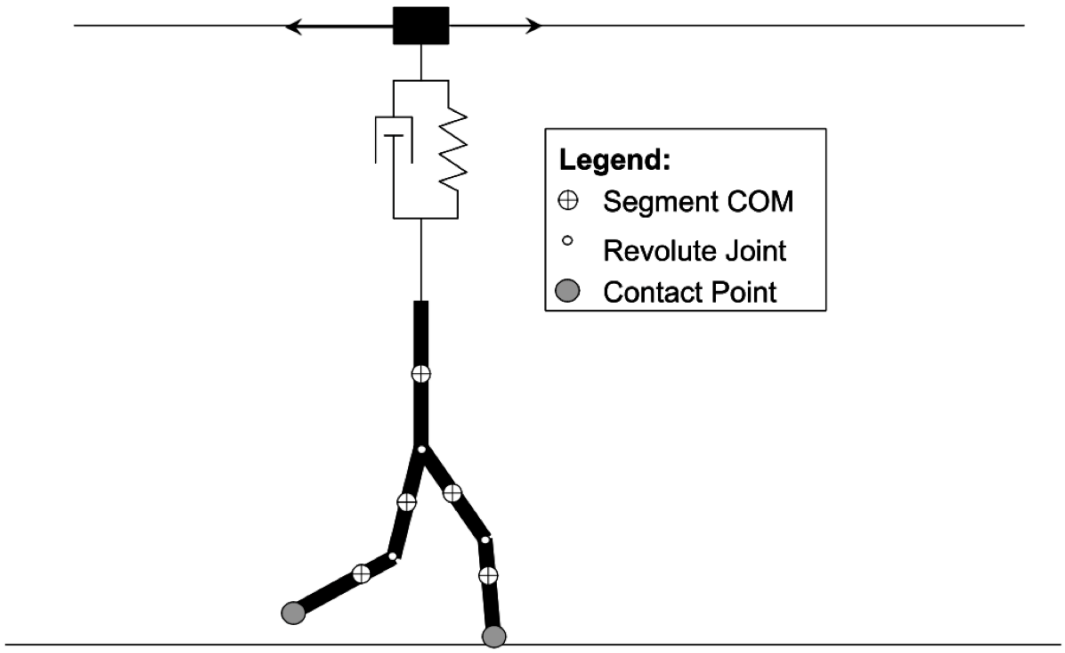

Figure 5.1: A schematic illustrating the mechanical model.

Ground Contact Model

Contact forces between the ground and the foot were applied at the end point of the shank segment. The vertical ground reaction forces were determined by the penetration of the contact point into the floor, by means of a nonlinear spring–damper system. The damping was restricted to a maximal value by the use of a cubic spline interpolation function (indicated by *c* in Figure 5.2). This model was developed by Peasgood (2004) and improved by Millard (2006). This representation has been shown to have reasonable correspondence to ground reaction forces recorded during normal locomotion. The equations that govern this interaction were shown in Figure 5.2, the specific properties of the ground contact model were given in Appendix A.

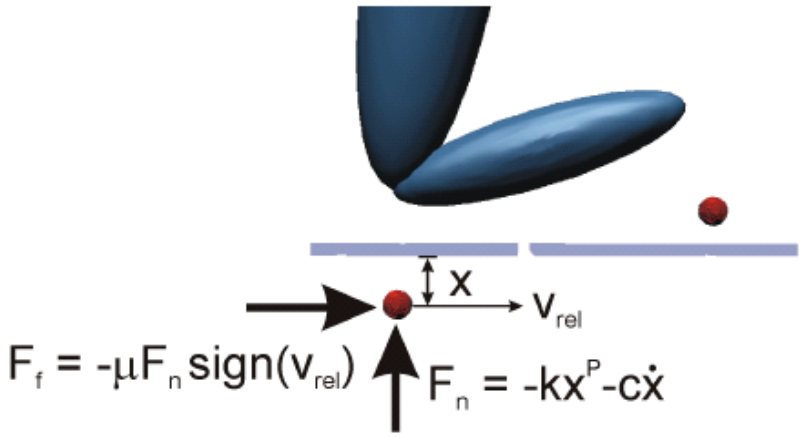

Figure 5.2: Details of the ground contact model. See description text below. Note that a foot with two contact points is presented in this figure. However, the model used in this study only had one contact point at the distal end of the leg segment. From Millard (2006).

F_f was the frictional force, μ was the coefficient of friction, F_n was the normal force v_{rel} was the relative velocity of the contact point to the ground, k was the stiffness of the spring in the spring damper, x was the penetration of the contact point into the floor, p was the power value which gives the non-linearity of the spring damper function, c was the cubic step interpolation function, which was shown in Equation 5.1, this function scaled the damping value between 0 (b_{min}) and a maximal damping value of b_{max}. The maximum damping occurred when the contact point reactions reached a prescribed penetration depth into the ground (d_{max}). Note that Figure 5.2 indicated two contact points, whereas only one was used in the model, as the foot segment was not represented in our mechanical model.

$$cubicStep(x,b_{\min},d_{\max},b_{\max}) = c_{\min} + (b_{\max} - b_{\min})\left(\frac{x}{d_{\max}}\right)^2 (3 - 2\left(\frac{x}{d_{\max}}\right))$$

Equation 5.1

The frictional force (F_f) applied by the ground was determined by a Coulomb friction model, with the coefficient of friction (μ) being varied depending on the horizontal velocity of

the contact point. The cubic step interpolation was used to interpolate the value of μ between limit values of v_{rel} for static (v_s) and dynamic (v_d) friction. Figure 5.3 shows how μ was altered for different values of v_{rel}.

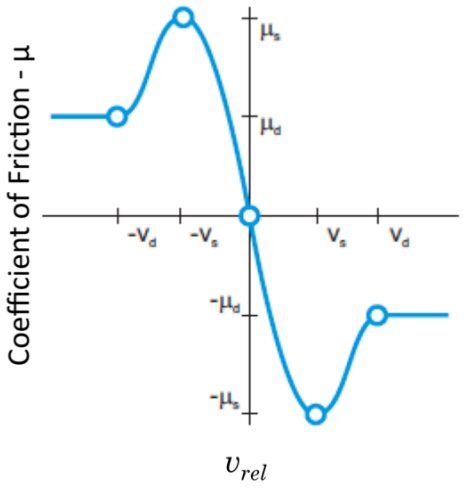

Figure 5.3: Relationship between coefficient of friction and relative horizontal velocity of the contact point. From Millard (2006).

Musculoskeletal Geometry Model

The current model was actuated by four muscles per limb, which represented a hip flexor (ie. Psoas Major), a hip extensor (ie. Gluteus Maximus), a knee flexor (ie. Short Head of Biceps Femoris) and a knee extensor (ie. Vastus Group). To define the muscle attachment points a local coordinate system was established for each segment, with the local origin at the distal endpoint of the segment and the local y-axis defining the long axis of the segment, and the local x-axis pointing in the anterior direction. The local coordinate systems used to determine the muscle attachment points were shown in Figure 5.4, with the local origin and insertion coordinates being given in Table 5.2. The local muscle attachment points were obtained from Hoy et al (1990) and scaled to fit the current model.

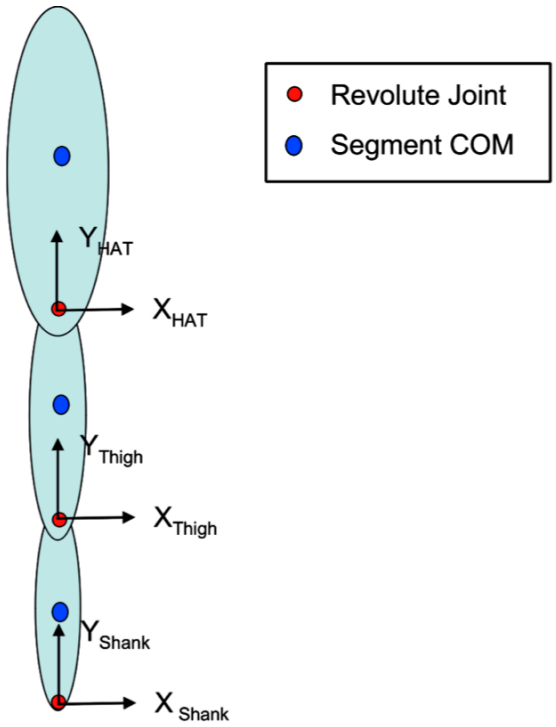

Figure 5.4: Local coordinate systems used to determine the muscle attachment points.

Table 5.2: Origin and insertion coordinates used in model

Muscle	Origin Coordinate System	Origin X (m)	Origin Y (m)	Insertion Coordinate System	Insertion X (m)	Insertion Y (m)
Knee Flexor	Thigh	-0.0007	0.17863	Shank	-0.0504	0.33228
Knee Extensor	Thigh	0.0106	0.20263	Shank	0.0400	0.36998
Hip Flexor	HAT	0.0250	0.13500	Thigh	0.0000	0.3519
Hip Extensor	HAT	-0.0578	0.075403	Thigh	-0.0158	0.3810

A plot of the musculoskeletal geometry is shown in Figure 5.5.

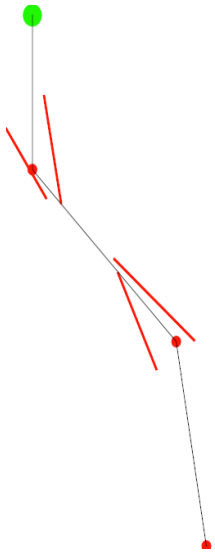

Figure 5.5: Plot of the musculoskeletal geometry used in the model.

Although muscle moment arms actually vary with the posture of the model, a constant moment arm was assumed for each muscle in order to simplify the calculation of joint moments. The nominal moment arms used in the model are shown in Table 5.3. Nominal moment arm values were obtained from literature sources (Raikova and Prilutsky 2001). Muscle lengths were estimated by determining the straight point-to-point distance between the origin and insertion points.

Table 5.3: Nominal moment arm values used in the model. A positive moment arm represents a joint flexor moment arm while a negative moment arm represents an extensor moment arm.

Muscle	**Moment Arm Value (m)**	
	Hip	**Knee**
Knee Flexor		-0.045
Knee Extensor		0.045
Hip Flexor	0.025	
Hip Extensor	-0.100	

Passive Joint Range of Motion Model

Each joint was constrained to a physiologic range of motion by a nonlinear rotational spring, which produced an opposing moment when the joint approached the end range of motion. The equations for the joint constraints were based on passive moments measured *in vivo* by Silder et al (2007), and were given in equations 5.2 and 5.3 below. These equations take into account the different ranges of motion that were possible depending on different joint configurations, for example the range of motion at the knee would be altered depending on the position of the hip joint. The β values were constants that dictated the shape of the passive moment curves, while α values indicated the angular position of a joint where that term of the equation became active and produced an opposing moment. Lastly, the joint angles were represented by θ_h, θ_k and θ_a for the hip, knee and ankle respectively. The values for β and α are given in Appendix A; all values were taken from Slider et al (2007). For the purposes of the ankle angle in this model, it was assumed that the ankle would be in a constant neutral posture that would be observed during normal quiet standing (0° Plantarflexion). These passive moments that limit the range of motion would be applied by passive muscle tension, ligaments and skeletal anatomy *in vivo*. This model also included the passive contribution that would be applied by muscles that were not present in the model to more closely represent the passive moment that would occur *in vivo.*

$$M_h = e^{-\beta_h^{RF}(\theta_h-(\beta_k^{RF}/\beta_h^{RF})\theta_k-\alpha^{RF})} + e^{-\beta_h^{HF}(\theta_h-\alpha^{HF})}\ldots$$
$$-e^{\beta_h^{HAM}(\theta_h-(\beta_k^{HAM}/\beta_h^{HAM})\theta_k-\alpha^{HAM})} - e^{\beta_h^{HE}(\theta_h-\alpha^{HE})}$$

Equation 5.2

$$M_k = -\left(\frac{\beta_k^{RF}}{\beta_h^{RF}}\right) e^{-\beta_h^{RF}(\theta_h - (\beta_k^{RF}/\beta_h^{RF})\theta_k - \alpha^{RF})} - e^{\beta_k^{HE}(\theta_k - \alpha^{KE})} \ldots$$
$$+\left(\frac{\beta_k^{RF}}{\beta_h^{RF}}\right) e^{\beta_h^{HAM}(\beta_h - (\beta_k^{HAM}/\beta_h^{HAM})\theta_k - \alpha^{HAM})} + e^{\beta_h^{KF}(\theta_h - \alpha^{HE})} \ldots$$
$$+ e^{\alpha_k^{GAS}(\theta_k - (\beta_a^{GAS}/\beta_k^{GAS})\theta_a - \alpha^{GAS})}$$

Equation 5.3

The results of these passive joint moment equations are shown in Figure 5.6, over the range of joint angles that would typically be observed in human walking. The effect of adjacent joints on the passive joint angles was also shown in Figure 5.6.

Joint motion was also subject to viscous damping which opposed the direction of movement; damping coefficients (*B*) of 0.1 Nm.s/rad were used at the hip and the knee joints. Light damping of the joints was required to maintain computational stability during integration of the equations of motion for the model (Anderson and Pandy 1999). The equations for the damping moment were shown below, where M_d was the damping moment, *B* was the damping coefficient, and ω was the angular velocity of the joint.

$$M_d = -B\omega$$

Equation 5.4

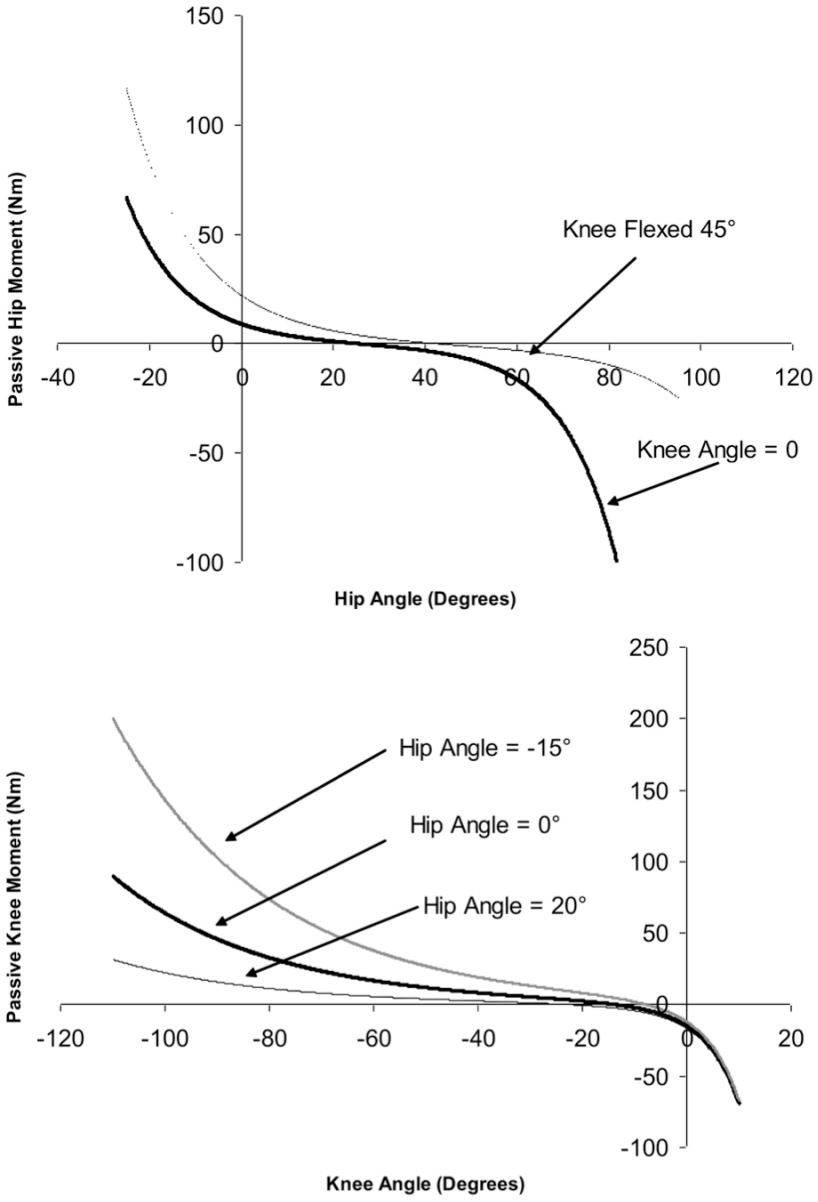

Figure 5.6: Passive moment vs. angle relationships for the hip (top) and knee (bottom) joints. The effect of the posture of adjacent joints on the passive moments is shown. At the hip joint positive angles represent flexion, while a positive moment indicates an extensor moment. At the knee joint a negative joint angle indicates knee flexion, while a positive moment represents a knee extensor moment.

Muscle Model

The muscle model used was similar to that which was used in the pendulum model, and was fully described in Chapter 3. The muscle properties that were used for this model were

shown in Table 5.4. These values were taken from literature sources (White et al. 1989; Hoy et al. 1990; Anderson and Pandy 1999), except for the value of P_O for the knee extensors, which was nominally set to be lower than typical literature values, since the use of typical literature values (approximately 6000N) produced erratic motion.

Table 5.4: Muscle Model Properties Used in the Model

Muscle	L_O (cm)	L_{SEC} (cm)	V_{max} (L_O/s)	P_O (N)
Hip Extensor	10.7	3.4	9.8	1730
Hip Flexor	7.4	15.1	9.3	1320
Knee Extensor	22.5	4.6	10.0	2000
Knee Flexor	10.4	9.0	6.9	2814

Muscle forces were calculated based on the kinematics of the mechanical model and the neural inputs that were given by the output of the CPG model, which will be described later in this chapter, after being subjected to a first order delay process which represented excitation-contraction coupling ECC. The differential equation used to represent ECC was presented previously, in Equation 3.2.

Central Pattern Generator Model

The basis of the CPG model used for this study was similar to that used in the pendulum simulations (Chapters 3 & 4), but had been expanded to incorporate multiple joints. As stated earlier, the numerical CPG model was based on a set of differential equations that were introduced by Matsuoka (1985; 1987). These equations use mutual inhibition and an adaptation effect to produce a reciprocal firing pattern for two half-centre neurons. The model was extended

beyond those introduced by Matsuoka, by incorporating several joints into the CPG model. Two different CPG models were used in this study. For the first aspect of this study the CPG only activated the muscles of the hip joint while no neural signals were activated at the knee joint. For the second portion of this study, the CPG model was expanded to incorporate the knee joints into the model.

A schematic indicating the connectivity of neurons in the CPG model for the hip joints is shown in Figure 5.8. The CPG contained a separate half centre for each hip, with a flexor and extensor neuron for each joint, which activated the appropriate muscle in the mechanical model. The half centre neurons mutually inhibited each other, such that only one half centre may be active at a time for a given joint. The neurons also had an inhibitory connection to the same neuron of the contralateral half-centre, such that the flexor neuron of the left hip's half centre would inhibit the flexor neuron in the right hip's half centre, and vice versa. These contralateral connections were also present for the extensor neurons. Expansions to this CPG model would be made to include the knee joint.

These neurons were also subject to an adaptation effect (self-inhibition), where sustained activity would lead to a decrease in output, allowing for oscillations to occur between the half centres. There was also a constant input (q_t) to each neuron in the model, which affected the magnitude of the output of the CPG.

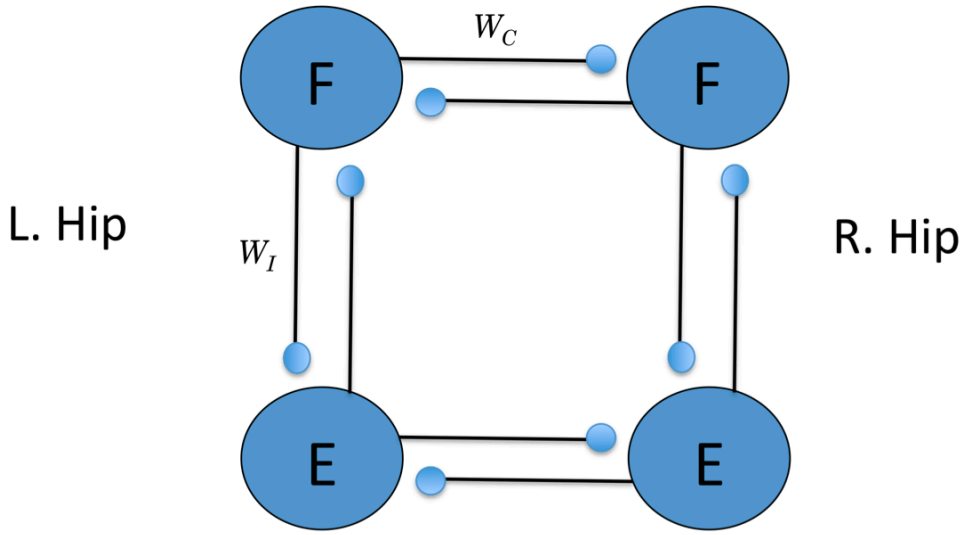

Figure 5.7: Connectivity of the CPG neurons for the hip joints. The flexor neurons are indicated with an 'F' while the extensor neurons are indicated with an 'E'. W_C is the weight of the connections between contralateral neurons, while W_I is the weight of the connections between ipsilateral neurons. The tonic input to each neuron (q_t) is not shown in this diagram.

The differential equations that describe the activity of these neurons differed slightly from the basic half-centre CPG model that was used in the previous chapters. The inner states of the neurons had an additional term to indicate the connections between the contralateral neurons, as shown in Equation 5.5:

$$\dot{u}_F = \frac{1}{\tau_{rise}}(q_t - u_F - \beta v_F - W_I y_E + W_C y_{CF})$$

and

$$\dot{u}_E = \frac{1}{\tau_{rise}}(q_t - u_E - \beta v_E - W_I y_F + W_C y_{CE})$$

Equation 5.5

Where, τ_{rise} was a time constant for the rise time of the output of the neurons and was set to 10 ms, q_t was the tonic input which specifies the magnitude of the output, u_f and u_e were the

current internal states of the neurons, v_f or v_e was the adaptation term, which was calculated in the same manner previously described and influenced how long the neuron woud remain active before its activity diminished. The variables y_f, and y_e indicated the output of the ipsilateral neurons, and W_I was a weighting value that represents the strength of the inhibitory connection between the half centre neurons. The activity of the contralateral neurons was indicated by y_{CE} for the contralateral extensor and y_{CF} for the contralateral flexor, W_C was a weighting factor that determines the strength of the inhibitory connections between the contralateral neurons. Once the inner state of the neuron was calculated, the output was calculated in a similar manner to that used in the previous chapter, as shown in Equation 5.6.

$$y_F = \max(0, u_F) \text{ and } y_E = \max(0, u_E)$$

Equation 5.6

Once the output of the CPG model was determined, the outputs of the various neurons provided the neural input to the appropriate muscles in the mechanical model. In the following section, the values of certain parameters were systematically manipulated in order to assess the function of the CPG circuit. The ability of the CPG model to produce a walking like movement pattern was assessed by examining the kinematics of the musculoskeletal system. The ability to alter walking speed by manipulating the parameters of the CPG model was also assessed in this study.

Overall Data Flow

Once the muscle forces were determined, the moment of force at each joint was given by the following general equation:

$$M_j = I(\ddot{q}) + C(\dot{q}) + G(q) + GRF(\dot{q}, q) + F_{MUS} \times r_{mus} + M_{PASS}(\dot{q}, q)$$

Equation 5.7

Where, M_j was a vector of the total joint moments for the system, q was a vector of the state variables (position and velocity) for the system, I was the inertial tensor for the system, C represented Coriolis effects for each joint, G represented gravitational effects at each joint, GRF represented the moment created by the ground reaction force, F_{mus} was a matrix of muscle forces and r_{mus} was a vector of the moment arms for each muscle. M_{PASS} represented the passive moments acting at the joints and included joint damping and end-range stiffness.

The equations of motion for the system were integrated in Simulink using the *ODE23t* integrator, to determine the velocity and position of the model. The *ODE23t* integrator was a moderately stiff variable time-step integrator that used a maximum step time of 10^{-2} s and minimum step time of 10^{-15} s, with an initial step size of 10^{-4} s.

A flowchart showing the flow of signals from the CPG model to the mechanical model is shown in Figure 5.8.

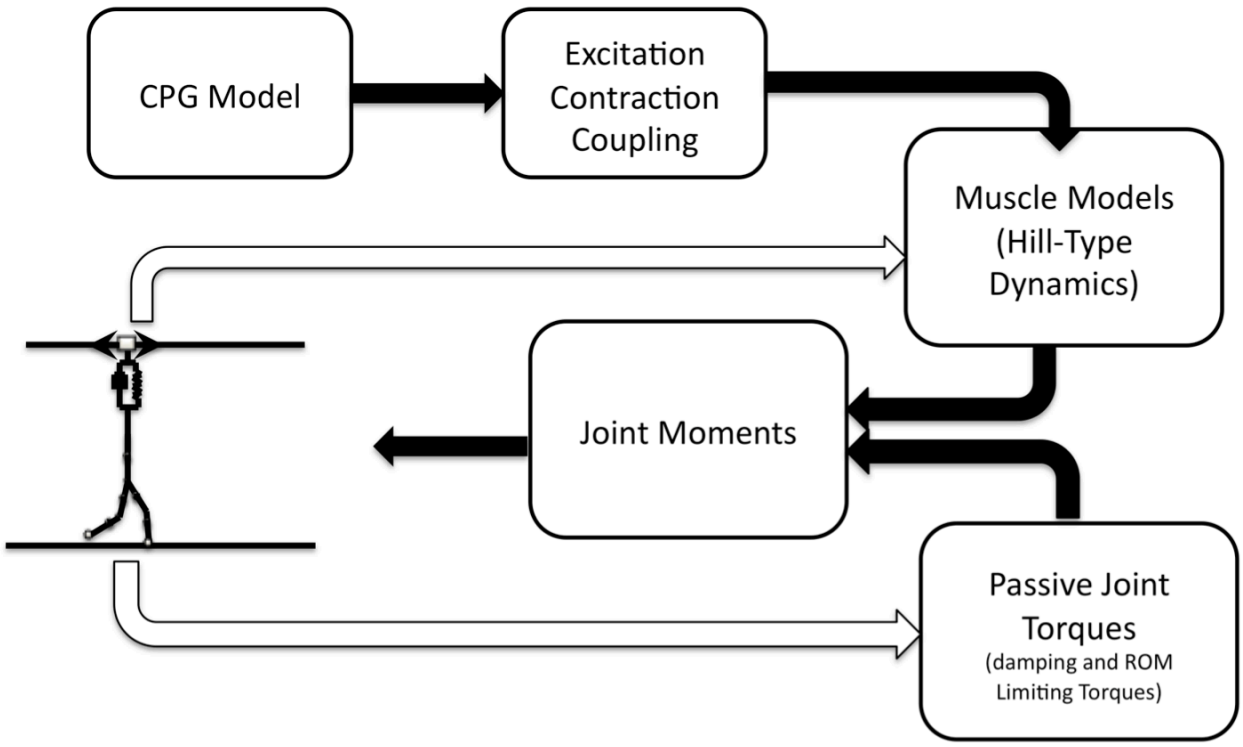

Figure 5.8: Flowchart showing the flow of data through the model. The black arrows represent the flow of data from the CPG model to the mechanical model's kinematics, while the white arrows indicate where kinematic data from the mechanical model is used to calculate muscle forces and passive joint moments.

Simulation Descriptions and Results

All simulations were carried out over a 50s simulation period, with signals generated by the CPG model being used to provide the activation inputs to the muscle model, which then produced force to actuate the mechanical model, as shown in the flowchart in Figure 5.8. This simulation time allowed for the analysis of approximately 40s of steady state walking, as the model took approximately 10s to begin to progress in the forward direction in a consistent manner. The same initial conditions were used for all simulations, with the mechanical model held in space and all joint angles and velocities set to zero, with the center of mass of the HAT segment being held at a height of 1.25 m above the ground (contact points were approximately 15.5 cm off the ground). The CPG model was initialized with the right limb entering the

extension phase of the cycle. These initial conditions were chosen based on pilot testing and chosen because they allowed a walking pattern to naturally emerge.

Experiment #1: Effect of W_c on CPG Output

Before the output of the CPG model was applied to the mechanical model, the effect of the weight of contralateral connections (W_C) was assessed on the frequency and amplitude of the CPG output. Six series of simulations were carried out with the value of τ_{ad} set to 0.1, 0.15, 0.25, 0.35, 0.5 and 0.75. For each set of simulations the value of W_C was systematically incremented from -1.0 to 0, in steps of 0.01. The constant input value (q_t) was set to 1.0 for all the following simulations.

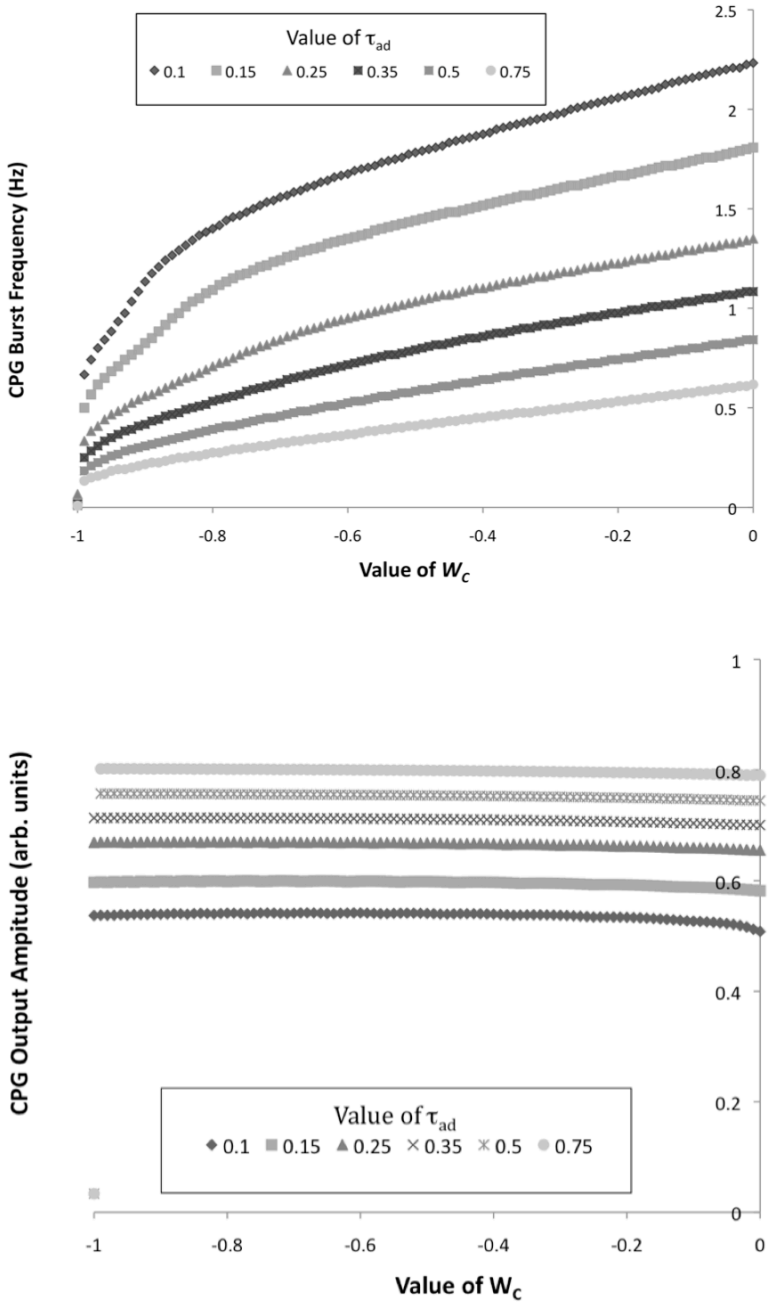

Figure 5.9: The effect of W_C and τ_{ad} on the burst frequency of the CPG model output frequency (top) and CPG model output amplitude (bottom).

The combined effect of τ_{ad} and W_C on the frequency and amplitude of the CPG output is shown in Figure 5.9. It could be seen that increasing the weight the inhibitory connection

between the contralateral neurons (W_C) led to a decrease in the burst frequency of the CPG model, while increasing the value of τ_{ad} also led to a decrease in the burst frequency of the CPG model, as was seen in the pendulum studies. The CPG model no longer produced an oscillatory output when the value of W_C reached -1.0, due to the input from the contralateral connection overwhelming the inhibitory connection from the ipsilateral neuron. It was observed that increasing the value of τ_{ad} led to an increase in the amplitude of the CPG output, due to the longer period of time that the neuron output was allowed to integrate before decreasing, however the value of W_C appeared to have very little effect on the amplitude of the CPG output until the value of W_C reached -1.0, when the amplitude of the CPG output dramatically decreased.

Experiment #2: Effect of τ_{ad} and W_C on the Walking Pattern of the Model

A series of simulations were carried out where the output of the CPG model served as muscle activation signals for the mechanical model as seen in the flowchart in Figure 5.8. For this set of simulations, the value of τ_{ad} was incremented from 0.1 to 2.5s, in increments of 0.01. These simulations were repeated with W_C set to values of 0.0, -0.25 and -0.5.

The outcome measure for this set of simulations was the average forward walking speed over the simulation, which indicated how well the model was able to progress in the forward direction. A normal walking speed in a healthy adult would be approximately 1.2 to 1.8 m/s (Andriacchi et al. 1977), therefore the range of parameters that led to this range of walking speeds will be noted of particular importance. In order to assess the variability in the forward walking speed, the bias was removed from the forward walking velocity signal, and the root-mean-square (V_{RMS}) was determined. This calculation was performed on the walking speed data from the final 40s of the trial to remove any influence of the initiation of the simulation. A low

V_{RMS} value indicates the forward walking velocity was very consistent over the time period analyzed, while a higher V_{RMS} value indicates more variability in the walking speed.

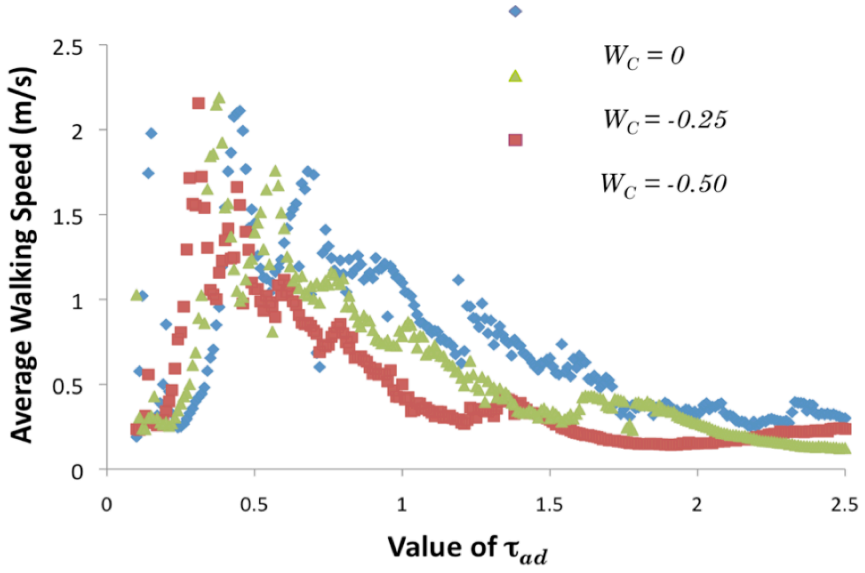

Figure 5.10: Average walking over a 50s simulation for values of τ_{ad} between 0.1 and 2.5, with the value of W_C set to 0.0 (diamonds), -0.25 (triangles) and -0.50 (squares).

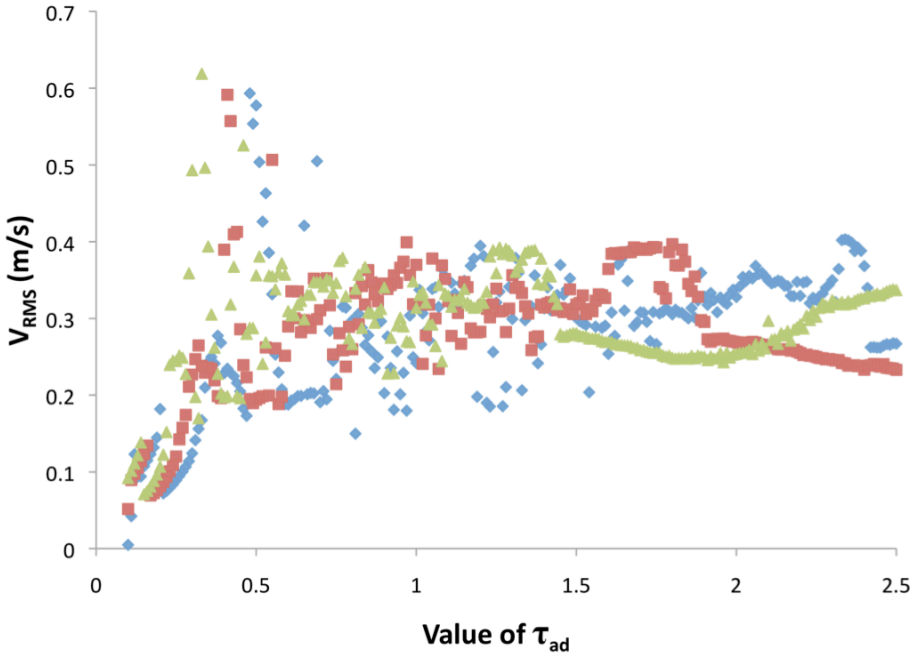

Figure 5.11: RMS velocity in the forward direction across values of τ_{ad} from 0.1 to 2.5, with W_C set to 0.0 (diamonds), -0.25 (triangles) and -0.50 (squares).

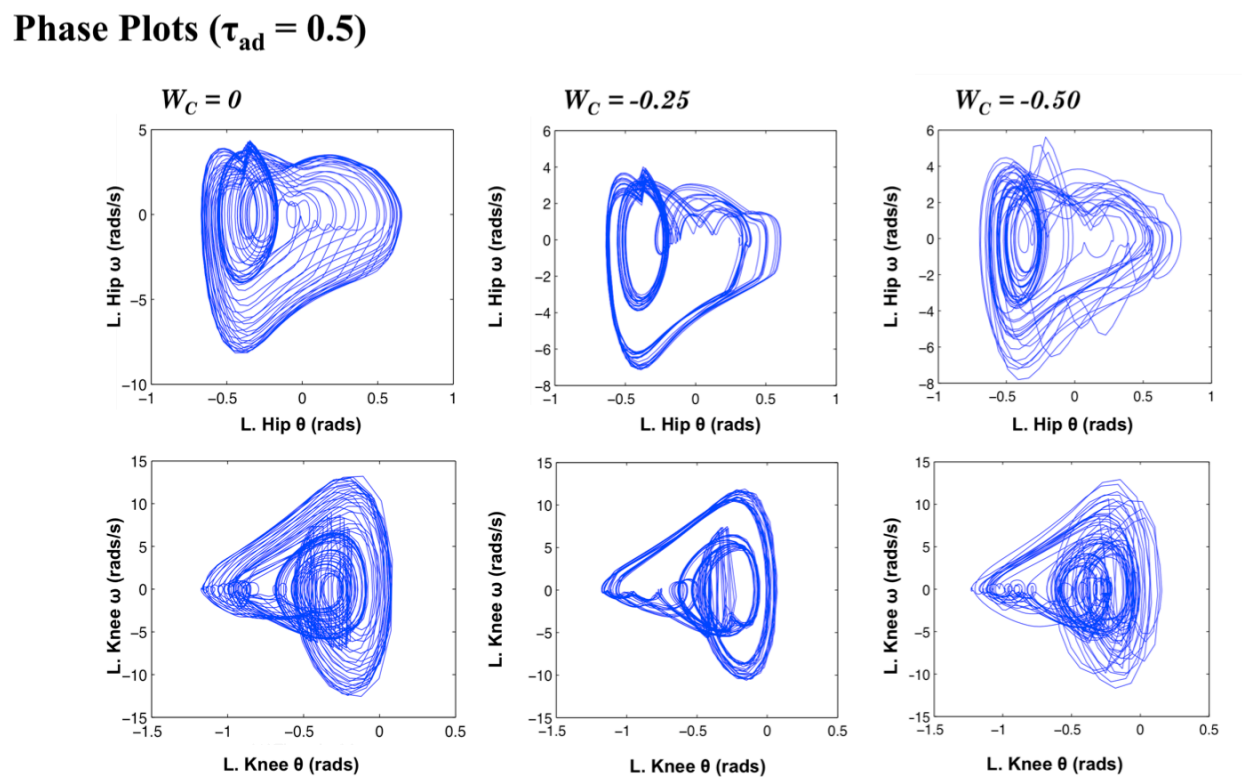

Figure 5.12: Phase plots for the left hip (top) and knee (bottom), when τ_{ad} = 0.5s, when W_C = 0, -0.25 and -0.5.

The results presented in Figure 5.10 showed that modifying a single variable could control the walking speed of a feedforward biped model, although there was a large degree of variability in this relationship. The mechanical model had a reasonable walking speed (> 1.0 m/s) when the value of τ_{ad} was approximately between 0.3 and 0.9s. This range of τ_{ad} values corresponds to those that would produce a normal walking speed, however there were instances when the walking speed was greater than 2.0 m/s, which is greater than a normal walking speed. Also, it was not assessed whether the biped model was truly walking or whether there were instances when both contact points were off the ground, which would be classified as running. When the values of τ_{ad} were below 0.3, there was an inadequate accumulation of force in the

muscle model, leading to lower muscle forces. When the value of τ_{ad} was higher than 1.0s there was too much time between cycles, resulting in slower walking speeds.

The weight of the contralateral connection also had an effect on the relationship between the τ_{ad} and the walking speed of the model. When τ_{ad} was within the range that permitted normal walking speeds (0.3-0.9s) the variability of the walking pattern resulted in a large variation in walking speed with all values of the contralateral connection weights (Figure 5.11). However, when the value of τ_{ad} was greater than 0.9s, increasing the inhibitory weight between contralateral half centres resulted in lower walking speeds for similar values of τ_{ad}.

The kinematics of the biped model's walking pattern were also affected by the weight of the connection between ipsilateral neurons (W_C). Phase plots showing the kinematic patterns of the biped when τ_{ad} was set to 0.5s are shown in Figure 5.12. From the phase plots it can be observed that the most stable walking pattern occurred when WC was set to -0.25, indicating for this particular case that a moderate amount of connectivity between the hip joint's neurons led to a more stable walking pattern, whereas too much inhibition between the neurons led to a decrease in the stability of the walking pattern. This effect was also seen in Figure 5.13, where the kinematics of the walking pattern were illustrated. This relationship however did not hold across all values of τ_{ad}. For example, when τ_{ad} was set to 0.6s, the phase plots show that a more cyclic walking pattern was achieved when there was no connectivity between the contralateral neurons (Shown in Figure 5.16).

The weight of the contralateral connections also had an effect on the coordination between the left and right hip joints. This was examined by plotting the value of the left hip angle against the value of the right hip angle over a simulated walking trial, and was shown in Figure 5.14. This approach to studying the coordination between contralateral limbs has been

previously used to examine changes in coordination during human walking (Byrne et al. 2002a). As could be observed in Figure 5.14, there was not a large degree of coordination between the left and right hip joints in any of the simulations plotted, however this was somewhat expected due to the lack of feedback mechanisms in the model. For comparison purposes, a similar plot that was obtained from a trial of human treadmill walking (walking speed= 1.43m/s) was shown in Figure 5.15. The most noticeable difference between the hip joint coordination between the simulated walking pattern obtained from the model and the recorded human walking were differences in the biases of the axis crossing locations. This was likely due to the fact that the HAT segment of the model was maintained in a completely upright position, whereas the trunk angle was not controlled in the human walking trials.

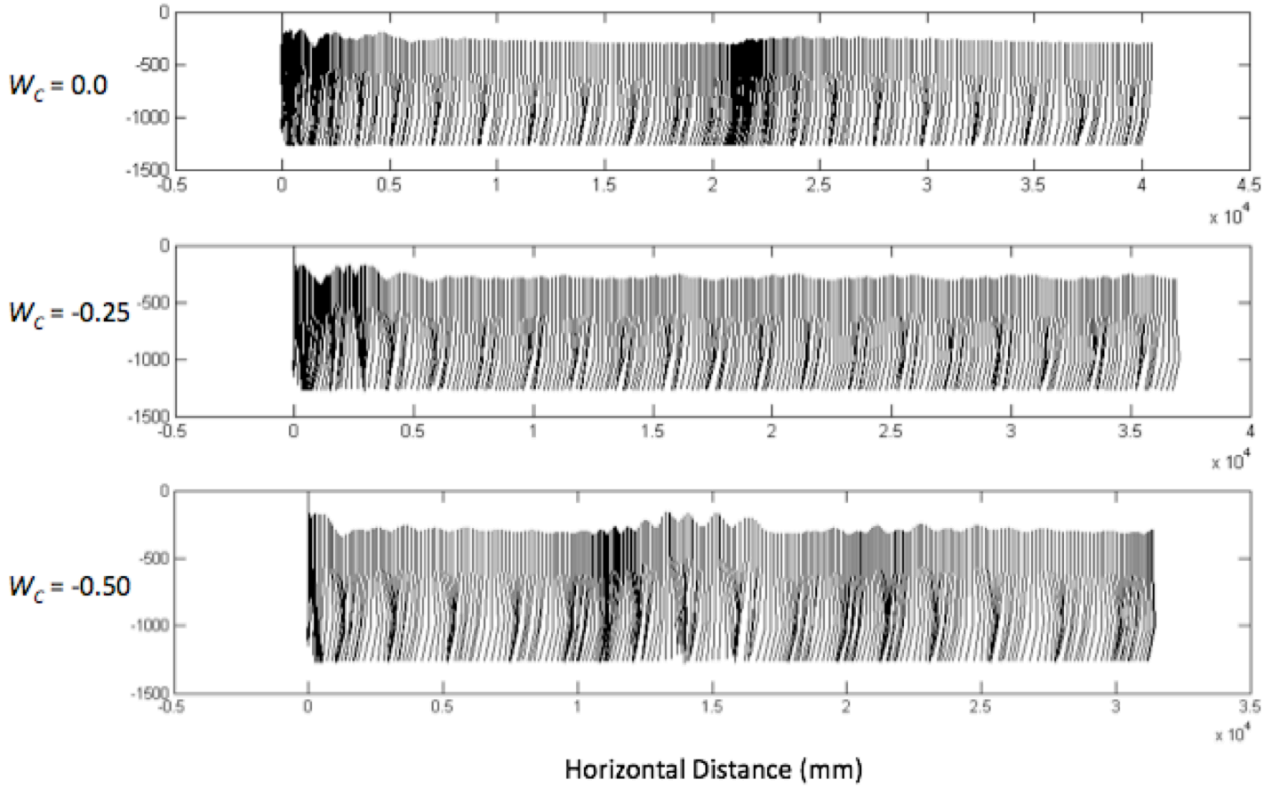

Figure 5.13: Kinematic walking patterns of the biped model, with τ_{ad} = 0.5s and W_C being set to 0.0, -0.25 and -0.5. The right side of the biped model was traced every 0.1s.

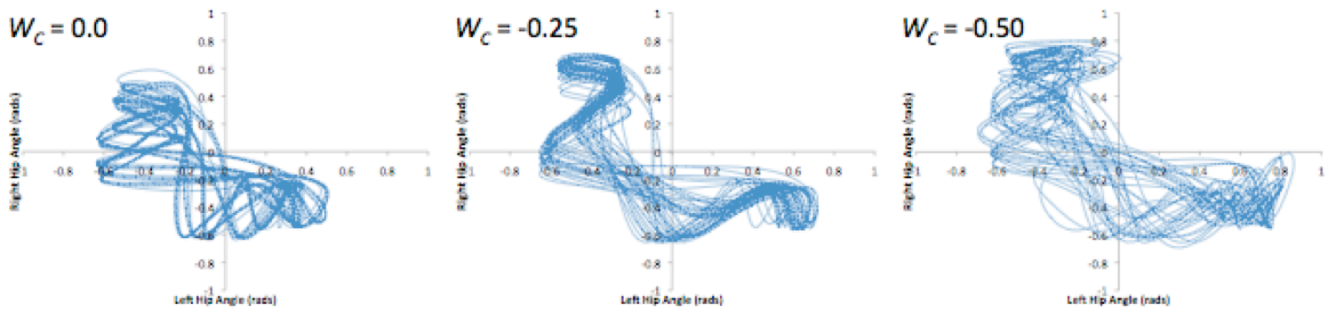

Figure 5.14: Angle-Angle plots comparing the angles of the left and right hip joints for the three levels of W_C tested in the simulation. The right hip angle is plotted on the vertical axis, while the left hip angle is plotted on the horizontal axis.

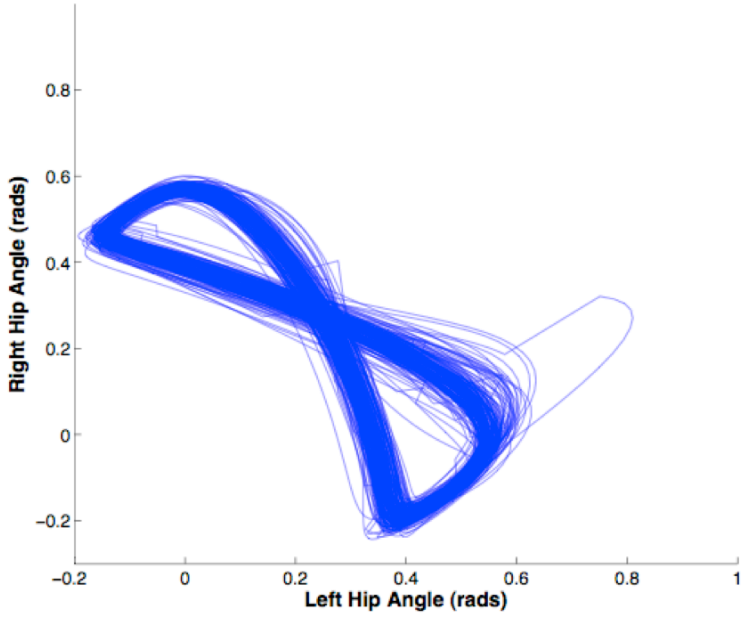

Figure 5.15: Angle-angle plot comparing the angles of the left and right hip angles recorded during human walking. The participant was walking on a treadmill at a speed of 1.43 m/s. The right hip angle is plotted on the vertical axis, while the left hip angle is plotted on the horizontal axis.

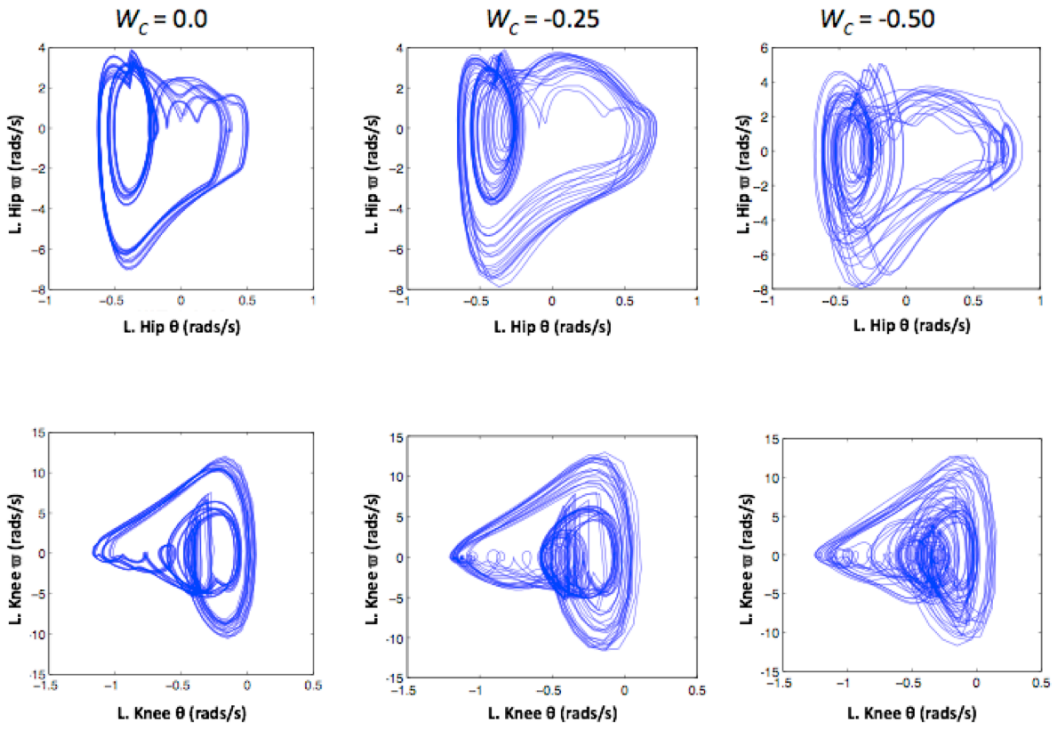

Figure 5.16: Phase plots of the left limb of the biped model when τ_{ad}= 0.6s at the three levels of W_C tested.

Experiment #3: Independent Effects of Bilateral Hip Joint Connectivity on the Walking Pattern of the Model

In order to independently assess the effects of the inhibitory contralateral connections in the CPG model, without altering any other parameters within the model, a series of 20 simulations were carried out with τ_{ad} being set to 0.5s and the value of W_C being systematically incremented for 0 to -1.0, by steps of 0.05. The average forward walking speeds for these simulations were shown in Figure 5.17. Initially, increasing the weight of the inhibitory connections between contralateral hip neurons led to a decrease in the walking speed achieved by the mechanical model. However, increasing the weights of the inhibitory connections to a

moderate value led to an increase in the walking speed of the model. Further increases to the value of W_C led to decreases in the observed walking speed of the model, most likely to the decreased frequency of the CPG output that was observed with the increase of W_C, as shown in top panel of Figure 5.9.

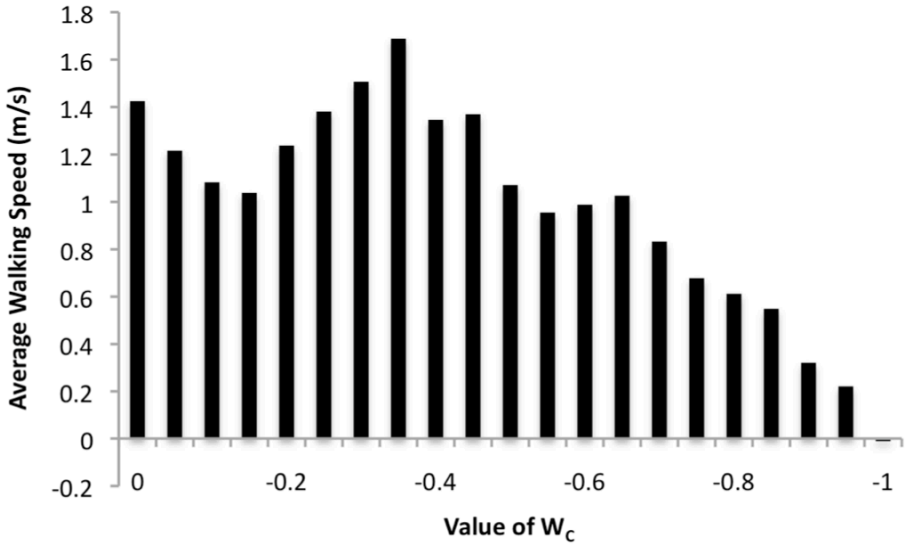

Figure 5.17: Average walking speed of the biped model at various values of W_C, when τ_{ad} = 0.5 s.

The variability of the forward velocity (V_{RMS}) for these simulations was shown in Figure 5.18. The simulations that resulted in greater average walking speeds corresponded to the simulations were there was a lower amount of variability in the forward walking speed, indicating that the variations in the walking speed were mainly due to slowdowns in the model.

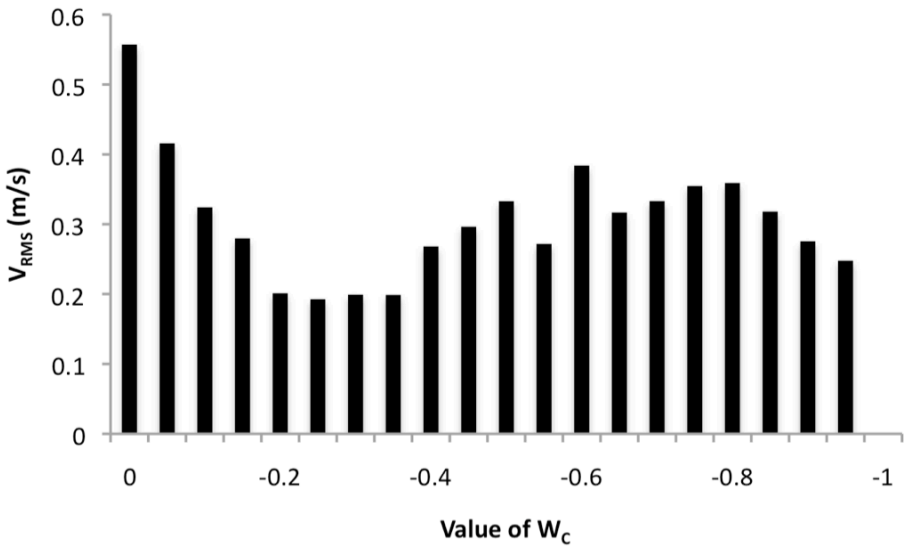

Figure 5.18: Effect of the weight of inhibitory bilateral hip neuron connections on the variability of the forward walking speed of the model, represented by the root-mean-square (RMS) of the forward walking speed.

Experiment #4: Addition of Knee Joint Muscles to the Biped Model

In order to assess the impact of the addition of the knee joint muscles to the mechanical model, the CPG model had to be modified to produce output signals for the knee joint. The basic organization of the CPG with the knee joint included was shown in Figure 5.19. The organization of the CPG model was based on that of Taga et al. (1991), where both of the neurons of the hip half-centre had inhibitory projections to the ipsilateral knee extensor neuron. A common connection weight (W_{HK}) was used for the connections from the ipsilateral hip flexor and hip extensor neurons to the knee extensor neuron. This connectivity allowed for the neurons of the knee half-centre to have an asymmetrical cycle, where the flexors were active for more than 50% of the cycle time.

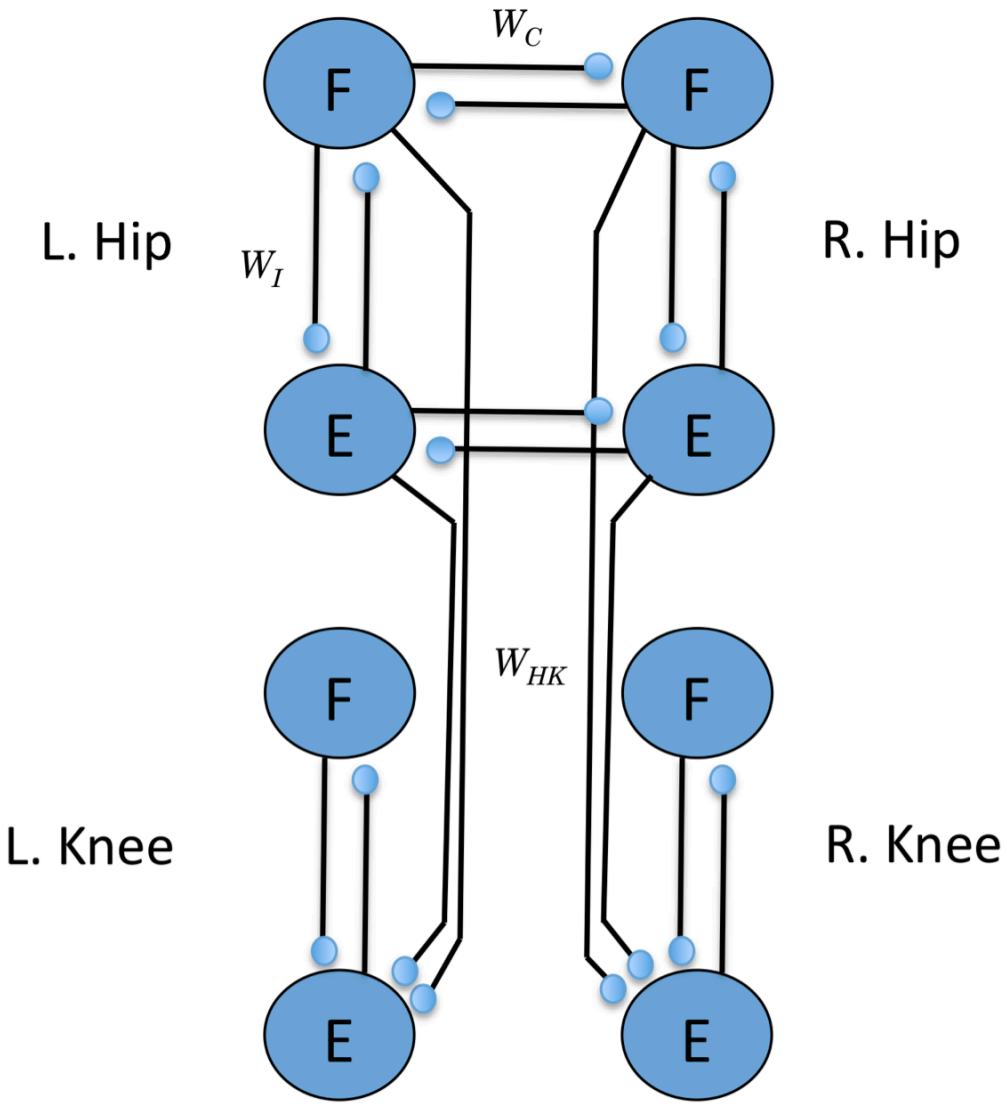

Figure 5.19: Organization of the CPG model with the addition of the knee joint. W_{HK} indicates the weight of the inhibitory connections between the neurons of the hip and the knee extensor neuron. The circular synaptic connections represent inhibitory connections.

The connections from the neurons of the hip were accomplished by adding another term to the calculation of the inner state of the neuron, as shown in Equation 5.8.

$$\dot{u}_F = \frac{1}{\tau_{rise}}(q_t - u_F - \beta v_F - W_I y_E + W_C y_{CF} + W_{HK} y_{HE})$$

and

$$\dot{u}_E = \frac{1}{\tau_{rise}}(q_t - u_E - \beta v_E - W_I y_F + W_C y_{CE} + W_{HK} y_{HE})$$

Equation 5.8

Where, y_{HE} was the output of the ipsilateral hip extensor neuron and W_{HK} was the weight of the inhibitory connection between the ipsilateral hip extensor neuron and the neurons of the knee half-centre. Once the inner state of the neurons (u) had been calculated, the output of the neurons (y) was calculated in a similar fashion to that used previously (Equation 5.7). These neural outputs then activate the appropriate muscles in the musculoskeletal model.

A series of simulations were carried out to examine the combined effect of τ_{ad} and W_{HK} on the walking pattern of the biped model. Simulations were carried out with values of W_{HK} set to 0, -0.5 and -1.0, with τ_{ad} being incremented by 0.01s between 0.1s and 2.5s for each value of W_{HK}. The walking speeds from these simulations are shown in Figure 5.20.

When the knee muscles were added to the model, there was a decrease in the variability in the relationship between τ_{ad} and the walking velocity of the biped. This could be observed by comparing the top panel of Figure 5.20 to Figure 5.10. It was also observed that the addition of knee muscles to the model led to higher walking speeds at lower values of τ_{ad}, when compared to the walking speeds of the biped with no knee muscles. It was also observed that the connectivity between the hip joints and the knee joints led to increased variability in the relationship between τ_{ad} and the walking speed of the model.

$W_{HK} = 0$

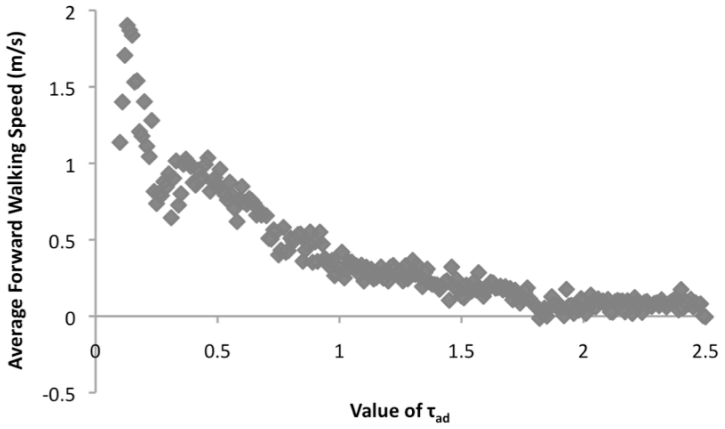

$W_{HK} = -0.5$

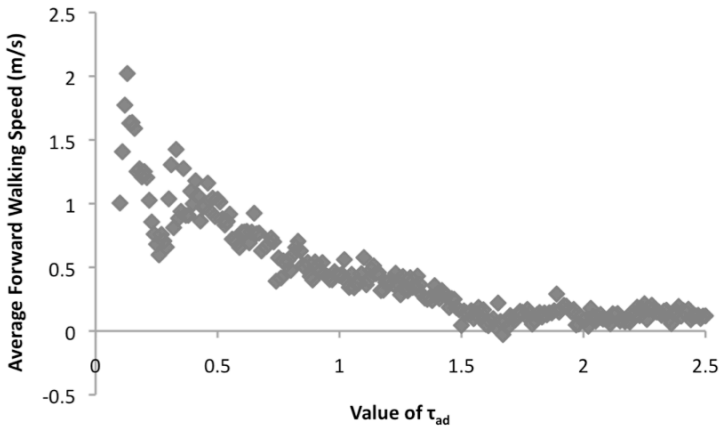

$W_{HK} = -1.0$

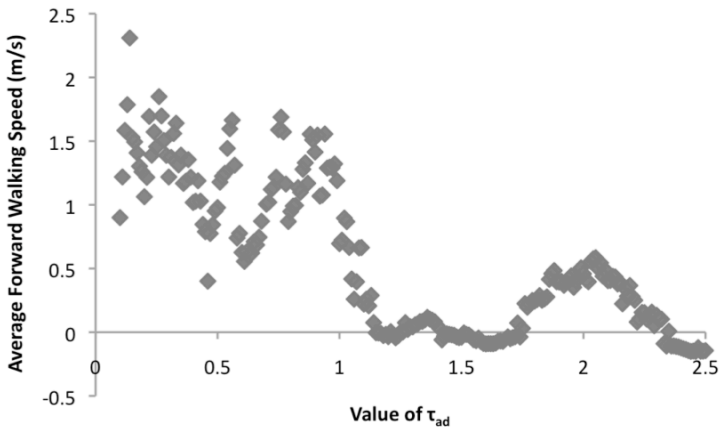

Figure 5.20: Walking speeds for various values of τ_{ad}, with different values of W_{HK}.

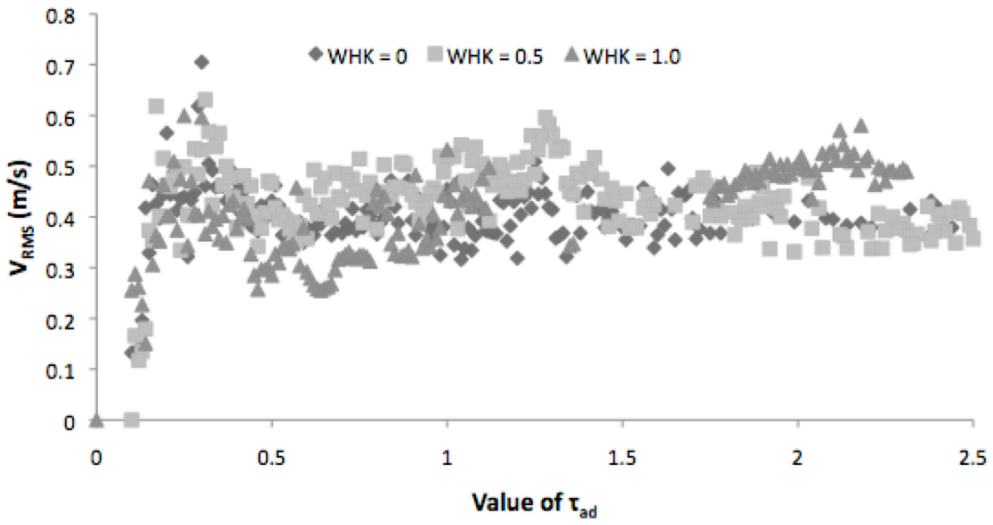

Figure 5.21: Variability in forward velocity at different values of τ_{ad}, when knee muscles were used in the model. The black diamonds indicate the variability when there were no connections between the neurons of the hips and the knees, the light grey squares indicate when the inhibitory connection between the hips and the knees was set to 0.5, while the dark grey triangles indicate the variability when the inhibitory connection was set to 1.0.

The addition of knee muscles to the model led to a slight increase in the variability in the forward walking speed (Compare Figure 5.21 with Figure 5.11), although direct comparisons were difficult to make since the addition of the knee muscles to the model also altered the relationship between walking velocity and τ_{ad}. The addition of an inhibitory connection between the hip neurons and the knee extensor neurons did not lead to any significant changes in the variability of the forward walking speed, as could be seen by the overlap of data in Figure 5.21. The addition active control of the knees also resulted in an increase in the variability of the kinematic pattern of the joints, as could be seen in the phase plots in Figure 5.22. The addition of knee joints in the model led to a lower range of τ_{ad} values that would lead to walking speeds in the range of human walking. When W_{HK} was 0 or -0.5, τ_{ad} values greater than 0.5s led to walking speeds that were less than 1.0 m/s, which is below values typically observed in normal human walking. When W_{HK} was set to -1.0, there was a wider range of τ_{ad} values that could lead to

normal walking speeds, however there was more variability in the relationship between τ_{ad} and the walking speed of the biped model. With the stronger connection between the hip and the knee joint, τ_{ad} values greater than 1.0s led to very slow walking speeds.

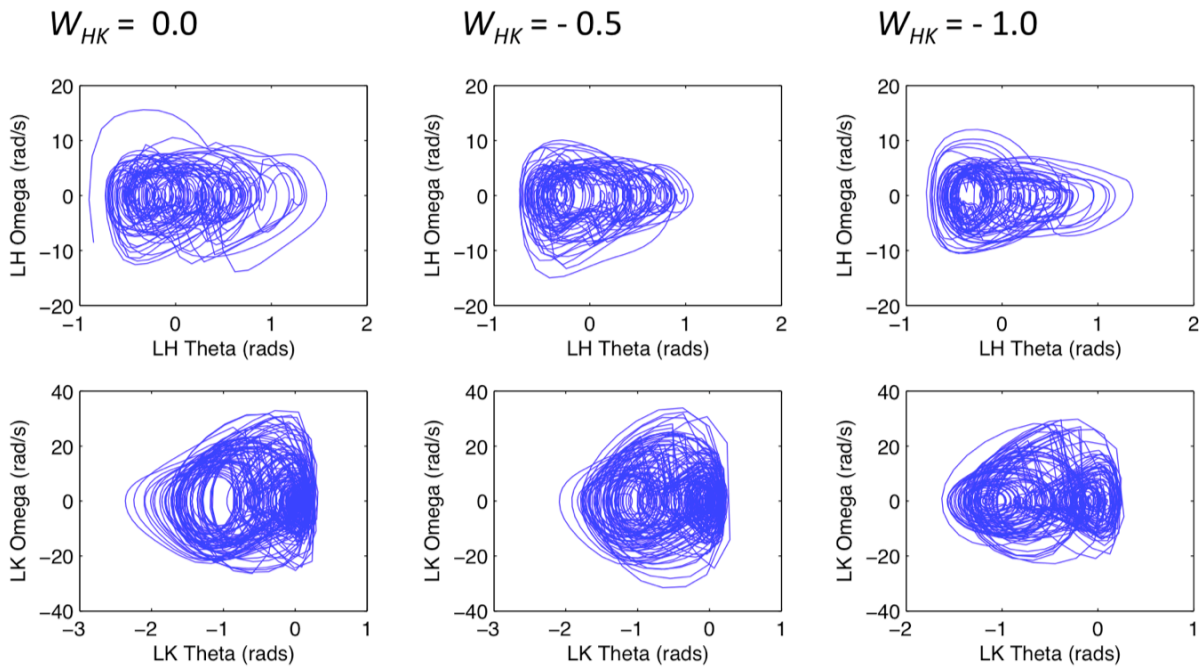

Figure 5.22: Phase plots of the left hip joint (top) and left (knee) joint of the biped model with different levels of inhibition between acting on the knee extensors from the hip neurons.

Experiment #5: Effect of Upper Body Support System Properties on the Walking Pattern

Up to this point all of the simulations have been carried out with similar properties of the upper body support system. The upper body support system consisted of a spring and damper in parallel, with a set rest-length, attached to a segment with negligible mass above the model (See Figure 5.1). The overhead segment was attached to a rod by a prismatic joint that allowed translation in the forward or backward directions. The advantage of a having the HAT segment supported by a spring-damper system was that motion of the HAT segment was still possible in the vertical direction, which is necessary for a normal walking pattern. All of the previously

described simulations were carried out with the stiffness of the spring set to 650 N/m the damping constant set to 100 N.s/m, with the resting length of the system set to 0.6m. This system supported a very large percentage (approximately 90%) of the total body mass of the mechanical model, while still allowing forward locomotion of the mechanical model to occur.

The goal of this series of simulations was to determine a relationship between the stiffness of the support system and the ability to generate forward propulsion. A series of simulations were carried out where the stiffness of the spring within the support system was adjusted to be between 0 N/m and 1000 N/m in increments of 25 N/m. Both the hip and knee muscles were active for this series of simulations, and the properties of the CPG were as follows: τ_{ad} = 0.25s, q_t = 1.0, W_C = -0.15 and W_{HK} = 0.5. The forward walking velocity was assessed for each simulation. It was found that a walking pattern was not possible when the support did not provide adequate support (0 - 300 N/m), or when the support system provided too much support (800-1000 N/m) and the mechanical model was unable to make contact with the ground. The average walking speed for the range of stiffness values tested was shown in Figure 5.23.

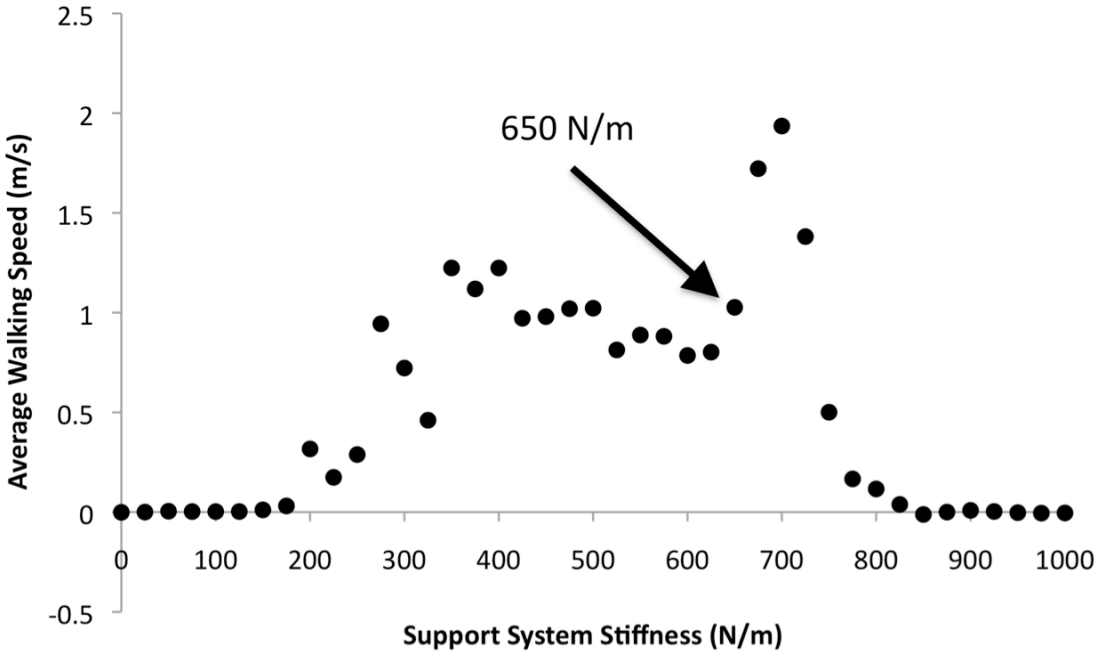

Figure 5.23: Average walking speed of the biped model during simulations where the stiffness of the support system was altered.

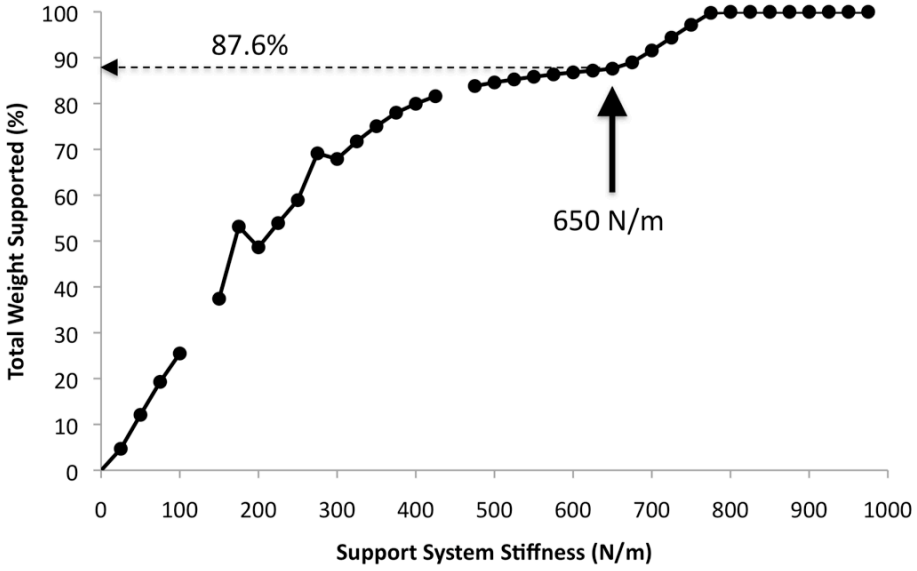

Figure 5.24: The total weight supported by the support system across the range of stiffness values used. Missing data points indicate that the simulation did not converge for that particular level of support system stiffness.

When a moderate amount of support (300-700 N/m) was provided to the HAT segment, the model was able to generate propulsion and progress in the forward direction, at a speed of approximately 1m/s for the CPG parameters tested. When the stiffness of the support system was set so that the model could just touch the ground the model progressed in the forward direction at a much faster rate, due to the fact that the body was able to just skip off the ground and avoid long periods of contact with the ground.

A separate series of simulations were carried out to determine what percentage of the mechanical systems weight the support system model took up. Once again the stiffness of the spring within the support system was adjusted to be between 0 N/m and 1000 N/m in increments of 25 N/m, however in this case the CPG model was not active. The mechanical model was essentially dropped from the starting position and the support system was left to hold up the HAT segment. The contact force with the ground was recorded during these simulations and the total percentage of the model's weight that was being supported by the support system model was calculated after the motion of the biped model's HAT segment stabilized. The results from this series of simulations were shown in Figure 5.24. It was seen that the total percentage of weight supported increases in a non-linear fashion as the stiffness of the spring was increased. The complete weight of the mechanical model was supported when the stiffness of the spring was set to 775 N/m.

There were some points missing from this series of simulations as the numerical integrator used for this study was not well suited for this type of simulation, where the model was simply dropped and then allowed to come to rest. This was particularly evident at lower

stiffness values where the model essentially fell over. If the simulation completed 5s of simulation time, then the final time point that could be calculated was used for Figure 5.24. If the simulation was unable to complete 5s of simulation time then the data point for that simulation was not used. If the full simulation was able to be completed, then the points on the graph were determined from the average contact force, once this signal had stabilized.

Discussion

In this chapter, a simplified model of the human neuromusculoskeletal system was developed. This model was able to produce movement patterns that produced forward locomotion from neural signals that were produced by a feedforward CPG mechanism. It was found that the modulation of the frequency of the CPG output had an impact on the movement pattern of the biped model, as did the nature of the connectivity within the CPG model. There was a great amount of variability observed in the kinematics during a large number of the simulations carried out in this chapter due to the fact that only a feedforward control mechanism was used. The major limitation that was associated with the use of a feedforward control mechanism was that the control system would be unable to respond to any perturbations applied to the system (Kuo 2002). In the simulations in this chapter, perturbations were applied to the model via the interaction of contact points with the ground and through intersegmental dynamics, where the motion of one segment will affect the motion of other segments within the system. It is hypothesized that the addition of feedback mechanisms to the neural control model will reduce the kinematic variability in future iterations.

In all of the simulations carried out for this study, the walking speed of the mechanical model could be controlled by adjusting the time constant for the adaptation effect within the CPG (τ_{ad}). By adjusting this time constant it was possible to effectively control the frequency of

the CPG output as was shown in Chapter 3. This finding has some correspondence to the findings of Shik et al (1969), who found that the speed of locomotion could be controlled by the magnitude of a simple signal to the brainstem, although it is not known whether the connections of from the MLR would affect the adaptation property of the neurons in the circuitry of the CPG. The effect of altering the magnitude of the CPG output was not tested in this chapter, but was addressed in the next chapter when feedback pathways were added to the model.

The walking pattern of the model was most realistic when only the hip joints were actuated by muscles while the knee joint moments were only determined by the passive moment model. There have been previous models where only the hip joint was actuated and realistic walking patterns have been realized, particularly when robotics were used for the mechanical model ie. (Lewis et al. 2003). It is possible that realistic walking patterns could be achieved with the addition of knee joint muscles to the model however it is likely that the phasing of the neural signals would have to be altered to produce an appropriate rhythmic pattern (Paul et al. 2005) or feedback mechanisms would have to be used to alter the neural signals driving the knee muscles (Ogihara and Yamazaki 2001). In the following chapter feedback mechanisms were added to the model in attempt to produce a more normal walking pattern.

The connections between the hip joints reduced the variability in the relationship between the frequency of the CPG output and the walking speed of the mechanical model. This was seen in Figure 5.10. Although the inhibitory neural connections appeared to reduce the variability in the above stated relationship, there was still a great deal of variability in the forward walking velocity of the mechanical model, as seen in Figure 5.11, due to the lack of feedback mechanisms in the model. Inhibitory connections between the contralateral hip joints have been used in previous neuromechanical models (Taga et al. 1991; Ekeberg and Pearson 2005) and

have been found to improve the stability of the walking pattern in the only study to date that has manipulated this connection (Ekeberg and Pearson 2005). The results from the simulations that tested the strength of the inhibitory connections between contralateral hip joints in this study remain somewhat inconclusive. It was seen in Figure 5.14 that a moderately weighted inhibitory connection between the contralateral hip joints appeared to improve the coordination between the left and right hip joints, although it was still quite different from the coordination that is observed during normal human walking (Figure 5.15). It was also observed that further increasing the weight of the inhibitory connections between the neurons of the hip joints led to a decrease in the walking speed of the model. This is likely due to the decreased frequency of the CPG output that was accompanied with the increased strength of the inhibitory connection. Moderate levels of inhibition between the contralateral neurons in the half-centres of the hip joints appeared to produce the most consistent motion in the forward direction (Figure 5.18) and fastest average walking speed (Figure 5.17), indicating that these connections help ensure forward progress was made.

The effects of placing inhibitory connections between the neurons of the hip joint half-centres and the extensor neuron of the ipsilateral knee joint were difficult to establish. Adding this connection to the model resulted in the knee flexor neuron being active for a greater percentage of the cycle of the CPG output. This connection was added based on the work of Taga (1991) who had placed such a connection in his model, but did not test the effect of altering the weight of these connections. The relationship between the frequency of the CPG output and walking speed was least variable when there were no connections between the neurons of the hip and knee joints and the strength of this connection appeared to have no significant effect on the variability of the forward walking speed. Phase plots of the mechanical model's kinematics

(Figure 5.22) also appeared to indicate that adding a neural connection between the knee the hip joints had little effect on reducing the kinematic variability of the model. It is possible that the connection between the hip and knee joint's neurons placed in the model by Taga (1991) was to serve a purpose that was specific to his model and may not be generalizable to other biped models. The only other model that has used the neural model proposed by Taga was developed by Zhang et al (2007), but used an optimization approach to determine the weights of the connections between neurons in the CPG model.

The decision that was made to have a stiff support system that supported the majority of the body weight of the mechanical model likely had a strong effect on the results that were observed in this study. In the final series of simulations, it was observed that providing too much or not enough body weight support prevented the model from moving in the forward direction. With moderate amount of body weight support, the model could achieve a fairly normal walking speed. There was a small range of support system stiffness values where the model just made contact with the ground and "skipped" forward at a faster than normal speed. The stiffness value used in this model was towards the higher end of the stiffness values that allowed for normal walking speeds to occur and supported approximately 90% of the weight of the mechanical model. The results that were found for the simulations in this study may be specific to the level of body weight support that was chosen for this study however it is felt that the level of body weight support selected for this study is appropriate. Previous animal work has shown that a significant level of body weight support was required to allow for walking patterns to occur when produced by the CPG in isolation (Grillner and Zangger 1979). In humans, some patients who have suffered a spinal cord injury were also able to produce a basic walking pattern when body weight support was provided ie.(Dimitrijevic et al. 1998; Ivanenko et al. 2009). To date, the

body weight support system that was modeled for these simulations appears to be unique and may provide an excellent means to further develop neuromechanical simulations of human locomotion.

Limitations of the Musculoskeletal System Model

The mechanical model developed in this chapter was adequate for the questions posed in this study, however it was quite simplified when compared to the human locomotor apparatus. One of the major limitations of the mechanical model used in this study was that there are no feet in the present model. Segments representing the foot were included in earlier versions of the mechanical model (that are not described in this thesis), however was removed due to erratic behavior of the ankle joint. Due to the low mass and the large moment producing capabilities of the muscles that cross the ankle joint the foot often underwent large rotations that could not be controlled using a passive angle-moment relationship or damping moments. The removal of the foot from the model had very little effect on the remaining portions of the mechanical model. When the foot was included in the model there were two contact points included in the model that roughly corresponded to the heel and the ball of the foot. When the foot was removed from the model, the number of contact points was reduced to one per limb and was placed where the ankle joint would have been located. The angle of the ankle joint also serves as an input to the passive moment - joint angle relationship of the knee joint, which was shown in Equation 5.3, and therefore the ankle angle was assumed to be in a neutral position throughout the simulations, which would have a minor effect on the passive moment that was observed at the knee joint.

Although it has been well documented that biarticular muscles have an important role in the control of walking (Wells 1988; Winter 1991; Prilutsky et al. 1998; Zajac 2002), the addition of biarticular muscles to the model greatly increased the complexity of control system that would

be required to control this system. For this reason biarticular muscles were excluded from the neuromechanical model.

Due to the differences in the mechanical model and the human locomotor apparatus, the strategy used to achieve forward propulsion in the model differs significantly when compared to human walking. It has been shown that approximately 80% of the power required for forward propulsion in human walking was generated by the plantarflexors of the ankle joint (Winter 1991). Because the ankle joint was removed from the model the forward propulsion is being achieved by a combined action of the hip and knee extensors, when present.

Limitations Caused by the Body Weight Support System Model

The body-weight support system that was represented in this chapter was unique among neuromechanical models in that it allowed the testing of a wide range of control parameters of the CPG model without having any balance control models in place. One limitation that was caused by the particular implementation of this model was the fact that the amount of body-weight supported by the harness was particularly high at 87%. While these types of systems may be used as a rehabilitation tool in clinical populations, the amount of weight support that would be used in these applications is substantially lower than what was used in this study and is usually set based on the patient's abilities (Wessels et al.). The high levels of support used in this study will cause very low vertical ground reaction forces to be applied, which will also affect the horizontal ground reaction force, because it is calculated from the vertical force. The limitations imposed by the high levels of body-weight support are important to consider when interpreting the results of this study.

Simulations showed that when body-weight support was removed that the model was unable to produce forward propulsion, which is likely due to the lack of support generating

mechanisms built into the model. Future implementations of the model should include feedback mechanisms that are capable of providing support to the HAT segment in the model.

Limitations of the CPG Model

The CPG model used for these simulations was admittedly a very simple representation of the spinal mechanisms involved in the control of locomotion. There are a number of more sophisticated CPG models that have been previously published; however the properties of these models did not lend themselves to being used in neuromechanical simulations of locomotion. As discussed earlier, the Matsouka oscillator model has several desirable features that make this model useful for inclusion in neuromechanical models. Firstly, this model produces a series of continuous signal that oscillate at a controllable frequency, based on principles that have long been speculated to be involved in the control of locomotion (Brown 1911; Brown 1914). These continuous signals can be thought of as representing the firing rate of the neurons in the model. Some more recent models have used spiking neuron models to more accurately represent neural dynamics, however these models did not lend themselves to most commonly used muscle models (Simoni and DeWeerth 2007).

There has been a great deal of evidence that CPG mechanisms in the spinal cord are made up of networks of a great number of neurons (Rossignol et al. 2006). Two of these networks were most commonly described in models of CPG activity; these networks were a timing network, which defines the basic locomotor rhythm, and a shaping network, which specifies the dynamics of the neural output to a specific muscle. Prentice et al used a artificial neural network approach to model both timing (Prentice et al. 1995) and shaping networks (Prentice et al. 1998) of the CPG. While it was initially proposed to extend these models to be used in the neuromechanical simulations it proved impossible to integrate these models with the dynamic

mechanical model, it proved difficult to include information regarding the simulation time within the artificial neural networks. A CPG model that includes both shaping and timing networks and temporal dynamics has been developed by McCrea (2001), however the complexity of this model that was caused by the large number of neurons in the model would dramatically increase the computational resources required to carry out the simulations in this study.

While CPG model used in this study was quite simple compared to other existing CPG models, the timing of the CPG model was able to be controlled by specifying the time constant of the adaptation effect of the neurons (τ_{ad}) and the shaping of the CPG output is able to be somewhat controlled by altering the weights of the various inputs. More extensive shaping of the neural output should be possible with the addition of feedback to the CPG model. There has been also evidence that the addition of sensory information increases the dynamic nature of the CPG output (or provides more shaping information) (Grillner and Zangger 1984; McCrea 2001; Yakovenko et al. 2004).

Conclusions

This study was successful in developing a mechanical model that can be used to test the basic mechanisms thought to be involved in the control of human locomotion. The novel body weight support system that was developed for this study allows for analysis of various neural aspects of locomotor control that could not be previously examined. For example we were able to specifically manipulate the frequency of the signals produced by a CPG model and apply these neural signals to a musculoskeletal model and analyze the effect of the CPG frequency on the ability to produce forward propulsion. Previous neuromechanical models have not been able to isolate the activity of the basic rhythm generator due to the lack of a support system. While the results obtained for several of the simulations in this study may be specific to the parameters that

were chosen for the support system, basic neural mechanisms involved in the control of locomotion may be examined using this model.

A basic movement pattern, that resembled human walking, could be produced using a simple CPG model. This movement pattern was most consistent when only the hip joints were actively actuated and there was a moderate inhibitory connection between the contralateral neurons in the half-centres of the hip joint. When the knee joints were actively actuated, the relationship between the frequencies of the CPG output was less variable, although the overall kinematic pattern of the model was more variable. It was hoped that the kinematic patterns of the mechanical model should be able to be improved with the addition of feedback mechanisms such as stretch reflexes to the neural control model.

Chapter 6: Sensory Feedback in a Neuromechanical Biped Walking Model

Introduction

Sensory feedback regarding the position of the limbs is crucial for the maintenance of a normal locomotor pattern. Although it has been shown that walking can be produced in the absence of sensory feedback there are components of the walking pattern that are absent, and the walking pattern is notably different from the normal walking pattern (Grillner and Zangger 1984; Lajoie et al. 1996). In a human subject that lost all sensory feedback from muscle receptors, it was observed that the complexity of the walking was reduced which was primarily shown by a decrease in knee flexion. It was also shown that the patient walked with poorer spatiotemporal gait measures and that the walking pattern lacked the normal 'fluidity' that is present in human gait (Lajoie et al. 1996). In both humans and cats, it has been observed that the removal of sensory information leads to changes in the muscle activation patterns involved in locomotion, with a decrease in the complexity of the muscle activation patterns (Grillner and Zangger 1984; Lajoie et al. 1996).

While walking patterns can be observed in the absence of sensory feedback, proprioceptive feedback makes important contributions to the control of the walking pattern. Sensory feedback from muscle receptors has been shown to have two primary roles in the control of locomotion. The first role is to regulate the level of extensor tone during the stance phase (Hiebert and Pearson 1999), this was demonstrated by foot-in-hole experiments where cats walking on a treadmill step on a trap door that releases, thus eliminating any loading of the limb

during the stance phase. In these experiments there was a significant decrease in the extensor activity during stance phase when the limb was unloaded. Additionally it was shown that the decrease in extensor activity is proportional to the magnitude of the unloading (Hiebert and Pearson 1999). Based on this work, it can be determined that the loading of the limb has a positive or excitatory connection to the extensor centre of the CPG.

The second major way which sensory information is used during walking is to trigger phase transitions. The stretching of the hip flexor muscles has been shown to trigger a transition from stance to swing (Pearson 1995; Lam and Pearson 2002; Rossignol et al. 2006), while stretching of the hip extensor muscles will trigger a transition from swing to stance phase (Lam and Pearson 2001). In many cases, the stretching of the hip extensor is actually sufficient to initiate the walking pattern. Because of the mutually inhibitory nature of the half-centre CPG model, the circuits to trigger the phase transitions could be represented by either inhibitory or excitatory connections to the half centres of the CPG, or some combination of the two.

Much of our knowledge regarding the sensory contribution to the neural control of walking has come from work based on animal studies, although results from studies involving the stepping response in infants shows that circuitry involved in the sensory modulation of the CPG exists within the human spinal cord (Lam et al. 2003a; Lam et al. 2003b). Various attempts have been made to investigate the contributions of afferent input from muscle receptors to the walking pattern in adult humans; these studies have used various paradigms such as eliciting tripping responses (Eng et al. 1994), muscle vibration (Sorensen et al. 2002), stepping onto a complaint surface (Marigold and Patla 2005) or altering the mechanical properties of the musculoskeletal system (Noble and Prentice 2006). These types of studies have documented the kinematic and neuromuscular responses to various types of sensory perturbations during walking

to help further our understanding of the control of locomotion. All of these studies have found robust multi-muscle responses to these various stimuli that are appropriate for the current phase of the walking pattern, for example different responses were found for tripping responses that occurred during early swing, where an elevation response was found to increase the height of the foot, whereas in late swing a lowering response was found to quickly return weight support to that foot.

Another tool that has been used to investigate the contributions of feedback from muscle afferents to the walking pattern is the H-reflex (Hoffmann 1910; Pearson and Gordon 2000). This reflex is an electrical analogue of the monosynaptic stretch reflex that is elicited by electrically stimulating a nerve transcutaneously. This stimulus will lead to both a motor response and a monosynaptic excitation that occurs due to the stimulation of the IA afferents. Depending on the magnitude of the stimulus current, it is possible to isolate the motor response (M-wave) or the mono-synaptic stretch response (H-wave, or H-reflex) where the magnitude of the H-wave represents the gain, or sensitivity, of the monosynaptic stretch reflex (Pearson and Gordon 2000). The magnitude of the H-reflex has been shown to be modulated across the gait cycle, such that the gain of the stretch reflex is higher when a muscle should be active during the gait cycle and a muscle's stretch response is lower when the muscle is not active during the gait cycle (Capaday and Stein 1986). This modulation is thought to help improve the stability of the gait cycle by having a higher stretch reflex gain for a muscle when it is active, as it would help respond to a stretch perturbation to that muscle immediately, whereas stretching a muscle that is not active would have less consequences on the stability of the walking pattern (Capaday 2002).

Due to the difficulty of measuring the afferent pathways involved in the neural control of locomotion, studies of human locomotion can alter the input to the sensory systems, but only the

kinematic/kinetic output (via motion analysis/force platforms) or the neuromuscular input (via electromyography) can typically be measured. Studies where the sensory pathways are measured directly have only been carried out in animal models and are very difficult to carry out, see review by Rossignol (2006). The ability to directly modulate the level of afferent feedback from sensory receptors is also impossible in intact specimens, therefore computer simulations of the neural control mechanisms involved in the sensory control of locomotion provides a promising method to help further our understanding of the neural control of locomotion.

The use of neuromechanical models to assess sensorimotor interactions during locomotion was reviewed by Pearson et al (2006). These models consist of a model of the neural control systems involved in the control of locomotion that interacts with a model of the musculoskeletal system, which allows for a prediction of the motion patterns that would result from the neural control model. These models allow for the systematic manipulation of the properties of the neural control system and to view what the kinematics of the resulting walking pattern would look like. Although a number of neuromechanical models of animal locomotion have been produced, relatively few studies have used these models to examine the properties of the afferent feedback systems. The following section will review some previous neuromechanical simulations of human walking that included afferent feedback.

Neuromechanical Simulations Analyzing Afferent Feedback

It is widely acknowledged the concept of computational neuromechanical simulations of human locomotion were first developed by Taga et al (1991). This model used a model of the CPG to that received feedback regarding the position of the joints within the musculoskeletal model. Taga et al, stated that the walking pattern that resulted from this relatively simple control system was ‘self-organized’ which meant that the frequency of the CPG’s output was modulated

by the sensory signals, such that the frequency of the CPG was determined by the natural frequency of the lower-limbs of the model. This model was surprisingly adaptable; it was able to respond to a perturbation in the sagittal plane, by taking longer steps and was able to walk up a slight incline by responding with increased extensor moments. This initial model by Taga et al was also able to modulate the walking speed of the musculoskeletal model by modifying the tonic input to the CPG, which resulted in appropriate changes in both stride length and cadence. This initial model was later improved by Taga by adding muscles, including biarticular muscles, to the model to better represent the musculoskeletal model (Taga 1995a). This improved model was also able to adapt to various perturbations, such as a push from behind or changes in the mass of one of the segments in the musculoskeletal model (Taga 1995b), however the feedback still originated from the position and velocity of the joints, rather than simulated muscle receptors. The work of Taga was instrumental for developing the concept of a neuromechanical model, unfortunately the work is difficult to replicate due to the "parameter tuning" necessary to obtain similar walking patterns. The work of Taga also showed that sensory inputs from joint position were sufficient to modulate the frequency of the CPG output. Also there was little justification given for the sensory feedback pathways that were chosen by Taga's group, and some of the pathways used did not appear to be based on experiments that were carried out *in vivo*, which is likely due to incomplete knowledge of the time when these models were developed.

More recent work has attempted to investigate specific contributions of sensory feedback to the control of the walking pattern. Yakovenko et al (2004) examined the ability of stretch reflexes to respond to a tripping perturbation in a neuromechanical model of the cat's hind limbs. This study examined the walking patterns when only CPG output was used and found that a

surprisingly stable walking pattern could be achieved with only CPG output. However if the output of the CPG was weak then feedback from the muscle afferents could be used to help strengthen the walking pattern. It was also found that finite-state controls (if-then rules) were helpful for controlling phase transitions. The CPG model used in this experiment was different than the simple oscillator used by Taga. Yakovenko created typical muscle activation patterns for each muscle modeled that would repeat at a set frequency. Another neuromechanical model of the cat hind-limbs during walking was constructed by Ekeberg and Pearson (2005) to test the sensory contributions to the stance-to-swing transition during walking. It was found that signals from the force within the ankle extensors or from the position of the hip joint were sufficient to initiate swing. Although this paper was important for demonstrating the importance of these sensory signals for triggering phase transitions during walking, the CPG model that was used by these authors was not the typically used half-centre model. To simulate the central contribution to the neural activation pattern, these authors chose to use a state-specific control, which produced a muscle activation pattern that was determined based on the postural configuration of the musculoskeletal system and therefore was not a feedforward system. These authors however did investigate the coupling between the left and the right limbs, and found that if their state-specific controller was coupled between the two sides that the hip position was able to produce a stable walking pattern alone when the controllers were coupled.

Besides the work of Taga et al, there have been relatively few studies to test the contributions of sensory information in neuromechanical models of the human locomotor system. Paul et al (2005) created a model of the human musculoskeletal system that was driven by signals generated by a model of the locomotor control system based on findings from animal studies and performed simulations where the final output of the locomotor control system

consisted of weighted output from sensory sources (ie. The contributions from the muscle spindles, Golgi tendon organs and the CPG sources could be weighted to produce a single output). The findings of this study were similar to those made by Yakovenko et al (2004), in that input from the CPG could provide a stable walking pattern, however input from the sensory systems was able to produce a stable walking pattern with lower values of input from the CPG. However the main emphasis of this work was to publish the methodological considerations for this type of model and to consider the potential applications of such a model.

One of the most advanced neuromechanical simulations of human walking was recently developed by Jo (2008). This model included a feedforward model of the CPG, however this CPG model was a hybrid of the finite-state control model used by Ekeberg and Pearson (2005) and the half-centre model used by Taga et al (1991). This CPG model was based on studies that decomposed EMG signals from various muscles using Principle Component Analysis and found that the EMG signals from all of the muscles contained five underlying patterns that coincided with different phases of the walking pattern, ie. Foot Placement, Weight Acceptance, Push-Off, Limb Retraction, and Moving the Foot Forward (Ivanenko et al. 2004) . This CPG model is similar in nature to a model that was proposed by Prentice et al (1998), based on an Artificial Neural Network (ANNs) and is essentially the feedforward implementation of a similar ANN.

Goals and Hypotheses

The overall goal of this study is examine how the types of feedback provided by muscle receptors to the locomotor control system will affect the output of the CPG and the resulting walking pattern in a biped model of the musculoskeletal system. In particular this study examined the effects of applying feedback from stretch reflexes, which will also help facilitate

phase transitions in the gait cycle, and positive feedback from stance sensors on the extensor half centre of the CPG.

The first experiment in this study examined the contributions of simulated stretch reflexes to the control of the biped model's walking pattern. In the first experiment the feedback from these simulated stretch reflexes were applied across the entire gait cycle. It was expected that this type of feedback will have a dramatic effect on the walking pattern that the muscles will better respond to perturbations that occur from the interaction between the foot and the ground. It was expected that these reflexes would quickly respond to the stretching that may be induced due to contact with the ground. It was also expected that these reflexes would help stabilize the walking pattern, through the facilitation of phase transitions, as the circuitry that was involved in the control of these transitions are similar to the simple stretch reflex implemented in this model.

In the next experiment the stretch reflexes were delivered in a phase dependent nature, where the stretch reflex of the extensor muscles were active during the stance phase, and the reflexes of the flexor muscles were activated during the swing phase, based on literature from human studies that have found this type of stretch reflex modulation (Capaday and Stein 1986). It was expected that this type of feedback will facilitate a trade-off between the stability of the walking pattern and the average walking speed of the biped model, since the CPG would be able to better contribute to the generation of the gait pattern, since it will have less interference from the stretch reflexes and the stretch reflexes will be able to respond to some of the perturbations that occurred during walking due to the interaction with the ground. An additional experiment took place where the degree of modulation of the stretch reflexes was affected by how much weight the model was bearing. These results were compared to the results of the simulations where the stretch reflexes were modulated in a simple on-off fashion.

The final experiment in this chapter examined the role of positive feedback on the extensor half-centre during stance from sensors indicating the loading of the limb. This type of feedback was thought to be critical to the walking pattern, since in ensures that a foot will not be lifted off the ground while it was still bearing weight. Therefore this type of feedback should enhance the duration of the stance phase of walking and should produce higher walking speeds due to the higher levels of impulse that will be generated during this longer stance phase.

Methods

Musculoskeletal Model

The musculoskeletal model was the same as the model used in the previous chapter. Briefly, the model of the skeletal system consisted of five segments, 2 legs, 2 thighs and a HAT (head, arms and trunk) segment. The HAT segment was supported by a spring-damper system that was attached to a small mass-less segment that was attached to a prismatic joint that allowed for motion in the anterior-posterior direction. The spring had a spring constant of 550 N/m while the damper had a damping constant of 100 N.s/m. Contact between the ground and the musculoskeletal system occurred at the distal end of the leg segment, with the vertical ground reaction force being determined by a non-linear spring damper and the horizontal ground reaction force being determined by Columb friction. The equations that determine the ground reaction force were presented previously in Chapter 5.

As with the first biped model presented in Chapter 5 the model presented in this study was actuated by four uniarticular muscles representing a hip flexor and extensor for each limb. The origin and insertion coordinates of these muscles were given in Chapter 5, as were other muscle parameters, such as resting length and maximum isometric force.

The overall flow of data through the model was shown in Figure 6.1. The CPG model was the same model that was used in all of the previous studies of this thesis. This model was based on a set of differential equations that represent the output of two mutually inhibitory half centre (HC) neurons (Matsuoka 1985). It was shown in the previous chapters of this thesis that the frequency of this oscillator could be controlled by specifying the time constant of the adaptation effect of the HC neurons (τ_{ad}), while the amplitude of the CPG's output could be controlled by specifying the magnitude of a tonic input to the CPG. The equations that govern the behaviour of this were previously shown in Chapter 3.

The output of the CPG was then subjected to a first-order delay to represent the dynamics involved in excitation contraction coupling (ECC). The differential equation used to implement this delay was shown in Chapter 3. The output of the ECC model then served as the muscle activation signal and input to the muscle model. The details of the muscle model were previously given in Chapter 3. Briefly, the muscle activation signal scaled the maximum isometric force output, in conjunction with scaling factors that represented the active and passive force-length relationships and the force-velocity relationship. The muscle forces were then used to calculate the active muscle moment, which was then applied to the joints. The ranges of joint motion of the musculoskeletal model were limited by passive moments that acted as non-linear rotational springs. The equations that govern the passive-moment joint-angle relationship were based on measurements that were made *in vivo* by Silder et al (2007); the equations that govern the passive were given in Chapter 5. The active and passive joint moments were summed and applied to the joints of the musculoskeletal model.

The kinematics of the musculoskeletal model were determined through the use of forward dynamics. This involved the integration of the equations of motion with the knowledge of the

joint moments and ground reaction forces. The equations of motion were integrated with the *ode23t* integrator in MATLAB, which is a moderately stiff, variable time-step trapezoidal integrator. The properties of the integrator were the same as those that used in the previous chapter. Once the kinematics of the musculoskeletal system were known they were used to calculate the muscle length and velocity, which were in turn used to calculate the force in the muscle model and the muscle spindle output.

The muscle spindle model was the same as that used to provide feedback to the CPG in Chapter 4. The output of the spindle model was a combination of the muscle's velocity and a length that was subject to a first order delay; the equations governing the output of the model are given by Prochazka and Gorassini (1998). The outputs from the muscle spindle models were then processed by a set of feedback rules, which were different depending on the purpose of the particular simulation. These feedback rules will be described more in upcoming sections.

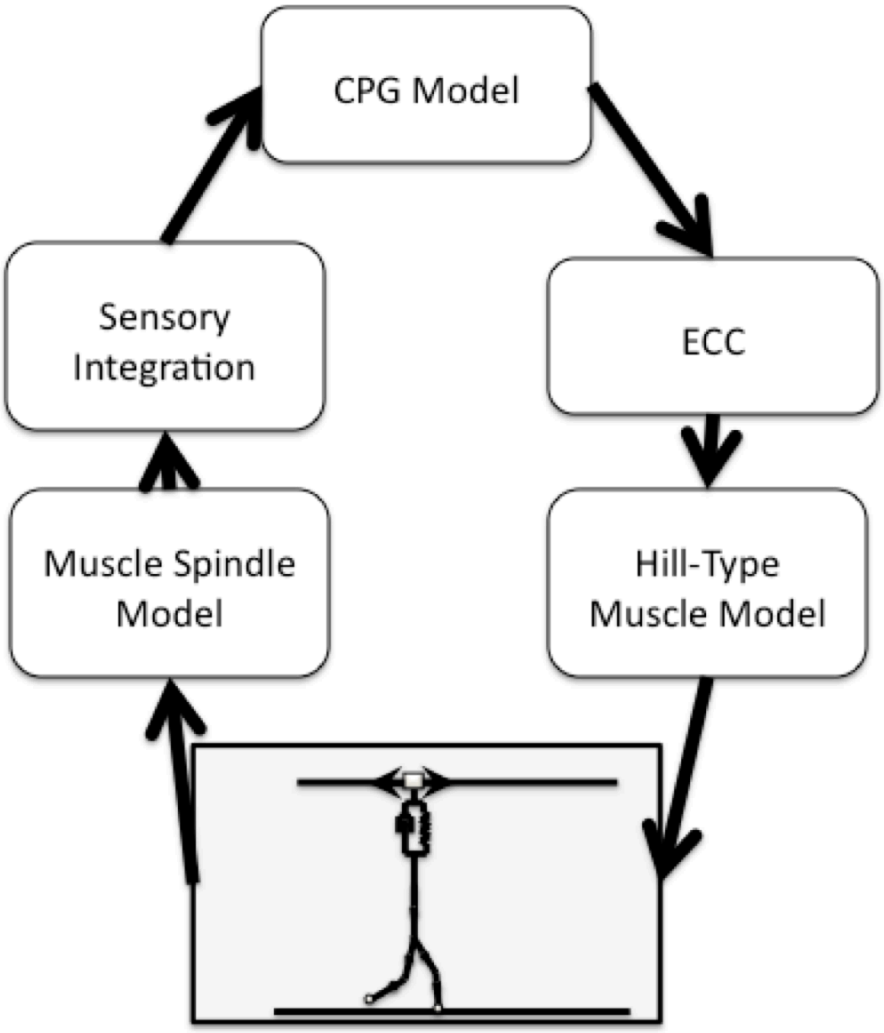

Figure 6.1: Flowchart of the data through the biped FB model. Neural signals originated from the CPG model, based on the Matsouka oscillator, which were then subjected to a first-order delay to represent excitation-contraction coupling. These signals then served as muscle activation signals for the Hill-type muscle models, which produced forces, which in turn created a moment about the hip joints of the mechanical model. Forward dynamics were then used to predict the kinematics from these torques. These kinematics then determined the length and the velocity of the muscles, which in turn served as input to the muscle spindle model. These signals were then integrated with the CPG signals, to produce the future CPG output.

CPG Model

The CPG model used for this study was similar to model that was used throughout this thesis and was based on the model by Matsuoka (1985). Briefly, this model includes two

mutually inhibitory neurons, which are subject to an adaptation effect, which describes the property of neurons where the neurons' output will stop responding when subjected to the same input. Matsuouka's model was modified to accept feedback signals, which were shown to be able to prolong the phase of the CPG's output, in Chapter 3. Matsuouka's model was also modified to have an inhibitory connection between contralateral neurons (ie. inhibition between the left and right hip flexor neuron). A figure illustrating the connections in this model was shown previously in Figure 5.7. The equations that dictate the behaviour of the CPG model will be briefly summarized below as well as the mechanisms that were used to influence the activity of the CPG via feedback signals.

The inner state of the HC neurons was determined by the following differential equations:

$$\dot{u}_F = \frac{1}{\tau_{rise}}(q_t - u_f - \beta v_f - w y_E - FB_{gain} Q_{fbF})$$

and

$$\dot{u}_E = \frac{1}{\tau_{rise}}(q_t - u_e - \beta v_e - w y_F - FB_{gain} Q_{fbE})$$

Equation 6.1

Where u_F and u_E were the inner states of the flexor and extensor HC neurons respectively and τ_{rise} was the time constant for the rise time of the neural output. The tonic input to the HC neurons was indicated by q_t, the adaptation term for the neuron's output was given by v_F and v_E, which was shown in Equation 6.3.The variables y_F and y_E represent the output of the HC flexor and extensor HC, and are subjected to a weighting factor w. The feedback from various sources

was combined into a single signal for each HC neuron Q_{FB}, as shown in Equation 6.2, which was subject to a weighting factor FB_{GAIN}.

$$Q_{fbF} = S_e - S_f \text{ and } Q_{fbE} = S_f - S_e$$

Equation 6.2

As in the previous chapters, the adaptation term was given by the following equations:

$$\dot{v}_F = \frac{1}{\tau_{ad}}\left(y_F - v_F\right) \text{ and } \dot{v}_E = \frac{1}{\tau_{ad}}\left(y_E - v_E\right)$$

Equation 6.3

Where, τ_{ad} was the time constant for the adaptation effect and was the primary mechanism used to control the burst frequency of the CPG model, y_E and y_F are the neural outputs of the HC neurons (Matsuoka 1987).

The output of the HC neurons was given by the following equation, which produces an output when the inner state of neuron was a positive value.

$$y_F = \max(0, u_F) \text{ and } y_E = \max(0, u_E)$$

Equation 6.4

Modelled Feedback Pathways

The feedback used in this model originated from two different sources; from simulated muscle spindles and from tactile sensors that detected when the 'foot' of the model was in contact with the ground. The feedback from both of these sources were weighted and summed by the sensory integration block in Figure 6.1.

The muscle spindles were based on work by Prochazka and Gorassinni (1998), which showed that the ensemble firing rate of muscle spindles could be represented by a weighted

combination of the muscle length and velocity that has been subjected to a first order delay. The first estimate of the muscle spindle's output was given by the following equation for each muscle:

$$MS_{Out} = K_{vel} \cdot v_{mus}^{p} + K_{len} \cdot l_{mus} - 1$$

Equation 6.5

Where MS_{Out} was the muscle spindle output, v_{mus} was the stretch velocity of the muscle, p was an exponent for the nonlinearity of the muscle velocity relation, l_{mus} was the length of the muscle and K_{vel} and K_{len} are gains for the muscle velocity and length components respectively. The muscle velocity muscle must be positive to give a real output (since $p < 1$), a positive muscle velocity corresponded to muscle stretch. If the muscle was shortening, the muscle spindle model will only output a value based on the current muscle length and not the velocity of shortening.

The result of equation 6.5 was then subject to a first order delay, which was given in the frequency domain by the following equation:

$$H(s) = \frac{1}{\tau s + 1}$$

Equation 6.6

Where τ was the time constant for the delay and s was the Laplace operator. The final output was then:

$$Ia = K_{IA} \cdot MS_{OUT} \cdot H(s)$$

Equation 6.7

The exact pathway that the muscle spindle signals were involved in for each simulation will be detailed in the *Simulation Descriptions* section.

Simulation Descriptions and Results

Experiment #1: Effect of Stretch Reflex Gains And CPG Parameters On The Walking Pattern Of The Biped Model When Feedback Was Applied Across the Entire Gait Cycle

The effect of CPG parameters (τ_{ad} and q_t) and the feedback gain from the muscle spindle signals were assessed. For this series of simulations, the output of the muscle spindle models caused excitation of the muscle that was stretched and inhibition of the antagonist muscle, similar to the feedback mechanism described by Pearson and Gordon (2000). A schematic illustrating the connectivity of the neurons in the neural control system for this simulation was shown in Figure 6.2.

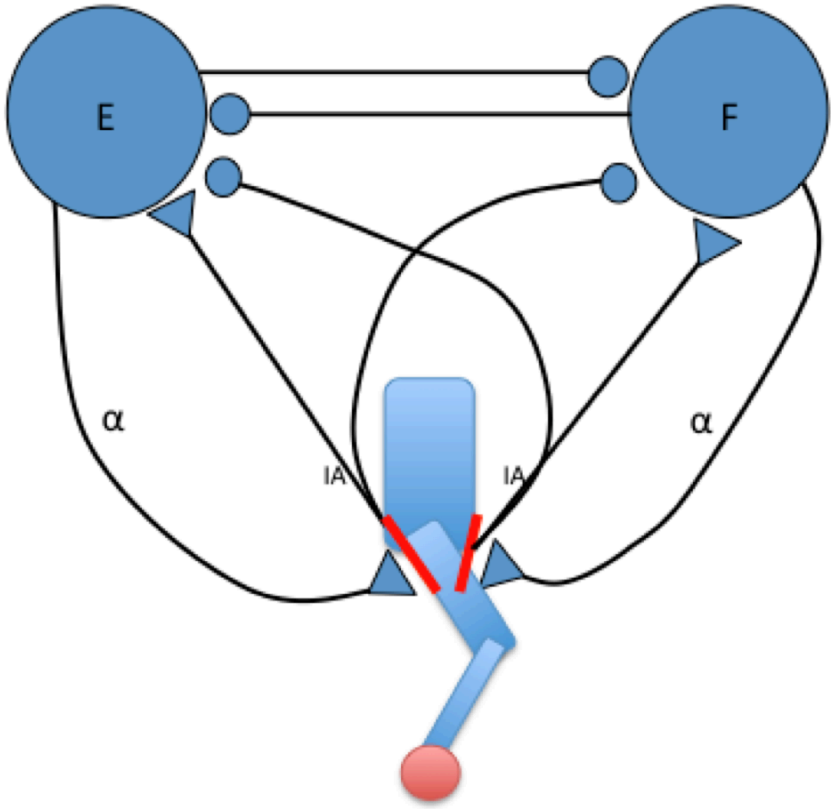

Figure 6.2: Schematic illustrating the neural connectivity that was used for Simulation #1. Muscles were activated by signals that originate from the half-centre neurons of the CPG, and were delivered through the α-motor neurons. Feedback from the muscle spindle models (indicated in the figure by 'IA') activated the half-centre of a stretch muscle while inhibiting the half-centre of the antagonistic neuron. Note that a triangular synapse represents an excitatory connection while a circular synapse indicates an inhibitory connection.

Four series of simulations were carried out to determine the effect of sensory feedback on the walking pattern of the biped model, when only hip muscles were used to actuate the model. Four series of 252 individual simulations were carried out to determine the interaction between the time constant of the adaptation effect of the CPG neurons and the feedback gains. During this series of simulations, the CPG only received feedback from the muscle spindle pathways that were presented in Figure 6.2, and feedback from the muscle spindle models was applied over the entire locomotor cycle. Four levels of tonic input to the CPG were tested (q_t = 1.25, 1.0, 0.75, and 0.5). These particular values of q_t were chosen based on pilot testing which showed that q_t

values greater than 1.25 tended to cause an erratic motion pattern and values of q_t less than 0.5 were insufficient to cause forward motion. Based on the finding in Chapter 3, τ_{ad} was incremented between 0.25s and 2.5s in steps of 0.1s, while the feedback gain was incremented from 0.0 to 1.0 in steps of 0.1. As in Chapter 5, the walking speed and the variability in forward walking speed were assessed for each simulation.

The average forward walking speed from each simulation is shown in Figure 6.3, while the variability of the walking speed is shown in Figure 6.4. For the majority of simulations carried out for this experiment, the walking speeds were generally slower than those observed when only FF control was used, such as the simulation that were carried out in Chapter 5. Both τ_{ad} and FB_{GAIN} had an effect on the walking speed of the biped model with higher values of the feedback gain tending to lead to slower walking speeds. The effect of the time constant was not as consistent as was observed in the previous study. The highest walking speed was observed when the tonic input was set to 1.0, when the feedback gain was set to a very low value.

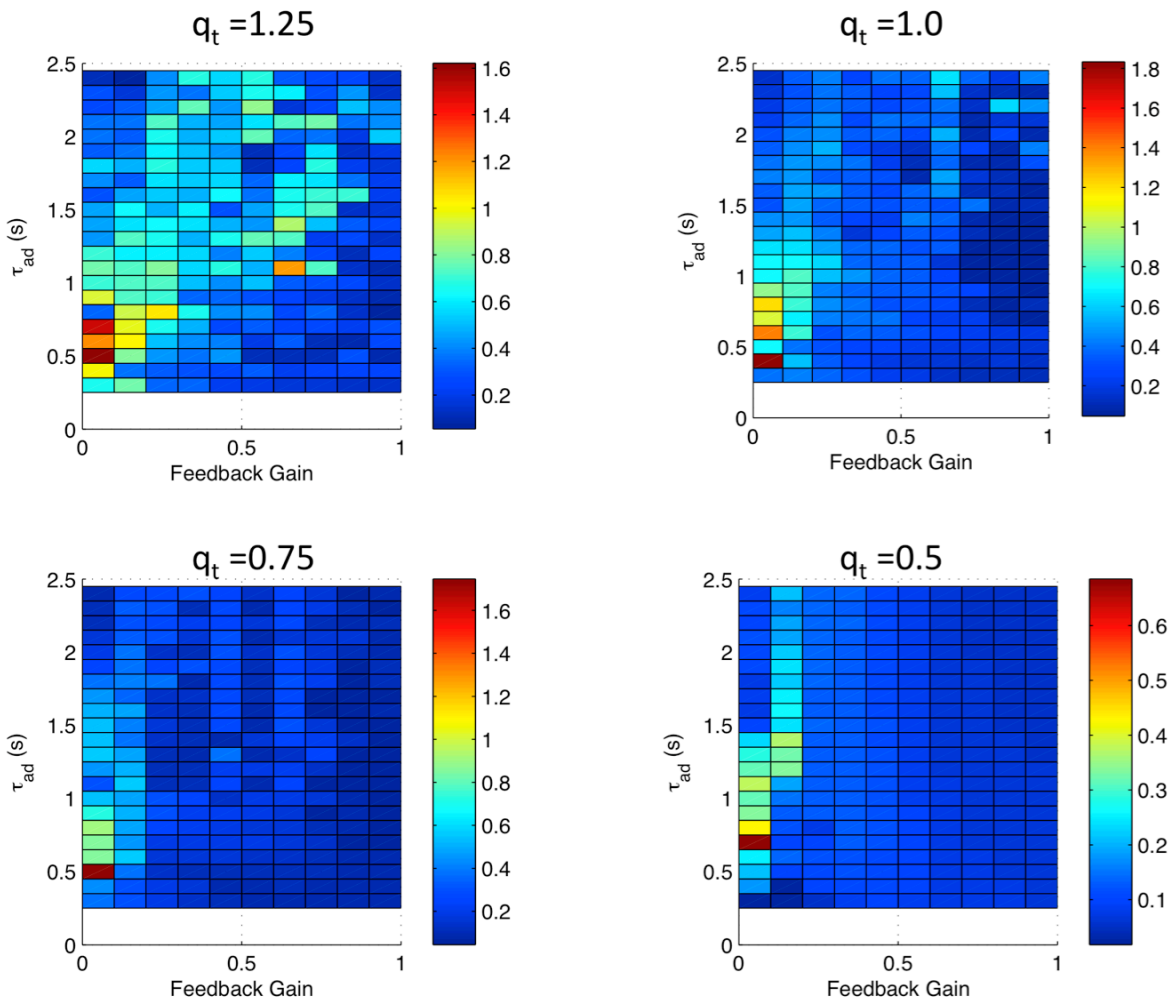

Figure 6.3: Plots showing the effect of the adaptation time constant (τ_{ad}) and the feedback gain on the average walking speed of the biped model, across four levels of tonic input to the CPG (q_t), when feedback was applied over the entire gait cycle. Red areas represent higher walking speeds, while blue areas represent lower walking speeds.

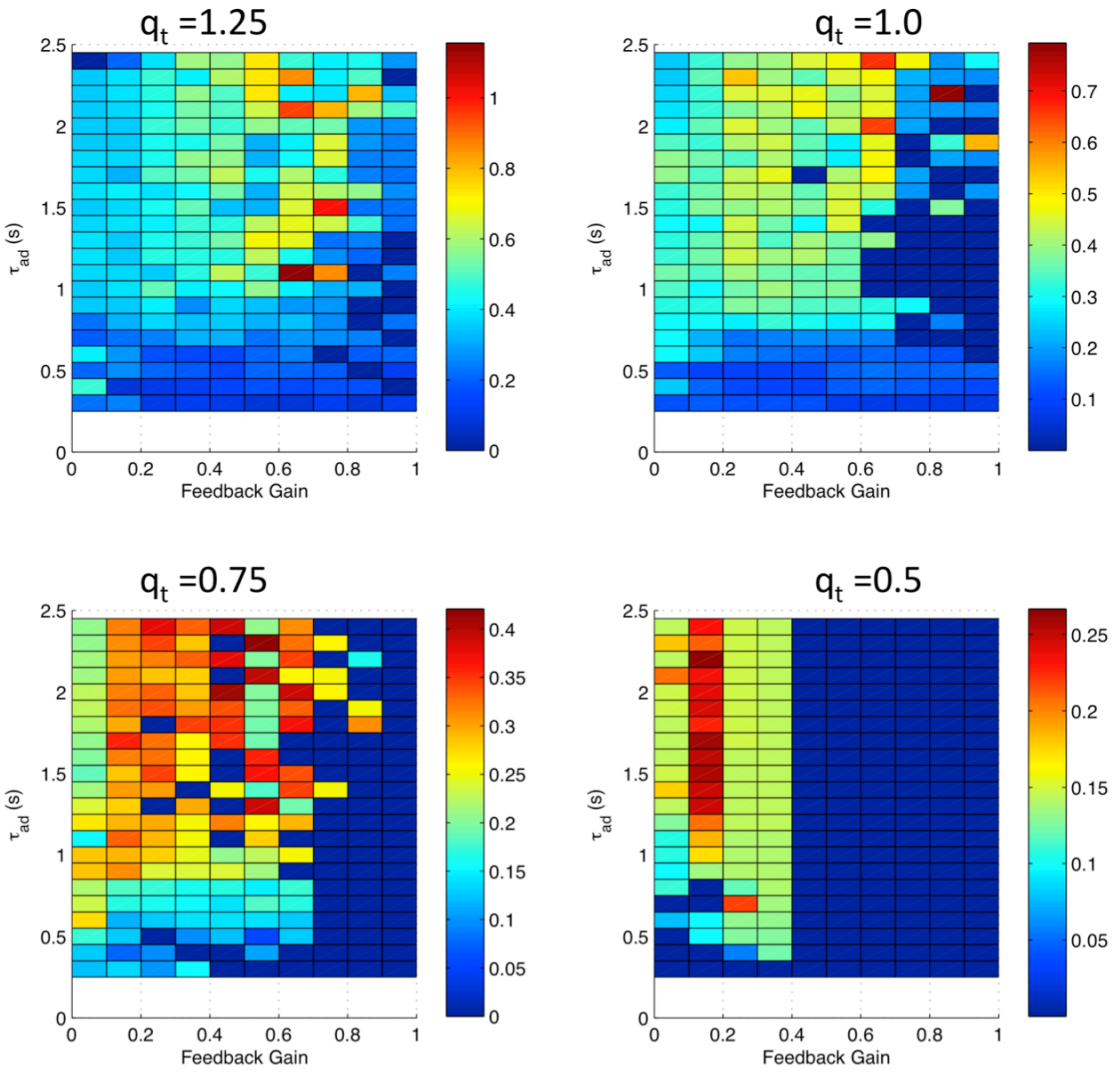

Figure 6.4: Plots showing the effect of the adaptation time constant (τ_{ad}) and the feedback gain on the variability of the walking speed of the biped model, across four levels of tonic input to the CPG (q_t), when feedback was applied over the entire gait cycle. Red areas represented higher variability in walking speed, while blue areas represented lower variability in walking speed.

The overall walking appeared to resemble a fairly normal walking pattern, although the joint kinematics of the walking pattern were not analyzed for each simulation. A plot comparing the walking pattern with other feedback mechanisms used in this study was shown in Figure 6.8.

Experiment #2: Analyzing the effect of phase dependent feedback on the walking patterns of the biped model

The set of simulations that were carried out for Experiment #1 were repeated with phase dependant feedback being delivered to the CPG. During these simulations feedback to the extensor HC was delivered during the stance phase and feedback from flexor muscle spindles was active during the swing phase. Four series of 252 individual simulations were carried out to determine the interaction between the time constant of the adaptation effect of the CPG neurons and the feedback gains. During this series of simulations the CPG only received feedback from the muscle spindle models. Four levels of tonic input to the CPG were tested (q_t = 1.25, 1.0, 0.75, and 0.5). As in experiment #1 in this chapter, the walking speed and the variability in forward walking speed was assessed for each simulation. The walking speed and walking speed variability results from these simulations were shown in Figures 6.5 and 6.6 respectively.

By comparing the walking speeds in Figure 6.3 to 6.6, it can be observed that typically higher walking speeds were achieved when phase-dependent feedback was applied. On average the walking speeds were 21-34% higher, depending on the value of q_t, when feedback was applied in a phase dependent nature, compared to when feedback was applied over the entire gait cycle. When the variability of the walking speed was compared between experiment #1 and experiment #2 it was found that the variability in the walking speed was greater when in experiment #2 when phase dependent feedback was applied. The variability in the walking speed was found to be 7-28% greater, again depending on the value of q_t, when phase dependent feedback was applied, compared to the simulations when feedback was applied across the entire gait cycle.

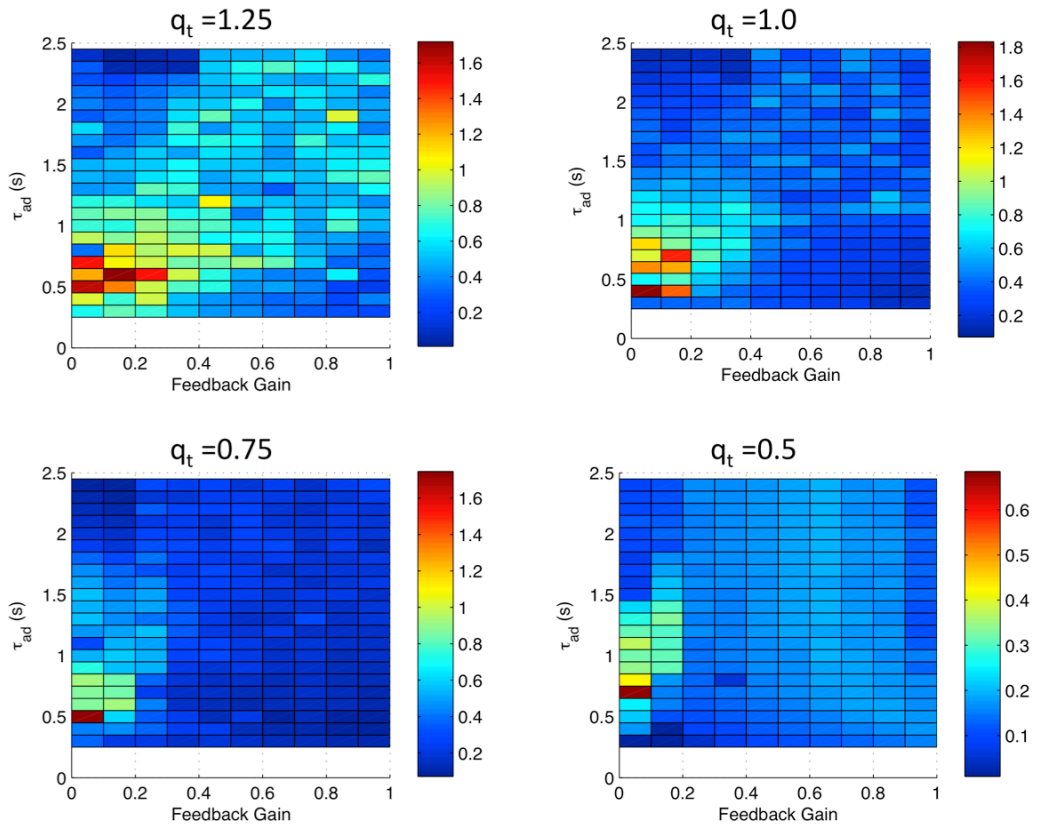

Figure 6.5: Plots showing the effect of the adaptation time constant (τ_{ad}) and the feedback gain on the <u>average walking speed</u> of the biped model, across four levels of tonic input to the CPG (q_t), when phase dependant feedback was applied. Red areas represented higher walking speeds, while blue areas represented lower walking speeds.

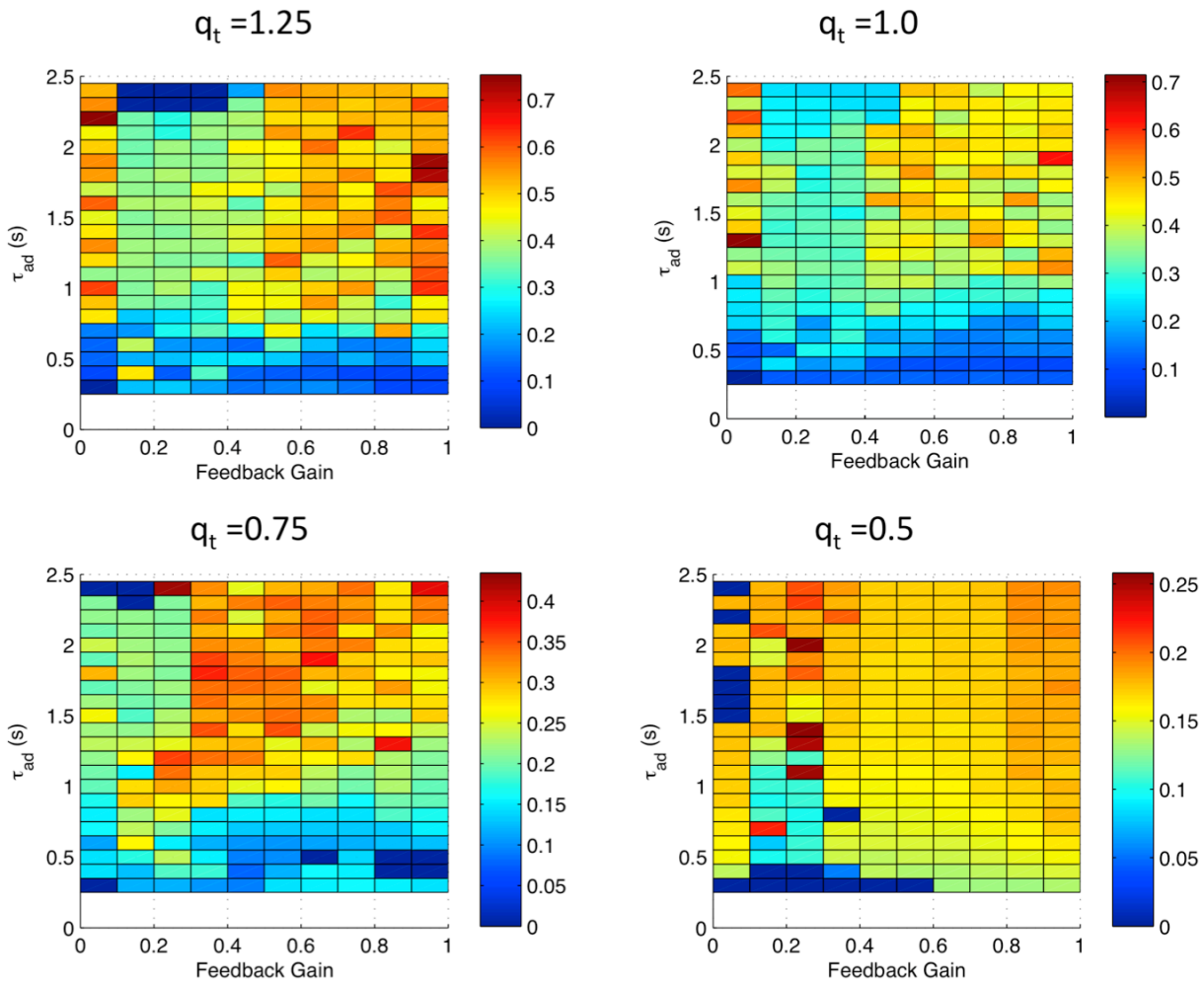

Figure 6.6: Plots showing the effect of the adaptation time constant (τ_{ad}) and the feedback gain on the variability of the walking speed of the biped model, across four levels of tonic input to the CPG (q_t), when phase dependent feedback was used. Red areas represent higher variability in walking speed, while blue areas represented lower variability in walking speed.

The typical horizontal displacements of the HAT segment's COM were shown in Figure 6.7. These simulations were carried out with the same tonic input to the CPG, the same time constant of the adaptation effect on the CPG and the same magnitude of the feedback gain (q_t = 1.0, τ_{ad} = 0.25, FB_{GAIN} = 1.0). This figure illustrated the main findings of the previous figures, where the highest levels of walking speed were found when no feedback was applied, while the

lowest walking speed was achieved when feedback was applied across the entire gait cycle, and the use of phase-dependent feedback produced a moderate walking speed. The variability in the walking speed was also assessed in Figure 6.7, by observing variations in the forward trajectory of the HAT segment. It could be seen that the use of phase dependent feedback and purely feedforward control led to some variation in the forward walking velocity while the use of feedback across the entire gait cycle led to a very consistent forward walking speed. Similar conclusions was made by viewing traces of the walking pattern, which were shown in Figure 6.8, and the phase plots of the joints motion, which were shown in Figure 6.9, 6.10 and 6.11.

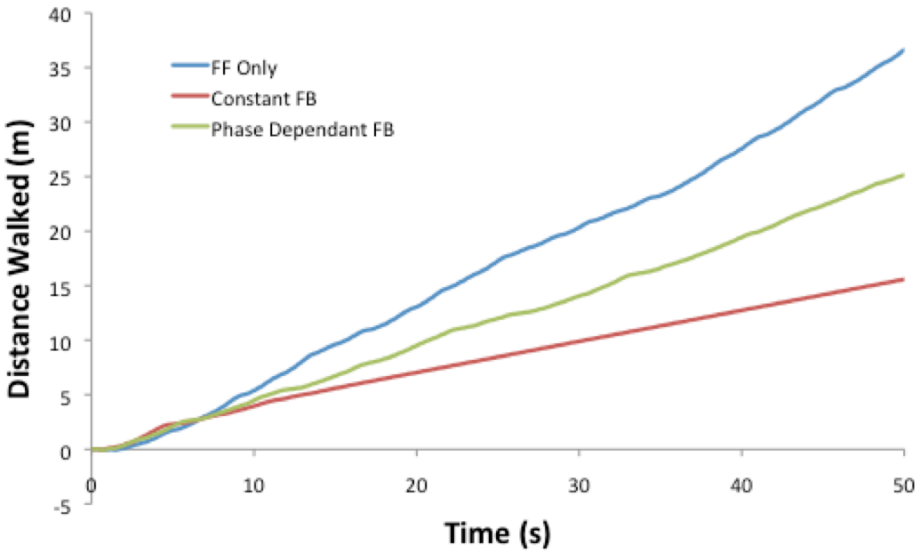

Figure 6.7: The effect of the feedback type (no FB, Constant FB, Phase Dependent FB) on the horizontal displacement of the HAT segment over the entire simulation. The settings were the same for all the simulations were identical (q_t = 1.5, τ_{ad} = 0.25, FB_{GAIN} = 1.0).

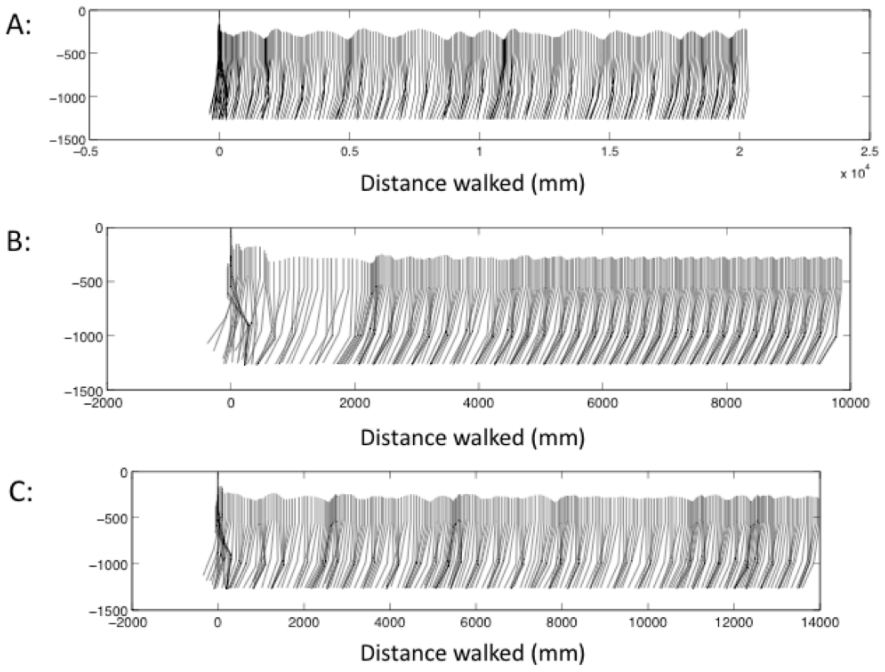

Figure 6.8: The walking pattern when different types of feedback were used: feedforward only (A), constant feedback (B) and phase dependent feedback (C). The right limb of the biped model was traced every 0.1s.

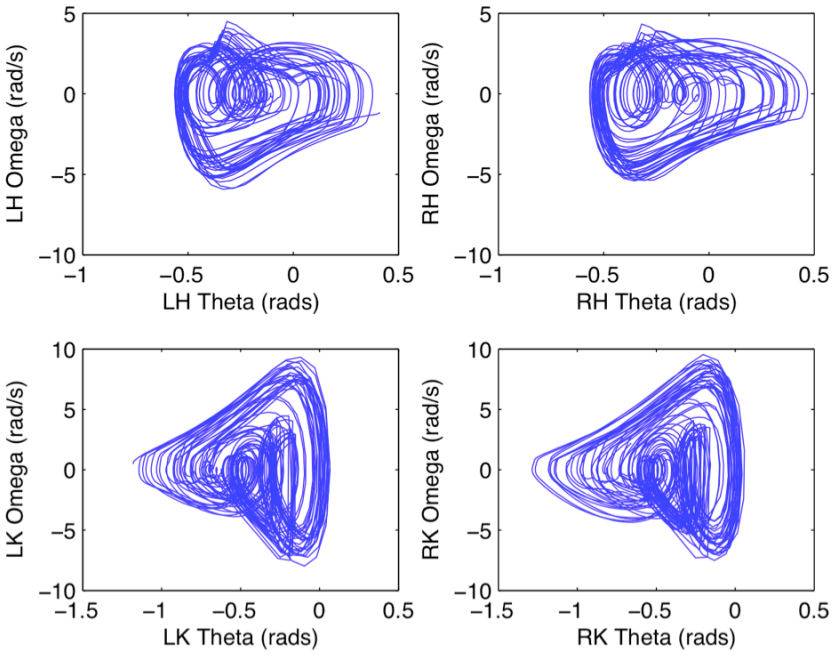

Figure 6.9: Phase plots showing motion of the limbs when only feedforward control was used.

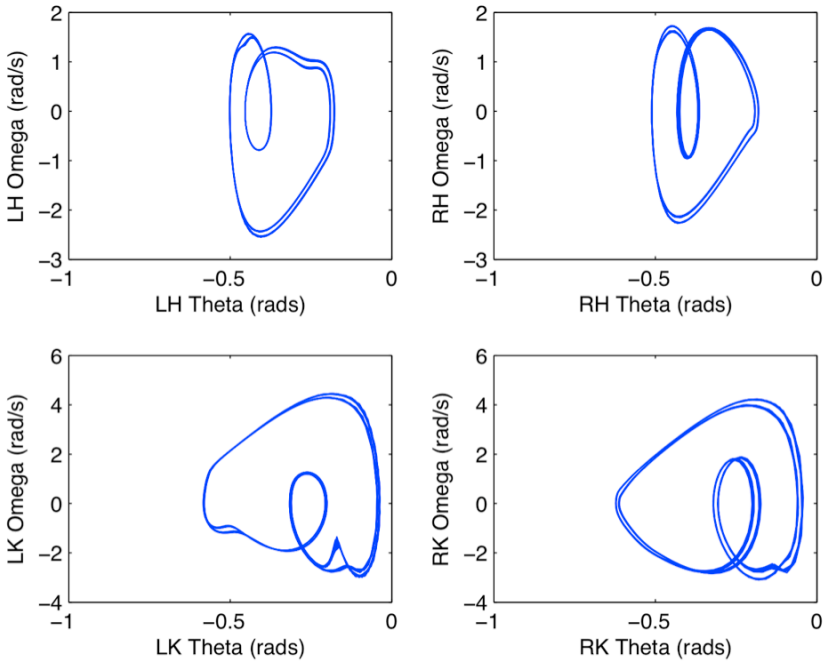

Figure 6.10: Phase plots showing motion of the limbs when feedback was applied across the entire gait cycle.

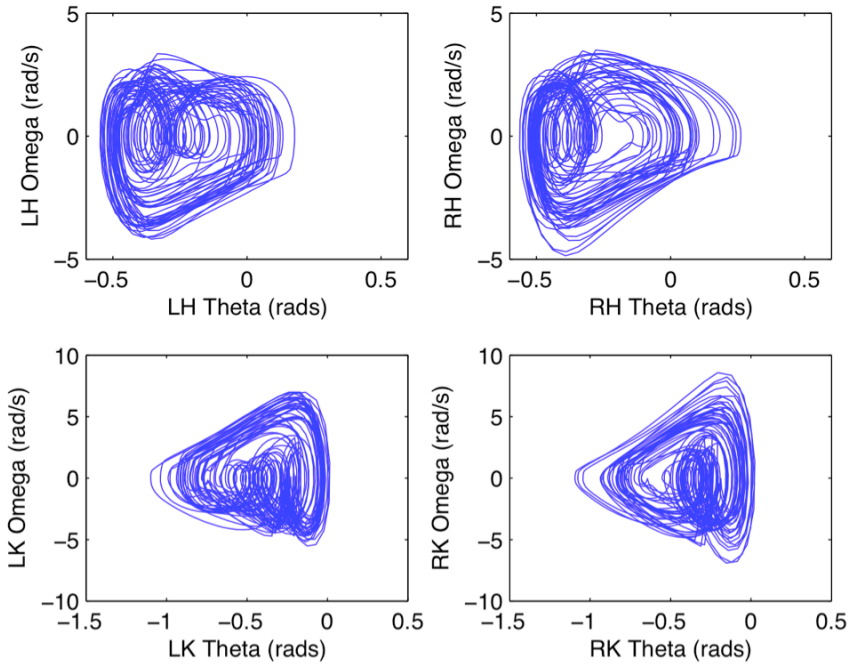

Figure 6.11: Phase plots showing motion of the limbs when phase-dependent feedback control was used.

Experiment #3: Effects of Modulating the Feedback Gain Based on Ground Contact Force

It has been demonstrated in animal (Akazawa et al. 1982) and human (Capaday and Stein 1986) work that the magnitude of the stretch reflex was dependent on the magnitude of the muscle's activation. To test the effect of this type of modulation of sensory reflexes, a series of simulations were carried out that were similar to those previously described to test the influence of τ_{ad} and FB_{GAIN} on the walking pattern of the biped model, except with the value of the feedback gain being determined by stance sensors at the contact points. These sensors signal the magnitude of the vertical ground reaction force, with a value of 1.0 being produced when full body weight was being supported by that stance sensor. The feedback gain for the extensor muscles in the model was multiplied by the value from the stance sensor, while the feedback gain for the flexor muscles were multiplied by the value of the stance sensor subtracted from 1.0.

As in the last experiment, four series of 252 individual simulations were carried out to determine the interaction between the time constant of the adaptation effect of the CPG neurons and the feedback gains. Despite having the feedback gain modulated by the stance sensor, an overall feedback gain (FB_{GAIN}) was also applied to the feedback signals prior to the integration with the CPG model. The feedback pathways were the same as those modeled in the previous experiment, and were shown in previously in Figure 6.2. Four levels of tonic input to the CPG were tested (q_t = 1.25, 1.0, 0.75, and 0.5).

The walking speeds from these simulations are shown in Figure 6.12. The results of these simulations were similar to those in Experiment #2 when phase dependent feedback was applied. This can be seen by comparing the average walking speed results in Figures 6.12 and 6.5. Although not depicted graphically, similar results were obtained when the variability in the walking speed was compared to the previous experiment. Again, the fast majority of the walking

speeds that were achieved in this experiment were substantially lower than normal human walking speeds.

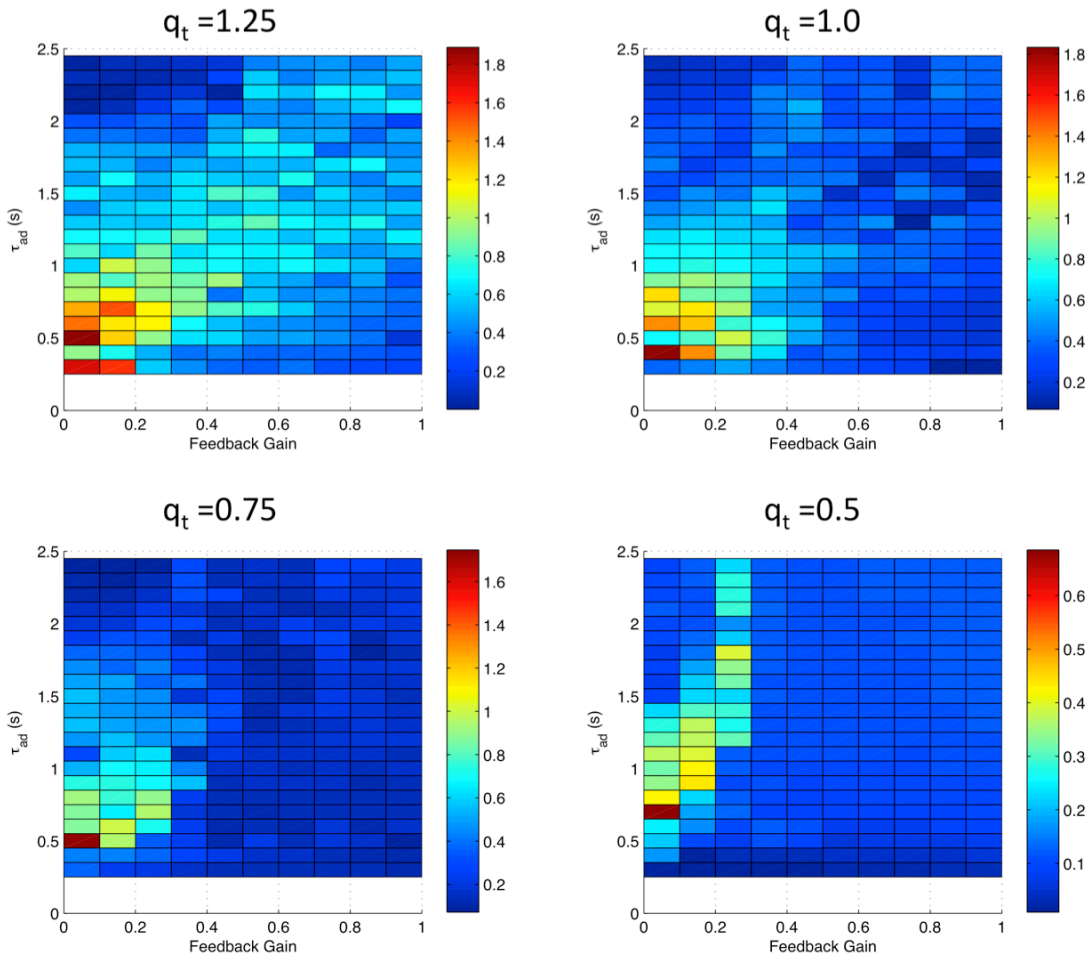

Figure 6.12: Plots showing the effect of the adaptation time constant (τ_{ad}) and the feedback gain on the average walking speed of the biped model, across four levels of tonic input to the CPG (q_t), when phase dependent feedback was produced based on the amount of body weight detected by the stance sensors. Red areas represent higher walking speeds, while blue areas represent lower walking speeds.

Experiment #4: Effects of Stance Feedback

The next simulations analyzed the effect of the positive feedback from loading with limbs to the extensor half-centre of the CPG. This set of simulations altered the stance feedback from the ground reaction forces to the extensor half-centre between 0 and 1.0 and made similar

analyses of the walking pattern, including the walking speed and variability of walking speed. The simulations were carried out with the same parameters that were used for the specific examples presented in the previous experiment ($q_t = 1.5$, $\tau_{ad} = 0.25$, $FB_{GAIN} = 1.0$). For this set of simulations there was an excitatory connection from the stance sensors on the bottom of the feet of the model to the extensor half centre of the CPG model. The signal from the stance sensor was normalized such that when the full body weight, a value of 1.0 would be generated. A gain was applied to this sensory signal originating from the foot sensor. A total of 21 simulations were carried out with this stance feedback gain being incremented from 0 to 1.0, in units of 0.05. All of the other parameters used for these simulations were similar to those previously run.

The average walking speed results from these experiments were shown in Figure 6.13. It was found that when the stance feedback gain was greater than 0.4, there was a dramatic increase in the walking speed of the biped model, with walking speeds ranging between 1.0 and 1.8 m/s, which was approximately the range of normal walking speeds in humans. It was found that when the stance feedback gain was less than 0.4, the walking speed was quite slow with a range of 0.2 to 0.5 m/s. The variability of the walking speed for these simulations was examined in two different ways, in absolute terms as was done in the previous experiments and as a percentage of the average walking speed for that particular simulation. These results were illustrated graphically in Figure 6.14. In absolute terms it can be observed that the variability in the walking speed shared a similar pattern to the average walking speed values over the same simulations, indicating that there was greater variability in the walking speed when the stance feedback gain was greater than 0.4.

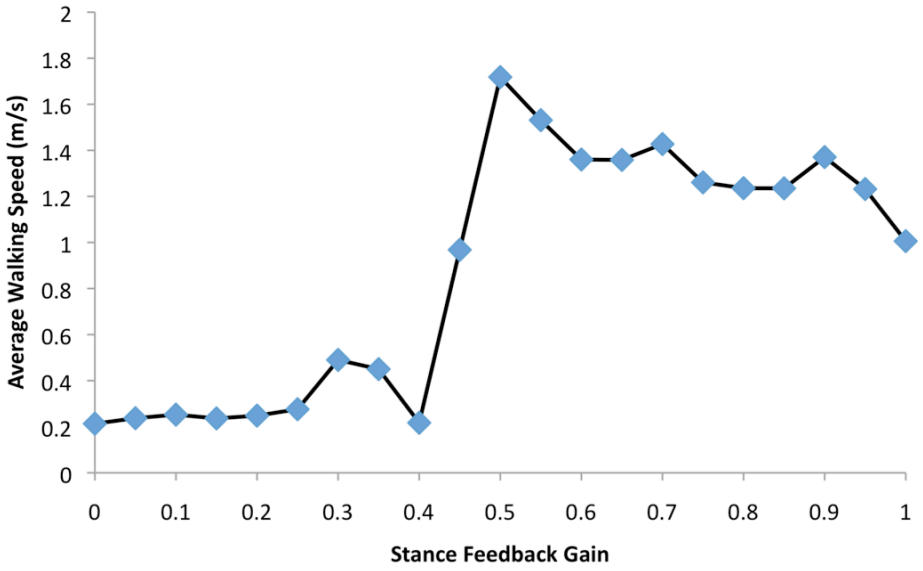

Figure 6.13: Average walking speed for each simulation, when the gain of the stance feedback mechanism was systematically manipulated.

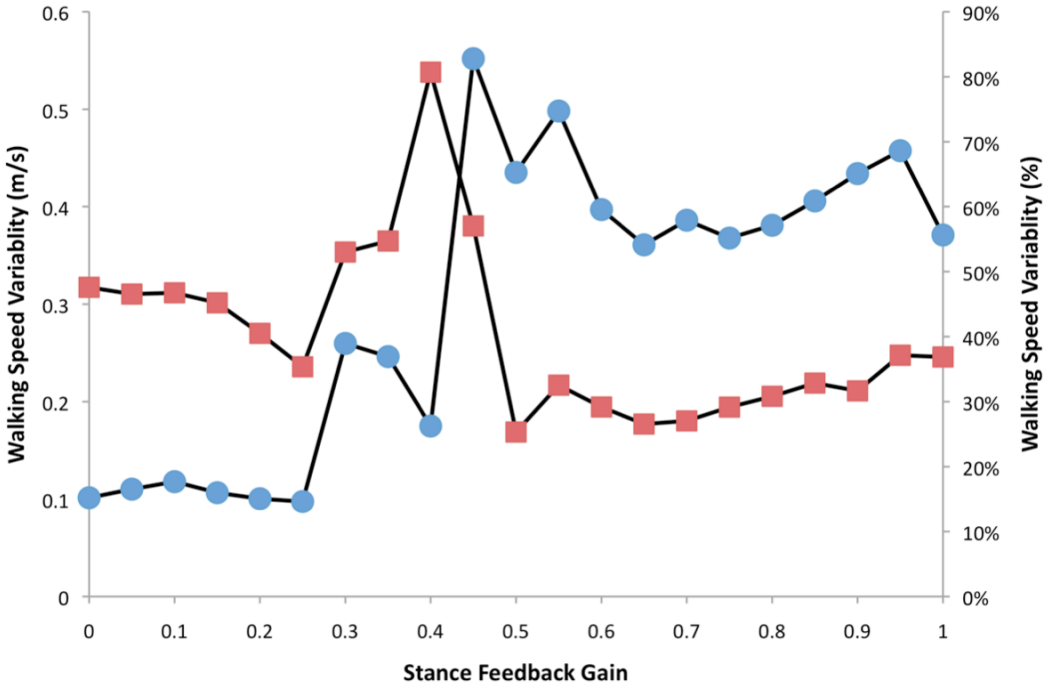

Figure 6.14: Walking speed variability across different values of the stance feedback gain. The values are shown in absolute terms (blue circles) on the left axis and as a percentage relative to the average walking speed for that simulation (red squares) on the right vertical axis.

To test the combined effect of the stance related feedback and stretch reflex modulation a series of simulations were carried out that modulated the time constant of the CPG and the spindle's feedback gain. A single series of simulations were carried out with the tonic input to the CPG set to 1.5 ($q_t = 1.5$), the time constant of the CPG ranging between 0.25 and 1.5 in increments of 0.1, while the feedback gain ranging between 0 a 1.0, in increments of 0.2. It was decided to only test this configuration of the neural control model with the tonic input set to 1.5, since based on the previous simulations this level of tonic input was found to produce the most realistic walking speeds. The level of stance feedback was set to 0.5, which based on the previous experiment, was shown to produce a greater level of forward walking velocity. The outcome measures evaluated were the same as those used in the previous experiments in this chapter, namely the average walking speed of the biped model, and the variability in the walking speed over the simulation time. The results of these simulations are presented in Figure 6.15.

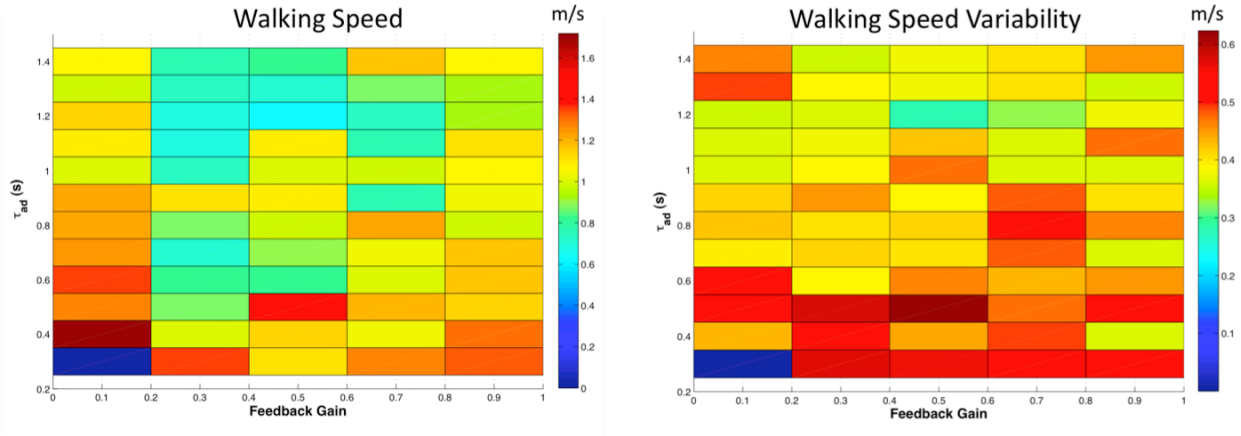

Figure 6.15: Plots showing the effect of the adaptation time constant (τ_{ad}) and the feedback gain on the average walking speed and walking speed of variability of the biped model. Red areas represent higher walking speeds, while blue areas represent lower walking speeds.

It was difficult to assess the results of these simulations due to the large amount of variability in the results. It could be observed in Figure 6.15, that the highest walking speed was achieved when the value of τ_{ad} was 0.4 and when the gain of the stretch reflexes was low (< 0.2).

These findings indicate that stretch reflexes have a role in slowing down the walking pattern. A trend can also be observed that lower walking speeds resulted with higher values of τ_{ad}, presumably by reducing frequency of the CPG output, as was shown in Chapter 3. A trend was observed that lower levels of walking speed variability were achieved when the value of τ_{ad} was greater than 1.0, this could be the result of walking at lower overall walking speed. The kinematics of the walking pattern of the biped model were less consistent then those that were shown previously in experiment 1 in this chapter. This was seen in the example stick figures and phase plots shown in Figures 6.16 and 6.17 respectively. Due to the higher walking speeds that were achieved with the addition of positive feedback to the extensor half centre the stretch reflexes appeared to lose some of their ability to correct undesirable walking patterns. For the majority of the simulations that were carried out in this experiment, the walking speeds that were achieved were very close to normal walking speeds in humans (1.0 – 1.8 m/s). There were some simulations with moderate values of FB_{GAIN} (0.2-0.8) and higher τ_{ad} (>0.6s) values that led to slower than normal walking speeds.

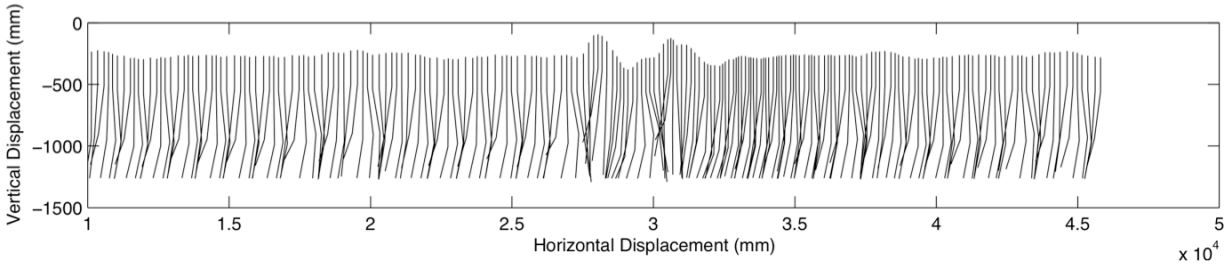

Figure 6.16: Stick figure illustrating the walking pattern of the biped model when stance feedback was applied to the activity of the extensor HC. The right limb of the biped model was traced every 0.1 s. The control system parameters for this simulation were: q_t = 1.5, τ_{ad} = 0.25, FB_{GAIN} = 1.0, Stance FB_{GAIN} = 0.5.

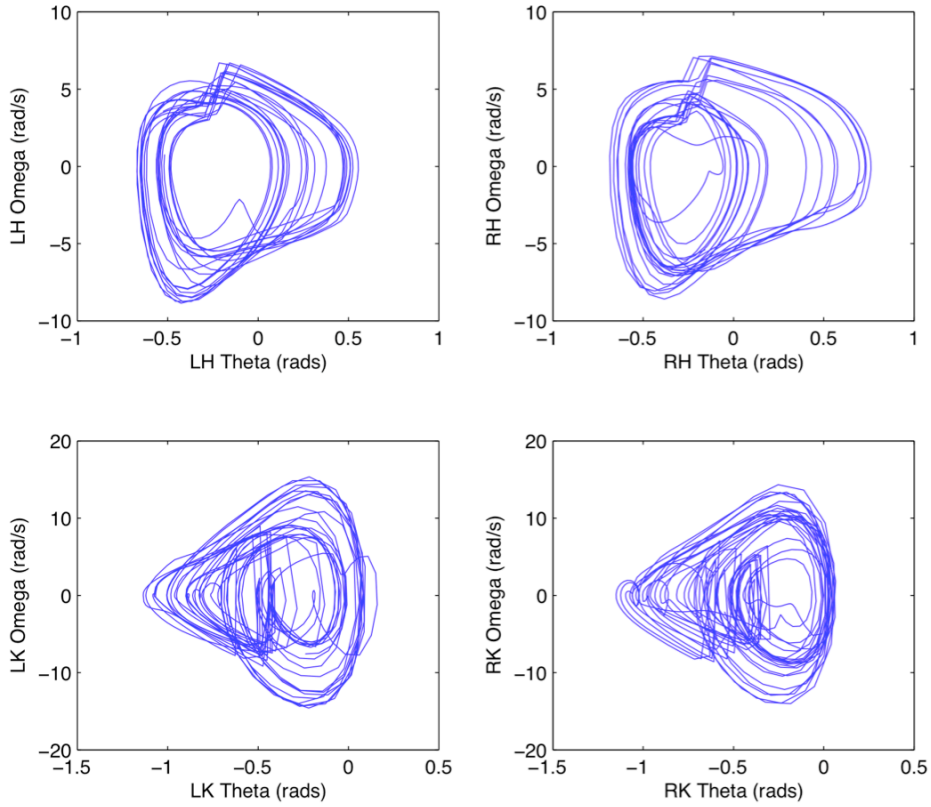

Figure 6.17: Phase plots of the biped model's limbs motion from the last 30s of the walking simulation when stance feedback was applied to the extensor HC's activity. The control system parameters for this simulation were: q_t = 1.5, τ_{ad} = 0.25, FB_{GAIN} = 1.0, Stance FB_{GAIN} = 0.5.

Discussion

This study focused on manipulating the properties of sensory feedback from muscle receptors and determining what their effect would be on the walking pattern of a model of the human musculoskeletal system. This study extended beyond previous work in this area by systematically altering the properties of the feedback system, where previous studies ran simulations with set properties of the feedback system and did not show simulation results with different feedback properties. When creating neuromechanical simulations, it is important to systematically test the effect of each component that was added to the model, to determine what

its effect would be on the overall behaviour of the model. If a model was constructed and each component was not independently verified, it cannot be known which component was determining the overall behaviour of the model. The work presented in this chapter extended beyond previously tested models by critically examining the effect of each feedback component that was added to the model.

The work in this chapter was divided into four independent experiments, which built upon the results of models that were previously presented in this thesis. In the first experiment, a series of simulations were carried out to determine the effect of a simple stretch reflex being applied on the muscles, which were actuating the walking pattern. This series of simulations applied the stretch reflex to varying degrees by systematically modifying the gain of this reflex. The effect of this reflex was tested in conjunction with modifying the properties of the CPG (q_t and τ_{ad}), which established the basic locomotor pattern. It was hoped that the application of this type of reflex would facilitate an improvement in the walking pattern of the biped model, because the circuitry involved in this feedback mechanism is similar to feedback mechanisms that have been found to facilitate phase transitions in the gait cycle in studies of animal locomotion. For example stretching of the hip extensor muscle that would occur at the end of the swing phase would trigger an excitation of the hip extensor HC and due to the mutual inhibition property of the CPG model that was used, the flexor neuron would be inhibited, thus producing a transition from swing phase to stance phase. Due to the nature of the circuitry, it was anticipated that a similar phenomenon would occur during the stance to swing transition through the inverse of the previously described mechanism. For the majority of simulations that were carried out for this particular manipulation it was found that the walking speed of the biped model was much lower than those found in the previous study, which only used feedforward control mechanisms

to drive the biped model's walking pattern. It was observed in Figure 6.3, that increasing the gain of the stretch reflex led to slower walking speeds. Thus the application of a stretch reflex significantly slowed down the walking pattern of the biped model. This was likely due to the inhibitory nature of the stretch reflex keeping overall levels of muscle activation lower, and thus reducing the overall average walking speed. The walking speeds that were closest to normal walking speeds (1.2 - 1.8m/s) tended to occur when q_t was set to higher values (1.25 or 1.0), at lower FB_{GAIN} values (<0.3) and lower values of τ_{ad} (< 1.0s).

The stretch reflex also appeared to cause a reduction in the level of variability in the walking pattern, but this appeared to be more consistent across the magnitudes of the feedback gains applied. It could be observed in Figure 6.4, that the variability in the average walking speed was lower on the right side of the graphs and it was further observed in Figure 6.5 that the application of the stretch reflex across the entire gait cycle led to very little variation in the forward progression of the HAT segment. This finding showed the potential for a stretch reflex to stabilize the walking pattern, however there are obviously other control mechanisms that were required to achieve a more appropriate walking speed, and take longer steps. Based on the previous study in this thesis that tested the interactions of stretch reflexes with the CPG with a pendulum model, it was expected that the addition of stretch reflex to the model would reduce the overall variability of the model's behaviour due to the entrainment between the limb's motion and the CPG. This was observed by having walking speeds of the model that were in a relatively tight range despite the wide range of feedback parameters that were tested in this study.

The second series of experiments in this study analyzed the effect of applying the stretch reflex in a phase dependent nature, as has been observed in humans (Capaday and Stein 1986).

This type of feedback has been included in some previous neuromechanical simulations. For example Taga et al (1991), included a stance sensor in his model, which detected when the foot (or terminal end of the leg) was in contact with the ground. If the foot was in contact with the ground then the stretch reflexes were only applied to the extensor muscles in the model, if the stance sensor did not detect contact with the ground then the stretch reflexes were applied only to the extensor muscles in the model. A similar feedback mechanism was implemented in the neural control model used in this study, and extended beyond the work of Taga by systematically manipulating the magnitudes of the feedback signals during walking, as was done in the first experiment in this study. The results from this series of simulations were also compared to the previous experiment, so that the effects of applying phase dependent feedback could be examined. Overall it was found that the use of phase-dependent feedback led to greater walking speeds (approximately 20-30**%** higher) compared to the use of a stretch reflex across the entire gait cycle. It was also observed that the use of phase dependent feedback led to an increase in the variability of the walking pattern, which was observed in both the variability of the walking speed (Figure 6.5), in the phase plots of the biped's joint kinematics (Figure 6.11) and in plots of the HAT segments forward trajectory (Figure 6.7). This increased variability was likely due to the fact that some unexpected motion patterns are not being corrected by the stretch reflex. Despite achieving average walking speeds that were still substantially less than those that were observed when only feedforward control was used (In Chapter 5), there appeared to be a trade-off between the average walking speed of the biped model and the variability in the biped's movement pattern. While the use of phase dependent feedback allowed greater walking speeds, it does so at the expense of allowing more variability in the walking pattern.

The third series of simulations that were carried out in this study attempted to determine the effect of modulating the gain of the feedback signals based on the level of weight supported, as detected by the stance sensors in the model. Modulating the gain of the reflex based on the level of the weight support was previously done by Taga (1995a), however most models have modulated the level of the stretch reflex gains based on the baseline state of the CPG's output (Yakovenko et al. 2004; Paul et al. 2005). It was decided not to implement this method in this experiment due to difficulties that would occur with integrating these types of signals with the CPG model that was used in this neuromechanical model. Overall, it was found that modulating the magnitude of the stretch reflex had little effect when compared to using a simple phase dependent feedback was used. Although it may increase the biological fidelity of the model to include modulation of the stretch reflex based on more complex methods, there was little effect to when a more simple method was used.

The final series of simulations in this study examined the effect of adding positive feedback from the stance sensor to the activity of the extensor HC within the CPG. It was found that this type of feedback had the largest overall effect on the walking pattern, of those that were tested in this study. It was found that when the gain for this type of feedback was sufficient that there was a dramatic increase in the walking speed of the biped model. This type of feedback was slightly different than stance reinforcing feedback that has been previously been found in animal work, where it has been typically thought that Ib signals from Golgi tendon organs (GTO) from stance muscles have a positive feedback effect on the extensor HC (Hiebert and Pearson 1999). By using the ground reaction force as surrogate for loading of the extensor muscles, the feedback mechanism may have been slightly different than using the GTO signals. However, since both signals would represent the loading of the limb, it was thought that they could be used

interchangeably. This type of sensory feedback has also been used in other neuromechanical simulations of human walking, such as those of Taga (Taga et al. 1991; Taga 1995a). Additionally previous research analyzing the effect of muscle loading on the control of stance duration has focused on the loading of the ankle extensors. Since there was no ankle joint in the model, it was felt that stance reinforcement would have to occur through a more global representation of the limb's loading and the vertical ground reaction force was chosen to represent this. Using a neuromechanical model, Ekeberg and Pearson (2005) made a similar finding regarding the contribution of positive stance feedback to the control of stance was the most important role of sensory feedback during locomotion, and had the largest effect on the walking pattern. The fact the findings of Ekeberg and Pearson could be replicated in a simplified simulation in this study provided some concurrent validity to the fact that this mechanism was clearly important in the control of the locomotor pattern.

The addition of stance reinforcing feedback also led to an improvement of the walking pattern of the biped model, this was seen by the improved step length in stick figures presented in Figure 6.16 and reduced variability in the phase plots of the joint kinematics when compared to previous simulations. The improved stride length was attributed to the enhancement of stance activity, while the decreased variability that was observed in the stick figures and phase plots could be a result of a greater walking speed leading to decreased variability (Jordan et al. 2006). It was found that the absolute variation in the walking speeds when stance reinforcing feedback was used was approximately the same, or greater than the previous series of simulations, however when it was considered that the biped model was actually walking at a faster walking speed, the variability in forward progression was actually substantially lower than the levels that were observed in the previous simulations.

Therefore the main finding of this study was that positive reinforcement of stance activity was critical for producing a walking pattern at satisfactory speeds. Previous studies investigating this type of feedback with "foot-in-hole" experiments have found that this feedback contributes approximately 30% of the muscle activation signal (Lam and Pearson 2002; Prochazka et al. 2002). This reflex was very important for the safety of the locomotor pattern, as it ensures that the limb was not bearing weight before it was withdrawn. It was likely that with the addition of this feedback mechanism that the level of support from the body weight support system model that was included in this study could be reduced, as was done in Chapter 5 to test the efficacy of that system. However this experiment will have to be completed with future work, due to the focus of testing this ability of this feedback to increase the walking speed of the biped model. The use of an excitatory connection from the stance sensor to the extensor half centre of the CPG differs from the mechanisms that are thought to be responsible for the reinforcement of stance activity during mammalian locomotion. Donelan and Pearson (2004) found that this mechanism is likely due to IB afferents in the ankle extensors having an excitatory effect on the extensor centre of the CPG. Since there were no ankle extensors or IB pathways modelled in this work, it was decided to base this signal on the amount of body weight that was detected by the stance sensor at the contact point. The input to this feedback mechanism is more akin to pressure or mechanoreceptors that are present in the sole of the foot. While these types of receptors have been shown to have an influence on locomotor parameters, such as foot placement (Bouyer and Rossignol 2003) or balance control (Perry et al. 2001), there is no evidence that these types of receptors are capable of reinforcing stance activity during walking, although there is some evidence that these pathways may act on the extensor centres within the CPG (Rossignol et al. 2006).

The stretch reflex was found to have a powerful effect on the walking pattern of the biped model, particularly reducing the walking speed and the variability of the walking pattern. It was found that when these stretch reflexes were applied in a phase dependent nature that there were higher walking speeds and an increase in the variability of the walking pattern when it was compared to the series of simulations with the stretch reflexes applied across the entire gait cycle. This improvement in the walking pattern was not surprising, as previous work has found phase modulation of stretch reflexes across the gait cycle (Capaday and Stein 1986). It was somewhat surprising that further modulating the gain of the stretch reflexes based on the amplitude of the ground reaction force signals did not have a substantial effect on the walking pattern. This could be due to the fact that use of the support system limited the range in which the modulation could occur, meaning the gain of the stretch reflexes of the extensor muscles were limited by the fact that the level of ground support as quite low. While the focus of many neuromechanical simulation studies has been the analysis of simulated IA pathways, there is little evidence that these pathways play a large role in the control of normal steady-state locomotion. In animal work, it has been found that animals are still able to produce walking patterns in the absence of sensory feedback from muscle receptors (Grillner and Zangger 1984). Even human subjects who have lost sensation from muscle receptors are also able to produce walking patterns although they are more reliant of other sensory systems to walk (Lajoie et al. 1996). Despite the ability to walk without information from muscle receptors, neuromechanical simulations have focused on modeling the effects of these pathways since they are thought to have a large effect on the timing and the magnitude of the motor patterns that occur during walking (Rossignol et al. 2006). The IA pathways are also good candidates for beginning to

model locomotor control systems of since the effects of these pathways on the walking pattern are among the most studied (Rossignol et al. 2006).

While this study modeled some of the key feedback pathways that were involved in locomotor control, it was by no means a complete representation of the neural control mechanisms that are involved in human walking. Since the representation of the locomotor control system was incomplete, there are aspects of the biped's walking patterns that are not addressed in this study, most importantly the control of balance. The upper body in this model was supported by a spring-damper system, which ensures that the HAT segment will not collapse to the ground, or move too far about the hip joint. Previous neuromechanical simulations have included balance control mechanisms into their neural control models, but the overall mechanisms of balance control during walking were not yet fully understood, so it was not clear whether the methods of implementing balance control in neuromechanical simulations were appropriate. For example, Taga (1991) used the global angle of the HAT segment and the accelerations of the distal end of the HAT segment to generate hip moments that would balance the HAT segment. This control mechanism has some correspondence to the mechanisms that are involved in the control of the HAT segment during walking (Winter 1995a), however it was not clear whether the signals used to generate these hip moments are appropriate.

Another aspect of the locomotor control system that was not represented in this study was the cerebellum. It was known from observing patients that have cerebellar deficits that it plays a crucial role in the control of walking (Ilg et al. 2008). It was thought that the cerebellum contributes to the control of walking by acting as a comparator of the sensory feedback resulting from the ongoing movement and the intended movement, via an efferent copy (Morton and Bastian 2004). Some recent neuromechanical models have attempted to replicate the role of the

cerebellum in their control model (Jo 2008), which has allowed for much more advanced walking patterns, such as stepping over obstacles or recovering from mechanical perturbations. These methods were not implemented in the present study due to the increased computational resources that would be required to carry out the simulations, however it was recognized that the addition of a cerebellar model would likely lead to an improvement in the walking pattern.

The main outcome measures for this study were the average walking speed, and the variability of the walking speed. Gait speed was a commonly used measure in clinical practice for determining the overall quality of gait due to the high level of coordination that was required to achieve higher walking speeds (Andriacchi et al. 1977). Variability in the gait speed can be seen has a measure of the stability of the walking pattern, since it is undesirable to have dramatic variation in the forward velocity during walking, and normal human walking was characterized by a very consistent forward velocity of the trunk (Winter 1991). The kinematics of the walking pattern were evaluated using phase plots which compare the angular displacement of a joint to the angular velocity of the joint. These types of plots were common in the evaluation of neuromechanical models, as it allows for an appreciation of the level of cyclical stability of the walking pattern (Paul et al. 2005). Plots of joint angles over a gait cycle were not always possible to construct in this study due to the variability that was seen in the walking pattern of the biped. The level of coordination between the hip and the knee joints (intra-limb coordination) was not considered in this study, since the knee was not actively controlled in this study. Future work should focus on finding better methods to quantify the amount of cycle-to-cycle variability from phase plots, so that the kinematic output of these neuromechanical models could be quantitatively evaluated. In chapter 4 of this thesis the range of the magnitude of the phase vector was chosen as a method to quantify the effect of the perturbation of the phase plots. This was

based on methods suggested by Hamil et al (2000), however to due the large amount of variability present in the data, the application of these methods to the phase plots that were constructed in this study was not possible. More recently methods such as using Fourier analysis of both the displacement and velocity components and using the geometric properties of the loops on the phase plot has been suggested a technique to quantify the variability of the phase plots (Polk et al. 2008), however this method has only been applied to a small number of loops on a phase plot and has not been applied to larger data sets such as those produced in this chapter. There are also nonlinear methods that may facilitate the quantification of the cyclical stability of the walking pattern, such as those used by Kang and Dingwell (2009).

Just as in Chapter 5, it is important to consider the limitations of the musculoskeletal system that was used for testing the neural control systems that were created for this study. In this study only the hip muscles were actuated, while the motion of the knees was allowed to occur passively. This type of control system has been used for testing locomotor control systems for robotic mechanical systems (Lewis et al. 2003). The uniarticular nature of the muscles that were used to provide the sensory feedback to the CPG may also have important effects on the walking patterns that were observed. It has previously been shown that feedback from muscle receptors biarticular muscles may have important contributions to the control of lower limb movement patterns (Van Ingen Schenaug et al. 1994). As was also stated in Chapter 5, it is important to consider that the amount of weight being supported by the upper body support system model is quite high and had a dramatic effect on the walking patterns of the biped model. The amount of weight supported by this model would have a particularly large effect in experiment #3 in this chapter, where the modulation of the stretch reflex was weighted based on the magnitude of the ground reaction force. Because the modulation of the stretch reflex was

over a small range, due to the low levels of the vertical ground reaction force, there was very little effect on the walking patterns when this feedback mechanism was implemented. Future work should modulate the amount of body-weight support that is provided by the support system model and examine this type of reflex modulation.

The last consideration of results that need to be considered with the use of the biped model is that the moment arms of the hip muscles were assumed to be constant regardless of the hip angle. For example, it is know that flexion of the hip joint will lead to a nearly linear decrease in the moment arm of the Gluteus Maximus muscle (Nemeth and Ohlsen 1985). Therefore as the hip angle increases the in vivo would have to generate more force to create the same moment. However, in the biped model the muscle force could remain constant at different hip angles and the same moments would be produced.

In conclusion, this study focused adding feedback pathways from muscle receptors and contact sensors to the locomotor control system of a neuromechanical model. It was found that the addition of a simple stretch reflex could lead to a more repetitive and cyclical motion pattern, but at the expense of a slower average walking speed. It was also found that delivering the stretch reflex feedback in a phase dependent manner led to an increase in the walking speed of the biped model, but at the expense of a walking pattern with a higher level of variability. Positive feedback to the extensor HC of the CPG was found to have the largest effect on the walking pattern of the biped model. The addition of this feedback led to a dramatic increase in the walking speed of the biped model across all of the CPG parameters and stretch feedback gains that were tested. Future work should focus on determining whether this type of feedback was adequate for reducing the level of support required for the HAT segment.

Chapter 7: Conclusions

The goal of this thesis was to integrate computational models of the human locomotor control system with a model of the musculoskeletal system involved in human walking to examine the interaction between these two systems during walking and to determine how the parameters of these two systems affected the overall walking pattern. Due to the complexities of the human musculoskeletal system, the first two studies of this thesis used a very simplified model of a swinging limb, in which a rod pendulum represented the limb. This representation of the human leg allowed for the establishment of some of the basic properties of controlling the amplitude and frequency of the walking pattern. The following two studies used a simplified representation of a walking biped, which consisted of two segments per limb and a lumped upper body segment. This model allowed for the testing of neural control models which where more complicated than those used in the first two studies, but not so complicated that the intricacies of the locomotor control system could not be identified. Future work will focus on adding more joints (ie. ankle joints) and muscles to the model and finding ways to incorporate these additional degrees of freedom in to the locomotor control system. Future simulations will also address the adaptability of the walking pattern, such as responding to perturbations and stepping over obstacles.

In the first study of the thesis, feedforward control of the frequency and amplitude of the swinging limb's motion was found to be controlled by specifying two parameters within a model of a Central Pattern Generator (CPG). It was found that there was a significant entrainment, or synchronization, between the CPG and the model of the swinging limb. It was also found that the behaviour of the swinging limb was different if the frequency of the CPG was above or below

the natural frequency of the limb. This study found that the motion of the CPG was most predictable when the frequency of the CPG's output was greater than the natural frequency of the limb. Comparisons were made to findings of previous work involving human subjects where it was difficult for humans to achieve movement frequencies that were greater than the natural frequency of the limb, and the most efficient movement pattern actually occurred when the movement occurred at the natural frequency of the limb.

The second study in this thesis added feedback in the form of a simulated stretch reflex to the pendulum model that was used in the first study. This feedback forced the CPG to become entrained to the natural frequency of the pendulum and dramatically increased the amplitude of the pendulum's motion, due to the extra muscle activation from the stretch reflex. The feedback from these stretch reflexes was also able to stabilize the motion following a perturbation. The stretch reflex was actually quite robust at responding to the perturbation, as it was able to stabilize the motion of the pendulum no matter where the perturbation was applied in its movement cycle. This study showed the power of a simple stretch reflex to stabilize a rhythmic limb movement and explained some of the mechanisms for the neural entrainment of the CPG to the natural frequency of the limb.

The third study applied the principles of the feedforward CPG neural control system to a simplified model of the human musculoskeletal system. Because there were no balance control mechanisms, the weight of the biped model had to be supported by a spring-damper system, which essentially acted as a harness and held up the model so that it would not fall. The walking speed of the biped model was able to be somewhat controlled by altering the time constant of the CPG's adaptation effect. As expected there was a trend where higher values of the time constant of the CPG's adaptation effect led to slower walking speeds of the biped model. Another

important aspect that was analyzed in this study was the effect of linking the CPG to produce muscle activation patterns for both limbs. By analyzing the phase plots of the biped's walking kinematics it was found that the most stable walking patterns were achieved when there was a moderate level of connectivity between the two sides.

The final study in this thesis conducted a series of simulations with the addition of sensory feedback from simulated muscle receptors and a contact sensor with the ground. It was found that positive feedback to the extensor HC from the contact sensor had the greatest effect on the walking pattern of the biped model. The addition of this feedback mechanism led to a dramatic increase in the walking speed of the biped model. The addition of simulated stretch reflexes from muscle receptors was found to severely limit the walking speed of the biped model, but led to an increase in the stability of the walking pattern, which was observed through more cyclic patterns in the phase plots of the biped model's kinematic pattern and a reduction in the variability of the forward walking speed of the model. A trade-off was found between the stability of the walking pattern and the average forward walking speed through the use of phase dependent feedback, where feedback from the simulated stretch reflexes were delivered only during the appropriate phase of the locomotor pattern.

Previously published models that incorporated neural control models and representations of the musculoskeletal system have been able to produce more robust walking patterns than the models presented in this thesis (ie. (Taga et al. 1991; Taga 1995a; Paul et al. 2005; Jo 2008)) and have even been able to incorporate adaptive aspects of locomotor control into their models, such as responding to perturbations (Taga 1995b) or stepping over obstacles (Taga 1998; Jo 2008). The main difference between these previously published models and the ones created in this thesis is that this thesis investigated what the effect of the altering the parameters of the neural

control model would have on the walking pattern, where these previous studies altered the values of the control parameters in a non-systematic fashion to achieve the most ideal walking pattern. By systematically manipulating the individual parameters of the locomotor control system, it was possible to directly indentify the effect that these parameters had on the walking pattern, which contributed to a better understanding of the neural control mechanisms of human walking.

One area of the neural control and biomechanics of human walking that still requires considerable research is the control of balance. While this thesis investigated several neural mechanisms of generating the walking pattern, it did not investigate any balance control mechanisms involved in human walking. Future work should focus on integrating these balance control systems with representations of other locomotor control systems and investigate how these systems interact with the CPG and feedback from sensory control systems. Jo and Massaquuoi (2007) carried out some promising work investigating the Cerebellar contributions to the control of balance, and perhaps these types of Cerebellar models could be incorporated in the locomotor control models presented in this thesis

Another area that requires work is to increase the complexity of the representations of the human musculoskeletal systems. The representations in this thesis were admittedly simple compared to the complexity of the real human body. This thesis limited the muscles included in the musculoskeletal model to uniarticular muscles as this greatly simplified the control of the walking pattern. Some recent work on investigating the control of walking and movement in general has found that uniarticular muscles may be responsible for generating the basic walking pattern and that feedback and passive forces originating from muscle receptors in biarticular muscles help refine the movement (Neptune et al. 2004; Whittington et al. 2008). It would be interesting to refine the CPG model presented in this thesis to include the generation of muscle

activation patterns for biarticular muscles, however this would require a significant modification to the representations of the CPG model that was used in this thesis.

The final consideration that must be understood when interpreting the results from this thesis was that these were the results from simplified representations of the nervous system and musculoskeletal system. While these models allowed for the systematic manipulation of a number of variables, it was unclear whether the same results would be attained if it were possible to manipulate these variables in human or animal subjects. Creating models of these systems and examining how they interact may be a valuable tool in furthering our understanding of the neural control mechanisms involved in the control of human walking (Pearson et al. 2006), however it was important to consider the validity of the models created in this thesis. A direct validation of these models was not possible, because it was impossible to measure, let alone manipulate, a number of the signals that were used in the control systems presented in this thesis. When these control models are more advanced it may be possible to compare the outputs of these neuromechanical simulations (muscle activation patterns or movement patterns) to equivalent signals directly recorded from human subjects. However, the state of these models, and other neuromechanical simulations of locomotion in the literature are still in an early stage of development. It is expected that the number of these types of models will increase in the future and the sub-models which comprise the components of the overall model will continue to improve in biological fidelity and validity and therefore improve our understanding of how human walking and other human movements are controlled by the CNS.

Novel Contributions of this Thesis

When evaluating any academic work it is important to consider what new contributions have been made to our collective knowledge. A large amount of the work that was completed in

this thesis involved the creation of computational models based on our current understanding of locomotor control and examining what the effects the various control parameters would have on the walking pattern of a mechanical model. In the first two studies a pendulum model was used to examine some of the basic principles involved in the control of rhythmic limb movements. The third and fourth studies used a basic biped model of the musculoskeletal system to investigate the neural control parameters involved in the control of locomotion.

One of the main goals of the first two studies was to develop models of that would be used in the final two studies, these include the CPG model, which was based on the work of Matsouka (Matsuoka 1985; Matsuoka 1987), the muscle model which was based on the work of Hill (Hill 1938) and heavily influenced by the work of McGill and Norman (McGill and Norman 1986). The main novel contribution was the combination of these models and the evaluation of a number of control parameters on the motion of the pendulum. A particularly novel contribution was to include the contraction dynamics of skeletal muscle (Force-Length and Force-Velocity Relationships) rather than simply representing the muscles as spring-damper complexes as has been done in several other past studies ie.(Hatsopoulos 1996; Kuo 2002). As was shown in Experiment 5 in Chapter 3, where the muscle attachment properties were altered and the effects on the motion of the pendulum were analyzed the properties of the muscles in the model could have dramatic effect on the motion of the pendulum. The addition of muscle contraction dynamics is a very important contribution to this area as it increases the level of biological fidelity to models that investigate the control of rhythmic limb movements.

One of the most novel aspects of the simulations that were carried out with the biped model is the fact that the motion patterns that were analyzed were allowed to emerge naturally from the control systems that were modelled, without the use of an optimization algorithm or any

parameter tuning. Of the previously published neuromechanical models only the work of Yakovenko (2004). The other novel aspect of this work is that a wide variety of parameters were tested to determine the effect of the control parameters on the walking speed and the variability of the walking pattern. Again the only other published neuromechanical model that used a similar approach was the work of Yakovenko (2004), who tested the ability of the control system that he developed to produce walking patterns over a wide range of parameters of the musculoskeletal system. The final major novel contribution was the use of a body-weight support system model to help hold up the HAT segment during the simulations. The use of this system allowed for the simulations to be carried out even if the neural control parameters were insufficient to provide support to the biped model. The main drawback to the use of this model in this thesis is that the amount of body-weight support that was provided by this system was very high; therefore the mechanisms that are used to provide propulsion are different than those that would be observed *in vivo*.

References

Akazawa, K., Aldridge, J. W., Steeves, J. D. and Stein, R. B. (1982). Modulation of stretch reflexes during locomotion in the mesencephalic cat. J Physiol **329**: 553-67.

Anderson, F. C. and Pandy, M. G. (1999). A Dynamic Optimization Solution for Vertical Jumping in Three Dimensions. Comput Methods Biomech Biomed Engin **2**(3): 201-231.

Anderson, F. C. and Pandy, M. G. (2001). Dynamic optimization of human walking. J Biomech Eng **123**(5): 381-390.

Andriacchi, T. P., Ogle, J. A. and Galante, J. O. (1977). Walking speed as a basis for normal and abnormal gait measurements. J Biomech **10**(4): 261-268.

Asai, Y., Nomura, T., Sato, S., Tamaki, A., Matsuo, Y., Mizukura, I. and Abe, K. (2003). A coupled oscillator model of disordered interlimb coordination in patients with Parkinson's disease. Biol Cybern **88**(2): 152-162.

Bent, L. R., Inglis, J. T. and McFadyen, B. J. (2004). When is vestibular information important during walking? J Neurophysiol **92**(3): 1269-1275.

Bosco, G. and Poppele, R. E. (1997). Representation of multiple kinematic parameters of the cat hindlimb in spinocerebellar activity. J Neurophysiol **78**(3): 1421-1432.

Bouyer, L. J. and Rossignol, S. (2003). Contribution of cutaneous inputs from the hindpaw to the control of locomotion. I. Intact cats. J Neurophysiol **90**(6): 3625-39.

Brown, T. G. (1911). The Intrinsic Factors in the Act of Progression in the Mammal. Proc Roy Soc B **84**(572): 308-319.

Brown, T. G. (1914). On the nature of the fundamental activity of the nervous centeres. J Physiol **48**: 18-46.

Browning, R. C., McGowan, C. P. and Kram, R. (2009). Obesity does not increase external mechanical work per kilogram body mass during walking. J Biomech.

Bryant, P. J. and Miles, J. W. (1990). On a Periodically Forced, Weakly Damped Pendulum. Part 1: Applied Torque. J. Austral. Math. Soc. Ser. B **32**: 1-22.

Byrne, J. E., Stergiou, N., Blanke, D., Houser, J. J., Kurz, M. J. and Hageman, P. A. (2002a). Comparison of gait patterns between young and elderly women: an examination of coordination. Percept Mot Skills **94**(1): 265-280.

Byrne, J. M., Gage, W. H. and Prentice, S. D. (2002b). Bilateral lower limb strategies used during a step-up task in individuals who have undergone unilateral total knee arthroplasty. Clin Biomech (Bristol, Avon) **17**(8): 580-585.

Calancie, B., Needham-Shropshire, B., Jacobs, P., Willer, K., Zych, G. and Green, B. A. (1994). Involuntary stepping after chronic spinal cord injury. Evidence for a central rhythm generator for locomotion in man. Brain **117 (Pt 5)**: 1143-59.

Caldwell, G. E. (2004). Muscle Modeling. Research Methods in Biomechanics. D. G. Robertson. Champain, IL, Human Kinetics.

Callaghan, J. P., Patla, A. E. and McGill, S. M. (1999). Low back three-dimensional joint forces, kinematics, and kinetics during walking. Clin Biomech (Bristol, Avon) **14**(3): 203-216.

Capaday, C. (2002). The special nature of human walking and its neural control. Trends Neurosci **25**(7): 370-376.

Capaday, C. and Stein, R. B. (1986). Amplitude modulation of the soleus H-reflex in the human during walking and standing. J Neurosci **6**(5): 1308-1313.

Chen, W. J. and Poppele, R. E. (1978). Small-signal analysis of response of mammalian muscle spindles with fusimotor stimulation and a comparison with large-signal responses. J Neurophysiol **41**(1): 15-27.

Cheng, E. J., Brown, I. E. and Loeb, G. E. (2000). Virtual muscle: a computational approach to understanding the effects of muscle properties on motor control. J Neurosci Methods **101**(2): 117-130.

Clarac, F. (2008). Some historical reflections on the neural control of locomotion. Brain Res Rev **57**(1): 13-21.

Cohen, A. H. (1992). The role of heterarchical control in the evolution of central pattern generators. Brain Behav Evol **40**(2-3): 112-124.

Conway, B. A., Hultborn, H. and Kiehn, O. (1987). Proprioceptive input resets central locomotor rhythm in the spinal cat. Exp Brain Res **68**(3): 643-56.

Dempster, W. T. (1955). Space requirements of the seated operator. Ohio: Wright-Paterson Air Force Base, Technical report WADC-TR-55-159.

Deshpande, N. and Patla, A. E. (2005). Dynamic visual-vestibular integration during goal directed human locomotion. Exp Brain Res **166**(2): 237-47.

Dietz, V. (2003). Spinal cord pattern generators for locomotion. Clin Neurophysiol **114**(8): 1379-1389.

Dietz, V. and Duysens, J. (2000). Significance of load receptor input during locomotion: a review. Gait Posture **11**(2): 102-10.

Dietz, V., Zijlstra, W. and Duysens, J. (1994). Human neuronal interlimb coordination during split-belt locomotion. Exp Brain Res **101**(3): 513-520.

Dimitrijevic, M. R., Gerasimenko, Y. and Pinter, M. M. (1998). Evidence for a spinal central pattern generator in humans. Ann N Y Acad Sci **860**: 360-376.

Doke, J., Donelan, J. M. and Kuo, A. D. (2005). Mechanics and energetics of swinging the human leg. J Exp Biol **208**(Pt 3): 439-445.

Donelan, J. M. and Pearson, K. G. (2004). Contribution of sensory feedback to ongoing ankle extensor activity during the stance phase of walking. Can J Physiol Pharmacol **82**(8-9): 589-598.

Drew, T. (1988). Motor cortical cell discharge during voluntary gait modification. Brain Res **457**(1): 181-187.

Drew, T., Prentice, S. and Schepens, B. (2004). Cortical and brainstem control of locomotion. Prog Brain Res **143**: 251-261.

Drew, T. and Rossignol, S. (1984). Phase-dependent responses evoked in limb muscles by stimulation of medullary reticular formation during locomotion in thalamic cats. J Neurophysiol **52**(4): 653-75.

Durkin, J. L., Dowling, J. J. and Andrews, D. M. (2002). The measurement of body segment inertial parameters using dual energy X-ray absorptiometry. J Biomech **35**(12): 1575-1580.

Dutra, M. S., De Pina, F. i. A. and Romano, V. F. (2003). Modeling of a bipedal locomotor using coupled nonlinear oscillators of Van der Pol. Biol Cybern **88**(4): 286-292.

Duysens, J., Van de Crommert, H. W., Smits-Engelsman, B. C. and Van der Helm, F. C. (2002). A walking robot called human: lessons to be learned from neural control of locomotion. J Biomech **35**(4): 447-53.

Edamura, M., Yang, J. F. and Stein, R. B. (1991). Factors that determine the magnitude and time course of human H-reflexes in locomotion. J Neurosci **11**(2): 420-427.

Ekeberg, O. and Pearson, K. (2005). Computer simulation of stepping in the hind legs of the cat: an examination of mechanisms regulating the stance-to-swing transition. J Neurophysiol **94**(6): 4256-4268.

Eng, J. J., Winter, D. A. and Patla, A. E. (1994). Strategies for recovery from a trip in early and late swing during human walking. Exp Brain Res **102**(2): 339-49.

Eng, J. J., Winter, D. A. and Patla, A. E. (1997). Intralimb dynamics simplify reactive control strategies during locomotion. J Biomech **30**(6): 581-588.

Fitzpatrick, R. C., Wardman, D. L. and Taylor, J. L. (1999). Effects of galvanic vestibular stimulation during human walking. J Physiol **517 (Pt 3)**: 931-9.

Forssberg, H., Grillner, S. and Halbertsma, J. (1980a). The locomotion of the low spinal cat. I. Coordination within a hindlimb. Acta Physiol Scand **108**(3): 269-281.

Forssberg, H., Grillner, S., Halbertsma, J. and Rossignol, S. (1980b). The locomotion of the low spinal cat. II. Interlimb coordination. Acta Physiol Scand **108**(3): 283-295.

Forssberg, H., Grillner, S. and Rossignol, S. (1977). Phasic gain control of reflexes from the dorsum of the paw during spinal locomotion. Brain Res **132**(1): 121-39.

Futakata, Y. and Iwasaki, T. (2008). Formal analysis of resonance entrainment by central pattern generator. J Math Biol **57**(2): 183-207.

Gage, W. H. (2003). The Role of the Knee Joint Sensory System in Human Postural Control. Kinesiology. Waterloo, University of Waterloo. **PhD**.

Ghez, C. and Thach, W. T. (2001). Cerebellum. Principles of Neural Science. E. R. Kandel, J. H. Schwartz and T. M. Jessel. New York, Wiley.

Gilchrist, L. A. and Winter, D. A. (1996). A two-part, viscoelastic foot model for use in gait simulations. J Biomech **29**(6): 795-798.

Goldberg, M. E. (2001). Control of Gaze. Principles of Neural Science. E. R. Kandel, J. H. Schwartz and T. M. Jessel. New York, Wiley.

Gorska, T., Zmyslowski, W. and Majczynski, H. (1999). Overground locomotion in intact rats: interlimb coordination, support patterns and support phases duration. Acta Neurobiol Exp **59**(2): 131-144.

Grillner, S., Wallen, P., Dale, N., Brodin, L., Buchanan, J. and Hill, R. (1987). Transmitter, membrane properties and network circutry in the control of locomotion in the lamprey. Trends Neurosci **10**: 34-41.

Grillner, S. and Zangger, P. (1979). On the central generation of locomotion in the low spinal cat. Exp Brain Res **34**(2): 241-261.

Grillner, S. and Zangger, P. (1984). The effect of dorsal root transection on the efferent motor pattern in the cat's hindlimb during locomotion. Acta Physiol Scand **120**(3): 393-405.

Gunther, M. and Ruder, H. (2003). Synthesis of two-dimensional human walking: a test of the lambda-model. Biol Cybern **89**(2): 89-106.

Hamill, J., Haddad, J.M., McDermott, W.J. (2000). Issues in Quantifying Variablity From a Dynamical Systems Perspective. Journal of Applied Biomechanics **16**: 407-18.

Hasan, Z. (1983). A model of spindle afferent response to muscle stretch. J Neurophysiol **49**(4): 989-1006.

Hatsopoulos, N. G. (1996). Coupling the neural and physical dynamics in rhythmic movements. Neural Comput **8**(3): 567-81.

Hiebert, G. W. and Pearson, K. G. (1999). Contribution of sensory feedback to the generation of extensor activity during walking in the decerebrate Cat. J Neurophysiol **81**(2): 758-770.

Hill, A. V. (1938). The Heat of Shortening and Dynamic Constants of Muscle Proc Roy Soc B **126**: 136-195.

Hill, S. W. (2004). Recovery Responses to Unexpected Medial/Lateral Trunk Perturbations During Over-Ground Human Locomotion: The Influences of Perturbation Magnitude, Phase of Gait, Medial/Lateral Walkway Constraint, Lower Field of Vision, and Advanced Knowledge of Perturbation. Kinesiology. Waterloo, University of Waterloo. **PhD**.

Hof, A. L., Gazendam, M. G. and Sinke, W. E. (2005). The condition for dynamic stability. J Biomech **38**(1): 1-8.

Hoffmann, P. (1910). Beitrag zur Kenntnis der menschlichen Reflexe mit besonderer Berucksichtigung der elektrischen Erscheinungen. Arch Anat Physiol. **1**: 223-246.

Houk, J. C., Rymer, W. Z. and Crago, P. E. (1981). Dependence of dynamic response of spindle receptors on muscle length and velocity. J Neurophysiol **46**(1): 143-66.

Hoy, M. G., Zajac, F. E. and Gordon, M. E. (1990). A musculoskeletal model of the human lower extremity: the effect of muscle, tendon, and moment arm on the moment-angle relationship of musculotendon actuators at the hip, knee, and ankle. J Biomech **23**(2): 157-169.

Hulliger, M., Nordh, E. and Vallbo, A. B. (1985). Discharge in muscle spindle afferents related to direction of slow precision movements in man. J Physiol **362**: 437-53.

Iida, H. and Yamamuro, T. (1987). Kinetic analysis of the center of gravity of the human body in normal and pathological gaits. J Biomech **20**(10): 987-95.

Ilg, W., Giese, M. A., Gizewski, E. R., Schoch, B. and Timmann, D. (2008). The influence of focal cerebellar lesions on the control and adaptation of gait. Brain **131**(Pt 11): 2913-27.

Ilg, W., Golla, H., Thier, P. and Giese, M. A. (2007). Specific influences of cerebellar dysfunctions on gait. Brain **130**(Pt 3): 786-98.

Ivanenko, Y. P., Poppele, R. E. and Lacquaniti, F. (2004). Five basic muscle activation patterns account for muscle activity during human locomotion. J Physiol **556**(Pt 1): 267-282.

Ivanenko, Y. P., Poppele, R. E. and Lacquaniti, F. (2009). Distributed neural networks for controlling human locomotion: lessons from normal and SCI subjects. Brain Res Bull **78**(1): 13-21.

Iwasaki, T. and Zheng, M. (2006). Sensory Feedback Mechanism Underlying Entrainment of Central Pattern Generator to Mechanical Resonance. Biol Cybern: 1-17.

Jensen, L., Prokop, T. and Dietz, V. (1998). Adaptational effects during human split-belt walking: influence of afferent input. Exp Brain Res **118**(1): 126-130.

Jo, S. (2007). A neurobiological model of the recovery strategies from perturbed walking. Biosystems **90**(3): 750-68.

Jo, S. (2008). Hypothetical neural control of human bipedal walking with voluntary modulation. Med Biol Eng Comput **46**(2): 179-93.

Jo, S. and Massaquoi, S. G. (2007). A model of cerebrocerebello-spinomuscular interaction in the sagittal control of human walking. Biol Cybern **96**(3): 279-307.

Jordan, K., Challis, J. H. and Newell, K. M. (2006). Walking speed influences on gait cycle variability. Gait Posture.

Kably, B. and Drew, T. (1998). Corticoreticular pathways in the cat. I. Projection patterns and collaterization. J Neurophysiol **80**(1): 389-405.

Kang, H. G. and Dingwell, J. B. (2009). Dynamic stability of superior vs. inferior segments during walking in young and older adults. Gait Posture **30**(2): 260-3.

Kingma, I., de Looze, M. P., Toussaint, H. M., Klinjnsma, H. G. and Buijen, T. B. M. (1996). Validation of a full body 3-D dynamic linked segment model. Hum Mov Sci **15**: 833-860.

Kuo, A. D. (2002). The relative roles of feedforward and feedback in the control of rhythmic movements. Motor Control **6**(2): 129-145.

Lajoie, Y., Teasdale, N., Cole, J. D., Burnett, M., Bard, C., Fleury, M., Forget, R., Paillard, J. and Lamarre, Y. (1996). Gait of a deafferented subject without large myelinated sensory fibers below the neck. Neurology **47**(1): 109-115.

Lam, T. and Pearson, K. G. (2001). Proprioceptive modulation of hip flexor activity during the swing phase of locomotion in decerebrate cats. J Neurophysiol **86**(3): 1321-1332.

Lam, T. and Pearson, K. G. (2002). The role of proprioceptive feedback in the regulation and adaptation of locomotor activity. Adv Exp Med Biol **508**: 343-55.

Lam, T., Wolstenholme, C., van der Linden, M., Pang, M. Y. and Yang, J. F. (2003a). Stumbling corrective responses during treadmill-elicited stepping in human infants. J Physiol **553**(Pt 1): 319-31.

Lam, T., Wolstenholme, C. and Yang, J. F. (2003b). How do infants adapt to loading of the limb during the swing phase of stepping? J Neurophysiol **89**(4): 1920-1928.

Lavoie, S. and Drew, T. (2002). Discharge characteristics of neurons in the red nucleus during voluntary gait modifications: a comparison with the motor cortex. J Neurophysiol **88**(4): 1791-1814.

Lewandowski, A. (1982). Issues in model validation. International Institute for Applied Systems Analysis **RR-82-37**: 1-11.

Lewis, M. A., Etienne-Cummings, R., Hartmann, M. J., Xu, Z. R. and Cohen, A. H. (2003). An in silico central pattern generator: silicon oscillator, coupling, entrainment, and physical computation. Biol Cybern **88**(2): 137-51.

MacKay-Lyons, M. (2002). Central pattern generation of locomotion: a review of the evidence. Phys Ther **82**(1): 69-83.

MacKinnon, C. D. and Winter, D. A. (1993). Control of whole body balance in the frontal plane during human walking. J Biomech **26**(6): 633-644.

Marigold, D. S. (2008). Role of peripheral visual cues in online visual guidance of locomotion. Exerc Sport Sci Rev **36**(3): 145-51.

Marigold, D. S., Bethune, A. J. and Patla, A. E. (2003). Role of the unperturbed limb and arms in the reactive recovery response to an unexpected slip during locomotion. J Neurophysiol **89**(4): 1727-37.

Marigold, D. S. and Eng, J. J. (2006). Altered timing of postural reflexes contributes to falling in persons with chronic stroke. Exp Brain Res **171**(4): 459-68.

Marigold, D. S. and Patla, A. E. (2002). Strategies for dynamic stability during locomotion on a slippery surface: effects of prior experience and knowledge. J Neurophysiol **88**(1): 339-53.

Marigold, D. S. and Patla, A. E. (2005). Adapting locomotion to different surface compliances: neuromuscular responses and changes in movement dynamics. J Neurophysiol **94**(3): 1733-50.

Massion, J. (1988). Red nucleus: past and future. Behav Brain Res **28**(1-2): 1-8.

Massion, J., Alexandrov, A. and Frolov, A. (2004). Why and how are posture and movement coordinated? Prog Brain Res **143**: 13-27.

Matsuoka, K. (1985). Sustained oscillations generated by mutually inhibiting neurons with adaptation. Biol Cybern **52**(6): 367-376.

Matsuoka, K. (1987). Mechanisms of frequency and pattern control in the neural rhythm generators. Biol Cybern **56**(5-6): 345-353.

Matthews, P. B. and Stein, R. B. (1969). The regularity of primary and secondary muscle spindle afferent discharges. J Physiol **202**(1): 59-82.

McCrea, D. A. (1996). Supraspinal and segmental interactions. Can J Physiol Pharmacol **74**(4): 513-517.

McCrea, D. A. (2001). Spinal circuitry of sensorimotor control of locomotion. J Physiol **533**(Pt 1): 41-50.

McCrea, D. A. and Rybak, I. A. (2008). Organization of mammalian locomotor rhythm and pattern generation. Brain Res Rev **57**(1): 134-46.

McFadyen, B. J., Magnan, G. A. and Boucher, J. P. (1993). Anticipatory locomotor adjustments for avoiding visible, fixed obstacles of varying proximity. Hum Mov Sci **12**: 259-272.

McGill, S. M. and Norman, R. W. (1986). Partitioning of the L4-L5 dynamic moment into disc, ligamentous, and muscular components during lifting. Spine **11**(7): 666-678.

McGowan, C. P., Neptune, R. R. and Kram, R. (2008). Independent effects of weight and mass on plantar flexor activity during walking: implications for their contributions to body support and forward propulsion. J Appl Physiol **105**(2): 486-94.

Millard, M. (2006). Implimentation of an Infinite-Step Human Gait Simulation. SYDE 750 Course Report, University of Waterloo.

Mills, P. M. and Barrett, R. S. (2001). Swing phase mechanics of healthy young and elderly men. Hum Mov Sci **20**(4-5): 427-446.

Misiaszek, J. E. (2006). Neural control of walking balance: if falling then react else continue. Exerc Sport Sci Rev **34**(3): 128-134.

Mori, S. (1987). Integration of posture and locomotion in acute decerebrate cats and in awake, freely moving cats. Prog Neurobiol **28**(2): 161-95.

Morton, S. M. and Bastian, A. J. (2004). Cerebellar control of balance and locomotion. Neuroscientist **10**(3): 247-59.

Morton, S. M. and Bastian, A. J. (2006). Cerebellar contributions to locomotor adaptations during splitbelt treadmill walking. J Neurosci **26**(36): 9107-9116.

Nathan, P. W. and Smith, M. C. (1982). The rubrospinal and central tegmental tracts in man. Brain **105**(Pt 2): 223-269.

Nelson-Wong, E., Howarth, S., Winter, D. A. and Callaghan, J. P. (2009). Application of autocorrelation and cross-correlation analyses in human movement and rehabilitation research. J Orthop Sports Phys Ther **39**(4): 287-95.

Nemeth, G. and Ohlsen, H. (1985). In vivo moment arm lengths for hip extensor muscles at different angles of hip flexion. J Biomech **18**(2): 129-40.

Neptune, R. R., Zajac, F. E. and Kautz, S. A. (2004). Muscle force redistributes segmental power for body progression during walking. Gait Posture **19**(2): 194-205.

Noble, J. W. and Prentice, S. D. (2006). Adaptation to unilateral change in lower limb mechanical properties during human walking. Exp Brain Res **169**(4): 482-495.

Obusek, J. P., Holt, K. G. and Rosenstein, R. M. (1995). The hybrid mass-spring pendulum model of human leg swinging: stiffness in the control of cycle period. Biol Cybern **73**(2): 139-47.

Ogihara, N. and Yamazaki, N. (2001). Generation of human bipedal locomotion by a bio-mimetic neuro-musculo-skeletal model. Biol Cybern **84**(1): 1-11.

Orlovsky, G. N. and Feldman, A. G. (1972). Role of afferent information in the generation of stepping movements. Neurophysiology **4**: 304-310.

Palliyath, S., Hallett, M., Thomas, S. L. and Lebiedowska, M. K. (1998). Gait in patients with cerebellar ataxia. Mov Disord **13**(6): 958-964.

Pandy, M. G. and Berme, N. (1988). Synthesis of human walking: a planar model for single support. J Biomech **21**(12): 1053-1060.

Patla, A. E. (1992). The Neural Control of Locomotion. Mobility and Gait. B. S. Spivack. New York, Marcel Dekker, Inc.

Patla, A. E. (1996). Neurobiomechanical bases for the control of human locomotion. Clinical Disorders of Balance, Posture and Gait. A. M. Bronstein, T. Brandt and M. Woollacott. London, Arnold**:** 19-40.

Patla, A. E., Calvert, T. W. and Stein, R. B. (1985). Model of a pattern generator for locomotion in mammals. Am J Physiol **248**(4 Pt 2): R484-94.

Patla, A. E. and Prentice, S. D. (1995). The role of active forces and intersegmental dynamics in the control of limb trajectory over obstacles during locomotion in humans. Exp Brain Res **106**(3): 499-504.

Paul, C., Bellotti, M., Jezernik, S. and Curt, A. (2005). Development of a human neuro-musculo-skeletal model for investigation of spinal cord injury. Biol Cybern **93**(3): 153-170.

Pearson, K., Ekeberg, O. and Buschges, A. (2006). Assessing sensory function in locomotor systems using neuro-mechanical simulations. Trends Neurosci **29**(11): 625-631.

Pearson, K. and Gordon, J. (2000). Spinal Reflexes. Principles of Neural Science. E. R. Kandel, J. H. Schwartz and T. M. Jessel. New York, McGraw-Hill.

Pearson, K. G. (1995). Proprioceptive regulation of locomotion. Curr Opin Neurobiol **5**(6): 786-791.

Pearson, K. G. (2004). Generating the walking gait: role of sensory feedback. Prog Brain Res **143**: 123-129.

Peasgood, M. (2004). Determinants of Increased Energy Cost in Prosthetic Gait. Systems Design Engineering. Waterloo, University of Waterloo. **M.A.Sc.:** 139.

Peasgood, M., Kubica, E. and McPhee, J. (2007). Stabilization of a Dynamic Walking Gait Simulation. ASME Journal of Couputational and Nonlinear Dynamics **2**: 65-72.

Pepin, A., Norman, K. E. and Barbeau, H. (2003). Treadmill walking in incomplete spinal-cord-injured subjects: 1. Adaptation to changes in speed. Spinal Cord **41**(5): 257-270.

Perry, S. D., Santos, L. C. and Patla, A. E. (2001). Contribution of vision and cutaneous sensation to the control of centre of mass (COM) during gait termination. Brain Res **913**(1): 27-34.

Piazza, S. J. and Delp, S. L. (1996). The influence of muscles on knee flexion during the swing phase of gait. J Biomech **29**(6): 723-733.

Polk, J. D., Spencer-Smith, J., DiBerardino, L., Ellis, D., Downen, M. and Rosengren, K. S. (2008). Quantifying variability in phase portraits: application to gait ontogeny. Infant Behav Dev **31**(2): 302-6.

Pozzo, T., Berthoz, A. and Lefort, L. (1990). Head stabilization during various locomotor tasks in humans. I. Normal subjects. Exp Brain Res **82**(1): 97-106.

Pozzo, T., Levik, Y. and Berthoz, A. (1995). Head and trunk movements in the frontal plane during complex dynamic equilibrium tasks in humans. Exp Brain Res **106**(2): 327-38.

Prentice, S. D. and Drew, T. (2001). Contributions of the reticulospinal system to the postural adjustments occurring during voluntary gait modifications. J Neurophysiol **85**(2): 679-698.

Prentice, S. D., Patla, A. E. and Stacey, D. A. (1995). Modelling the time-keeping function of the central pattern generator for locomotion using artificial sequential neural network. Med Biol Eng Comput **33**(3): 317-322.

Prentice, S. D., Patla, A. E. and Stacey, D. A. (1998). Simple artificial neural network models can generate basic muscle activity patterns for human locomotion at different speeds. Exp Brain Res **123**(4): 474-480.

Prilutsky, B. I., Gregor, R. J. and Ryan, M. M. (1998). Coordination of two-joint rectus femoris and hamstrings during the swing phase of human walking and running. Exp Brain Res **120**(4): 479-486.

Prochazka, A. and Gorassini, M. (1998). Models of ensemble firing of muscle spindle afferents recorded during normal locomotion in cats. J Physiol **507 (Pt 1)**: 277-91.

Prochazka, A., Gritsenko, V. and Yakovenko, S. (2002). Sensory control of locomotion: reflexes versus higher-level control. Adv Exp Med Biol **508**: 357-367.

Prochazka, A., Hulliger, M., Zangger, P. and Appenteng, K. (1985). 'Fusimotor set': new evidence for alpha-independent control of gamma-motoneurones during movement in the awake cat. Brain Res **339**(1): 136-40.

Prokop, T., Berger, W., Zijlstra, W. and Dietz, V. (1995). Adaptational and learning processes during human split-belt locomotion: interaction between central mechanisms and afferent input. Exp Brain Res **106**(3): 449-456.

Proske, U. and Gandevia, S. C. (2009). The kinaesthetic senses. J Physiol **587**(Pt 17): 4139-46.

Raikova, R. T. and Prilutsky, B. I. (2001). Sensitivity of predicted muscle forces to parameters of the optimization-based human leg model revealed by analytical and numerical analyses. J Biomech **34**(10): 1243-1255.

Rassier, D. E. and Herzog, W. (2005). Force enhancement and relaxation rates after stretch of activated muscle fibres. Proc Biol Sci **272**(1562): 475-480.

Rassier, D. E., Lee, E. J. and Herzog, W. (2005). Modulation of passive force in single skeletal muscle fibres. Biol Lett **1**(3): 342-5.

Rassier, D. E., MacIntosh, B. R. and Herzog, W. (1999). Length dependence of active force production in skeletal muscle. J Appl Physiol **86**(5): 1445-57.

Reisman, D. S., Block, H. J. and Bastian, A. J. (2005). Interlimb coordination during locomotion: what can be adapted and stored? J Neurophysiol **94**(4): 2403-2415.

Rogers, M. W. (1996). Disorders of posture, balance, and gait in Parkinson's disease. Clin Geriatr Med **12**(4): 825-845.

Rossignol, S. (1996). Neural control of sterotypic limb movements. Handbook of Physiology: Sec. 13. Exercise: Regulation and Integration of Multiple Systems. L. B. Rowell and J. T. Shepherd. New York, Oxford University Press. **12**.

Rossignol, S., Brustein, E., Bouyer, L., Barthelemy, D., Langlet, C. and Leblond, H. (2004). Adaptive changes of locomotion after central and peripheral lesions. Can J Physiol Pharmacol **82**(8-9): 617-27.

Rossignol, S., Dubuc, R. and Gossard, J. P. (2006). Dynamic sensorimotor interactions in locomotion. Physiol Rev **86**(1): 89-154.

Rybak, I. A., Stecina, K., Shevtsova, N. A. and McCrea, D. A. (2006). Modelling spinal circuitry involved in locomotor pattern generation: insights from the effects of afferent stimulation. J Physiol **577**(Pt 2): 641-58.

Saibene, F. and Minetti, A. E. (2003). Biomechanical and physiological aspects of legged locomotion in humans. Eur J Appl Physiol **88**(4-5): 297-316.

Selles, R. W., Bussmann, J. B., Wagenaar, R. C. and Stam, H. J. (2001). Comparing predictive validity of four ballistic swing phase models of human walking. J Biomech **34**(9): 1171-1177.

Sherrington, C. S. (1910). Flexion-reflex of the limb, crossed extension-reflex, and reflex stepping and standing. J Physiol **40**(1-2): 28-121.

Shik, M. L., Severin, F. V. and Orlovskii, G. N. (1966). [Control of walking and running by means of electric stimulation of the midbrain]. Biofizika **11**(4): 659-66.

Shik, M. L., Severin, F. V. and Orlovsky, G. N. (1969). Control of walking and running by means of electrical stimulation of the mesencephalon. Electroencephalogr Clin Neurophysiol **26**(5): 549-.

Silder, A., Whittington, B., Heiderscheit, B. and Thelen, D. G. (2007). Identification of passive elastic joint moment-angle relationships in the lower extremity. J Biomech **40**(12): 2628-2635.

Simoni, M. F. and DeWeerth, S. P. (2007). Sensory feedback in a half-center oscillator model. IEEE Trans Biomed Eng **54**(2): 193-204.

Sorensen, K. L., Hollands, M. A. and Patla, E. (2002). The effects of human ankle muscle vibration on posture and balance during adaptive locomotion. Exp Brain Res **143**(1): 24-34.

Sutarno, C. G. and McGill, S. M. (1995). Isovelocity investigation of the lengthening behaviour of the erector spinae muscles. Eur J Appl Physiol Occup Physiol **70**(2): 146-153.

Taga, G. (1995a). A model of the neuro-musculo-skeletal system for human locomotion. I. Emergence of basic gait. Biol Cybern **73**(2): 97-111.

Taga, G. (1995b). A model of the neuro-musculo-skeletal system for human locomotion. II Real-time adaptability under various constraints. Biol Cybern **73**(2): 113-121.

Taga, G. (1998). A model of the neuro-musculo-skeletal system for anticipatory adjustment of human locomotion during obstacle avoidance. Biol Cybern **78**(1): 9-17.

Taga, G., Yamaguchi, Y. and Shimizu, H. (1991). Self-organized control of bipedal locomotion by neural oscillators in unpredictable environment. Biol Cybern **65**(3): 147-159.

ten Donkelaar, H. J. (1988). Evolution of the red nucleus and rubrospinal tract. Behav Brain Res **28**(1-2): 9-20.

Thelen, E. (1979). Rhythmical stereotypies in normal human infants. Anim Behav **27**(Pt 3): 699-715.

Van Ingen Schenaug, G. J., Pratt, C. A. and Macpearson, J. M. (1994). Differential use and control of mono- and biarticular muscles. Hum Mov Sci **13**: 495-517.

Verdaasdonk, B. W., Koopman, H. F. and Helm, F. C. (2005). Energy efficient and robust rhythmic limb movement by central pattern generators. Neural Netw.

Verdaasdonk, B. W., Koopman, H. F. and Van der Helm, F. C. (2007). Resonance tuning in a neuro-musculo-skeletal model of the forearm. Biol Cybern **96**(2): 165-80.

Wadden, T. and Ekeberg, O. (1998). A neuro-mechanical model of legged locomotion: single leg control. Biol Cybern **79**(2): 161-173.

Wells, R. P. (1988). Mechanical energy costs of human movement: an approach to evaluating the transfer possibilities of two-joint muscles. J Biomech **21**(11): 955-964.

Wessels, M., Lucas, C., Eriks, I. and de Groot, S. (2010). Body weight-supported gait training for restoration of walking in people with an incomplete spinal cord injury: a systematic review. J Rehabil Med **42**(6): 513-9.

Whelan, P. J. (1996). Control of locomotion in the decerebrate cat. Prog Neurobiol **49**(5): 481-515.

White, O., Bleyenheuft, Y., Ronsse, R., Smith, A. M., Thonnard, J. L. and Lefevre, P. (2008). Altered gravity highlights central pattern generator mechanisms. J Neurophysiol **100**(5): 2819-24.

White, S. C., Yack, H. J. and Winter, D. A. (1989). A three-dimensional musculoskeletal model for gait analysis. Anatomical variability estimates. J Biomech **22**(8-9): 885-893.

Whittington, B., Silder, A., Heiderscheit, B. and Thelen, D. G. (2008). The contribution of passive-elastic mechanisms to lower extremity joint kinetics during human walking. Gait Posture **27**(4): 628-34.

Whittlesey, S. N., van Emmerik, R. E. and Hamill, J. (2000). The swing phase of human walking is not a passive movement. Motor Control **4**(3): 273-292.

Williams, C. A. and DeWeerth, S. P. (2007). A comparison of resonance tuning with positive versus negative sensory feedback. Biol Cybern **96**(6): 603-14.

Winter, D. A. (1980). Overall principle of lower limb support during stance phase of gait. J Biomech **13**(11): 923-7.

Winter, D. A. (1991). The Biomechanics and Control of Human Gait: Normal, Pathological, Elderly. Waterloo, ON, Waterloo Biomechanics.

Winter, D. A. (1992). Foot trajectory in human gait: a precise and multifactorial motor control task. Phys Ther **72**(1): 45-53; discussion 54-6.

Winter, D. A. (1995a). Human balance and posture control during standing and walking. Gait Posture **3**: 193-214.

Winter, D. A. (1995b). Kinetics: our window into the goals and strategies of the central nervous system. Behav Brain Res **67**(2): 111-120.

Winter, D. A. (2004). Biomechanics and Motor Control of Human Movement, 3rd Edition, Wiley.

Winter, D. A., Patla, A. E., Prince, F., Ishac, M. and Gielo-Perczak, K. (1998). Stiffness control of balance in quiet standing. J Neurophysiol **80**(3): 1211-1221.

Winters, J. M. (1990). Hill Based Muscle Models: A System Engineering Perspective. Multiple Muscle Systems. J. M. Winters and S. L. Woo. New York, Springer**:** 69-93.

Winters, J. M. and Stark, L. (1987). Muscle models: what is gained and what is lost by varying model complexity. Biol Cybern **55**(6): 403-420.

Yakovenko, S., Gritsenko, V. and Prochazka, A. (2004). Contribution of stretch reflexes to locomotor control: a modeling study. Biol Cybern **90**(2): 146-155.

Yang, J. F., Stephens, M. J. and Vishram, R. (1998a). Infant stepping: a method to study the sensory control of human walking. J Physiol **507 (Pt 3)**: 927-937.

Yang, J. F., Stephens, M. J. and Vishram, R. (1998b). Transient disturbances to one limb produce coordinated, bilateral responses during infant stepping. J Neurophysiol **79**(5): 2329-37.

Yu, W. and Ikemoto, Y. (2007). An artificial reflex improves the perturbation-resistance of a human walking simulator. Med Biol Eng Comput **45**(11): 1095-104.

Zajac, F. E. (1989). Muscle and tendon: properties, models, scaling, and application to biomechanics and motor control. Crit Rev Biomed Eng **17**(4): 359-411.

Zajac, F. E. (2002). Understanding muscle coordination of the human leg with dynamical simulations. J Biomech **35**(8): 1011-1018.

Zajac, F. E., Neptune, R. R. and Kautz, S. A. (2002). Biomechanics and muscle coordination of human walking. Part I: introduction to concepts, power transfer, dynamics and simulations. Gait Posture **16**(3): 215-232.

Zatsiorsky, V. M. (2002). Kinetics of Human Motion. Champlain IL, Human Kinetics.

Zehr, E. P. (2005). Neural control of rhythmic human movement: the common core hypothesis. Exerc Sport Sci Rev **33**(1): 54-60.

Zernicke, R. F., Schneider, K. and Buford, J. A. (1991). Intersegmental dynamics during gait: implications for control. Adaptability of Human Gait. A. E. Patla**:** 187-202.

Zernicke, R. F. and Smith, J. L. (1996). Biomechanical insights into neural control of movement. Handbook of Physiology. **Section 12:** 293-330.

Zhang, D. and Zhu, K. (2007). Modeling biological motor control for human locomotion with functional electrical stimulation. Biol Cybern **96**(1): 79-97.

Appendix A: Model Parameter Values

Mechanical Model Properties

Vertical Ground Reaction Force Contact Model

Variable Name	Description	Value (Units)
k	Stiffness of spring in the spring-damper	800, 000 N/m
p	Exponent for non-linear stiffness	2.2
B_{min}	Minimum damping value	0 N.s/m
B_{max}	Maximum damping value	1000 N.s/m
d_{max}	Penetration depth where maximum damping occurs	0.01 m
$s_y(x)$	Function that prescribes the height of the floor.	$s_y(x) = -1.25$ m

Horizontal Ground Reaction Force Model

Variable Name	Description	Value (Units)
μ_s	Static co-efficient of friction	0.8
μ_d	Dynamic co-efficient of friction	0.2
v_s	Velocity limit for static friction.	±0.05 m/s
v_d	Velocity limit for dynamic friction	±2 m/s

Passive Joint Moment Parameters

Muscle Group	**α (degrees)**	β	
		Proximal	**Distal**
Rectus Femoris (RF)	24.4	3.1	1.9
Hamstrings (HS)	30.8	5.1	3.9
Gastrocnemius (GAS)	26.0	4.5	4.7
Hip Flexors (HF)	19.5	5.1	
Hip Extensors (HE)	27.3	2	
Knee Flexors (KF)	12.8	5.8	
Knee Extensors (KE)	101.9	3.5	

Body Weight Support System Model

Variable Name	**Description**	**Value (Units)**
K_s	Spring Stiffness	650 N/m
B_s	Damping Constant	100 N.s/m
L_s	Resting length of Support System	0.6 m

Muscle Model Properties

Excitation-Contraction Coupling Model Parameters

Variable Name	**Description**	**Value (Units)**
τ_{rise}	Time constant for rise of output	20 ms
τ_{rise}	Time constant for fall of output	40 ms

Hill-Type Muscle Model Parameters

Symbol	Description	Value
P_o	Maximum Isometric Muscle Force	2000 N (in Pendulum model)
P_S	Maximum Eccentric Muscle Force	1.8 * P_o
L_o	Resting Length	0.383 m (in Pendulum model)
V_{max}	Maximum rate of shortening where force can be produced	10 L_0/s
τ_{rise}	Time constant for rise of muscle activation signal	0.19 s
τ_{fall}	Time constant for decrease in muscle activation	0.4 s
L_{SEC}	Length of Series Elastic Component	0.2 m (in Pendulum model)
A	Shaping factor for F-V relationship	0.25 * Po
B	Shaping factor for F-V relationship	a*Vmax/Po

Central Pattern Generator Model Parameters

Variable Name	Description	Value (Units)
τ_{rise}	Time constant for increase in neuron activity	10ms
τ_{ad}	Time constant for adaptation effect	Various values used
β	Weight for adaptation term	2.0
W_I	Weight factor for ipsilateral neuron connection	2.0
W_C	Weight factor for ipsilateral neuron connection	Various values used
w	Weight for mutual inhibition term	-2.0
q_t	Tonic input value	Various values used
y_1 (For Right Flexors and Left Extensors)	Initial Condition for CPG output	0.2
y_1 (For Left Flexors and Right Extensors)	Initial Condition for CPG output	0
τ_{fall}	Time constant for fall of output	40 ms

Muscle Spindle Model

Variable Name	Description	Value (Units)
K_{vel}	Velocity Gain	2.0
K_{len}	Length Gain	1.0
p	Power for Velocity Term	0.5
t	Time Constant for 1st Order Delay	10 ms